NASA Contractor Report 187229

NASA-CR-187229
19920011242

Environmental and Strain Rate Effects on Graphite/Epoxy Composites

Konstantinos Peimandis
Northwestern University
Evanston, Illinois

October 1991

Prepared for
Lewis Research Center
Under Grant NAG3–423

National Aeronautics and
Space Administration

TABLE OF CONTENTS

TABLE OF CONTENTS cont.

Page

LIST OF TABLES

LIST OF TABLES cont.

LIST OF TABLES cont.

LIST OF TABLES cont.

LIST OF FIGURES

LIST OF FIGURES cont.

LIST OF FIGURES cont.

LIST OF FIGURES cont.

LIST OF FIGURES cont.

LIST OF FIGURES cont.

LIST OF FIGURES cont.

LIST OF FIGURES cont.

LIST OF FIGURES cont.

LIST OF FIGURES cont.

LIST OF FIGURES cont.

LIST OF FIGURES cont.

LIST OF FIGURES cont.

LIST OF FIGURES cont.

LIST OF FIGURES cont.

LIST OF FIGURES cont.

I. INTRODUCTION

Some applications of composite materials involve dynamically loaded components and structures under variable hygrothermal conditions. For example, composite jet engine blades are exposed to the hazards of foreign object damage (FOD), such as bird impact on rotating blades. Such impact loadings are of short duration and produce stress (strain) wave pulses with strain rates up to a few hundred (m/m) per second. Composite automobile bodies are continuously exposed to high temperature variations and variable hygroscopic conditions. For example, on a hot summer day, a composite automobile engine hood could reach temperatures well above 65°C(150°F). Reliable design of composite components requires characterization of the composite material at high strain rates, high temperatures and under various hygrothermal conditions.

The effects of strain rate on properties of composites under ambient environmental conditions have been investigated before [1,2]. It was found that, in general, fiber-dominated properties are not affected by strain rate, contrary to matrix-dominated properties which show rate, moisture and temperature sensitivity.

A need was recognized for determining the influence of environmental parameters, such as moisture and temperature, on high strain rate properties of composites. Although a great deal of work has been reported on the effects of moisture and temperature, the study of the combined effects of strain rate, temperature and moisture is of particular interest.

The work presented here, deals with the hygrothermal characterization of a unidirectional graphite/epoxy composite material over a range of strain rates.

Special techniques developed for such hygrothermal characterization are described. The mechanical properties of the composite material were obtained and analyzed by means of a time-temperature-moisture superposition principle.

II. OBJECTIVES AND SCOPE

The objective of this work is to study the individual and combined effects of temperature, moisture and strain rate on the mechanical behavior of graphite/epoxy composite materials, and to provide a detailed and complete database of mechanical properties for a typical (AS4/3501-6) graphite/epoxy material under various moisture, temperature and strain rate conditions. The ultimate goal of this work is to develop constitutive relations for the material, including rate, temperature and moisture effects. Supported by the above experimental results, an attempt will be made to develop a method which can be used to predict material behavior under any set of service conditions, from data of tests performed in the laboratory, under other conditions which are less difficult to simulate.

The first goal of this program was to develop a new method for testing composites under extreme environmental and strain rate conditions. For this purpose the embedded strain gage technique was used. A complete reliability study of embedded gages was undertaken and their performance was evaluated by a close comparison with other valid strain measurement techniques. Secondly, the material under consideration was evaluated completely under various thermal, hygroscopic and mechanical loading conditions. Approximately four hundred tests were performed under various conditions, and over one thousand stress-strain, strain-strain, strain vs time and other related curves were developed and analyzed in order to provide all the necessary data. Ultimately this work has as scope to provide a better understanding of the combined effects of moisture, temperature and strain rate on the mechanical behavior of composite materials.

III. THEORETICAL BACKGROUND AND LITERATURE SURVEY

3.1 Hygrothermal Effects In Composite Materials.

The matrix-controlled mechanical behavior of graphite/epoxy fiber composites can be significantly influenced by loading and environmental parameters such as strain rate, temperature, and moisture as previously mentioned. For this reason, a great deal of work has been done on the effects of the above parameters in the behavior of composite materials. Some investigators have used the diffusion equation to describe the sorption of moisture by composite materials [3-5]. Early papers dealt with a constant coefficient of diffussion and, initially, with dry material exposed to constant surface moisture. Later work included time-dependent diffussion coefficients [6] and varying moisture boundary conditions [7]. Some mechanical properties were predicted by micromechanical analysis by calculating thermal and swelling stresses arround fibers [8]. Some experiments were also conducted on thermal and moisture effects on strength and moduli of unidirectional fiber-reinforced lamina [9,10]. Specificaly, a series of tests on unidirectional graphite/epoxy composites (T300/5208) were conducted by Lifshitz [11] and arrived at the following conclusions on the effect of temperature, moisture and strain rate on material properties:

a. Matrix-controlled mechanical properties of fiber reinforced composites are influenced by temperature, moisture and strain rate.
b. The strongest influence is on the in-plane shear behavior.

c. The effects of the three applied parameters appear to be similar, suggesting that an equivalence between them could be established.
d. Fiber-controlled modulus and major Poisson's ratio (E_1, v_{12}) are not influenced by temperature, moisture or strain rate.
e. The longitudinal strength accepted as a fiber controlled property, was influensed appresiably by temperature and moisture. This is attributed to uneven tension on fibers and the behavior of the matrix near broken fibers.

The various investigations on the effects of moisture, temperature and strain rate on the behavior of composites thus far have generated significant fundamental knowledge for:

1. identifying the variables and mechanisms which bring about this influence,
2. establishing some key relationships between these variables, and
3. suggesting the existence of an integrated theory for predicting the hygrothermomechanical (HGTM) response of advanced composites.

In this work, some of the key mechanisms by which moisture, temperature and strain rate affect the mechanical properties of Hercules 3501-6 neat resin, and derived AS4/3501-6 graphite fiber composites are investigated. Also, the basis for developing an integrated theory able to predict the HGTM responce of advanced composite materials is described in detail.

3.1.1 Moisture Absorption

Epoxy resins absorb atmospheric moisture apparently by instantaneous surface absorption and subsequent diffusion through the interior. The absorbed water is not liquid, but exists rather in the form of hydrogen-bounded molecules

or clusters within the polymer. Liquid water may however be transported by capillary action along cracks and (in composites) along the fiber-matrix interfaces and may appear in interior voids. The absorbed water softens epoxy resins, causes them to swell, and lowers their glass transition temperature (T_g) (explained later). Thus absorbed moisture can reduce the temperature range over which matrix diminated composite properties remain stable.

The moisture distribution in laminated composites can be predicted by Fick's second law. For one dimensional diffusion through the thickness of a composite plate, Fick's law states

$$\frac{dc}{dt} = D \frac{d^2c}{dz^2} \qquad (3.1)$$

where c = moisture concentration

D = diffusivity through the thickness

t = time

z = thickness coordinate

Equation (3.1) can be solved analytically if the diffusion constant is independent of concentration and appropriate boundary conditions are specified. For the case of a plate with a large surface area relative to its thickness (h) suspended in a moist atmosphere, the boundary conditions are:

$c = c_o$ at t=0 for all x

$c = c_\infty$ at z=0 and z=1 at t>0 and,

$c = c_\infty$ at $t=\infty$ at all x

Equation (3.1) then gives

$$\frac{c_t - c_0}{c_\infty - c_0} = 1 - 4\pi^{-1} \sum_{n=0}^{n=\infty} (2n+1)^{-1} \sin[(2n+1)\pi z h^{-1}] \exp[-(2n+1)^2 D t h^{-2}] \qquad (3.2)$$

where h = thickness of the plate,

c_0, c_t, c_∞ = concentrations of water at a point z in the plate at times 0, t, and ∞ respectively, and

n = integer

The total weight of the absorbed water in the material is given by

$$m = \int_0^h c_{(z,t)} dz \qquad (3.3)$$

which yields

$$G = \frac{M_t - M_0}{M_\infty - M_0} = 1 - 8\pi^{-2} \sum_{n=0}^{n=\infty} (2n+1)^{-2} \exp[-D(2n+1)^2 \pi^2 z h^{-2}] \qquad (3.4)$$

where

M_0, M_t, M_∞ = moisture content at times 0, t and infinity respectively

Another solution to equation (3.1) given the same boundary conditions, is

$$G = \frac{M_t - M_0}{M_\infty - M_0} = 4 \cdot Dt^{1/2} \{\pi^{-2} + 2 \sum_{n=0}^{n=\infty} (-1)^n \operatorname{erfc}[nz(4dt)^{-1/2}]\} \qquad (3.5)$$

This equation is more suitable for small times while equation (3.4) is best used for moderate and long times. The value of diffusivity (D) can be deduced from the initial gradient of a graph of G as a function of reduced time ($t^{1/2}/h$) that is

$$D=\frac{\pi}{16}\left(\frac{G}{t^{1/2}/h}\right)^2 \qquad (3.6)$$

In practice a graph of G versus ($t^{1/2}/h$), the reduced sorption plot will be linear for $G<0.6$ with less than 1.2% deviation [12]. It can also be shown from the Boltsmann solution of Fick's laws [11,14] that this method for determining D can also be usefull when D depends on penetrant concentration.

Experimental evidence indicates that the maximum moisture content of a material (M_∞), is insensitive to temperature but depends on the environment moisture content according to the relationship

$$M_\infty=\alpha\phi^b \qquad (3.7)$$

where

M_∞ = equilibrium moisture content

ϕ = fractional relative humidity

α = equilibrium moisture content at 100% relative humidity, and

b = constant (both a and b are empirical values)

Examination of equations (3.4) and (3.5) indicates that the rate of moisture absorption is a function of several variables two fo them being, time of exposure and thickness of the laminate. The diffusivity is a much more complex variable, and can be a function of temperature, fiber obstruction, moisture concentration

in the laminate, or even swelling of the laminate. The dependence on moisture concentration is generaly believed to be caused by swelling of the polymer matrix by the water molecules, leading to a loosening of the polymer structure which facilitates the moovement of the diffusing molecules [14]. The mathematical and experimental approach to concentration-dependent diffusion offers considerable difficulties. Crank and co-workers [12,26] in particular, have developed the mathematical treatment for concentration-dependent diffusion coefficient and methods for their experimental determination.

In deriving equations (3.2) and (3.3), it was assumed that the laminate dimensions remain constant. However, for situations where the laminate swells, these equations can still be used provided a frame of reference is taken with respect to the moisture in the laminate, Von Amerongen [12] describes in detail two methods which can be used to approach this problem.

In the activated transition state theory of diffusion, originally proposed by Erwing [11] and further developed for polymeric materials by Barrier [13], the temperature dependence of diffusion can be expressed by

$$D = D_o \exp(-E_d/RT) \qquad (3.8)$$

where

D_o = frequency factor

E_d = activation energy for diffusion

R = gas constant, and

T = temperature

This temperature dependence will be utilized later in the experimental procedure to accelerate moisture conditioning of graphite/epoxy specimens.

In order to determine variations of mechanical properties as a function of moisture content, it is essential that moisture distribution through-out the specimen be as uniform as possible. The time required to yield a uniform distribution was determined as a series solution of equation (3.1) with the boundary conditions given above. In the case of initially dry specimens, the solution becomes

$$\frac{C_{(x,t)}}{C_\infty} = \sum_{n=1}^{n=\infty} (-1)^{n+1} \left\{ \frac{\text{erf}\,(2n-1)-2x/h}{2t^{*1/2}} + \frac{(2n-1)+2x/h}{2t^{*1/2}} \right\} \qquad (3.9)$$

where erf is the error function and t^* is a dimensionless time parameter given by

$$t^* = 4Dt/h^2 \qquad (3.10)$$

For an eight-ply specimen, equation (3.9) has been evaluated numerically by Lifshitz [11] to be about 16 days. This time period was much less than the time required for the specimens to reach the moisture level required for the tests performed in this work. Thus, all specimens tested had a uniform moisture distribution.

3.1.2 Glass Transition Temperature.

The glass transition temperature (T_g) of a polymer is defined as the temperature above which the polymer is soft and below which it is hard. The hard polymer is a glasslike material, while the soft polymer varies from a rubbery material for very high molecular weights to a liquid for very low molecular weights. Thus, for epoxy resins the T_g is the temperature at which the polymer goes from a glassy solid to a rubbery solid.

In practice, a single glass transition temperature does not exist. It is more appropriate to refer to a glass transition temperature region where T_g is conveniently taken as the temperature at which there is a very rapid change in polymer physical properties [13].

An accepted theory states that at and bellow the transition temperature, 1/40 of the total volume of the material is free volume. If this is true, then the T_g can be altered by changing its free volume at a given temperature. If a polymer were mixed with a miscible liquid that contains more free volume than the pure polymer, then the T_g will be lowered. In particular, if it is assumed that the free volumes are additive, then the diluent-polymer solution will contain more free volume at any given temperature than would the polymer alone. As a result, the plasticized polymer must be cooled to lower temperature in order to reduce its free volume to 1/40 of the total volume of the diluent-polymer combination. This is the process which occurs when moisture is absorbed into an epoxy resin. Based on the above assumptions Bueche and Kelley [14] derived the following expression for the T_g of a plasticized system

$$T_g = \frac{a_p V_p T_{gp} + a_d(1-V_p)T_{gd}}{a_p V_p + a_d(1-V_p)} \qquad (3.11)$$

where

T_{gp} = polymer glass transition temperature

T_{gd} = diluent glass transition temperature

a_p = expansion coefficient of polymer

a_d = expansion coefficient of diluent, and

V_p = volume fraction of polymer

It should be noted that in this case, (a) is not the usual linear coefficient of thermal expansion. It is a_l-a_g where a_l is the linear thermal expansion

coefficient above the T_g and a_g corresponds to the same below T_g. In terms of the percent weight gain in the polymer, M, V_p is given by

$$V_p = \frac{1}{1+\rho_p/\rho_d[0.01 M]} \qquad (3.12)$$

where ρ_p and ρ_d are the densities of the polymer and diluent respectively.

It is obvious from equation (3.11) that the presence of moisture within a composite laminate will reduce the glass transition temperature of the matrix, as shown in figure (3.1) in which case a sharp decrease in matrix modulus is taken as an indicator for establishing the glass transition region. This in turn causes a reduction of the operating temperature of the composite structure of which the particular polymer is a material constituent

3.1.3 Hygrothermal Deformation.

Absorption of moisture and temperature change cause deformation of composite structures (hygrothermal deformation). The matrix material is much more susceptible to dimensional change than the fiber. Therefore, the hygrothermal deformation of a unidirectional composite is much higher in the transverse direction than the longitudinal direction. Such anisotropy in deformation results in the presence of residual stresses in composite laminates.

a. Thermoelastic Stress-Strain Relations.

Analytically, when an orthotropic material (composite lamina) is subjected to a change in temperature, the stress-strain relations are modified to account for the free thermal strains as follows

$$\varepsilon_1 - \alpha_1 \Delta T = \frac{\sigma_1}{E_1} - \frac{\nu_{21}\sigma_2}{E_2} + \frac{(0)\tau_{12}}{G_{12}} \qquad (3.13)$$

$$\varepsilon_2 - \alpha_2 \Delta T = -\frac{\nu_{21}\sigma_1}{E_1} + \frac{\sigma_2}{E_2} + \frac{(0)\tau_{12}}{G_{12}} \qquad \text{(3.13) cont.}$$

$$\varepsilon_{12} - (0)\Delta T = \frac{(0)\sigma_1}{E_1} + \frac{(0)\sigma_2}{E_2} + \frac{\tau_{12}}{G_{12}}$$

where

α_i = thermal expansion coefficients in the principal material coordinate system
T = local temperature distribution
σ_i, ε_i = mechanical stress, strain along principal material axes
ν_{12}, ν_{21} = major and minor Poisson's ratios respectively
i = 1, 2

in matrix form,

$$\varepsilon_i - \alpha_i \Delta T = S_{ij}\sigma_j \ , \quad (i, j = 1,2,6) \qquad (3.14)$$

$$\sigma_i = Q_{ij}(\varepsilon_j - \alpha_j \Delta T) \ , \quad (i, j = 1,2,6) \qquad (3.15)$$

where

S_{ij} = material compliance matrix, and

$S_{11} = 1/E_1$ $\quad S_{22} = 1/E_2$ $\quad S_{66} = 1/G_{12}$

$S12 = -\nu_{12}/E_1$ $\quad S_{21} = -\nu_{12}/E_1$ $\quad S_{26} = S_{61} = S_{62} = S_{16} = 0$

Q_{ij} = stiffness matrix, and

$Q_{11} = E_1/(1-\nu_{12}\nu_{21})$ $\quad Q_{22} = E_2/(1-\nu_{12}\nu_{21})$

$Q_{21} = \nu_{12}E_2/(1-\nu_{12}\nu_{21})$ $\quad Q_{12} = \nu_{21}E_1/(1-\nu_{12}\nu_{21})$

$Q_{66} = G_{12}$ $\quad Q_{21} = Q_{16} = Q_{62} = Q_{61} = 0$

For an arbitrary coordinate system, of orientation (θ), the thermoelastic compliance and stiffness relations are:

$$\begin{aligned}
\varepsilon_x - \alpha_x \Delta T &= S_{xx}\sigma_x + S_{xy}\sigma_y + S_{xs}\tau_{xy} \\
\varepsilon_y - \alpha_y \Delta T &= S_{xy}\sigma_x + S_{yy}\sigma_y + S_{ys}\tau_{xy} \\
\gamma_{xy} - \alpha_{xy} \Delta T &= S_{xs}\sigma_x + S_{ys}\sigma_y + S_s\tau_{xy}
\end{aligned} \tag{3.16}$$

and

$$\begin{aligned}
\sigma_x &= Q_{xx}(\varepsilon_x - \alpha_x \Delta T) + Q_{xy}(\varepsilon_x - \alpha_y \Delta T) + Q_{xs}(\gamma_{xy} - \alpha_{xy} \Delta T) \\
\sigma_y &= Q_{xy}(\varepsilon_x - \alpha_x \Delta T) + Q_{yy}(\varepsilon_x - \alpha_y \Delta T) + Q_{ys}(\gamma_{xy} - \alpha_{xy} \Delta T) \\
\tau_{xy} &= Q_{xs}(\varepsilon_x - \alpha_x \Delta T) + Q_{ys}(\varepsilon_x - \alpha_y \Delta T) + Q_s(\gamma_{xy} - \alpha_{xy} \Delta T)
\end{aligned} \tag{3.17}$$

where

$$\begin{aligned}
\alpha_x &= m^2\alpha_1 + n^2\alpha_2 \\
\alpha_y &= n^2\alpha_1 + m^2\alpha_2 \\
\alpha_{xy} &= 2nm(\alpha_1 - \alpha_2)
\end{aligned} \tag{3.18}$$

and

$$\begin{aligned}
m &= \cos\theta \\
n &= \sin\theta \\
s &= \text{subscript denoting shear}
\end{aligned} \tag{3.19}$$

The transformed material compliances and stiffnesses for any orientation (θ) are given in the following matrix multiplication table:

Table 3.1 Transformation of Stiffness and Compliance matrices.

on-axis	Q_{11}/S_{11}	Q_{22}/S_{22}	Q_{12}/S_{12}	$Q_{66}/(1/4)S_{66}$
off-axis				
Q_{xx}/S_{xx}	m^4	n^4	$2m^2n^2$	$4m^2n^2$
Q_{yy}/S_{yy}	n^4	m^4	$2m^2n^2$	$4m^2n^2$
Q_{xy}/S_{xy}	m^2n^2	m^2n^2	m^4+n^4	$-4m^2n^2$
Q_s/S_s	m^2n^2	m^2n^2	$-2m^2n^2$	$(m^2-n^2)^2$
$Q_{xs}/(1/2)S_{xs}$	$-m^3n$	$-mn^3$	mn^3-m^3n	$2(mn^3-m^3n)$
$Q_{ys}/(1/2)S_{ys}$	$-mn^3$	$-m^3n$	m^3n-mn^3	$2(m^3n-mn^3)$

b. Hygroscopic Stress-Strain Relations

The hygroscopic response of polymeric composites is totally analogous to the thermal response of the material. Hence, it is necessary to define two new material properties b_1 and b_2, the coefficients of moisture expansion along the principal material directions. For hygrothermal responce, equations (3.14-3.19) can now be rewritten as:

$$\varepsilon_i - \beta_i \Delta c = S_{ij}\sigma_j \ , \quad (i, j = 1,2,6) \tag{3.20}$$

$$\sigma_i = Q_{ij}(\varepsilon_j - \beta_j \Delta c) \ , \quad (i, j = 1,2,6) \tag{3.21}$$

$$\begin{aligned} \varepsilon_\chi - \beta_\chi \Delta c &= S_{xx}\sigma_x + S_{xy}\sigma_y + S_{xs}\tau_{xy} \\ \varepsilon_y - \beta_y \Delta c &= S_{xy}\sigma_x + S_{yy}\sigma_y + S_{ys}\tau_{xy} \\ \gamma_{\chi y} - \beta_{\chi y} \Delta c &= S_{xs}\sigma_x + S_{ys}\sigma_y + S_s\tau_{xy} \end{aligned} \tag{3.22}$$

and

$$\sigma_x = Q_{xx}(\varepsilon_\chi - \beta_\chi \Delta c) + Q_{xy}(\varepsilon_\chi - \beta_y \Delta c) + Q_{xs}(\gamma_{\chi y} - \beta_{\chi y} \Delta c) \tag{3.23}$$

$$\sigma_y = Q_{xy}(\varepsilon_x - \beta_x \Delta c) + Q_{yy}(\varepsilon_x - \beta_y \Delta c) + Q_{ys}(\gamma_{xy} - \beta_{xy} \Delta c) \qquad (3.23) \text{ cont.}$$

$$\tau_{xy} = Q_{xs}(\varepsilon_x - \beta_x \Delta c) + Q_{yy}(\varepsilon_x - \beta_y \Delta c) + Q_s(\gamma_{xy} - \beta_{xy} \Delta c)$$

where

$$\beta_x = m^2\beta_1 + n^2\beta_2$$

$$\beta_y = n^2\beta_1 + m^2\beta_2 \qquad (3.24)$$

$$\beta_{xy} = 2nm(\beta_1 - \beta_2)$$

and

$$m = \cos\theta \qquad (3.25)$$

$$n = \sin\theta$$

c = moisture concentration

s = subsript denoting shear

(all other symbols were previously defined)

c. Combined Expansional Stresses

In many practical applications it is likely that both moisture and temperature will be present. For such a case, it is necessary to account for the combined effect of thermal expansion and hygroscopic expansion. In order to develop effective laminate expansional stresses, it is necessary to define expansional force resultants as

$$N_x^E = N_x^T + N_x^H$$

$$N_y^E = N_y^T + N_y^H \qquad (3.26)$$

$$N_{xy}^E = N_{xy}^T + N_{xy}^H$$

where

E, T, H = supercripts denoting effective, thermal and hygroscopic, respectively

The thermal force resultants (N_x^T, N_y^T, N_{xy}^T) are obtained from the lamina stiffnesses Q^k_{ij}, and coefficients of thermal expansion α_j^k, where (i,j =1,2,6). The superscript k denotes the lamina. This superscript was not used in sections a and b above, because there was no need for distinction since the whole discussion concerned the unidirectional lamina and the concept of a laminate, which is a stack of laminae at prescribed orientations, had not yet been introduced. The laminate thermal force resultants are given as:

$$N_x^T = \sum_{k=1}^{n} (Q^k_{11}\alpha^k_1+Q^k_{12}\alpha^k_2+Q^k_{16}\alpha^k_6)(h_k-h_{k-1})\cdot\Delta T$$

$$N_y^T = \sum_{k=1}^{n} (Q^k_{12}\alpha^k_1+Q^k_{22}\alpha^k_2+Q^k_{26}\alpha^k_6)(h_k-h_{k-1})\cdot\Delta T \qquad (3.27)$$

$$N_{xy}^T = \sum_{k=1}^{n} (Q^k_{16}\alpha^k_1+Q^k_{26}\alpha^k_2+Q^k_{66}\alpha^k_6)(h_k-h_{k-1})\cdot\Delta T$$

where α^k_1, α^k_2, α^k_6 are equivalent to α^k_x, α^k_y, and α^k_{xy} as seen in figure 3.2.

The hygroscopic force resultants for a laminate consisting of n laminae are given as:

$$N_x^H = \sum_{k=1}^{n} (Q^k_{11}\beta^k_1+Q^k_{12}\beta^k_2+Q^k_{16}\beta^k_6)(h_k-h_{k-1})\cdot\Delta C$$

$$N_y^H = \sum_{k=1}^{n} (Q^k_{12}\beta^k_1+Q^k_{22}\beta^k_2+Q^k_{26}\beta^k_6)(h_k-h_{k-1})\cdot\Delta C \qquad (3.28)$$

$$N_{xy}^H = \sum_{k=1}^{n} (Q^k_{16}\beta^k_1+Q^k_{26}\beta^k_2+Q^k_{66}\beta^k_6)(h_k-h_{k-1})\cdot\Delta C$$

where β^k_1, β^k_2, β^k_6, are analogous to α^k_1, α^k_2, and α^k_6, respectively.

The effective expansional laminate strains for a unidirectional material are as follows:

$$\varepsilon^E_x = \frac{A_{22}N^E_x - A_{12}N^E_y}{A_{11}A_{22} - A^2_{12}}$$

$$\varepsilon^E_y = \frac{A_{11}N^E_y - A_{12}N^E_x}{A_{11}A_{22} - A^2_{12}} \qquad (3.29)$$

$$\varepsilon^E_{xy} = \frac{N^E_{xy}}{A_{66}} \cdot 0$$

where

$$A_{ij} = \sum_{k=1}^{n} Q^k_{ij}(h_k - h_{k-1}) \qquad (3.30)$$

are the laninate coupling coefficients

As previously mentioned, hygrothermal strains give rise to residual stresses in the laminae. These stresses may be calculated for a unidirectional material as follows:

$$\sigma^k_x = \frac{[(Q^k_{xx}A_{22} - Q_{xy}A_{12})N^E_x + (Q^k_{xy}A_{11} - Q^k_{xx}A_{12})N^E_y]}{A_{11}A_{22} - (A_{12})^2}$$

$$\sigma^k_y = \frac{[(Q^k_{xy}A_{22} - Q_{yy}A_{12})N^E_x + (Q^k_{yy}A_{11} - Q^k_{xx}A_{12})N^E_y]}{A_{11}A_{22} - (A_{12})^2} \qquad (3.31)$$

$$\tau^k_{xy} = \frac{[(Q^k_{xs}A_{22} - Q_{ys}A_{12})N^E_x + (Q^k_{ys}A_{11} - Q^k_{ys}A_{12})N^E_y]}{A_{11}A_{22} - (A_{12})^2}$$

In general, hot and humid environments are not necessarily detrimental for laminated composites because it is possible that in such environments, laminates may benefit from residual stresses. For example, consider a $[0/90]_s$ laminate subjected to a tensile load in the 0-degree direction. After fabrication, the residual stress σ_y in the 90° ply in tensile. However, as temperature and moisture concentration increase, σ_y will decrease and may become compressive. Thus, even though the transverse strength decreases, the 90° ply may fail at higher applied loads [15].

3.2 Time-Temperature-Superposition.

When an amorphous polymer is subjected to a stress or strain, above its glass transition temperature, the molecular chains tend to rearrange and take on the most probable configurations commensurate with the state of stress or strain. The rate of rearangement depends on the local resistance encountered by the chain. This resistance is given by a viscous friction coefficient which equals the force required to move a chain through the surrounding medium at unit velocity. The faster the chain is required to move, the greater is the force which must be applied. Likewise, the required force becomes greater as the temperature is decreased. Thus it appears that some relation should exist between the time and temperature dependence of viscoelastic quantities. The equivalence of time and temperature regarding the viscoelatic properties of polymers has been widely recognized and the validity of applying time-temperature equivalence to experimental data under many temperature and

strain rate conditions have been well established by experimentalists such as Staverman and Schwarzl [16], and Williams [17].

The most important assumption of time-temperature equivalence is that all relaxation (or retardation) times are affected the same amount by a temperature change. Thus, a temperature function a_T can be defined as

$$a_T = \tau/\tau_o \tag{3.32}$$

where τ in any relaxation time at temperature T, and τ_o is the correspondimg time at a selected reference temperature T_o. The other assumption is that the moduli of all elastic mechanisms are directly proportional to the absolute temperature and to the density of the polymer. Thus, the time-temperature superposition principle might be stated mathematically as:

$$\frac{E(T_1,t)}{\rho(T_1)\cdot T_1} = \frac{E(T_2,t/a_T)}{\rho(T_2)\cdot T_2} \tag{3.33}$$

where

E = modulus

ρ = density

T = temperature

t = time

a_T = temperature shift factor

which also takes into account an inherent change in the modulus brought about by a change in temperature.

Another mathematically clear description of this principle is given by Muki and Sternberg [18] as follows:

If E(t,T) is the relaxation modulus at time t and absolute temperature T_o such that

$$E'(t) = E(t,T_o) = f(\log t) \tag{3.34}$$

then the relaxation modulus at absolute temperature T is

$$E(t,T) = f[\log t + \psi(T)] \tag{3.35}$$

where $\psi(T)$ is the shift factor obeying the conditions

$$\psi(T_o) = 0$$

$$\frac{d\psi}{dT} > 0$$

Setting $\psi(T) = \log(a_T)$ we get

$$E(t,T) = G(\xi) \tag{3.26}$$

with $\xi = t \cdot a_T = t \cdot \phi(T)$

where $\phi(T_o) = 1$

$$\phi(T) > 0$$

$$\frac{d\phi}{dT} > 0$$

In other words, the time-temperature superposition principle asserts that the effects of temperature on linear viscoelastic polymer properties is to multiply (or divide) the time scale by a constant factor at each temperature. Thus, by translating curves E(t,T) along the log(time) axis to superpose with $E(t,T_o)$, a master curve covering a much wider range of log(time) can be constructed (Figure 3.3)

A paper of major importance, published in 1955 by Williams, Landel and Ferry (WLF) [17], showed that a_T for amorphous polymers above their glass transition temperature can be represented by an equation of the form

$$\log(a_T) = \frac{c_1(T-T_o)}{c_2+T-T_o} \qquad (3.37)$$

where

T_o = reference temperature empirically chosen so that the above relation fits experimental values

T = temperature

c_1, c_2 = empirically evaluated material constants

Another form af equation 3.37 reduced to the material glass transition temperature, and taking into account that material viscocity is a function of the free volume (volume taken by voids etc, V_f) which increases linearly with temperature as

$$V_f = V_{fg}+\alpha_f(T-T_g)\ , \quad \text{is}$$

$$\log(a_T) = \frac{-[B/(2.303\ V_{fg}](T-T_g)}{V_g/\alpha_f - T - T_g} \qquad (3.38)$$

where

V_{fg} = fractional free volume at $T=T_g$

T_g = glass transition temperature

B = empirical constant (usually B=1)

α_f = coefficient of thermal expansion

The above relation is identical in form with the WLF equation 3.37.

The time-temperature superposition principle enables one to predict viscoelastic behavior in regions of time not experimentally accessible. Short-term tests, carried out at temperatures somewhat higher than those normally encountered by the material, are used to predict long-term properties. The same reasoning may also be applied to dynamic tests where by an analogous

treatment, material responce at very high strain rates can be predicted from tests at more accessible rates at lower temperatures. This principle has been shown to be correct by a number of studies. Lohr [19] compared the time-temperature dependence of yield stress with that of stress relaxation for polymethylmethacrylate, polyethylene, terephthalate, polystyrene and polyvinylchloride. All of the yield stress data were found to be described by the relation

$$\sigma_y = k_1 + k_2 \ln(\dot{\varepsilon} a_T) \tag{3.39}$$

where

σ_y = yield strength

k_1, k_2 = material constants empirically obtained

$\dot{\varepsilon}$ = strain rate

Lohr also found that in regions below the glass transition temperature (T_g), the free volume treatment of the WLF equation is not applicable and the temperature dependence of a_T follows an equation of the simple Ahrenius form

$$\log(a_T) = \frac{\Delta H_a}{R}\left(\frac{1}{T} - \frac{1}{T_o}\right) \tag{3.40}$$

where

ΔH_a = apparent activation energy for relaxation or retardation process

R = resistance constant

T, T_o = temperature and initial temperature respectively

Thus, the temperature dependence of responses below T_g bears no relation to what would be extrapolated from the behavior above T_g, but the time-temperature superposition principle is still applicable.

There is currently a lot of work being done on determining the behavior of the shift function (a_T), and the development of any theory dealing with this issue is based primarily on empirical deductions from experimental data. The presence of moisture also complicates the material behavior and the possibility exists for a new moisture shift factor (a_H), and a time-moisture superposition principle analogous to that of time-temperature equivalence.

3.3 Integrated Theory for Predicting the Hygromechanical Responce of Composite Materials.

As mentioned previously, the validity of applying time-temperature equivelance to data obtained on certain types of polymers and consequently polymer matrix composites, under many test conditions has been well established by various experimental studies and as a consequence of current molecular theories. Many experimentalists, among them J. M. Lifshitz [11], have empirically observed that the effects of time, temperature and moisture on matrix dominated mechanical properties of composites appear to follow a similar pattern. This observation suggests the existence of an integrated time/temperature/moisture superposition principle for polymer dominated material properties of composite materials and polymeric materials in general.

Although there is reason to beleive in the existence of such an integrated hygrothermomechanical (HGTM) theory, to the writer's knowledge a complete statement of such has not yet been published. A possible reason for this may be the amount of work incvolved in producing a complete and reliable data base to support any such statement, and the complexity involved in formulating

a molecular theory which would incorporate the combined influence of time, temperature and moisture on the behavior of composite materials.

One of the most interesting and in depth works on developing a HGTM theory was done by C. C. Chamis [20]. In this case, an integrated theory was developed based on a combined theoretical, and experimental investigation of hygrothermal effects on the mechanical properties of unidirectional composites loaded along the material axes and off-axis, and those of angle-plied laminates. According to Chamis, a relationship among the wet resin mechanical properties and the room-temperature dry properties must exist such that:

$$\begin{aligned} &\text{Resin Mechanical Properties} \quad (E,\ v,\ F)_{wr} = \Phi_1[(E,\ v,\ F)_{dr},\ T_{gwr}] \\ &\text{Resin Thermal Properties} \quad\ (\alpha,\ k,\ c)_{wr} = \Phi_2[(\alpha,\ k,\ c)_{dr},\ T_{gwr}] \end{aligned} \tag{3.41}$$

where E, v and F denote modulus, Poisson's ratio and fracture stress, respectively, α, k and c denote thermal expansion coefficient, heat conductivity and heat capacity and subscripts w, d, r denote wet, dry and resin property, respectively. The glass transition temperature of the wet resin T_{gwr} is given in symbolic form as

$$T_{gwr} = \Phi_3(T_{gdr},\ m_r) \tag{3.42}$$

where T_{gdr} denotes glass transition temperature of the dry resin and m_r the moisture content of the resin. The form of function Φ_3 was previously given in section 3.1.2. In developing this HGTM theory, the following assumptions were made:

(1) Moisture diffusion in the composite is independent of the state of stress.

(2) The temperature distribution in the composite is independent of the state of stress.

(3) The underlying assumptions of linear micromechanics, macromechanics and linear laminate theory hold true.

By plotting retention ratios, defined as wet property at test temperature divided by room temperature dry property, versus temperature, a simple algebraic expression was found to approximate the functional relationships Φ_1 and Φ_2. It was found that

$$\frac{\text{wet resin mechanical property at test temperature}}{\text{dry resin mechanical property at room temperature}} = f_m = \left[\frac{T_s - T}{T_s - T_o}\right]^{1/2} \qquad (3.43)$$

is a good approximation for data in the range of 200^oK (-100^oF)$<T<T_s$

where

f_m = mechanical property retention ratio

$T_s = T_{gwr}$ (wet resin T_g)

T = test temperature

T_o = 273^oK (0^oF)

The corresponding relationship for the wet resin thermal properties was found to be of the form:

$$\frac{\text{wet resin thermal property at test temperature}}{\text{dry resin thermal property at room temperature}} = f_t = \left[\frac{T_s - T_o}{T_s - T}\right]^{1/2} \qquad (3.44)$$

where f_t denotes thermal property retention ratio. Now equations (3.41) can be expressed as

$$\text{Resin Mechanical Properties} \quad (E, v, F)_{wr} = (E, v, F)_{ro} f_m \qquad (3.45)$$

$$\text{Resin Thermal Properties} \quad (a, k, c)_{wr} = (a, k, c)_{ro} f_t$$

where

r_o = dry resin properties evaluated at room temperature, and

r = resin property

The governing micromechanics equations for predicting the ply elastic properties, longitudinal modulus (E_{11}), transverse modulus (E_{22}), major Poisson's ratio (v_{12}) and interlaminar shear modulus (G_{12}) are given by:

$$E_{11} = k_f E_{f11} + k_r f_m E_{r0}$$

$$E_{22} = \frac{f_m E_{r0}}{1-(k_f)^{1/2}(1-f_m E_{r0}/E_{f22})} \qquad (3.46)$$

$$v_{12} = k_f v_{f12} + k_r v_{r0}$$

$$G_{12} = \frac{f_m G_{r0}}{1-(k_f)^{1/2}(1-f_m G_{r0}/G_{f12})}$$

where

$$G_{r0} = \frac{E_r}{2(1+v_{r0})} \qquad (3.47)$$

and

r, f = subscripts denoting resin and fiber property,

1, 2 = subscripts denoting fiber and perpendicular to fibers orientations,

0 = subscript denoting room temperature and zero moisture and

k = volume ratio

The uniaxial ply strengths, transverse tension (F_{2T}), compression (F_{2C}), and interlaminar (in-plane) shear (F_{12}) are given respectively by the following micromechanics equations:

$$F_{2T} = \beta_{2T} \cdot \frac{F_{rT0}}{E_{r0}} \cdot \frac{E_{22}}{\beta_v \phi_{v2}}$$

$$F_{2C} = \beta_{2C} \cdot \frac{F_{rC0}}{F_{rT0}} \cdot \frac{E_{22}}{\beta_v \phi_{v2}} \qquad (3.48)$$

$$F_{12} = \beta_{12} \cdot \frac{F_{rT0}}{G_{r0}} \cdot \frac{G_{12}}{\beta_v \phi_{\mu 12}}$$

where

β_v = void magnification factor

ϕ_μ = strain magnification factor

F = fracture stress

T, C = subscripts denoting tension and compression

1,2,12 = subscripts denoting fiber direction, matrix direction and in-plane shear, respectively, and

r = subscript denoting resin property

The coefficients β_{2T}, β_{2C}, and β_{12} are correlation coefficients if needed; otherwise they are assumed to be unity. The void and strain magnification factors are given by

$$\beta_v = [1-(4k_v/\pi k_r)]^{-1/2}$$

$$\phi_{\mu 2} = \frac{1-(k_f)^{1/2} E_{22}/E_{f22}}{1-(k_f)^{1/2}} \qquad (3.49)$$

$$\phi_{\mu 12} = \frac{1-(k_f)^{1/2} G_{12}/G_{f12}}{1-(k_f)}$$

The uniaxial-ply longitudinal tensile strength (F_{1T}) and compressive strengths (F_{1C}) are given by

$$F_{1T} = F_{fT}[\beta_{fT}k_f + k_r f_m E_{r0}/E_{f11}]$$

$$F_{1C} = 0.5[F_{fC}(\beta_{fC}k_f + k_r f_m E_{r0}/E_{f11}) + (\beta_{CS}S_{12} + F_{rC0})] \quad (3.50)$$

where

F_{fT}, F_{fC} = fiber longitudinal and compressive strength respectively

β_{fT}, β_{fC} = correlation coefficients if needed, otherwise taken equal to unity

r, f, T, C, 0, 12 = subscripts denoting resin, fiber, tensile, compressive initial and shear, respectively

f_m = previously defined in equation 3.43

F_{12} = given by equation

It is important that the various correlation coefficients be evaluated from dry room-temperature data and should remain invariant with both temperature and moisture changes [21].

By comparing corresponding measured and predicted properties using the above relations, an agreement within 10% was observed, except for F_{1C} at room temperature, F_{12} at all temperatures tested and E_{22} and G_{12} at high temperatures. A probable explanation may have been the normal difficulties encountered in measuring these properties.

It is obvious from the material presented in sections 3.2 and 3.3, that a relationship between all three parameters of time, temperature and moisture must exist which would describe the mechanical behavior of a composite under a wide range of environmental and strain rate conditions. It is also clear, that such an integrated theory does not exist, although it has been proposed by many experimentalists. It is thus not possible to include an in-depth discussion

about time-temperature-moisture equivalence at this point. However, the scope of this work is to experimentaly prove the existence of a constitutive relationship between the above three parameters and propose a method for predicting the total hygrothermomechanical (including the efffect of strain rate) responce of polymer matrix composites. For this purpose, any discussion involving the three parameter superposition principle, or the existence of a time-temperature-moisture equivalence, will be presented in Chapter V and supported by a wide range data base on material properties for AS4/3501-6 graphite/epoxy, which was constructed for this purpose.

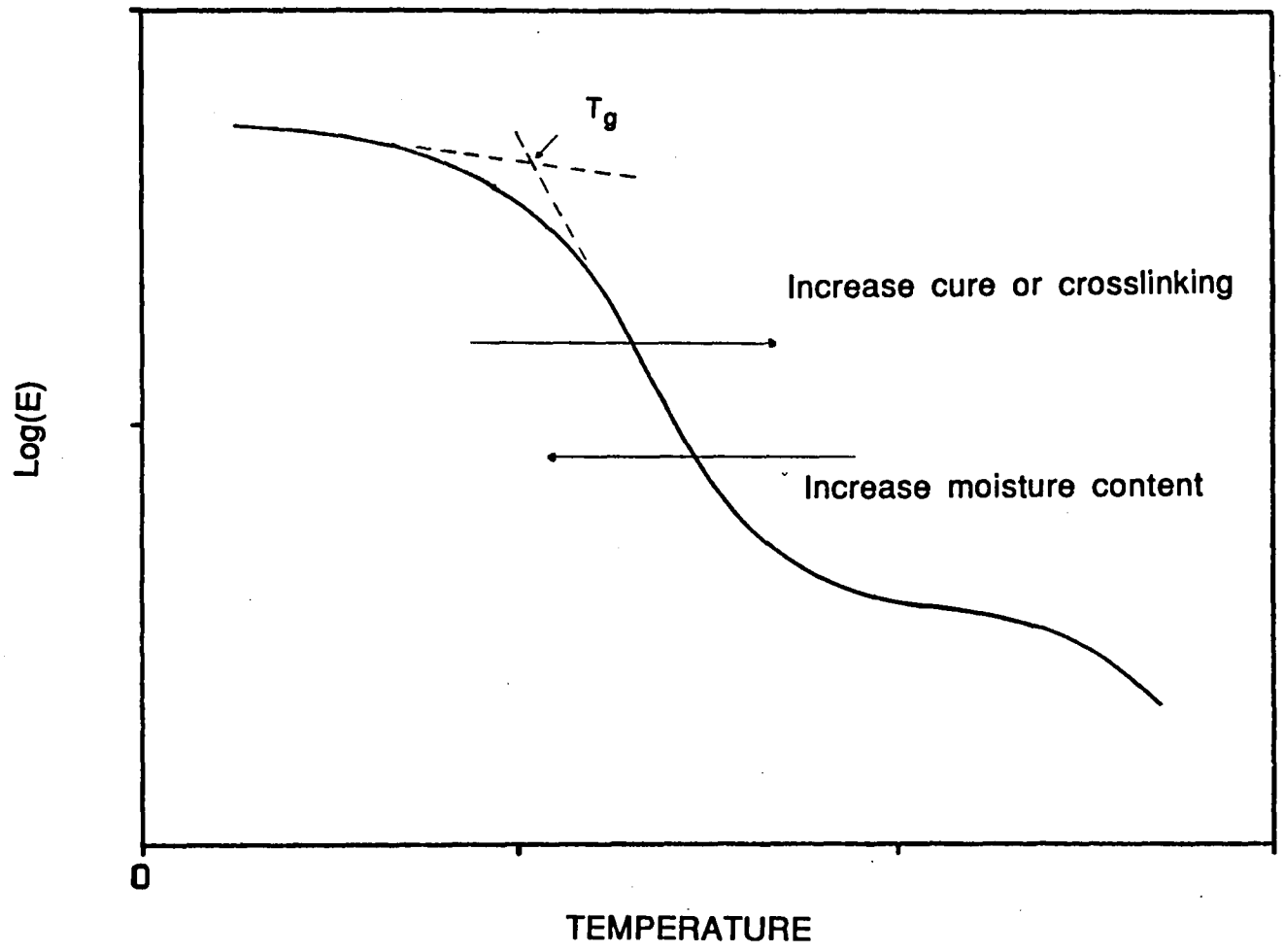

Figure 3.1 Modulus vs. temperature for typical epoxy resin, illustrating glass transition temperature

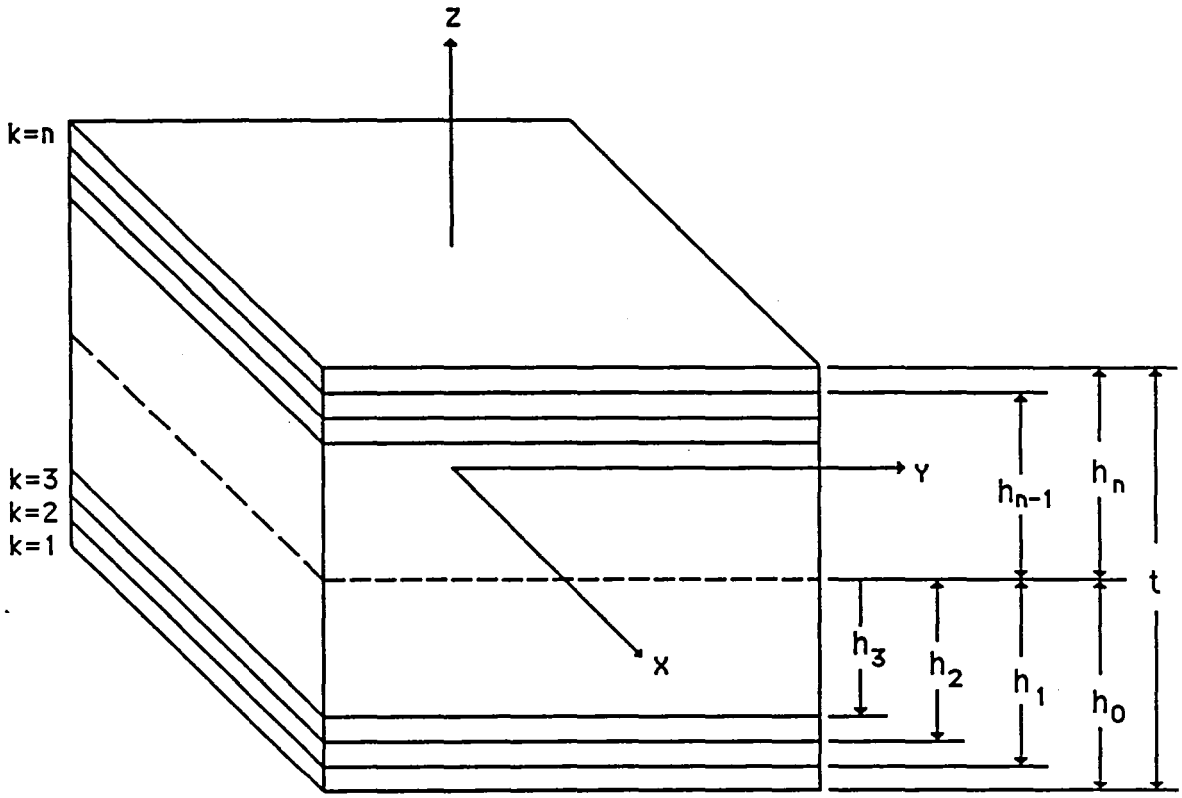

Figure 3.2. Section of Composite Laminate.

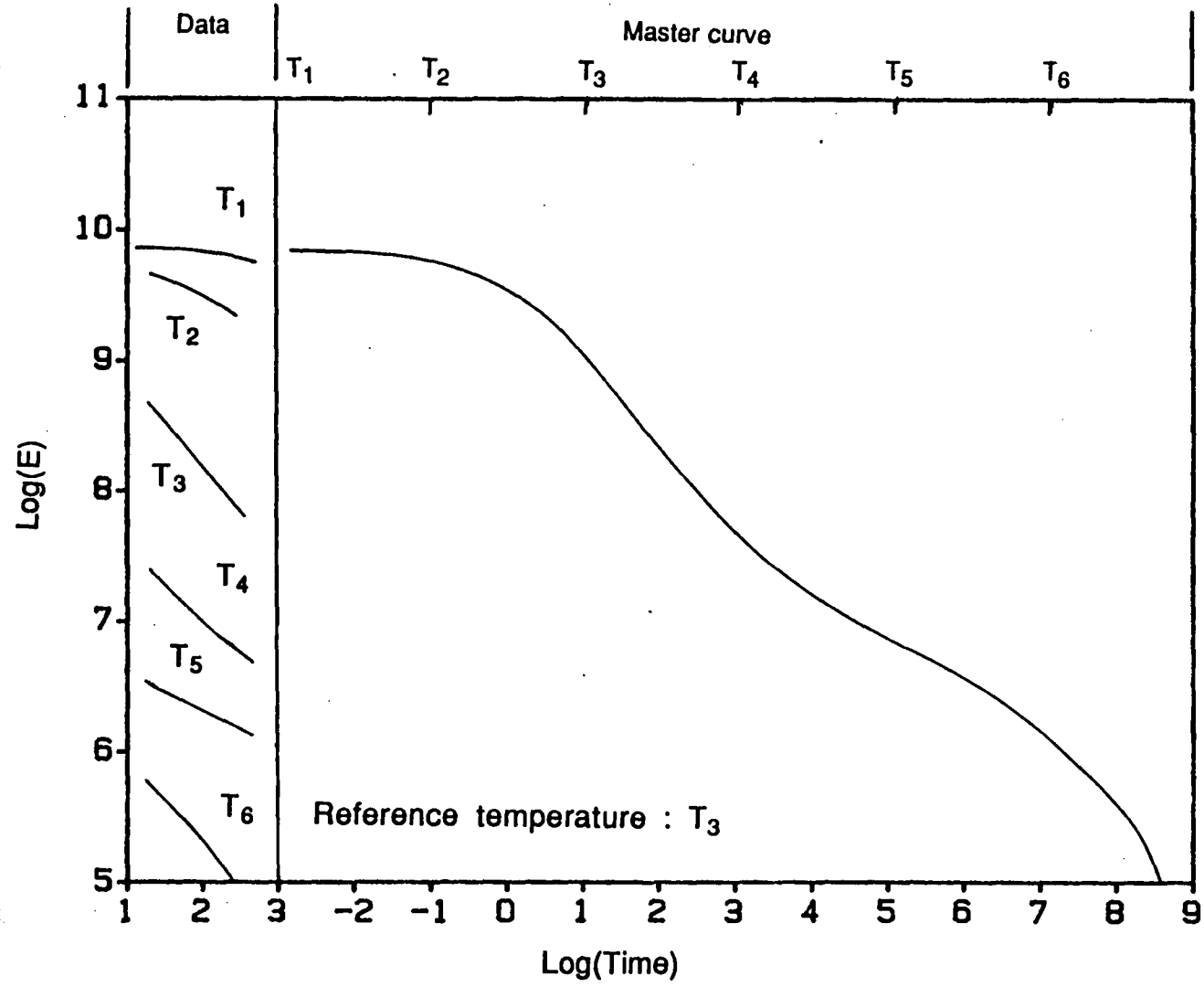

Figure 3.3 Preparation of a modulus (E) master curve from experimentally obtained modulus-time curves at various temperatures

IV. EXPERIMENTAL PROCEDURE

4.1. General.

In the case of mechanical characterization of moisture conditioned specimens, it is not usually possible to apply strain gages after conditioning. Conventional strain gage adhesives require curing at some elevated temperature which could alter the specimens moisture content appreciably. In some cases, and for imediate testing, a room-temperature curing anaerobic adhesive (Eastman 910 or M-Bond 200) was found to be adequate for bonding of gages after conditioning. For elevated temperature testing, a high-temperature fast-curing adhesive has been used [25]. In general, bonding of strain gages to moisture-conditioned specimens is not very reliable and may introduce additional problems. The use of extensometers, although simple in some cases, may pose problems especially at high strain rates due to their relatively high inertia. Also, their inability to measure shear at any event poses another limiting factor over their use.

To address the above problems, a new technique was developed, whereby encapsulated strain gages were embedded in the midplane of the specimen. The procedure for preparing encapsulated strain gages and fabricating the composite material with or without embedded gages is described in sections (4.2) and (4.3).

The experimental procedure is devided into two major phases, Specimen Conditioning and Actual Testing. Each phase consists of two stages.

In the first stage, extensive hygroscopic and mechanical tests are carried out in order to prove the reliability and consistency of the embedded gage

technique. This is achieved by examining wether the hygromechanical, and mechanical properties (at various strain rates, temperatures and moisture conditions) of the material were altered by the presence of embedded strain gages, in the laminate midplane surface.

Secondly, graphite/epoxy specimens of all three layups, $[0_6]$, $[90_8]$ and $[10_6]$, were mass-produced. Those which required conditioning prior to testing, contained embedded strain gages. All specimens were mechanically loaded to failure at four different temperatures, two strain rates and two moisture conditions. Strain data from embedded gages, extensometer or surface gages (depending on the test conditions) and load, were continuously recorded, processed and stored.

4.1.1. Strain gages and Wheatstone Bridge Circuit.

Strain gages are extensively used and relied upon for the majority of the tests presented in this work. It is thus essential to understand their operating principles and select the appropriate gages for each existing operating condition.

An electrical-resistance strain gage will change in resistance due to applied strain according to the relation

$$\frac{\Delta R}{R} = S_g \, \varepsilon_{xx} \qquad (4.1)$$

where R = original gage resistance

ΔR = change in resistance

S_g = is a calibration constant provided by the manufacturer, known as the gage factor.

The Wheatstone bridge is an electric circuit which is employed to convert the change in resistance (ΔR) of an electrical resistance strain gage due to an applied strain (ε_{xx}), to a voltage signal (ΔE) which can be measured with a recording instrument. The principle of operation of the Wheatstone Bridge (Figure 4.1) as a direct readout device for ΔE is as follows.

Usually R_1 is the resistance of the electrical resistance strain gage mounted on the specimen to be tested. R_2, R_3, R_4 are adjustable resistors within the bridge circuit. Resistor R_2, adjacent to R_1, may sometimes be used as a dummy resistor (strain gage mounted on a reference specimen as will be mentioned later in this work) for evaluating material tensile properties at high temperatures or at various hygroscopic conditions. It can also be used along with R_1 for direct measurement of shear strain, as mentioned later, at which case the circuit is self temperature and moisture compensated and no dummy specimen is needed.

The output voltage from the bridge, E , is related to the input or excitation voltage (V) and the circuit resistances (R_i, i=1,2,3,4) by

$$E = \frac{R_1R_3-R_2R_4}{(R1+R2)(R3+R4)} \cdot V \qquad (4.2)$$

The voltage (E) wil be zero , and the bridge will be considered balanced when

$$R_1R_3=R_2R_4 \qquad (4.3)$$

The bridge is initially balanced before strains are applied to the gage(s) in the bridge. Thus the voltage E is initially zero, and the strain induced voltage ΔE can be obtained by the relation

$$\Delta E = V \cdot \left[\frac{R_1 R_2}{(R_1+R_2)} \left(\frac{\Delta R_1}{R_1} - \frac{\Delta R_2}{R_2} + \frac{\Delta R_3}{R_3} - \frac{\Delta R_4}{R_4} \right) \right] \qquad (4.4)$$

The sensitivity (S_c) of a constant voltage bridge is given by the relation

$$S_c = \frac{V}{(1+r)^2} \cdot r \cdot n \cdot S_g \qquad (4.5)$$

where r = ratio of the resistances R_1/R_2
n = number of active arms int the bridge circuit

A plot of r versus $r/(1+r)^2$ (Figure 4.3) shows that the maximum efficiency is obtained when r=1. Thus, all strain gages were taken to have a resistance of (120+0.2) % Ω (Ohms), the same as those used by the Wheatston bridge conditioner (Kaye Instruments, Model BC-8) with a constant 3 Volt excitation voltage (V).

The effect of moisture and temperature on gage must be accounted for in the installation of the gage and in the analysis of the data. High temperature and moisture, degrades the strength and rigidity of the bond and reduces the effectiveness of the adhesive in transmitting the strain from the specimen to the gage. The high temperarure effect was overcome by using M-Bond AE 10 adhesive (Micro-Measurements) cured under pressure at 75°C(150°F) for 1 hour. In order to overcome moisture degredation, M-bond 300 adhesive (Micro-Measurements), recomended for its ability to resist moisture and be operational at high temperatures was considered. Preliminary testing employing surface gages bonded with this adhesive were unsuccesful due to gage debonding while the spesimen was in a moist environment. For this purpose and the fact that no other adhesive existed which would cure fast under room temperature and resist moisture, if the specimen was not to be tested imediately after

installation of the gage, surface gages were excluded for testing conditioned specimens, and an alternate technique (embedded gages) was developed and described in the next section.

The effect of temperature and time on the strain gage itself is given by

$$\Delta R = \frac{1}{R}\frac{df}{d\varepsilon}\Delta\varepsilon + \frac{1}{R}\frac{df}{dT}\Delta T + \frac{1}{R}\frac{df}{dt}\Delta t \qquad (4.6)$$

where $\frac{1}{R}\frac{df}{d\varepsilon} = S_g$ = gage factor

$\frac{1}{R}\frac{df}{dT} = S_T$ = gage sensitivity to temperature

$\frac{1}{R}\frac{df}{dt} = S_t$ = gage sensitivity to time

d = partial derivative

To nullify these effects, EA-06-125 TM-120 gages were employed having a gage factor of (2.01+10) % and $S_T << 1$, $S_t << 1$ which was too small to produce any noticeable difference under the present operating conditions.

The apparent strain due to thermal and moisture expansion of the composite specimen itself is taken care of by introducing a dummy specimen exposed to the same hygrothermal conditions as the active specimen, as shown in Figure 4.2, (R_2 is a dummy strain gage). In this case $(\Delta R_1/R_1)_{Hygrothermal} = (\Delta R_2/R_2)_{Hygrothermal}$ so that the only resistance change in the circuit is on R_1 (for axial tension tests) due to mechanical loading ($\Delta R_{2\ mechanical}=0$ and $\Delta R_{3\ total}=\Delta R_{4\ total}=0$). The net mechanical strain produced on the specimen can be obtained from the bridge circuit output voltage (ΔE) from equations (4.1) and (4.4) due to the above conditions, as

$$\Delta R_{total} = \Delta R_{mechanical} + \Delta R_{hygrothermal} \qquad (4.7)$$

and

$$\varepsilon_{xx} = \frac{1}{Sg\ V\ r} \cdot \frac{(1+r)^2}{} \cdot \Delta E \qquad (4.8)$$

4.1.2. 10° Off-Axis Testing

The 10° off-axis tensile test is commonly used for the determination of in plane shear properties of a unidirectional composite laminate [22]. The 10° angle is chosen to minimize the effects of longitudinal and transverse stress components on the shear response. The result is (Figure 4.4) that the material axes shear strain (intralaminar shear strain γ_{12}) is maximun at this angle and appears to be insensitive to small errors in angle. The specimen is a 6-ply unidirectional coupon with the fibers oriented at 10° with the loading axis. It is tabbed with tapered tabs and instrumented with a 2-gage rosette. The 2-gage rosette has one gage element oriented at -45 with respect to the fiber direction or -55° with respect to the loading axis, and one at 45° with respect to the principal material direction or 35° with respect to the loading axis (Figure 4.5). The shear strain is given by the relation [23]

for

$$\varepsilon_{45^o} = \varepsilon_A \qquad (4.9)$$

$$\varepsilon_{-45^o} = \varepsilon_B$$

$$\gamma_{12} = \frac{2(\varepsilon_A-\varepsilon_B)-(\varepsilon_{xx}-\varepsilon_{yy})(\cos\theta_A-\cos 2\theta_B)}{\sin 2\theta_A-\sin 2\theta_B} \qquad (4.10)$$

which reduces to

$$\gamma_{12} = \varepsilon_{45^o}-\varepsilon_{-45^o} \qquad (4.11)$$

and can be obtained directly in the bridge circuit by conecting the two strain gages (at 45° and -45° to fibers) to adjacent arms of the Wheatstone bridge circuit (equation 4.11). The in-plane shear stress corresponding to the fiber coordinate system is given by the stress transformation relation

$$\tau_{12} = \sigma_x \sin\theta\cos\theta = 0.171\ \sigma_x \qquad (4.12)$$

4.2. Preparation of Encapsulated Strain Gages.

The following is the sequence of steps required for the preparation of encapsulated gages:

1. Cut thin Nickel-Clad copper ribbon leads (GL-92R-50, Measurements Group, Inc.), of 0.025 mm thickness (0.001 in) and 0.4 mm (0.016 in) width into proper lengths.
2. Attach the ribbon leads to a strain gage using a very small amount of solder. For 10° off-axis specimens the leads had to be attached at 35° with respect to the gage principal axis because of the need to measure the strain at +35° and at 55° with respect to the loading direction.
3. Attach a 13 mm (0.5 in) strain gage wire strip at the ends of the ribbons to avoid breaking of exposed thin lead tips of the embedded gages. Tape the lead ends so the wire strips are straight and smooth.
4. Sandwich the gage with the attached leads between two sheets of glass skrim cloth of thickness 0.025 mm (0.001 in) impregnated in adhesive (Hysol Clear Epoxy). The assembly is then placed between two mylar sheets, clamped between two pressure plates and cured

under at 60°C (140°F) for two hours (Figures 4.7-4.8) (Be sure to apply release agent on mylar sheets and pressure plates).

5. Remove the Mylar sheets and trim the gage /lead/scrim-cloth sandwich to the minimum possible size (Figure 4.9).
6. Check the strain gage for continuity. Check insulation by immersing the sandwich in water, or by tracing the leads with a continuity indicator.

4.3. Composite Material Fabrication.

The material used in the present work was AS4/3501-6 Graphite/Epoxy (Hercules, Inc). Three types of laminates were fabricated:

$[90_8]$ unidirectional laminates with dimensions 25.4 cm by 30.5 cm (12" by 10") and an average thickness of 1.016 mm (0.04").

$[10_6]$ unidirectional laminates with dimensions 25.4 cm by 30.5 cm (10" by 12") and an average thickness of 0.762 mm (0.30").

$[0_6]$ unidirectional laminates with dimensions 25.4 cm by 30.5 cm (10" by 12") and an average thickness of 0.762 mm (0.30").

The laminates with the embedded strain gages showed no appreciable difference in thickness from those laminates with no gage. The sequence of steps necessary to complete the fabrication of the above laminates, with or without embedded strain gages is as follows:

1. Remove Graphite/Epoxy prepreg roll from storage freezer and allow it to reach room temperature (for approximately two hours).

2. Cut prepreg into unidirectional sheets of the necessary size and fiber orientation according to the material layup. Use roll edge as a reference for cutting.
3. Make air-tight packages of six and eight sheets of prepreg, and store in freezer for future use.
4. Clean the surface of both pressure plate and tool plate with fine abrasive and acetone. Apply generously mold release on both plates.
5. Cut 4 bleeder sheets (glass fiber cloth used to absorb any excess resin the prepreg might have while the material is being cured) of dimensions 25.4 cm by 30.5 cm (10" by 12"), and one of dimensions 25.4 cm by 40.6 cm (10" by 16"). Cut two teflon sheets and one perforated mylar sheet of dimensions 25.4 cm by 30.5 cm (10" by 12").
6. Construct a cork dam of dimensions similar to those of the material prepreg sheets on the tool plate. Lay two absorber sheets on the corked tool plate.
7. Layup half the Graphite/Epoxy prepreg sheets on top of a clean surface. Make sure that all laminae are alligned as accuratelly as possible.

If the plate does not contain embedded strain gages, go to step 10.

8. Position encapsulated strain gages normal to fiber direction for $[90_8]$ and $[0_6]$ plates and at 45° to the fiber direction for the 10° off-axis plates, by means of a transparent mylar template having the exact same dimensions as the prepreg sheets (Figures 4.10-4.11).
9. Mark the side used as a reference for positioning the template.
10. Layup the rest of the prepreg sheets.

11. If strain gages were positioned within the laminate, place the template on the top surface, and using the same side as in step 8 for reference, place distinct marks on both the plate and template for future alignment (Figure 4.12).
12. Cover both faces of the composite prepreg plate with the precut teflon sheets, and place assembly on tool plate within the cork-dam (Figure 4.13). Place the other two bleeder sheets over the composite plate. Position perforated mylar sheet over the last bleeder and cover the assembly with the pressure plate.
13. Cover tool plate with the remaining bleeder and form a vacuum over it by means of a nylon film and flexible adhesive tape (Figure 4.14).
14. Place the layup in the autoclave (Rapidoor) (Figure 4.15). Care must be taken if embedded gages are present in order no to breack off the lead tips.
15. Apply vacuum of at least 85 KPa (25 in. Hg).
16. Raise temperature to (116±6)°C, (240±10) °F at a rate of (1.7-2.0) °C/min.
17. Hold vacuum for (60-70) min.
18. Apply pressure of (690±35) KPa, (100±5) Psi and vent the vacuum bag to atmospheric presure.
19. Raise temperature to (117±6)°C, (350±10)°F at a rate of (1.7-2.0) °C/min, (3-5 °F/min).
20. Hold pressure for (120±10) min.
21. Shut down autaclave temperature.
22. Release pressure after temperature drops bellow 93°C (200°F).

23. Leave plate in the autoclave untill it cools down to ambient temperature.
24. Remove plate from autoclave. Special care must be taken when embedded gages are present in order not to demage the lead tips.

The curing cycle is also shown in Figure 4.16.

25. Carefully remove composite plate off the layup plate, cut off the edges (if gages have been embedded, do not cut off the side from were the leads are coming out) with a diamond saw and remove (with care) the excess matrix-filled, bleeder sheets.
26. If plate contains embedded strain gages, place template on marked surface, and draw reference lines for cutting specimens without damaging the gages.
27. Tab plate with four 5.08 cm (2") wide strips of 7-ply Scotchply 1002 (3M Company) glass/epoxy, bonded to the plate with High-Peel 1105 epoxy (Hysol Corp.). For high temperature tests, FM300 adhesive film (Cyanamid) was employed instead.
28. Cut plate into specimens of dimensions shown in Figure 4.18
29. Check all embedded gages for continuity.

4.4. Specimen Conditioning.

The main purpose of this phase of the experimental procedure was to induce a constant amount af moisture (condition) in sellected specimens prior to

mechanical testing. The conditioning phase is devided into two stages; strain gage reliability and specimen conditioning.

4.4.1. Strain gage reliability.

This stage was designed to examine the reliability of the embedded gages in measuring hygroscopic strains without being affected by moisture, and to provide calibration curves yielding the specimen moisture content as a function of time and hygroscopic strain. Two $[0_6]$ and two $[90_8]$ specimens were immersed in distilled water in a specially designed plexiglas container (Figure 4.19) to withstand temperature-induced (120°F) strains and provide proper support for fragile $[90_8]$ composite coupons. In order to minimize the loss of water due to vaporization, a special cover was designed. Water vapors were liquified when came in contact to it and slowly dropped back into the container. This eliminated the need to costantly observe the containers' distilled water level. It also eliminated the posibility of disturbing the specimens, and thus produce strains unacounted for, while adding water to the container. The container with the specimens was placed in an oven set at 49°C (120°F) (Fisher Isotemp. 2000). This temperature was selected because it was high enough to considerably accelerate the absorption process and low enough not to alter the material physical properties. Also, the temperature variations (inherent oven limitation) at this rate were low enough so no noticeable thermal strains were produced on specimens whose moisture induced strains were measured by embedded strain gages. The embedded gages from the immersed specimens were conected through a Wheatstone bridge circuit, to a data logger (Digistrip II, Kaye Instruments) where hygroscopic strains, air and water temperatures were simultaneously recorded. Two specimens of each layup ($[90_8]$, $[0_6]$ and $[10_6]$)

with and without embedded gages had their tabs cut off and were conditioned together with the tabbed specimens. They were used for water gain measurements, and were periodically weighed on an analytical balance with a resolution of 0.1 mg (Metller H31). The tabs were cut off because they were made of a material whose moisture absorption coefficient was not the same as that for graphite/epoxy. Both specimens with and without embedded gages were used in this case in order to prove the the presense of the gages will have no effect on the hygroscopic and hygroelastic properties of the material. Three other $[90_8]$ untabbed coupons were mounted into fixtures with dial gages (Figures 4.20-4.21), immersed in distilled water and placed in the same oven in order to obtain independent results of hygroscopic strains. The effects of purely thermal output was eliminated by using the first strain readings at 49°C (120°F) as reference and by keeping the water temperature controlled within +3°F. Nevertheless, a complete thermal evaluation of the composite specimen was also performed in order to see the effect of 3°F on total strain. For this purpose, a two gage rossete was mounted on a Titanium-Silicate (TiSi) specimen having practically a zero coefficient of thermal expansion. Another two-gage rossete was mounted on a unidirectional composite specimen with one gage allinged along the fiber direction and the other perpendicular to the fibers. The TiSi apparent thermal strain (although very small), was automatically subtracted from the strain of the composite in the Wheatstone bridge conditioner. This was an extra precaution (because as mentioned previously the strain gage used is self compensated for the range of temperatures under consideration) to eliminate any strains, as small as they may be, which are not thermal induced strains on the composite specimen itself. The net thermally induced strain was recorded as a function of temperature for both principal material directions and

used to obtain the material principal thermal expansion coefficients (α_1 and α_2). These values were different from those of the thermal expansion coefficients of the Scotchply, glass/epoxy tab material. This thermal incompatibility gave rize to residual stresses on the composite plate while bonding tabs with FM300 adhesive at elevated temperatures. To solve this problem, analysis showed that the glass/epoxy tab material will have the same axial thermal expansion coefficients as the graphite/epoxy plate if it was cut at 45° with respect to its' principal material axes. This is a good indicator of the flexibility of composite properties, which enable the engineer to actually taylor the material to fit his design needs.

4.4.2. Moisture Conditioning.

This stage consists of conditioning specimens for mechanical testing. It follows only after a thorough analysis of the hygroscopic (described above) and mechanical testing (descrided in phase 4.5 of the experimental prosedure) data proved that embedded gages provide reliable and consistent strain readings under all selected hygrothermal and strain rate conditions.

Three plexiglass containers were placed at the same time in an oven set to 49°C (120°F). Each container held 22 specimens of the same layup ($[0_6]$, $[90_8]$ $[10_6]$) immersed in distilled water. At least two specimens from each of the $[0_6]$ and $[90_8]$ containers were wired to the data logger through a Wheatstone bridge, to obtain a continuous record of hygroscopic expansion. This was necessary in order to determine the moisture content in the specimens, evaluated from the calibration curves obtained previously, and also make sure that the gages function properly. In addition, two untabbed specimens from

each layup were placed in a separate container for parallel water gain weighing.

4.5. Mechanical Testing.

This mechanical testing phase was also devided into two stages.

4.5.1. Strain gage Reliability.

This phase was designed to examine the reliability of the embedded strain gages in measuring mechanical strains without being affected by moisture, high temperature and high strain rates.

At first, a set of dry (unconditioned) specimens were tested mechanically to failure. The tensile tests were carried out on a servohydraulic testing machine (Instron 3200 series), (Figure 4.22) under stroke control. The outline of the system designed for aquiring the data is shown in Figure 4.23. Strains were measured in three different ways: using embedded gages, surface gages, and an extensometer. The strain gage output was transfered through an eight-channel Wheatstone bridge circuit (Kaye Instruments, Inc. BC-8SG) and amplifiers (100 x) to a digital processing oscilloscope (Norland 3001). Special care was taken in precise calibration of the amplifiers so that the signal amplification would be exact. Load measurements were measured by a load cell, from which the signals were transfered to the Norland. All data were then analysed and processed. At first, voltage readings were converted through propper factors into values of stress, strain and time. Next, the ultimate values of strain, load and time were recorded. The stress-strain and stain vs. time

curves were then displayed on the oscilloscope. The curves were smoothened (n-point average technique) corrected for any inconsistencies due to experimental error, as strain jump due to fiber breackage directly under the extensometer or zero shifting, etc. All data were then transfered to a microcomputer (Apple 2e) and stored on a floppy disc for further analysis (Figure 4.24).

Secondly, specimens with embedded gages, conditioned to a moisture content of 0.35% were tested under uniaxial tension to failure. These tests were conducted at three strain rate levels: low strain rates, a quasi-static rate of $\dot{\varepsilon}_{xx}=1.4 \cdot 10^{-4}\ s^{-1}$ and a high rate of $\dot{\varepsilon}_{xx}= 5.0\ s^{-1}$. Strains were measured simultaneously by means of embedded gages and an extensometer mounted on the specimen during the test. An environmental chamber for moisture control was proven unnecessary in all wet specimen tests because all specimens were kept submerged in water untill all testing conditions and instrumentation were set. Actual testing did not exceed (2-3) min. for room temperature and (3-4) min. for higher temperature tests, hense, neither a significant amount of moisture in the spesimen was desorbed nor the embedded gages in the midplane showed any strain change. Hygroscopic strains were subtracted from the total strain output during testing by connecting an identical (dummy) specimen to a Wheatstone bridge arm adjacent to the strain gage of the mechanically loaded specimen. The necessity to do so arose because hygroscopic strains were too large to balance by adjusting the potentiometer provided for such purpose in each of the Wheatstone bridge channels, and because it was impossible to account for changes in strains due to constant variations of specimen temperature and moisture (as small as they may be) during testing. After evaluating the reliability of the embedded gage

technique to measure hygrothermal and mechanical strains, specimens were subjected to full scale conditioning prior to mechanical testing (as described previously).

4.5.2. Final Testing.

Longitudinal properties, modulus, E_1, tensile strength, F_{1T}, ultimate tensile strain, ε_{1T}, and poisson's ratio, v_{12} were obtained by testing 6-ply 0° coupons (Figure 4.18). Transverse properties, modulus, E_2, tensile strength, F_{2T}, ultimate tensile strain, ε_{2T} and poisson's ratio, v_{21}, were obtained by testing 8-ply 90° coupons (Figure 4.18). Eight plies were used for transverse properties because thinner coupons were too fragile to handle. In-Plane Shear properties, modulus, G_{12}, shear strength, F_{12} and ultimate shear strain, γ_{12}, were obtained by testing 6-ply 10° off-axis coupons (Figure 4.18). The procedure for 10° off-axis testing was previously described. All tensile tests were carried out in a servohydraulic Instron testing machine (Figure 4.22) and under the following conditions.

Table 4.1. Hygrothermal and strain rate testing conditions.

Temperature, °C (°F)	22 (72)	60 (140)	91 (196)	128(263)
Moisture, content, %C (%M)	1 0	0	1 0	1 0
Average strain rate, s^{-1}	10^0 10^{-1} 10^{-3}	10^0 10^{-1} 10^{-3}	10^0 10^{-1} 10^{-3}	10^0 10^{-3} 10^{-3}

A computer program developed by Mr. Scott Cokeing and Dr. Gershon Yaniv of Northwestern University was used to set the Instron machine controls according to each specimen characteristics. High strain rate data were aquired at a rate of one point per 0.1 ms. by the digital oscilloscope (Norland 3001) trig gered by the load applied to the specimen. All tests above room temperature were conducted in a chamber (Associated Environmental Systems) controlled to within +0.6°C (+1°F), (Figure 4.25). The temperature was monitored by a thermocouple, (K type) through a data logger (Digistrip II, Kaye Instruments). During the tests, continuous records of load and strain for each specimen were obtained simultaneously by the digital oscilloscope as previously described. All data were processed and transferred to a microcomputer (Apple 2e) and filed on disk for further analysis.

The embedded gage output at elevated temperatures, is a combination of several effects including thermal expansion, hygroscopic expansion and mechanical strain. In the case of the 10° off-axis specimen, the hygrothermal effects on the -45° and +45° gages are identical and subtracted out when the gages are mounted on adjacent arms of the Wheatstone bridge. The algebraic difference of the two strain readings is the net mechanical in-plane shear strain, and is free of all hygrothermal effects and can be considered as self-compensated hygrothermally [5]. In the case of 0° and 90° specimens, temperature and moisture compensations of the strain gage output were performed by using identical reference specimens with no mechanical loading but at the same hygrothermal conditions. The longitudinal gages from the test and reference specimens were connented to adjacent arms of a Wheatstone bridge and the transverse gages to the adjacent arms of another bridge. Bridges of dry specimens were balanced (zeroed) at room temperature and

checked to see that the balance was maintained at the testing temperature. Bridges of a pair of wet specimens were balanced while the specimens were still immersed in the water container. Then, the container with the specimens was placed in the environmental chamber of the testing machine. The test and reference specimens were taken out from the container as close as possible to the very moment of mechanical testing. When the spesimens reached the desired temperature, the test specimen was loaded to failure and the output was recorded on the digital oscilloscope as the net induced mechanical strain. The load output was connected directly from the Instron to the digital oscilloscope (as previously mentioned). All data were processed, transferred to the microcomputer and filed for further analysis.

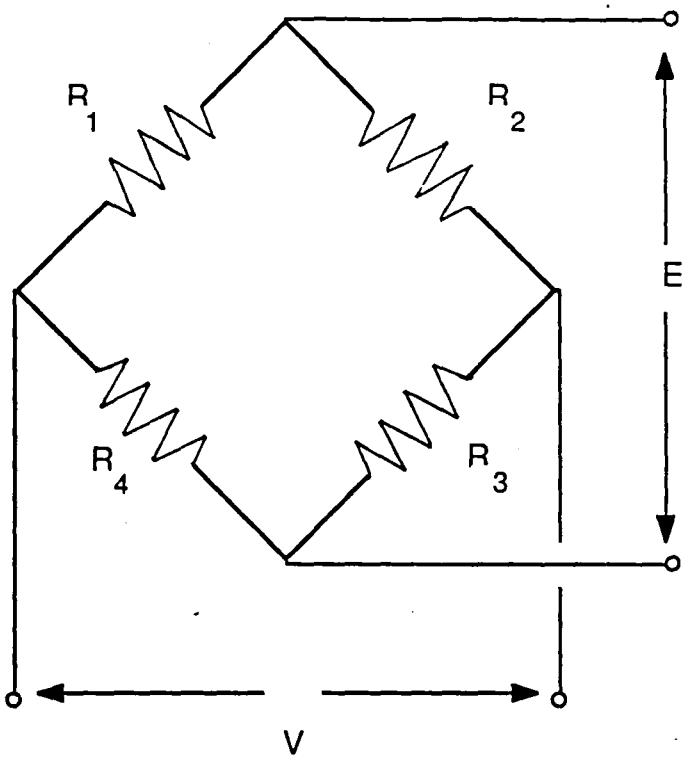

Figure 4.1 The Wheatstone bridge circuit.

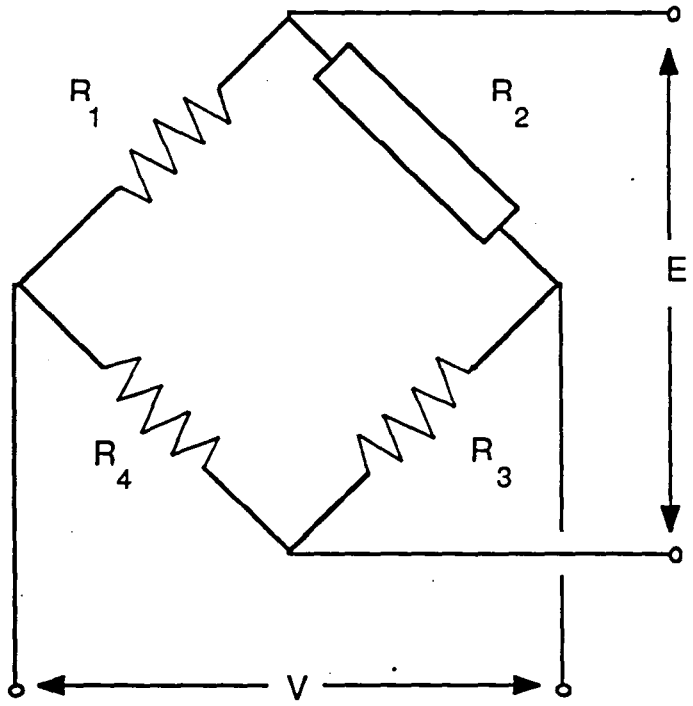

Figure 4.2 Wheatstone bridge with dummy strain gage.

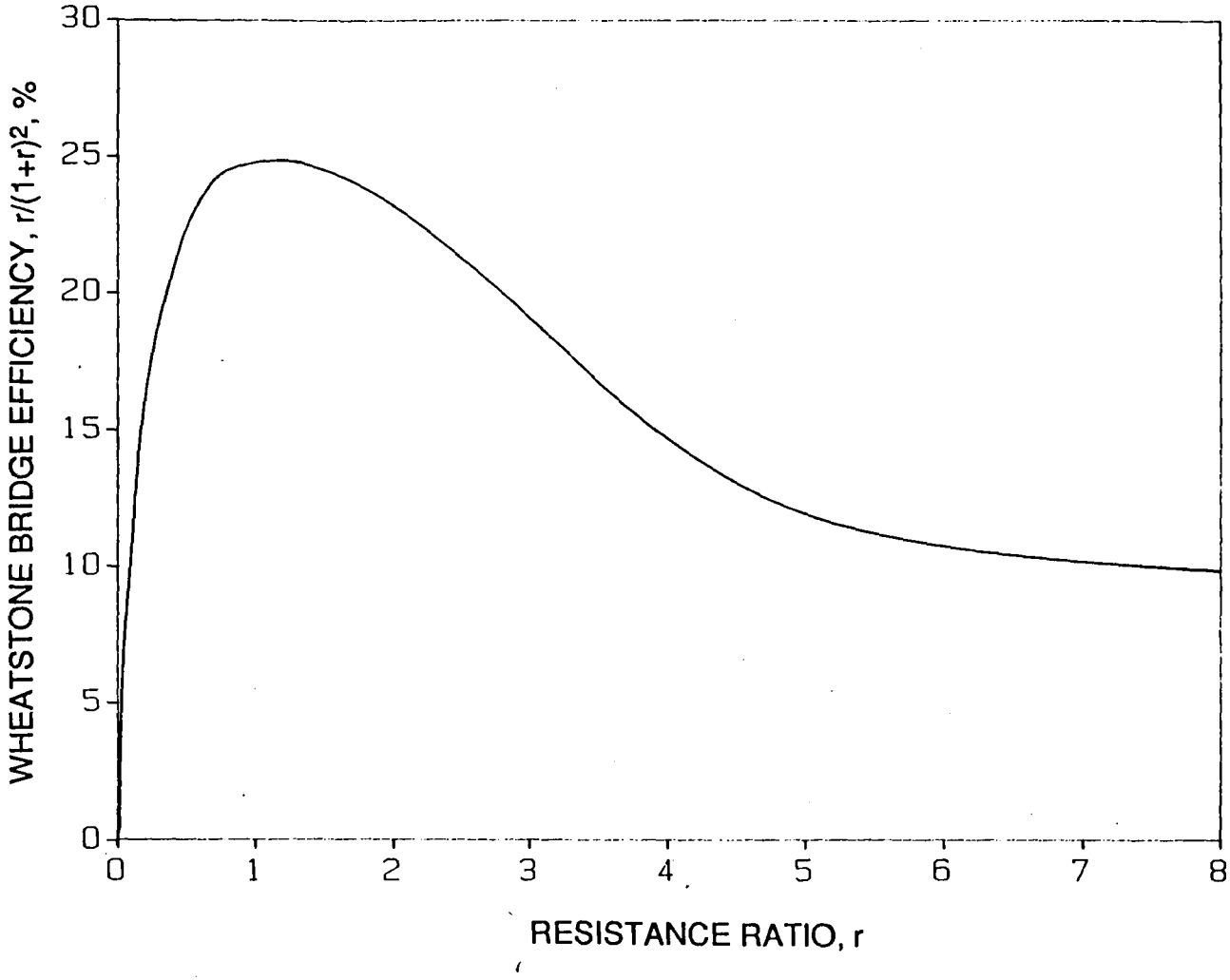

Figure 4.3 Wheatstone bridge circuit efficiency as a function of resistance ratio (r)

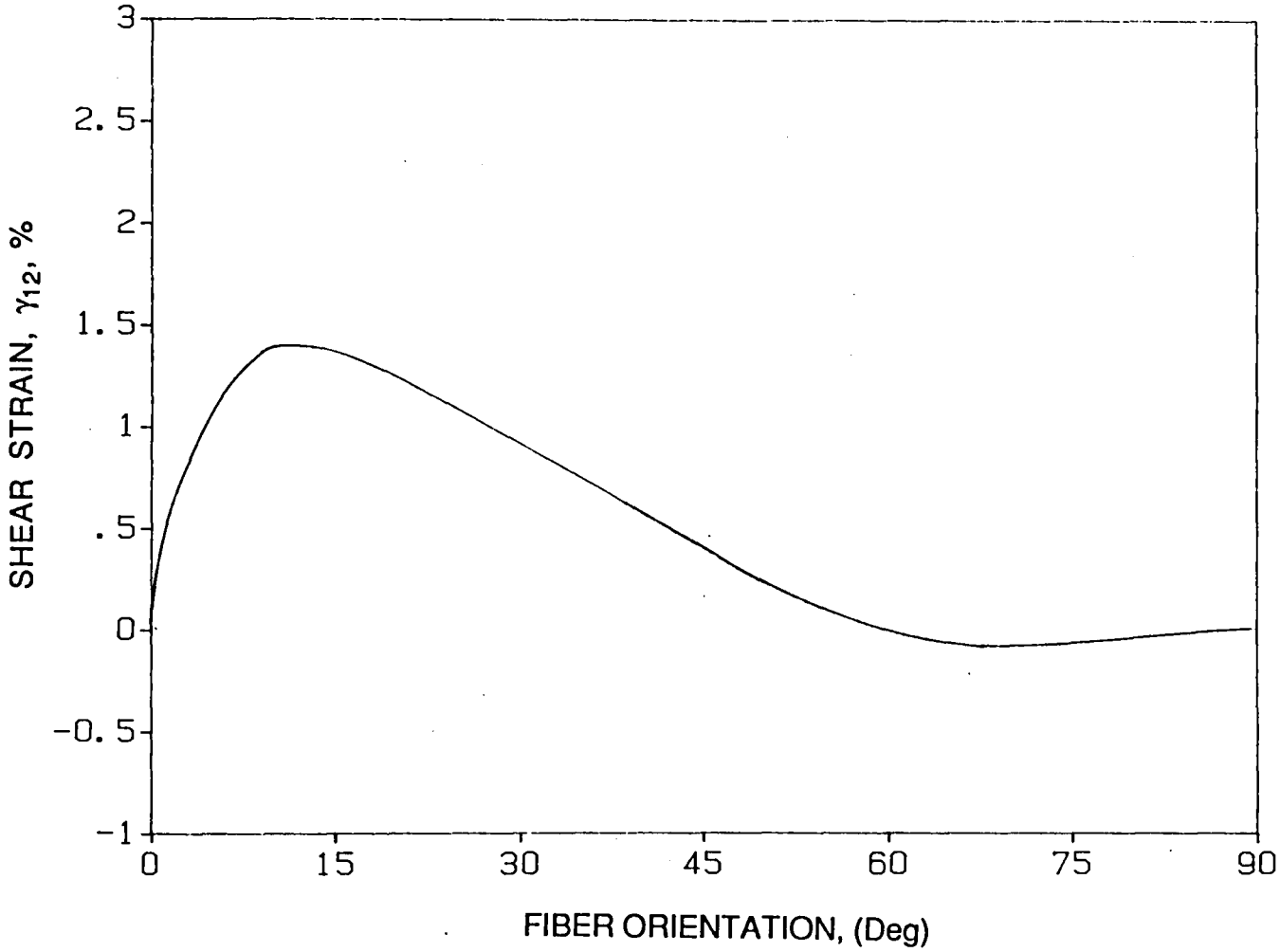

Figure 4.4 Shear strain as a function of fiber orientation for typical unidirectional Graphite/Epoxy material

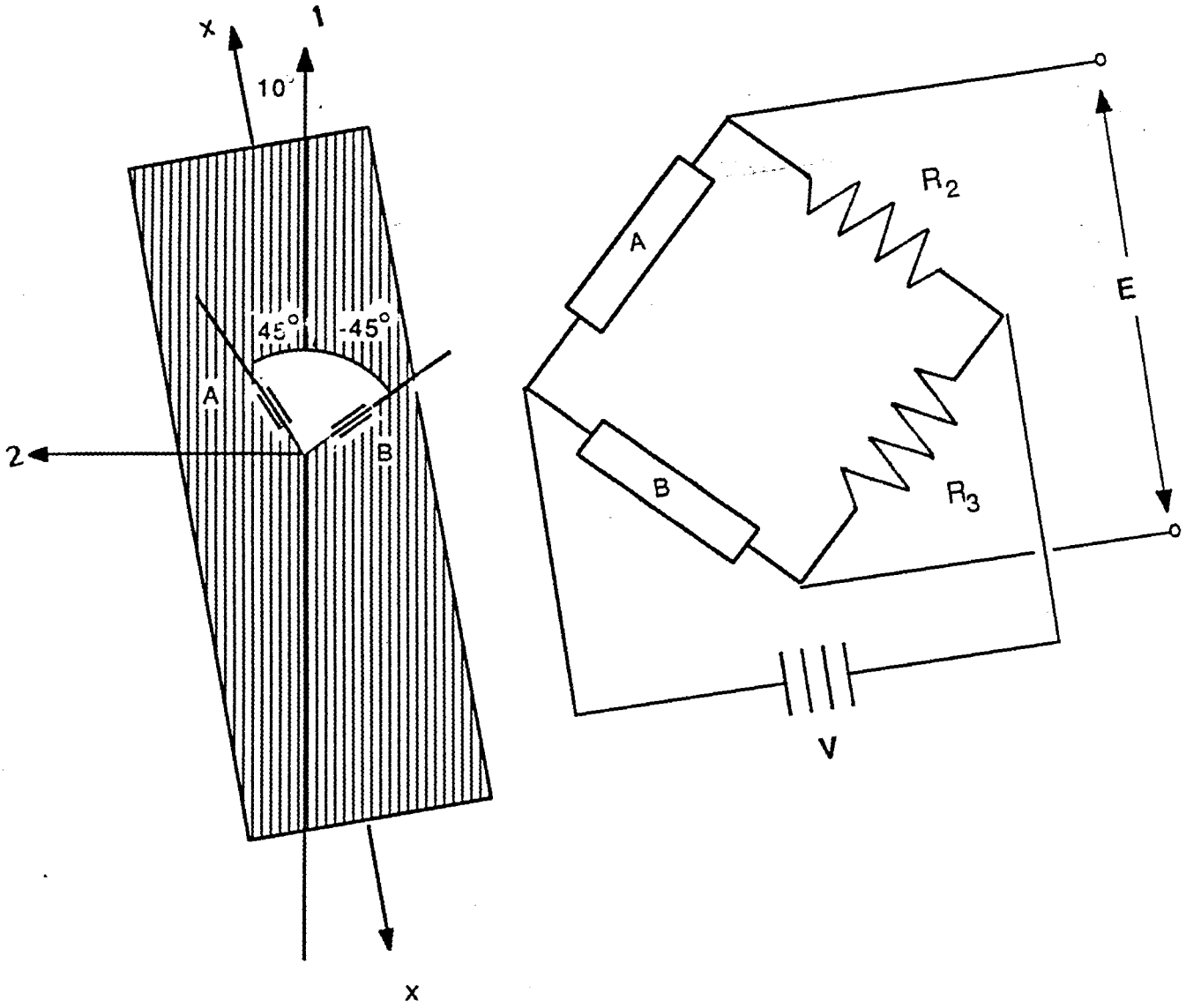

Figure 4.5 Arrangement of Strain Gages on an Off-Axis Composite Specimen for Direct Measurement of In-Plane Shear Strain.

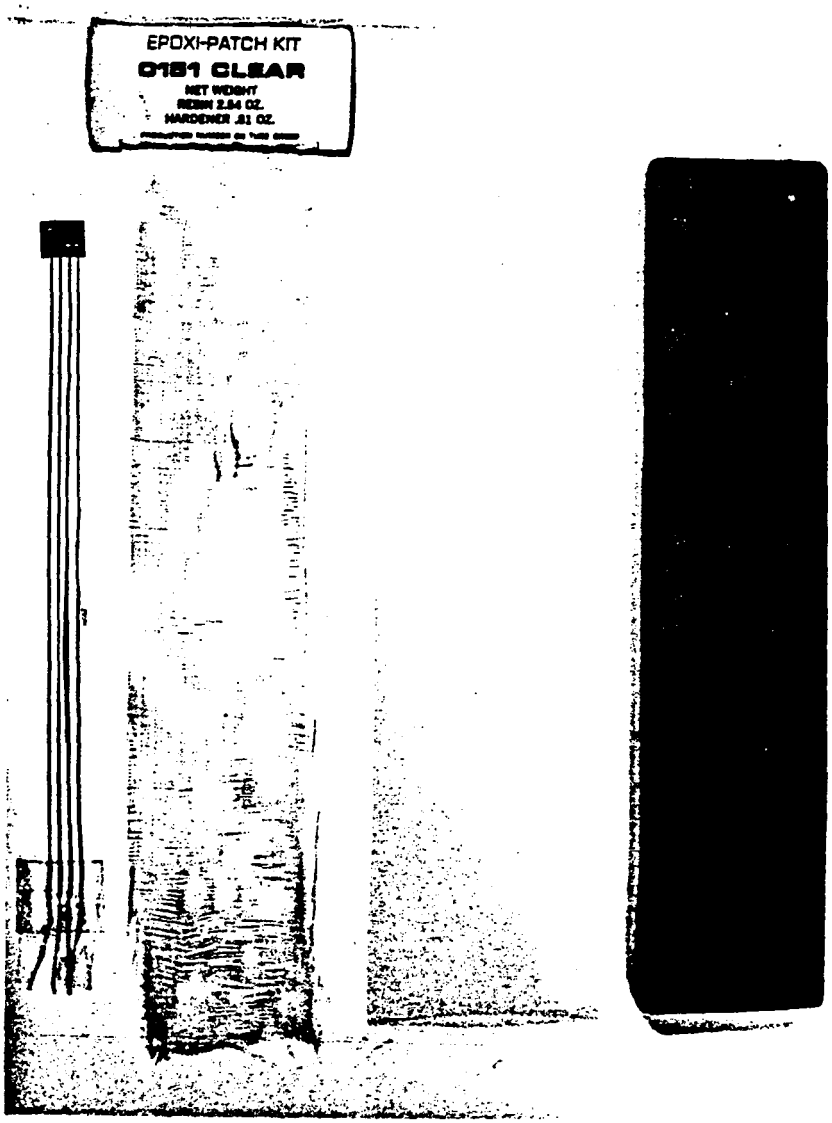

Figure 4.6 Materials necessary for the production of encapsulated strain gages.

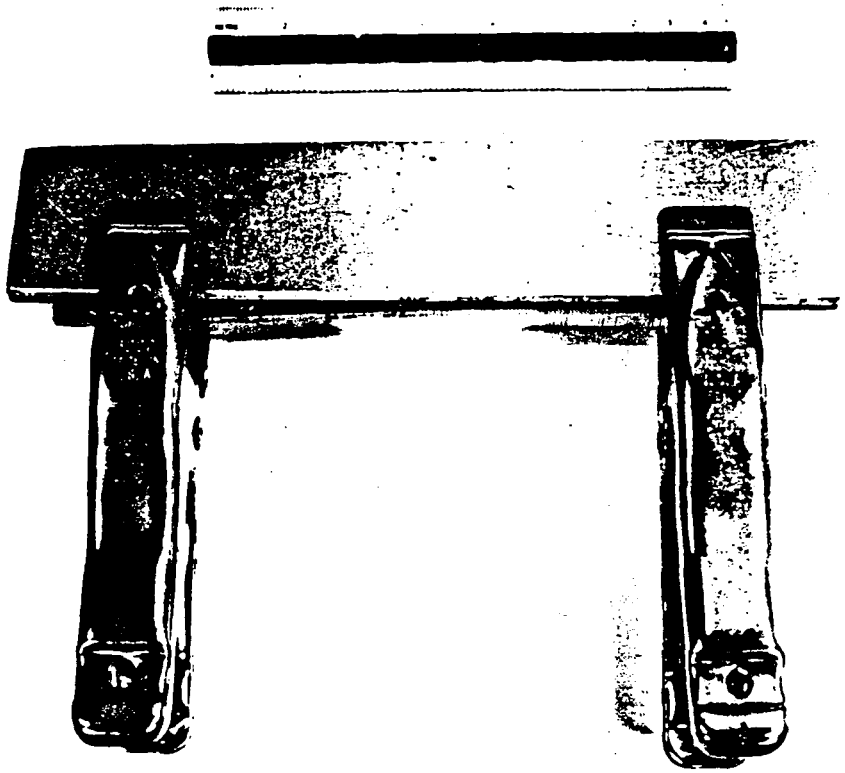

Figure 4.7 Uniform pressure applied to encapsulated gage by means of spring clamps.

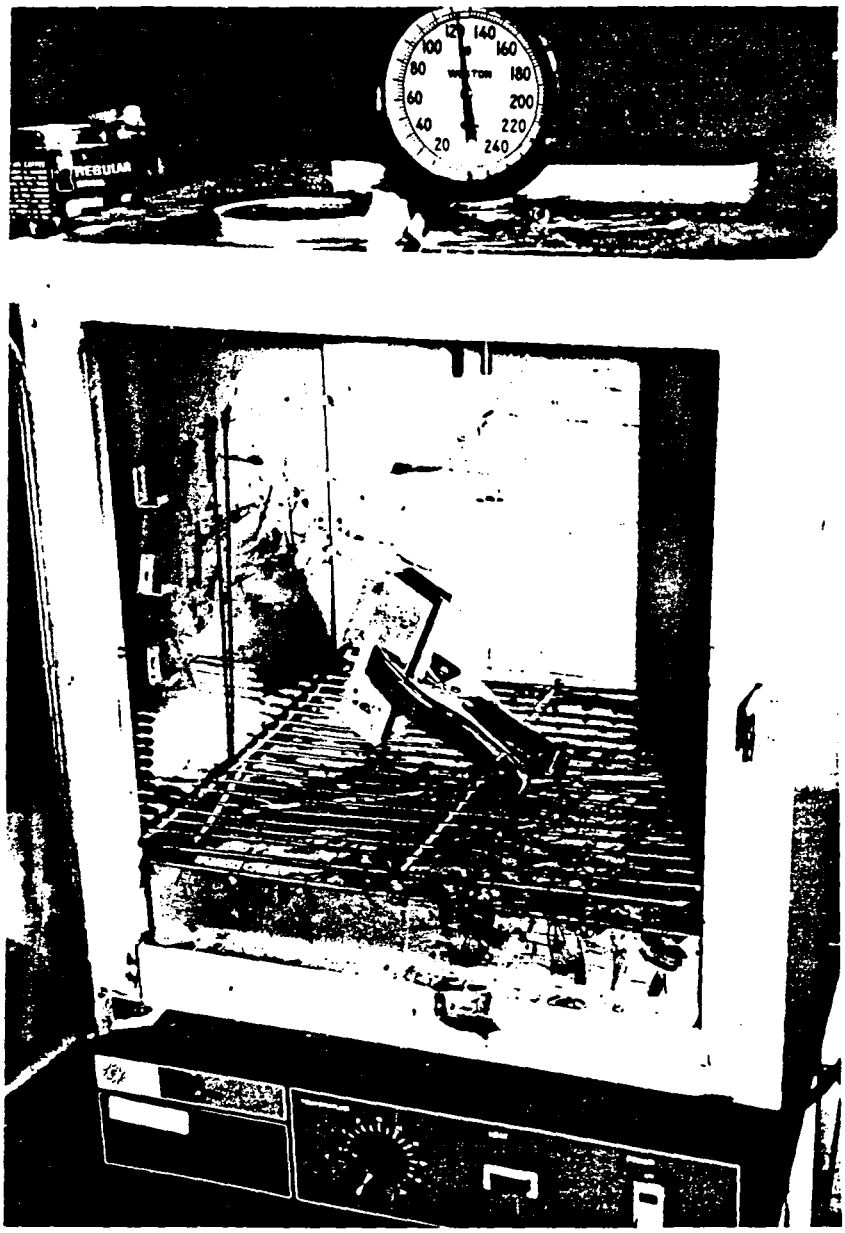

Figure 4.8 Curing of encapsulated strain gage at 60°C (140°F).

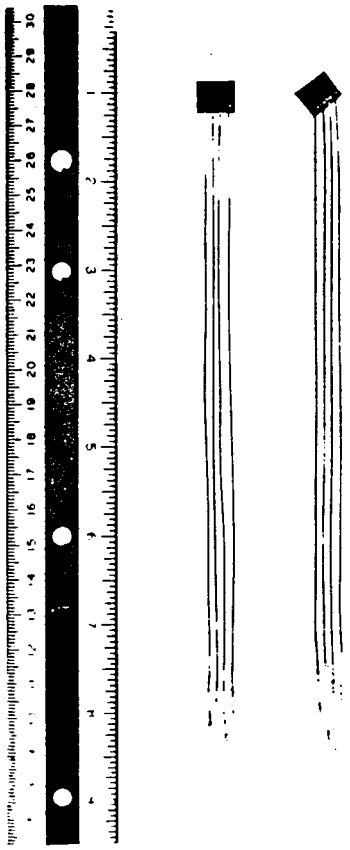

Figure 4.9 Prepared encapsulated gages.

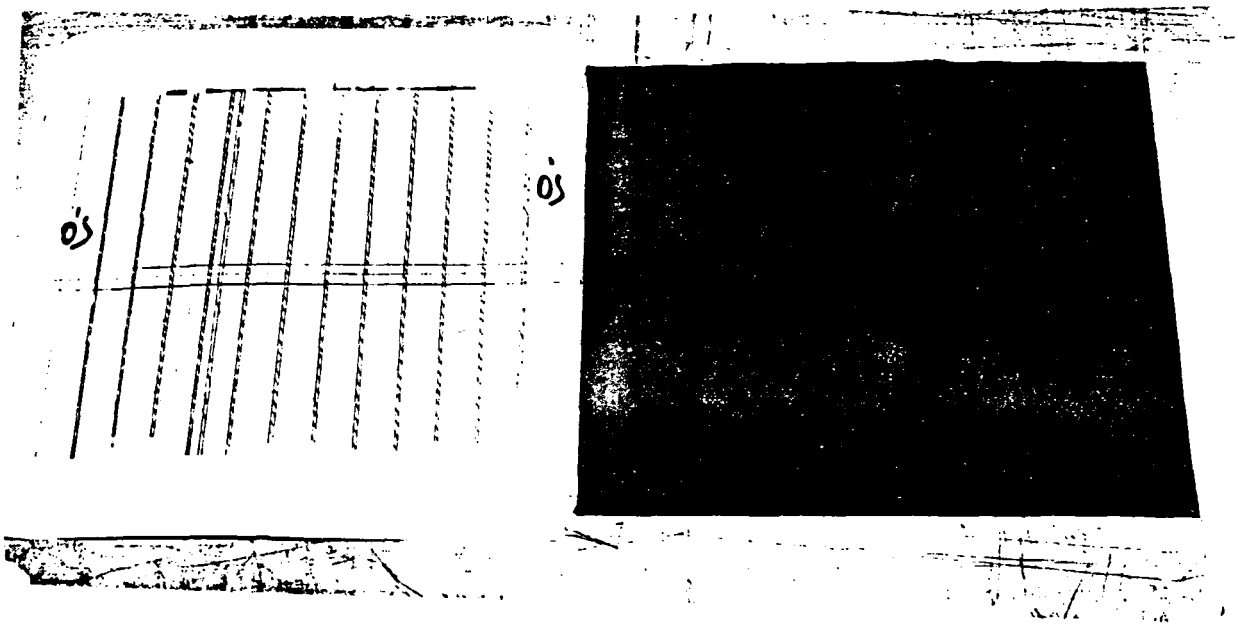

Figure 4.10 Template for positioning strain gages on a $[0_6]$ composite plate.

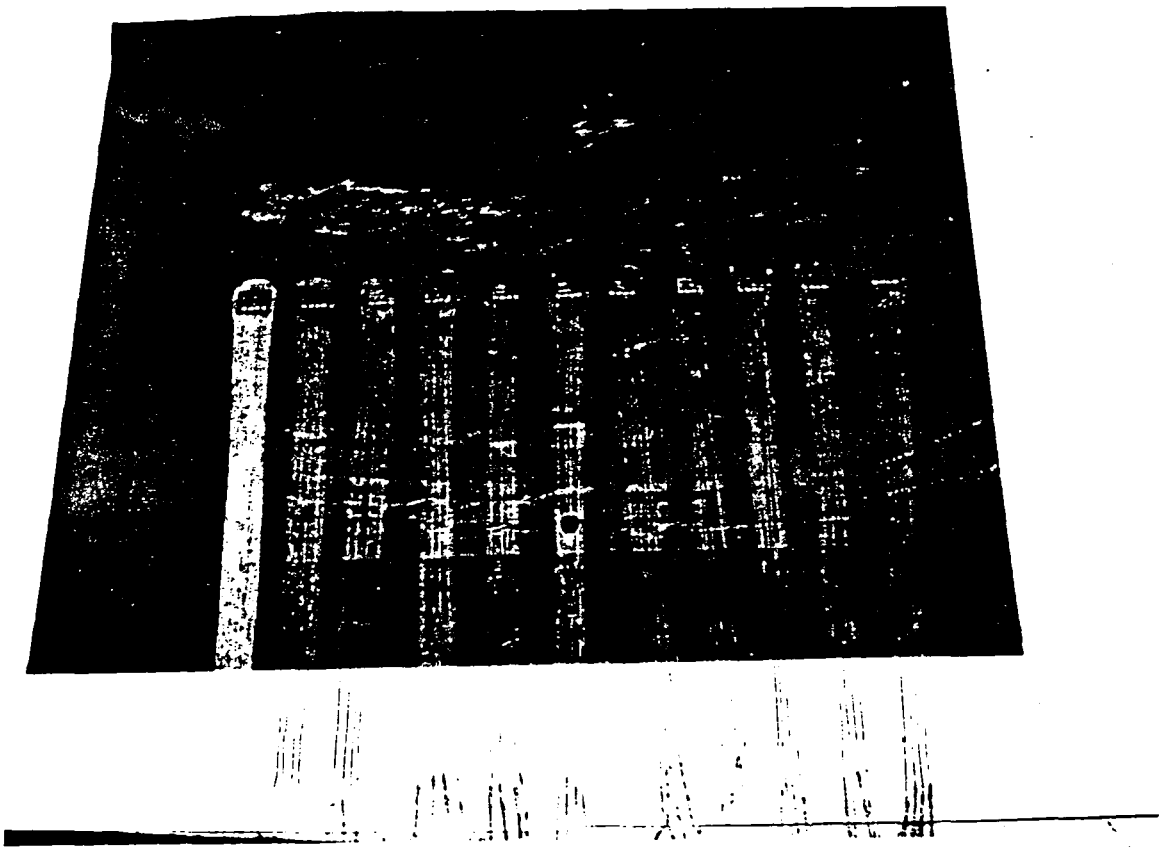

Figure 4.11 Positioned encapsulated strain gages in the mid-plane of a $[0_6]$ composite layup.

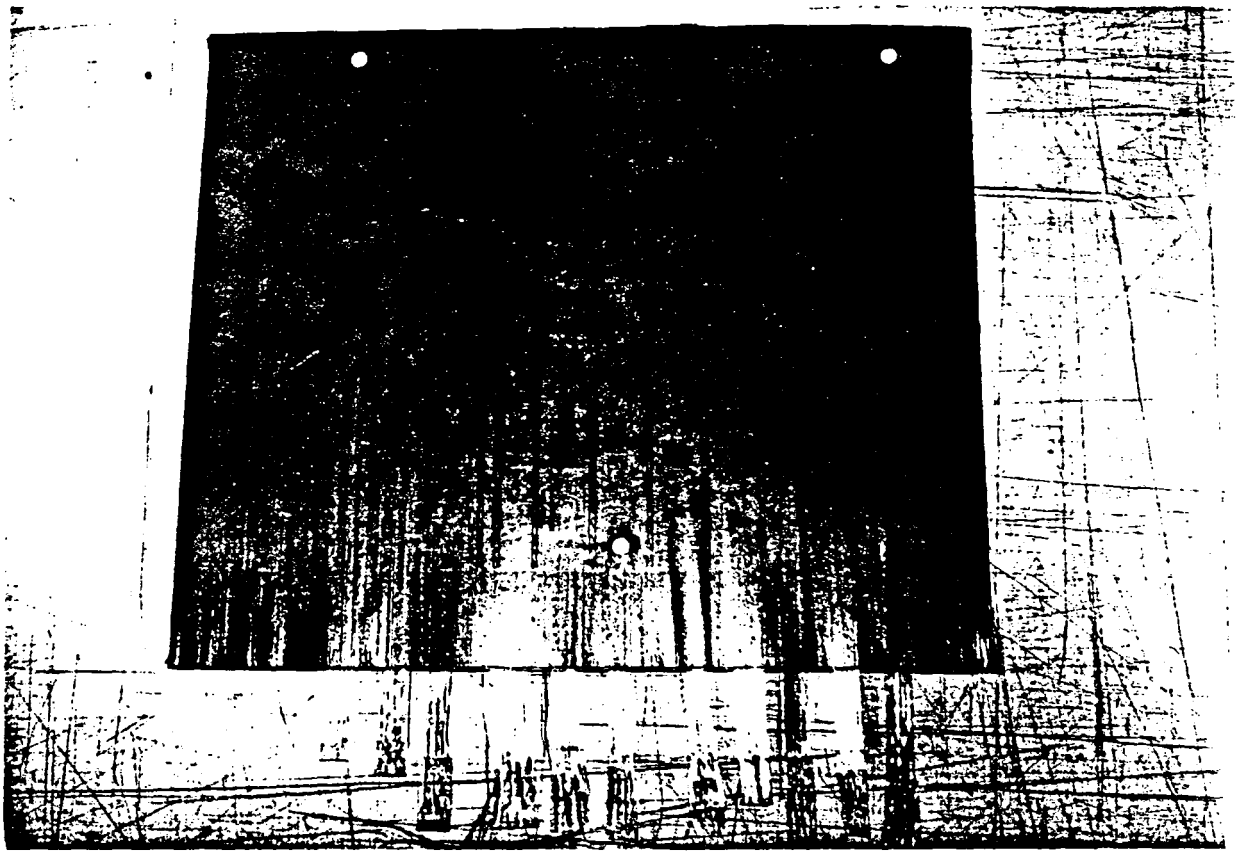

Figure 4.12 Reference position of template on outer surface of a $[0_6]$ composite layup containing embedded gages.

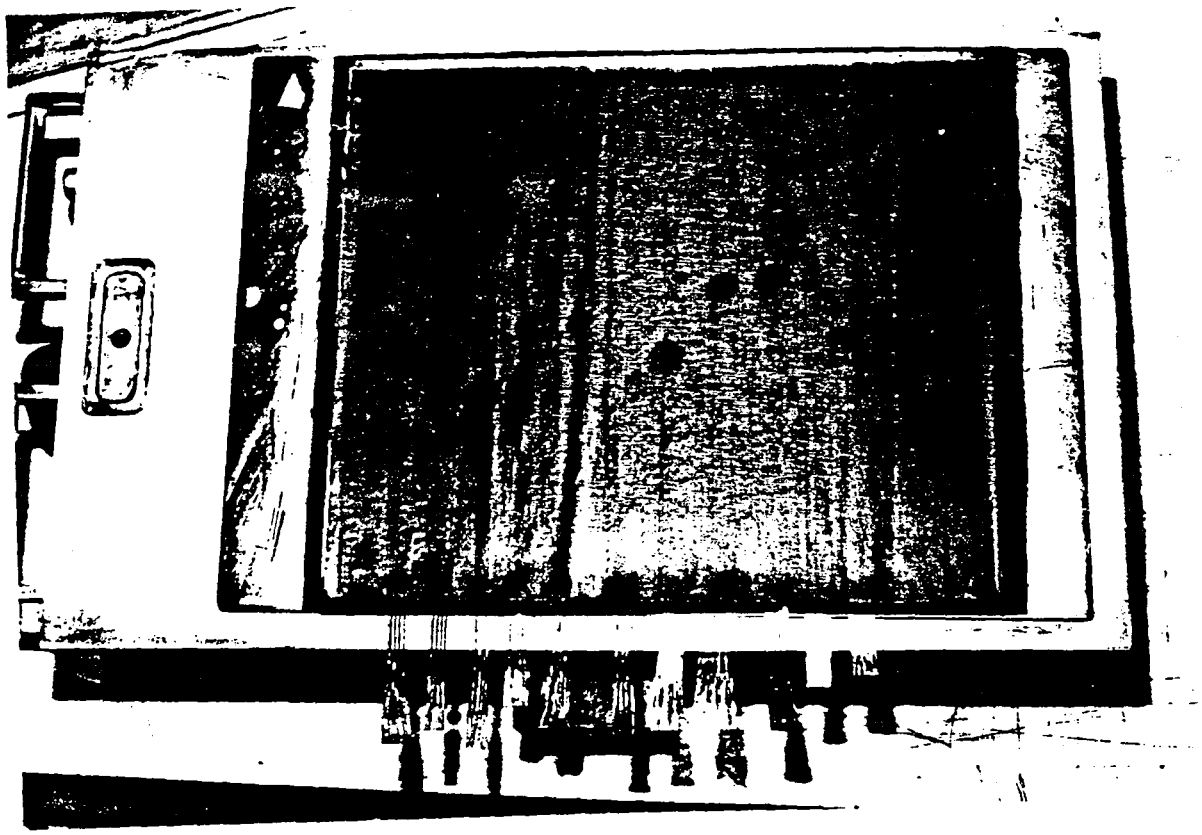

Figure 4.13 Composite plate containing embedded gages on cork dammed tool plate, prior to curing.

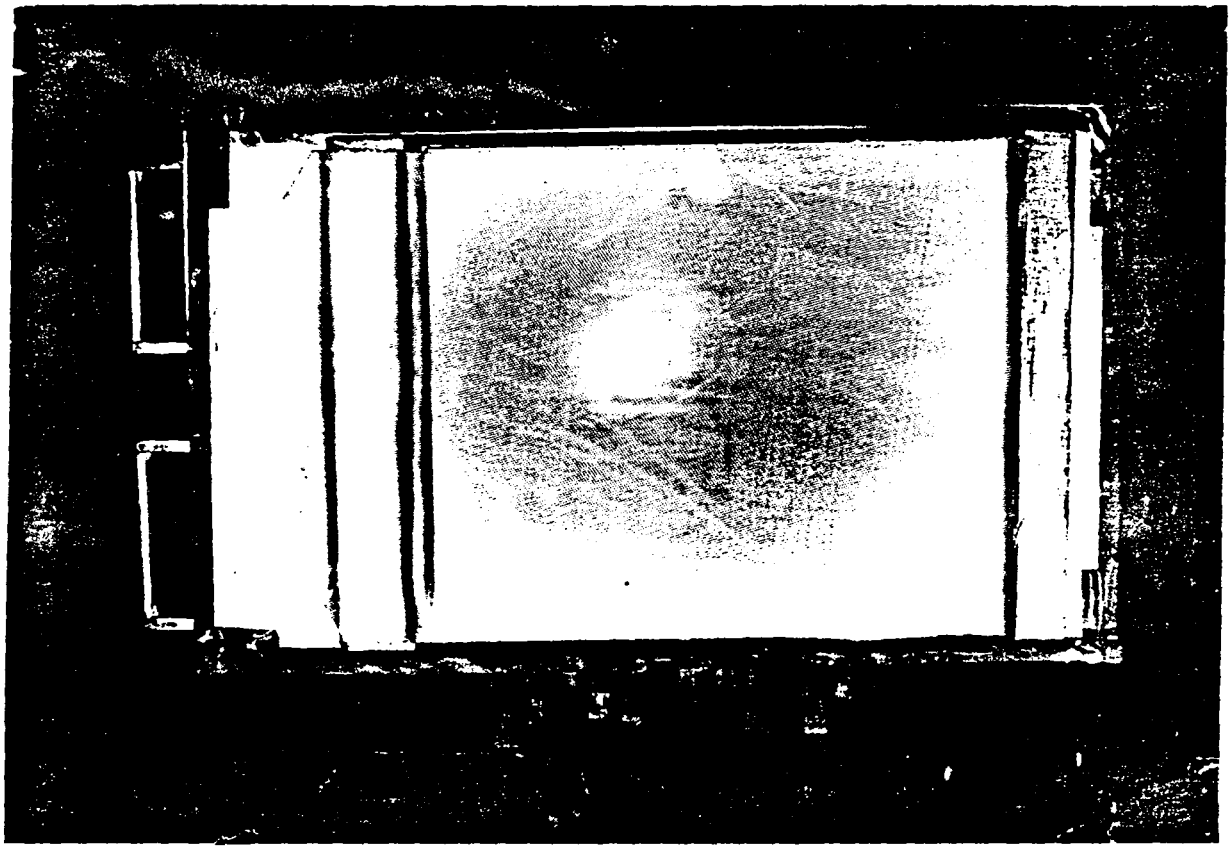

Figure 4.14 Vacuum bag over composite plate/tool plate assembly, prior to curing.

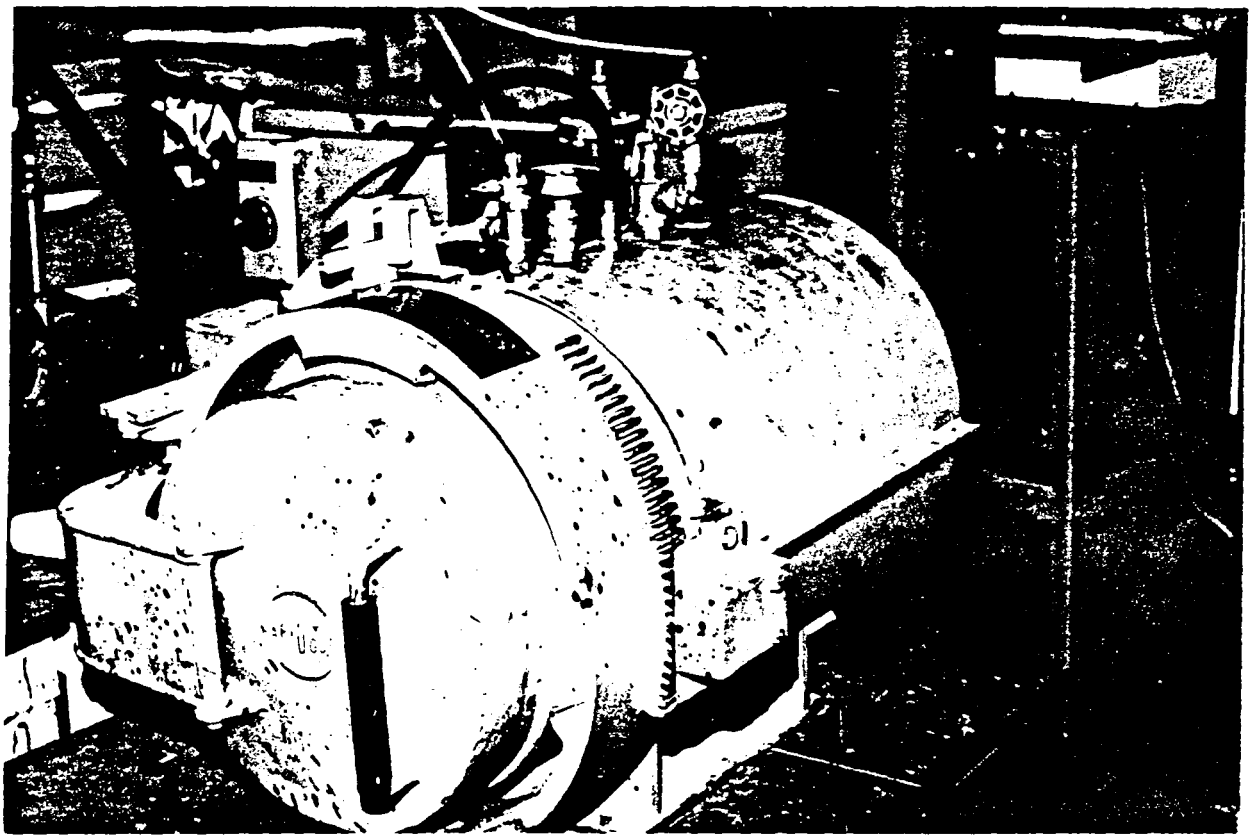

Figure 4.15 Rapidoor autoclave for curing of AS4/3501-6 Graphite/Epoxy material.

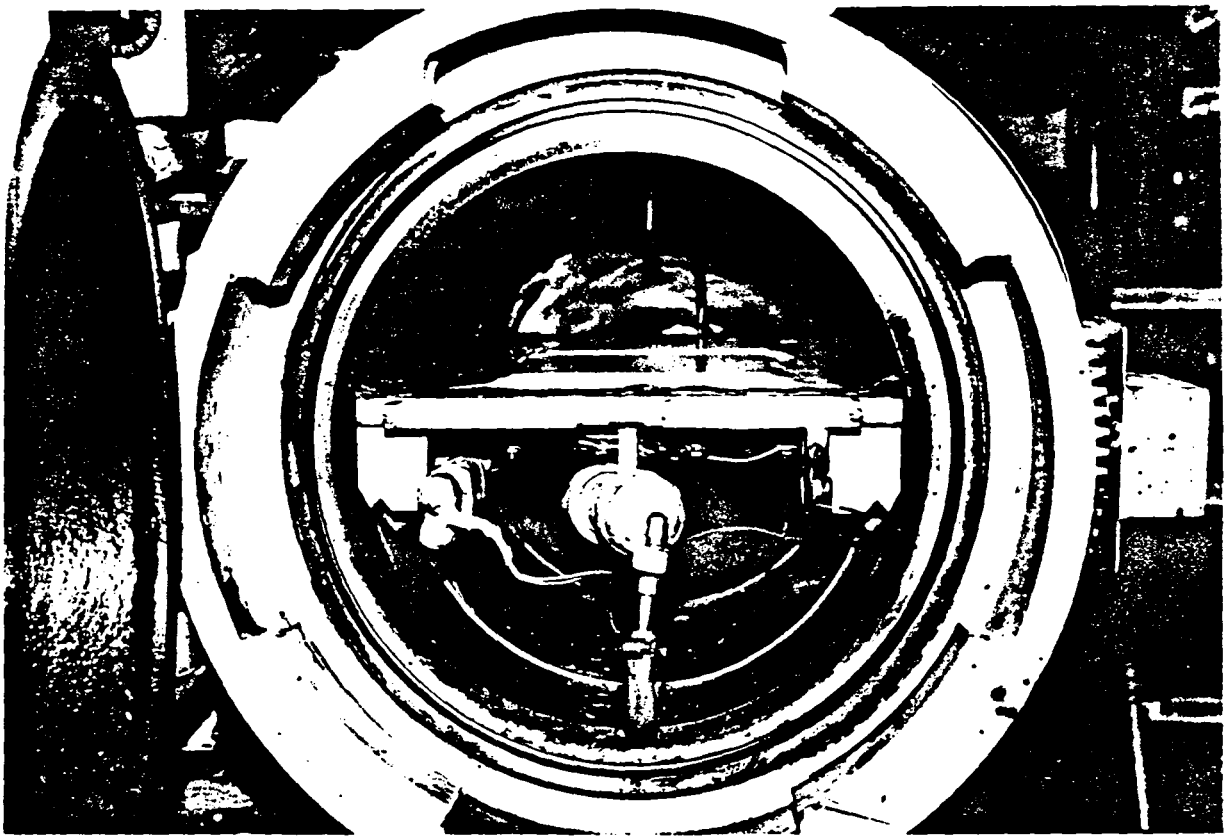

Figure 4.15.a Tool plate with composite layup inside autoclave prior to curing.

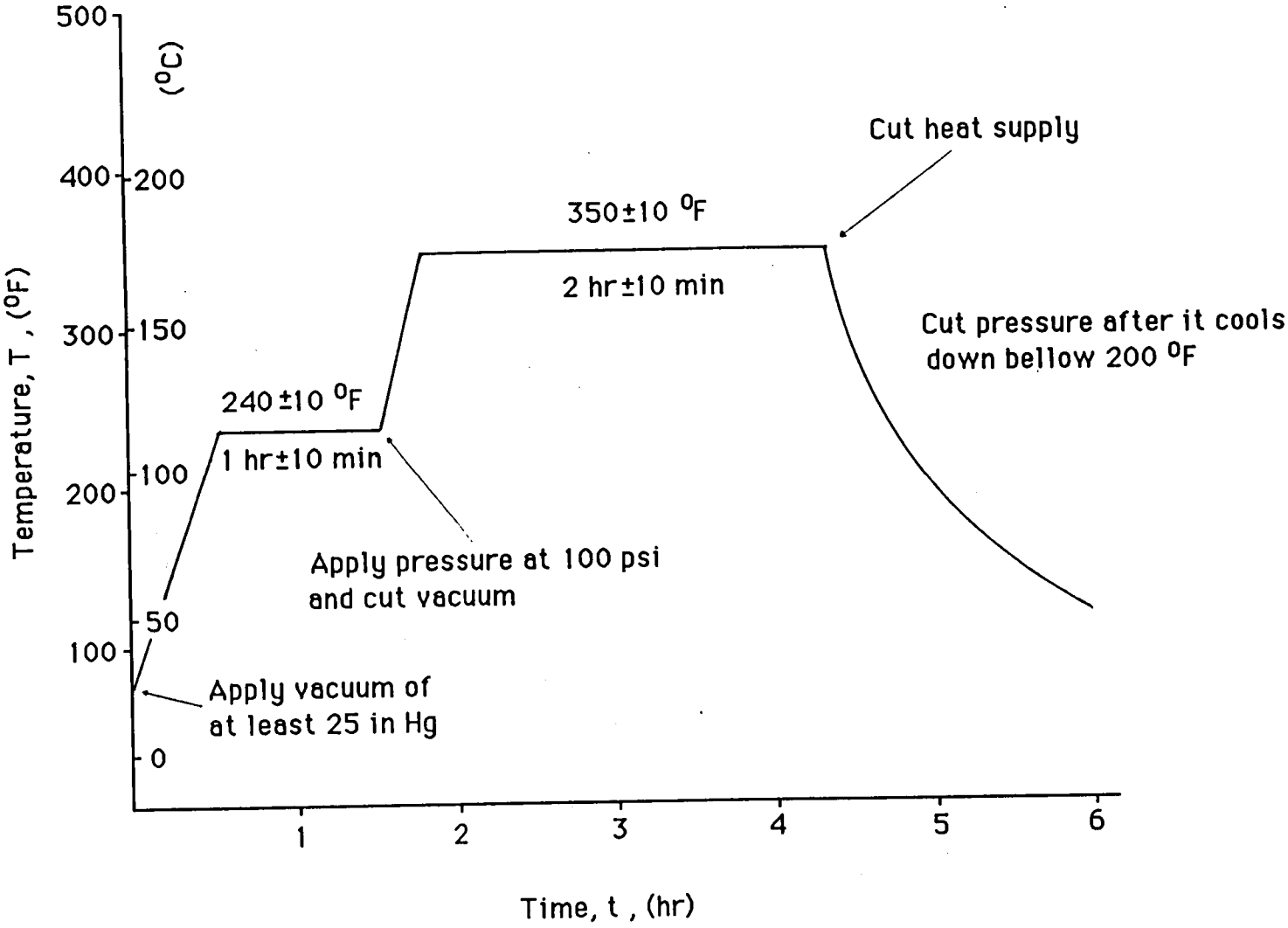

Figure 4.16 Curing schedule for AS4/3501-6 Graphite/Epoxy material

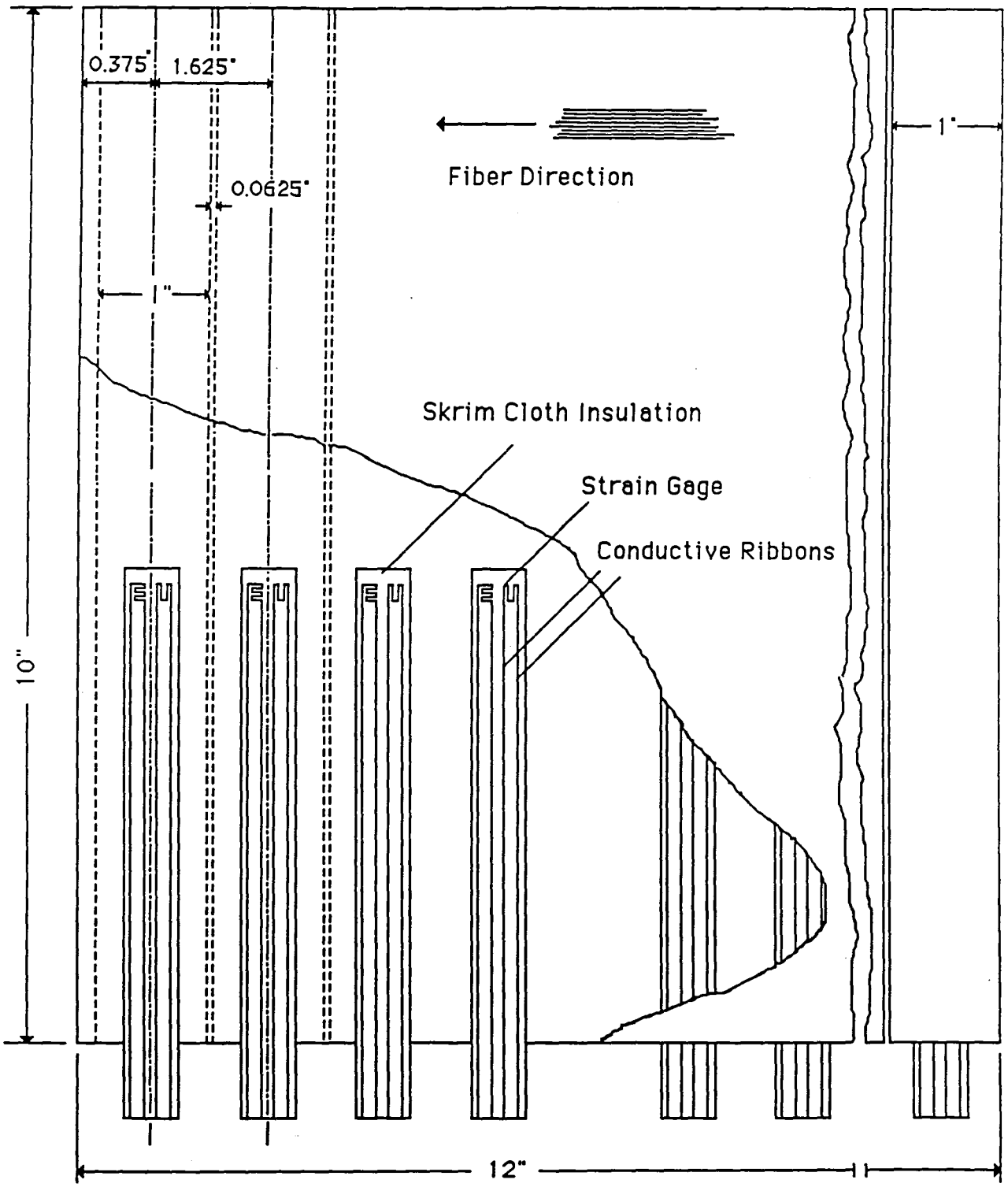

Figure 4.17 Embedded gage layout for unidirectional, $[90_8]$, Graphite/Epoxy specimens

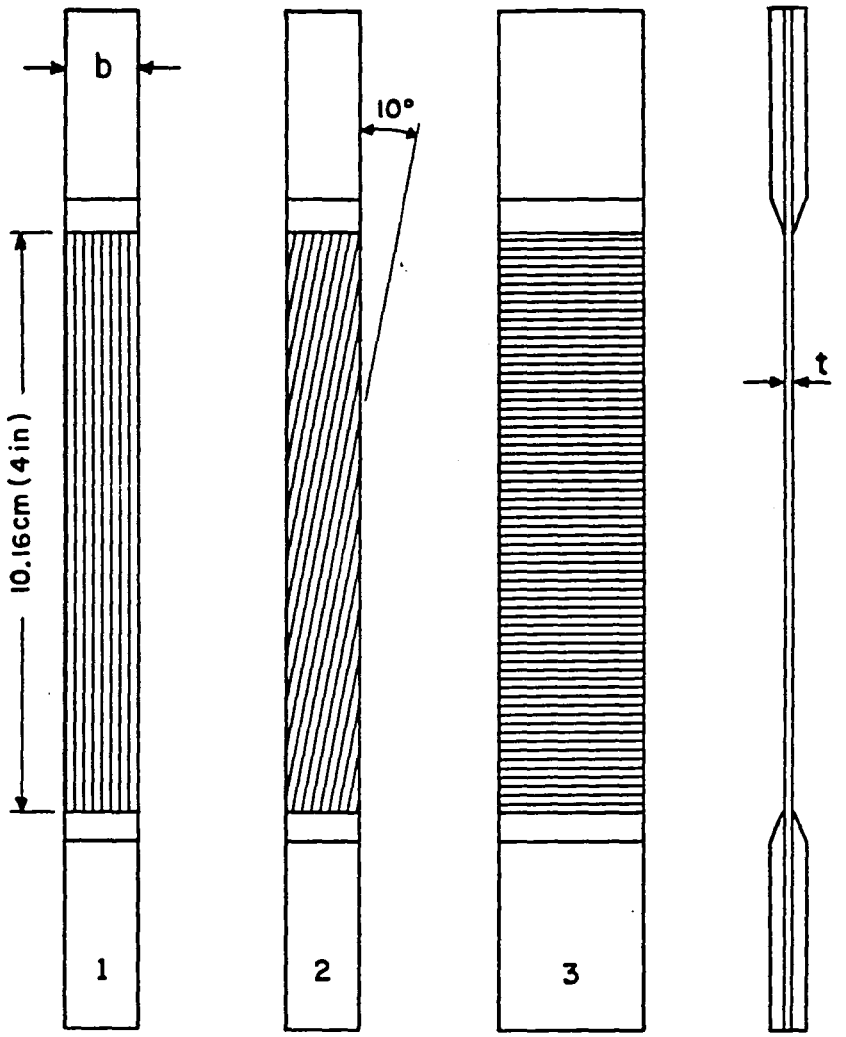

Specimen Type	Layup	Width, b cm (in.)	Thickness, t mm (10^{-3} in.)
1	$[0_6]$	1.27(0.5)	0.76±0.03(30±1)
2	$[10_6]$	1.27(0.5)	0.76±0.03(30±1)
3	$[90_8]$	2.54(1.0)	1.02±0.03(40±1)

Figure 4.18 Specimen geometries for characterization tests of Unidirection Graphite/Epoxy

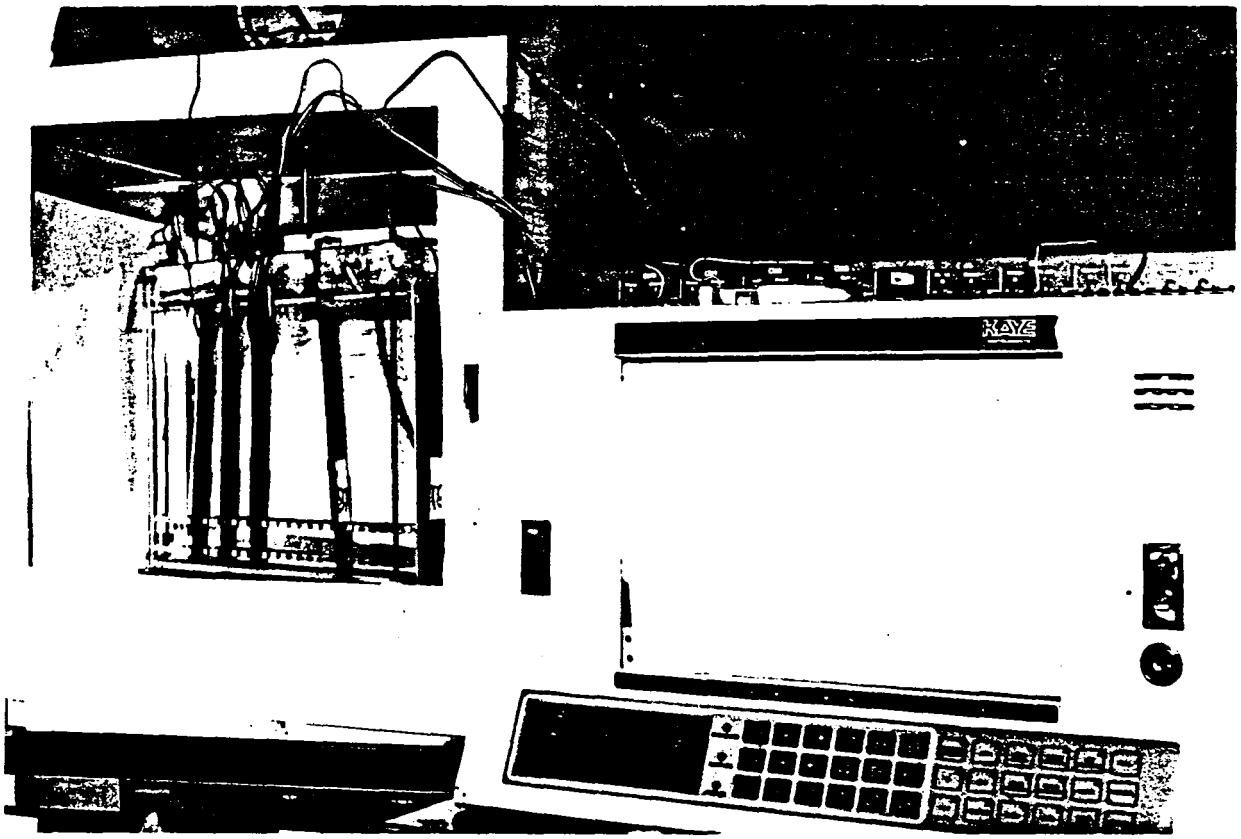

Figure 4.19 Moisture conditioning of composite specimens with parallel measurement of hygroscopic strain by means of embedded strain gages.

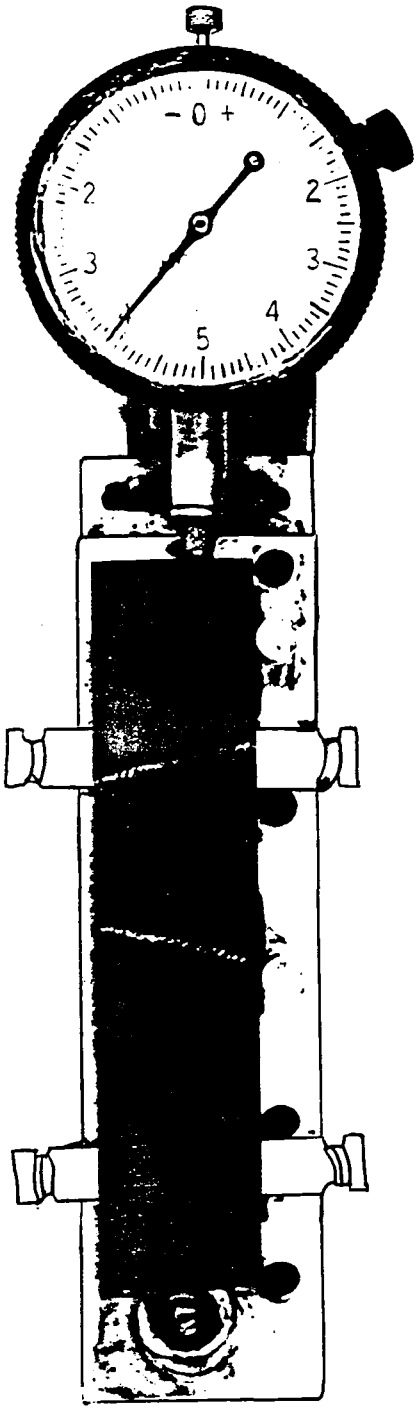

Figure 4.20 Fixture for measurement of moisture expansion with a dial gage, in a composite specimen.

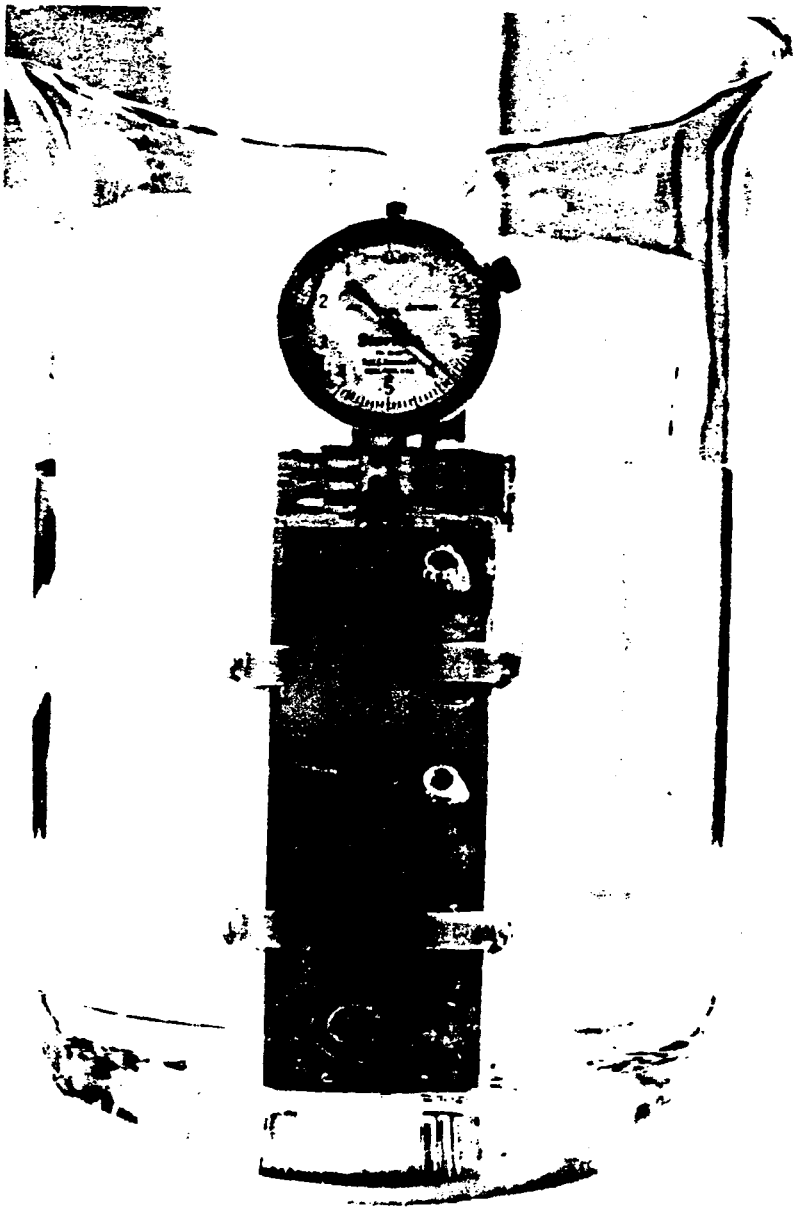

Figure 4.21 Composite specimen mounted on a dial gage fixture while moisture conditioning.

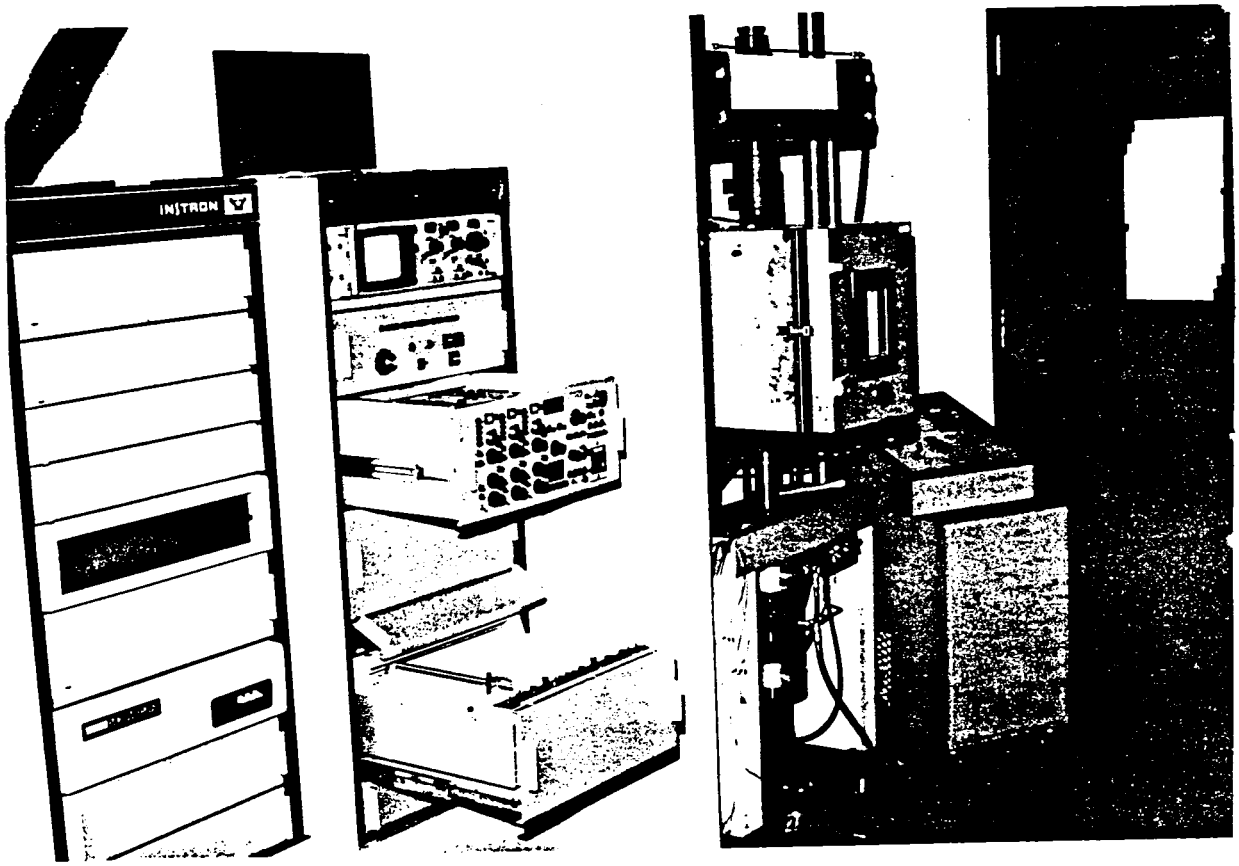

Figure 4.22 Servohydraulic Instron 1300 series testing machine with environmental chamber.

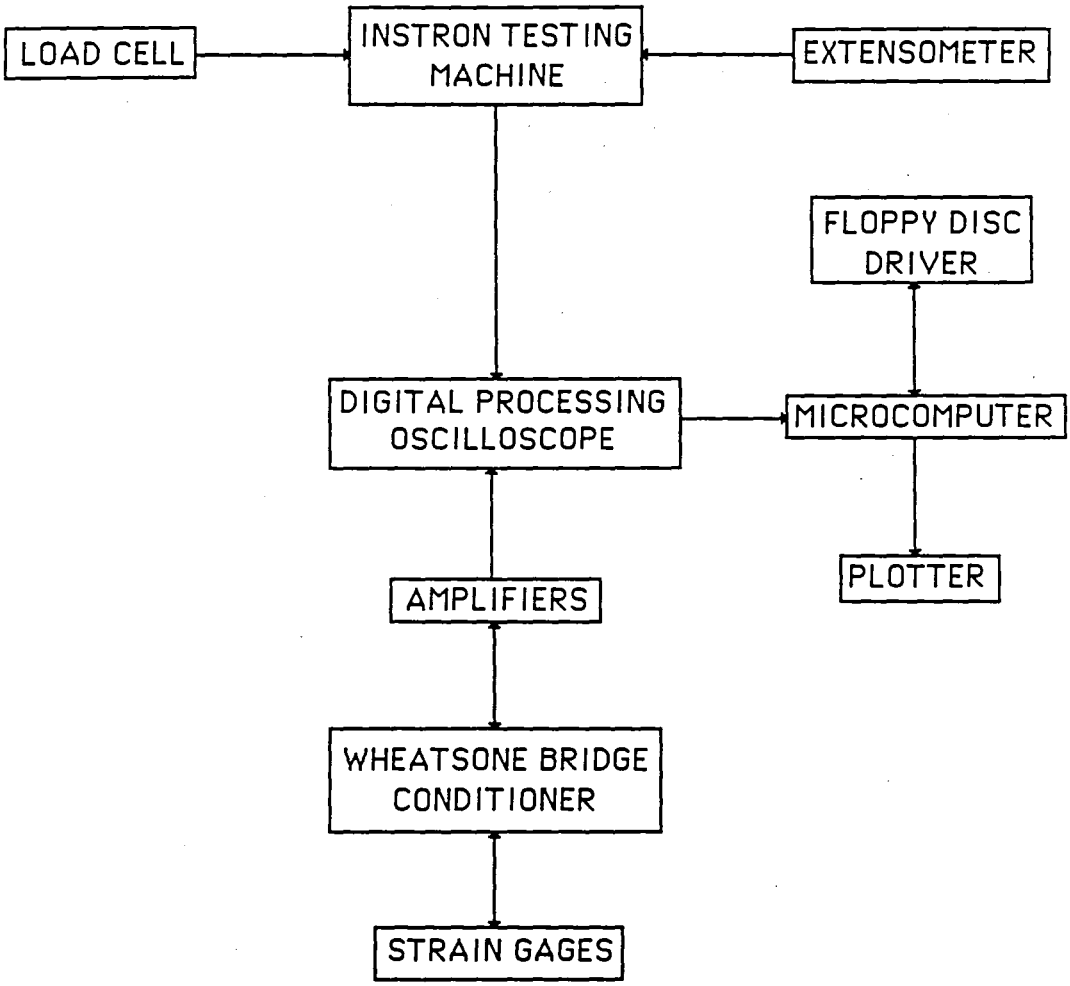

Figure 4.23 Configuration of data aquisition system.

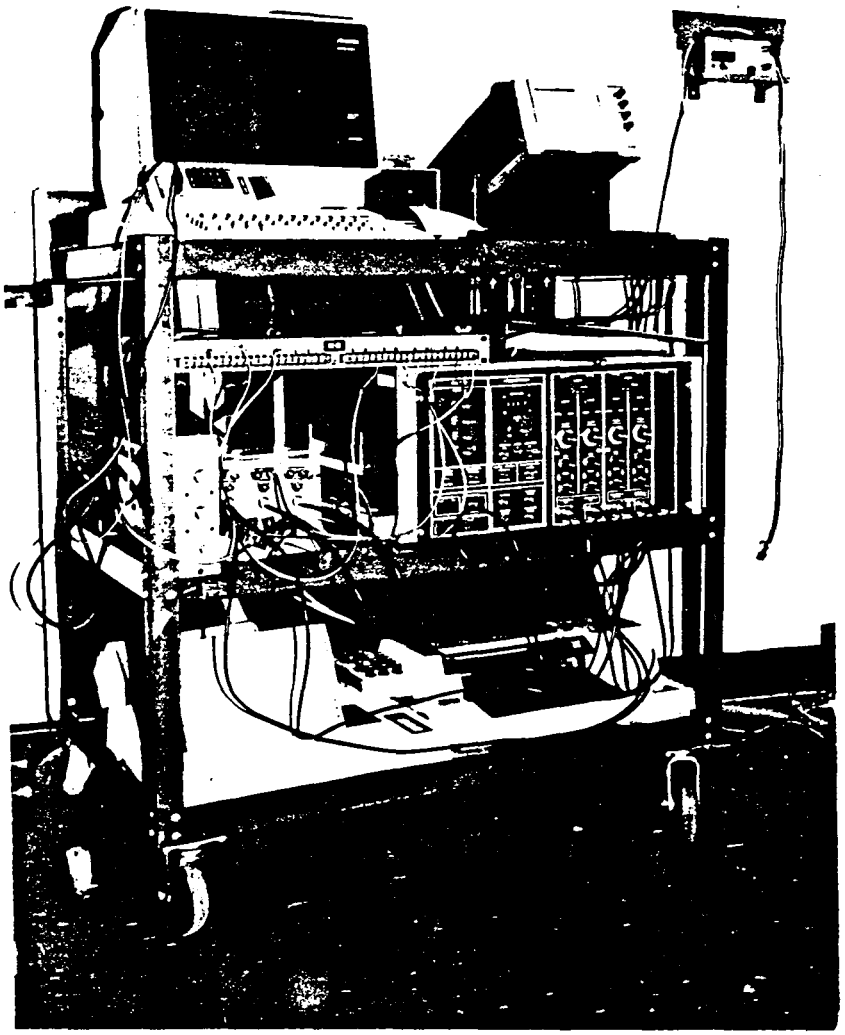

Figure 4.24 Data aquisition and processing system.

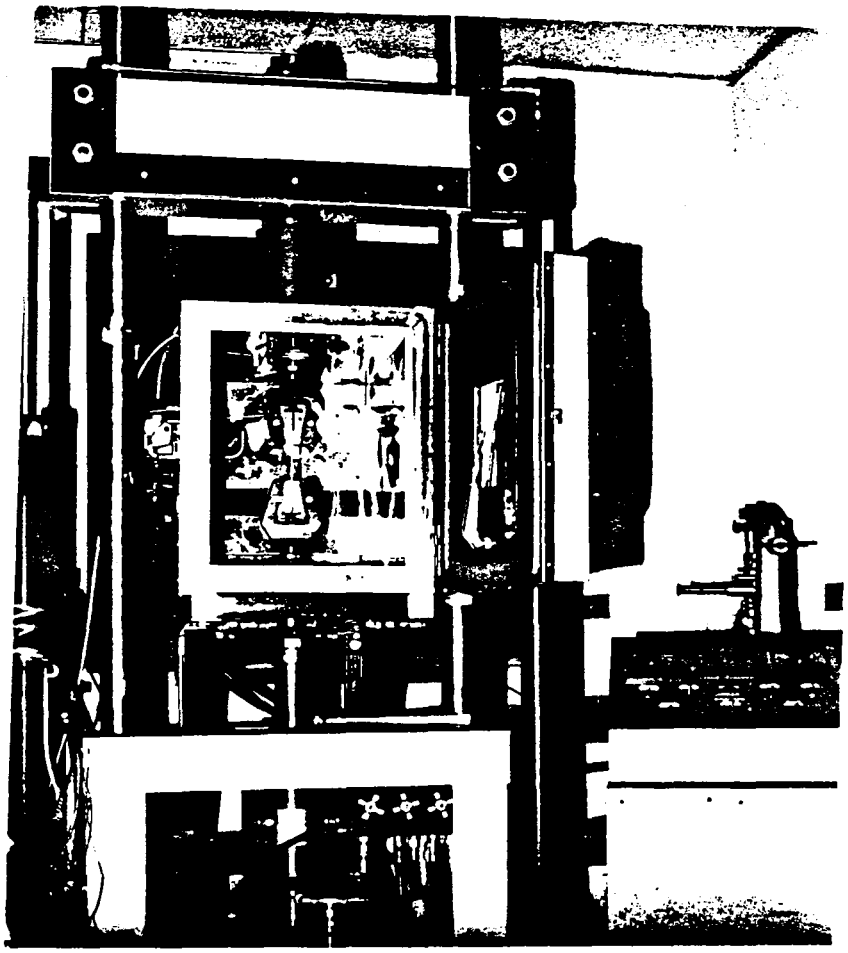

Figure 4.25 Composite specimen mounted on Instron testing machine, for high temperature/moisture testing inside environmental chamber.

V. RESULTS AND DISCUSSION

5.1. Embedded Etrain Gage Reliability.

As previously mentioned, encapsulated strain gages embedded within the specimen were used for strain measurements on wet (moisture conditioned) specimens. Since the embedded gage technique is not widely used, it was necessary to examine the method's reliability and consistency for tests performed under various hygrothermal and strain rate conditions, and to verify that the presence of gages within the composite laminate did not affect the material behavior in any way.

In sections 5.1.2 and 5.1.3 bellow, the results of the strain gage reliability tests along with a complete evaluation of the strain measurement technique are presented in detail.

5.1.1. Moisture Absorption Evaluation Tests.

In this stage, the ability of embedded gages to measure hygroscopic strains in a composite, without affecting the moisture absorption process was examined. The procedure for performing such experiments was previously described in sections 4.4.2 and 4.5.1.

Moisture content as a function of time for two specimens with embedded gages is shown in Figure 5.2. The conditioning phase took place in water at a temperature of 120°F (49°C). The data were normalized by plotting the percent weight gain (M) versus a reduced time parameter defined by:

$$t_r = (t/\pi)^{1/2}.(4/h) \qquad (5.1)$$

where

h = specimen thickness

t = time

t_r = reduced time parameter

Figures 5.1 and 5.2 indicate the presence of a non-Fickian anomaly. In Fickian diffusion, the absorption curves are linear for values of M less than 0.6 M_∞, and then became concave to the abscissa until M_∞ is reached. However, in graphs 5.1 and 5.2, the absorption curves have yet to come to an equilibrium moisture content and sudden jumps of moisture are observed at very long conditioning times where a gradual moisture equilibrium was expected. This phenomenon could have possibly been caused by moisture collecting in surface cracks and subsurface microvoids which were continually being formed during the weighing process by a cavitation mechanism. The process of removing the specimens from a 120°F (49°C) environment to room temperature for weighing and then returning them to a 120°F environment would expose the specimens to a mild thermal shock. This thermal shock could make the cavitation mechanism possible, and would be more pronounced in $[90_8]$ specimens as observed in Figure 5.1. Similar results were observed by Lifshitz [11] for conditioning at high temperatures. In the experiments performed in this work, non-Fickian anomalies were not as pronounced due to the relative low conditioning temperature. Lifshitz found that higher temperatures could considerably influence the material moisture absorpion pattern.

From Figure 5.2 and the relation

$$D = \frac{\pi}{16}\left(\frac{G}{t^{1/2}/h}\right)^2 \qquad (5.2)$$

where

$$G = \frac{M_t - M_0}{M_\infty M_0} = \frac{M_t}{M_\infty} \qquad (5.3)$$

and

M_t, M_0, M_∞ = moisture content at a time, t, zero and saturation respectively.

The diffusivity of both specimens was calculated from the Figure 5.2 to be

$$D = 4.31\ 10^{-11}\ in^2/s$$

for the $[90_8]$ specimen having equilibrium moisture content of 1.41%, and

$$D = 6.33\ 10^{-11}\ in^2/s$$

for the $[0_6]$ specimen having eqilibrium moisture content of 1.34%.

Next, the data of Figures 5.1 and 5.2 were plotted along with moisture absorption data obtained for specimens of various thickness and without embedded gages in Figures 5.3 and 5.4. From the reduced time graphs in Figure 5.4, it is evident that all specimens, with and without embedded gages, behave in a similar manner and have the same diffusivity D. It may be concluded, then, that the presence of embedded gages does not affect the moisture diffusion process.

Hygroscopic strains in the transverse to the fiber direction were measured using embedded gages and dial gages. All data were plotted against moisture content (M), as shown in Figure 5.5. Specimens, #17 and #11 contained embedded gages. The gage of specimen #11 was inactive, and hygroscopic strain was measured by a dial gage. Specimens #6 and #24 did not contain embedded gages and hygroscopic strain was also measured by means of a dial gage (Figure 4.20). The hygroscopic strain of specimen #17 containing an active embedded 2-gage rosette, was continually recorded through a Wheatstone bridge circuit on a data logger. From the graphs on Figure 5.5, it is obvious that embedded gages function properly and do not affect the hygroscopic stress state of the specimen since there is complete agreement between the hygroscopic strain readings obtained by both, the

embedded gage and the dial gage. Figure 5.5 will be used as a calibration curve for future moisture conditioning. This graph can also be used as a guide to insure the proper function of the embedded gages in conditioned specimens. This is achieved by comparing the embedded gage reading with the strain expected at that particular moisture content, as indicated by the calibration curve of Figure 5.5. These two values should show close agreement if the gage under consideration is functioning properly. The slope of the curve drawn through the data points of Figure 5.5 yields the transverse moisture expansion coefficient, β_2:

$$\beta_2 = (1/\rho_c)(d\varepsilon_H/dM) \qquad (5.4)$$

where

ρ_c = density of the composite specimen

$d\varepsilon_H/dM$ = slope of curve

For a density of 1.6 gr/cm^3 for AS4/3501-6 graphite/epoxy, β_2 was calculated to be 0.18 cm^3/gr which is in good agreement with published values for similar materials. Strain measurements in the fiber direction, with embedded gages, exhibited a scatter of 25-35% and yielded an average value of the order of β_1=0.01 cm^3/gr (Figure 5.6). This was expected since moisture has no effect on graphite fibers and the hygroscopic strain in this direction is the result of the swelling of the matrix restrained by the fibers. The high scatter was most likely due to inherent instabilities and high sensitivities to noise of the data aquisition system associated with high amplification of small strains. The possibility of using dial gages to record hygroscopic strains along the fibers was rejected as a very unreliable method. Strains in this direction were too small to be distinguished, and the human error involved in reading or in this case estimating such minute strain differences from the dial gage was larger than the

magnitude of the actual change. Such strains are very difficult to record and to the writer's knowledge no reliable values for the longitudinal moisture expansion coefficient have been published prior to this work.

It is obvious that all curves in Figures 5.5 and 5.6 show initially moisture content increase without the presence of hygroscopic strain. This is attributed to a rapid moisture absorption through microcrakcs to fill in material voids. Thus, the point where the hygroscopic strain versus moisture content curve intersects the abscissa gives an approximate value of the material void content.

5.1.2 Mechanical Loading Evaluation Tests.

The objective of this task was to examine the ability of embedded gages to measure mechanical strains without affecting the mechanical properties of the specimen. For this purpose, $[90_8]$ graphite/epoxy specimens were used since their mechanical behavior is mainly matrix controlled. These specimens would be most sensitive to the effects (if any) of embedding strain gages within the laminate.

Figure 5.7 shows typical stress-strain curves from quasi-static (strain rate of $5 \cdot 10^{-5}$ s^{-1}) tests for dry specimens. The mechanical strain of specimen #12 was measured by means of an embedded strain gage, a surface gage positioned directly "above" the embedded gage and an extensometer, carefully mounted such that both gages mentioned above would fall within it's gage length area. Specimen #9 was a reference specimen used for comparison and the strain was measured with an extensometer. It is clearly seen in Figure 5.7 that the results obtained by the three different strain measurement methods are in good agreement in terms of transverse modulus (E_{22}), transverse tensile strength (F_{2T}) and ultimate tensile strain ε_{2T}. This indicates that the embedded

gages record strains accurately and do not impair the integrity of the specimen. Furthermore, the stress-strain curves obtained with surface gages and the extensometer show some slight cuvature near the origin, possibly due to some straightening of the specimen. The curve for the embedded gage, however, is straight from the beginning, since the mid-surface of the specimen is not affected by this slight bending.

In order to evaluate embedded gage perfomance under moisture conditions, specimens conditioned to 0.35% moisture content were tested in uniaxial tension to failure at two strain rates, a quasi static strain rate of $5 \cdot 10^{-5}$ s^{-1} and a high rate of 5 s^{-1}. In both cases strains were measured with embedded gages and an extensometer. Stress-strain curves obtained under quasi-static loading (Figure 5.8) show excellent agreement between embedded gages and extensometer results for test specimen #10 and reference specimen #9. This is not true however, at high strain rates (Figure 5.9). Embedded gage results are relatively smooth and stable, whereas results from the extensometer test show large oscillations due to inertia effects on the extensometer itself. The small apparent fluctuations in the embedded gage results are attributed to the limitation of the servohydraulic machine, which is unable to control a ram function command at this rate.

From the above discussion, it can be derived that embedded gages provide a reliable, consistent and valid method for measuring strains under various hygromechanical conditions. Before accepting embedded gages as a solution to all our problems of measuring material properties under hostile environmental conditions, and as an additional measure of caution, thermal expansion tests were performed in order to study their behavior under thermal loading, the procedure of which has been explained in section 4.5. The results

are shown in Figures 5.10 and 5.11. The slopes of the curves give the thermal expansion coefficients for the material as:

$$\alpha_1 = \frac{\Delta\varepsilon_{11}}{\Delta T} = -7.2\ \mu\varepsilon/^oF \qquad (5.5)$$

$$\alpha_2 = \frac{\Delta\varepsilon_{22}}{\Delta T} = 12.3\ \mu\varepsilon/^oF \qquad (5.6)$$

where

$\Delta\varepsilon_{22}$, $\Delta\varepsilon_{22}$ = change in strain in principal material directions

ΔT = change in temperature

α_1, α_2 = thermal expansion coefficients along principal material axis

These values are in agreement with published values for similar material. These results indicate that embedded gages function properly at high ($75^oF<T<265^oF$) temperatures. Having the values of the thermal expansion coefficients may also prove useful as an alternate method (the other method is direct subtraction in the Wheatstone bridge by means of a reference specimen) for eliminating thermal strains from thermomechanical strain gage readings at high temperatures.

Thus far, a complete hygroscopic and thermal characterization of AS4/3501-6 graphite/epoxy has been conducted, and embedded gage reliablility, consistency and validity for measuring strains under various hygrothermomechanical service conditions was proven experimentally.

5.2 Mechanical Properties.

As previously mentioned, the scope of this work is to establish constitutive relations between time, temperature and moisture, and construct a complete and reliable data base to support a statement of a proposed HGTM theory. For this purpose a complete mechanical characterization of AS4/3501-6 graphite/epoxy was performed at various hygrothermal and strain rate conditions. The results of these tests are presented and explained in the following sections of this chapter.

5.2.1 Transverse Tensile Properties.

Transverse properties are expected to be highly affected by temperature, moisture and strain rate, since they are polymer-matrix-dominated [1-5]. Figures 5.12 to 5.15 show some typical stress-strain curves for dry specimens at room temperature and and various strain rates. The wavy shape of the stress-strain curves at the highest rates reflects the limitations of the testing machine and the inertia of the extensometer (whenever used) rather than true material behavior. Figure 5.16 shows the effect of strain rate on the transverse mechanical behavior of composites. Similarly, the effect of temperature is illustrated by typical stress-strain curves at different strain rates and temperatures for zero moisture content (dry) as shown in Figures 5.16 to 5.22. A more comparative graph of the stress-strain curves of these Figures, is shown in Figure 5.23 where the effect of temperature on material behavior is easily distinguished. The effect of moisture content is also pointed out by plotting stress-strain curves of wet specimens at various temperatures and strain rates as shown in Figures 5.24-5.27. Figure 5.28 which is a plot of stress-strain

curves for two similar specimens tested under the same thermomechanical conditions but at different moisture content levels, clearly shows this effect. The value of minor Poisson's ratio calculated from plots of the transverse strain versus longitudinal strain curves shown in Figures 5.29-5.34, should be considered as qualitative since the transverse strain was found to be of the same order of magnitude as the transverse sensitivity factor (k_t) of the gage used. It should be taken in mind that Figures 5.11-5.34 represent only a small sample of all the stress-strain, strain-strain, and strain-time curves prepared to evaluate the material transverse modulus (E_{22}), ultimate tensile strength (F_{2T}), ultimate tensile strain (ε_{2T}), minor Poisson's ratio (ν_{21}) and strain rate ($\dot{\varepsilon}_{22}$), which were 240 in total. A complete and detailed presentation of all data obtained for all hygrothermal and strain rate conditions tested are presented in Tables A-1 to A-18 in Appendix A. A summary of the average (from all performed tests) transverse properties for dry and wet specimens is given in Table 5.1.

In order to utilize the information contained in Tables A-1 to A-18, and to clearly see the effect that the three parameters under consideration have on material behavior (a sample of which was given in Figures 5.11-5.34), plots of material property versus strain rate were constructed for every tested temperature and moisture condition. Figures 5.35-5.38 show the effects of strain rate and elevated temperature on the transverse modulus (E_{22}). In this case, the values of E_{22} shown are initial values, as the modulus was observed to decrease as the load approached failure (Figures 5.11-5.26).

From the same Figures (5.11-5.26) it is deduced that transverse modulus increases with strain rate at a given temperature which is a common characteristic of many polymers. By comparing Figures 5.35 and 5.37 (dry

specimens) to Figures 5.40 and 5.41 (wet specimens) it is observed that the transverse modulus (E_{22}) of wet specimens is lower than that for dry specimens. Although a similarity exists between temperature and moisture effects on E_{22}, it is obvious that the effect of moisture is not as distinct as that of temperature. Thus, the modulus of the material is more sensitive to temperature changes (Figure 5.39) and the 1% moisture content shows negligible effects on this property (approximately 5% decrease). This small effect will become more pronounced when shift factors are introduced later in this section.

The ultimate properties, namely the transverse tensile strength (F_{2T}) and strain (ε_{2T}) do not exhibit such a uniform trend as the modulus (Figures 5.42-5.49). These properties tend to decrease with increasing strain rate at low temperatures, and increase with strain rate at high temperatures for dry specimens, and consistently decrease with strain rate for wet specimens, (Figures 5.50- 5.53).

The effect of temperature on ultimate properties is shown from Figures 5.42-5.53 for both dry and wet specimens to be similar to that on modulus. Specifically, both F_{2T} and ε_{2T} decrease with increasing temperature but not significantly. Of greater interest is the effect of moisture on these properties as seen in Figures 5.50-5.53. When compared to similar graphs at zero moisture, a high decrease of properties, of the order of 25%, is observed. Thus, moisture has a higher effect on F_{2T} and ε_{2T} than temperature, although a similar pattern between their influences is also observed. Minor Poisson's ratio was not included in this discussion due to its characteristic high scatter. The plasticizing effect of moisture on all transverse properties, along with their degradation due to high temperatures is evident from the above discussion.

It was previously mentioned that a similarity in the influence pattern of moisture and temperature on transverse properties was observed. Taking into consideration the existence of a time-temperature equivalence, the possiblity of a time-moisture, and even a time-temperature-moisture equivalence seems possible at this point. For this purpose, all curves, for dry and wet specimens separately were shifted horizontally (with respect to time) toward one of the curves which serves as a reference, and in this case was the room temperature curve. Thus, time-temperature master curves for both moisture conditions were constructed. The amount each individual property versus strain rate curve is shifted, is commonly known as the time-temperature shift function $\log(a_T)$. Similarly, the shifting may be done with respect to moisture, i.e., shifting curves obtained from specimens of different moisture content, but same temperature, toward a reference one, in this case the zero moisture content curve, to form a time-moisture master curve. The amount each curve is shifted is the time-moisture shift function $\log(a_H)$. The values of $\log(a_T)$ and $\log(a_H)$ for all the properties versus strain rate curves obtained, are shown in Tables 5.2 and 5.3 respectively.

From the values of these shift functions, one can easily see the effect of temperature or moisture on a certain material property. For example, the values of $\log(a_H)$ for ultimate transverse strain in Table 5.3, are 3.4 for room temperature, and 5.14 for 91°C (196°F). While the corresponding values for transverse modulus are zero for room temperature and 1.0 for 91°C (196°F). This indicates that moisture content has a higher effect on ε_{2T} than on E_{22}. By comparing the signs of $\log(a_H)$ and $\log(a_T)$ (positive or negative) in Tables 5.2 and 5.3 for a certain property, it is possible to distinguish a similarity in the influence pattern of temperature and moisture on material property, and thus

establish temperature and moisture constitutive relations, which will eventually lead to a time-temperature-moisture supermaster curve.

Time-temperature master curves were drawn for both dry and wet specimens in Figures 5.54-5.59. From these curves it is clearly seen that temperature is interchangeable with strain rate, i.e. the higher the temperature, the lower is the equivalent strain rate. Figures 5.60-5.62 show the logarithm of the time-temperature shift factor $\log(a_T)$, plotted versus temperature (T) for dry and wet specimens. In all cases the shifting is negative, i.e., higher temperature and/or moisture are equivalent to lower strain rates, and the traditional straight line may fit them all.

Time-moisture master curves are shown in Figures 5.63-5.68. These Figures emphasize the reduction of wet properties over the corresponding dry properties. The resulting time-moisture shift function curves, $\log(a_H)$ versus moisture content (C) are shown in Figures 5.69-5.71. Since shifting, in this case, is based on two points only, the curves show qualitative trends rather than true full range behavior.

Finally, time-temperature and time-moisture master curves were combined by shifting to room temperature, and dry state reference point. Time-temperature-moisture super-master curves were drawn for the transverse modulus (E_{22}), transverse tensile strength (F_{2T}) and ultimate tensile strain (ε_{2T}), as shown in Figures 5.72-5.74. From these curves it is seen, as mentioned previously, that both moisture and temperature are interchangeable with strain rate. These Figures also support the existence of a complete HGTM theory describing the natural behavior at a wide range of strain rate and/or temperature and moisture content. From these curves it is observed that the modulus increases gradually with strain rate as expected from previous works

[2,11,30]. The behavior of the transverse tensile strength (F_{2T}) and the transverse tensile strain (ε_{2T}) is different from that of modulus (E_{22}), but similar among each other. Initially, they both increase with strain rate, however at a strain rate of about 10^{-6} s^{-1} they reach a local maximum, and thereafter the trend is reversed. This phenomenon can be explained by the fact that, like most polymers, the failure mechanism associated with low rates is crazing, whereas at high rates it is cracking. The crazing failure load usually increases with loading rates up to the point where the crazes develop into cracks. This occurs because the loading rate is too high to allow the polymeric material to flow into the crazing zone. This phenomenon has been reported in the literature for polymers [31] and composites [1,32].

An interesting result is observed from the curves for transverse ultimate properties. It seems as if moisture is equivalent to higher strain rates, while temperature was found to affect properties in the opposite direction. This can also be seen from the opposite sign between a_T and a_H for these properties in Tables 5.2 and 5.3. However, since these properties indeed show a reduction with strain rate for dry specimens (for rates above 10^{-6} s^{-1}), the lower values obtained for wet specimens are indeed equivalent to higher rates (Figures 5.65-5.68). These results are reflected as positive slopes of the time-moisture shift function ($\log a_H$) curves in Figures 5.69-5.71.

Figure 5.75 shows the logarithm of the time-temperature shift factor, $\log(a_T)$, of all transverse properties, plotted against temperature (T) for both dry and wet specimens. In all cases the shifting is negative, i.e., higher temperature is equivalent to lower strain rates. The logarithm of the time-temperature shift factor, ($\log a_T$), is linearly related to the temperature, as commonly found in the literature, for room and intermediate temperatures only [30]. However, re-

examining the results at the highest test temperature of 128°F reveals that these points are off the straight line, as can be seen also in Figure 5.75. Recalling that the glass transition temperature (Tg) of the resin is approximately 130°C (248°F) explains the accelerated degradation in properties. Thus, it seems more appropriate to fit a second or higher order curve to the experimental data, on this semi-log scale, rather than a straight line. A second order curve describes the behavior of the transverse properties better over a wider range of temperatures. Moreover, this curve resembles perfectly the property curve over the transition region, also plotted on a semi-log scale. The range of temperatures where a straight line is fitted, corresponds to the glassy plateau whereas higher order curves may include the glass transition temperature.

According to the data presented in this section, it seems possible to describe the complete hygrothermomechanical response of a composite, the method of which is proposed and discussed in section 5.4.

5.2.2 In-Plane Shear Properties.

As seen in section 5.2.1 matrix dominated properties are sensitive to temperature and moisture content. Thus, in-plane shear properties namely the shear modulus (G_{12}), the shear strength (F_{12}), and the ultimate shear strain (γ_{12}), which are expected to reflect the effects of both matrix and fiber-matrix interface, will be highly affected by these external parameters. Typical shear stress-strain curves at various rates and temperatures are shown in Figures 5.76-5.83 for dry specimens. In general, the behavior in shear is similar to that in transverse tension. The shear properties are lower at elevated temperature, and higher at high strain rates. These observations could be better seen in Figures 5.88-5.99 where shear properties are plotted versus strain rate for dry specimens.

Figures 5.88-5.99 clearly show the stiffenning effect of strain rate on shear modulus (G_{12}). From Figure 5.91 it is evident that at higher temperatures, the stiffenning effect is more pronounced. This could be explained by the fact that higher temperatures tend to decrease the modulus, as seen in Figures 5.88-5.91, and the strengthing effect of high strain rates is more dominant at high temperatures. Of all shear properties, the ultimate shear strain seems to be the least affected by either temperature or strain rate. In fact, the shear strain increases slightly with increasing strain rate at high temperatures, and decreases at low temperatures. The shear strength (F_{12}) and shear modulus (G_{12}) are more sensitive to temperature and strain rate in a monotonic way.

Wet properties are also plotted versus strain rate at room and elevated temperatures (Figures 5.100-5.105). In all cases, the effect of moisture on the shear properties at room temperature is negligible, and the values obtained are the same as the corresponding dry specimen results. The combined condition of both high temperature and moisture has a considerable effect, and 20%-30% reduction in shear strength and shear modulus is observed. A summary of the average in-plane shear properties for dry and wet specimens is given in Table 5.4. The values, presented in this Table are average values obtained from a total number of 100 mechanical tests performed at various strain rates, temperatures, and moisture content. A sample of the data obtained is presented in Figures 5.76-5.87. The bulk of the data obtained was not possible to include within this work. All other shear stress versus shear strain, and shear strain versus time curves can be found in the Appendix of reference [33]. However, all the values obtained from these graphs are presented in Tables A-13 to A-36 in Appendix A.

To construct time-temperature master curves, the corresponding shift factors had to be evaluated. For this purpose, all curves for dry and wet specimens were, separately, shifted horizontally toward one of the curves. As in the case of 90° specimens, room-temperature, and dry and wet conditions (where applicable), were chosen as a reference to form time-temperature master curves for both moisture conditions. The amount each individual property versus strain rate curve is shifted is the time-temperature shift factor $\log(a_T)$. Similarily, the shifting was done with respect to moisture, i.e., shifting curves obtained from specimens of different moisture content, but same temperature, toward a reference one, in this case the zero moisture content curve. Thus, time-moisture shift factors were obtained. The values of $\log(a_T)$ and $\log(a_H)$ for all property versus strain rate curves presented here are shown in Tables 5.5 and 5.6, respectively.

The corresponding $\log(a_T)$ versus temperature curves for in-plane shear properties are shown in Figures 5.106-5.108. Again it is observed, from the summarizing graph of $\log(a_T)$ versus temperature (Figure 5.109) for all in-plane shear properties, that the results are similar to those obtained for the transverse tensile tests (Figure 5.75), and that the shift function seems to follow a second order curve. It is also obvious from the negative shifting in Figure 5.75 that higher temperatures are equivalent to lower strain rates. The corresponding $\log(a_H)$ versus moisture content curves for in-plane shear properties are shown in Figures 5.110-5.112. Since moisture has small effects on the in-plane shear properties, and the in-plane shear strength (F_{12}) and ultimate strain (γ_{12}) exhibited relatively wide scatter (Figures 102-105), difficulties were encountered while moisture shifting, and Figures 5.110-5.112 should be taken only as indicators of the moisture shift trend rather than accurate time-moisture

shift function data. Also, the fact that these curves consist of only two data points indicates their limitation.

Time-temperature master curves for dry and wet specimens are shown in Figures 5.113-5.118. As has been observed earlier, G_{12} and F_{12} decrease with moisture and temperature, and increase with strain rate. Similar results for in-plane shear properties had been observed and reported by Daniel [1,2,28]. The reduction of these properties for hot wet specimens is highly pronounced. The irregularity of the high increase in ultimate shear strain at high rates and temperatures of wet specimens is questionable, and necessitates additional testing at these extreme conditions.

Finally, time-temperature and time-moisture curves were combined to form the time-temperature-moisture super-master curves using dry and room temperature conditions as a reference (Figures 5.119-5.121). As seen from the individual master curves, the behavior in shear is similar to that in transverse tension. Nevertheless, experimental results of the in-plane shear properties are more scattered than other properties due to the sensitivity of the matrix-fiber interface to high moisture and temperature conditions. For example, the ultimate shear strain decreases slightly and monotonically with increasing strain rate. However, the results for the highest rate, at high temperature and moisture content, show an abrupt jump which can be attributed to the unsteady nature of the shear stress-strain behavior at these conditons, and to a possible measurement failure.

Similar effects of moisture, temperature, and strain rate on material behavior, as discussed above, have also been reported by Lifshitz [11] and Browning [13]. Of most importance in the results presented thus far for both transverse and shear properties, is the behavior of the shift factor ($\log a_T$). From

the $\log(a_T)$ versus temperature curves it is obvious that a function can be fitted to these data, thus making possible the prediction of the temperatue shift factor at any temperature (T). It is thus obvious, that thanks to the time-temperature equivalence principle, material behavior at a certain temperature and over a wide strain rate range can be predicted. Similar observations can be made for time-moisture equivalence through time-moisture master curves. Although in the present work only two moisture levels were investigated, and these results standing alone cannot support any general conclusions, it is possible to extend the current data base by including results obtained by other experimentalists [11]. In such a case it is observed that in a wider data domain, moisture does indeed follow the behavioral trend observed at the two moisture levels tested. Thus, in general, moisture effects may be considered similar to those of temperature, as previously mentioned, and graphically presentd by Lifshitz [11], and reported here in Figures 5.122 and 5.123.

5.2.3. Longitudinal Tensile Properties.

As seen in sections 5.1.3, both moisture and temperature tend to reduce matrix dominated mechanical properties. On the other hand, fiber dominated properties are not expected to change with temperature or moisture since graphite fibers remain virtually unaffected by these parameters. Typical stress-strain and transverse strain versus longitudinal strain curves for strain rates of 10^{-3} s^{-1} to 5 s^{-1} and temperatures of 22°C (72°F), 77°C (140°F), 91°C (196°F) and 128°C (263°F) are shown in Figures 5.124-5.139. All stress-strain curves are close to a straight line, except for a slight increase in slope as the load increases. Similar effects were observed by Lifshitz [11] and Sendeckyj et al [34]. This stiffening effect is an inherent property of graphite fibers [52] whose

proposed empirical stress-strain model is of second order ($\sigma=E_o\varepsilon+F\varepsilon^2$) where E_o and F are determined using a least square fit on the stress-strain data pairs. E_o is the initial modulus, and F is a measure of the degree of nonlinearity of the stress-strain curve. An explanation for the carbon fiber's increase in modulus has been proposed by Ruland [53]. Ruland's model of elastic unwrinkling assumes that the graphitic layers of a carbon fiber are linked together to form long, wrinkled ribbons along the fiber axis. A stress on the ribbons will increase the preferred orientation of the individual layers; therefore, the stiff axis of the individual layers is more closely alinged with the fiber axis leading to an increased fiber modulus. Except for this small variation, the longitudinal modulus (E_{11}) tends to increase slightly with both temperature and strain rate as seen from Figures 5.140-5.143 for dry specimens and Figures 5.144-5.145 for wet specimens. Moisture seemed to have a slight affect on modulus as seen in Figures 5.144-5.145 and represented by the small positive time-moisture shift factors $\log(a_H)$ as shown in Table 5.9. From Figures 5.146-5.151 where longitudinal strength is plotted versus strain rate, it is observed that temperature has almost no effect on this property. Moisture, on the other hand, was found to affect F_{1T} at both temperatures tested as seen from Figures 5.146, 5.148 and 5.150-5.151. The time-moisture shift factors $\log(a_H)$ shown in Table 5.9 show a slight increase of longitudinal tensile strength (F_{1T}) with moisture. This may be attributed to a possible uneven stress distribution accross the specimen which leads to failure of some fibers at an early stage of the loading process. At low temperatures and in dry specimens, the matrix material is more brittle, and thus, more sensitive to stress concentrations around broken fibers. This would result in the slightly lower observed laminate strength and a possible increase in data scatter. At higher temperatures and moisture content, the matrix material is

more ductile and less sensitive to stress concentration around broken fibers. This increase in ductility is also observed in the ultimate tensilte strain (ε_{1T}) versus strain rate curves shown in Figures 5.152-5.155 for dry specimens, and Figures 5.156-5.157 for wet specimens. It must be noted at this point that the property changes reported here are of the order of 5%-10%, and could be subject to the experimentalist's judgement. Similarly, no changes were recorded for the major Poisson's ratio (v_{12}) presented in Figures 5.158-5.161 plotted versus strain rate for dry, and in Figures 5.162-5.163 for wet specimens.

Average values for all longitudinal properties are presented in Table 5.7. Coresponding property values for all tests performed in this material direction are presented in Tables A-36 to A-52 in Appendix A. In order to construct time-temperature master curves, the coresponding shift factors were evaluated by shifting all property curves horizontaly (along the strain rate axis) toward the reference curve, which again in this case was the room temperature, dry and wet curves for dry and wet data, respectively. All time-temperature shift factors, $\log(a_T)$, are presented in Table 5.8, and graphicaly plotted versus temperature for both moisture conditions tested in Figures 5.164-5.167. Similarly, the corresponding time-moisture shift factors, $\log(a_H)$, are presented in Table 5.9, and plotted versus moisture condition for 22°C (72°F) and 91°C (196°F). Although fibers are not expected to behave as thermorheologically-simple materials, the logarithm of the time-temperature shift factors is linearly related to temperature for both dry and wet specimens. As previously mentioned, time-moisture shift factors shown in Figures 5.168-5.171 should be considered as qualitative since they are based on two points only.

Using the above shift factors, time-temperature master curves were constructed and presented in Figures 5.172-5.179 for all longitudinal properties

of dry (0% moisture) and wet (1% moisture) specimens, using room temperature as a reference point. Similarly, Figures 5.180-5.187 were constructed showing time-moisture master curves having dry condition as a reference point. In Figures 5.188-5.191, all master curves were combined to form time-temperature-moisture super-master curves of the longitudinal properties, using room-temperature and dry condition as a reference. In general from the results presented here, it can be said that the average longitudinal properties, i.e., modulus (E_{11}) and major Poisson's ratio (v_{12}) are similarly affected by moisture and temperature. These properties are shifted to the right. The increase with temperature and moisture, although small, implies that accelerated tests can be conducted at higher temperatures and moisture contents to predict these properties at higher strain rates. As far as the ultimate properties are concerned, i.e., strength (F_{1T}) and strain (ε_{1T}), the changes are within the experimental scatter and no definite conclusion can be drawn.

5.4. Time-Temperature-Moisture Superposition.

In the previous sections, time-temperature, time-moisture and time-temperature-moisture constitutive relations were established. Shift factors, $\log(a_T)$ and $\log(a_H)$ have been evaluated and plotted versus temperature and moisture content for all material properties. These curves were not fitted, and shift functions have not yet been drawn at this point. The most interesting result thus far is the experimental proof of the above constitutive relations which enables one to obtain a complete property curve at a certain hygrothermal condition over a wide range of strain rate, otherwise non-accessible to the

researcher. These constitutive relations may allow the experimentalist to obtain meaningfull material property data under a certain set of loading conditions, from similar data at another set of loading conditions, if the shift factor between these two states is known. In this work, it was found that keeping one of the condition variables constant while shifting with respect to the second to a reference, and then keeping the second constant while shifting with respect to the first to a reference, will yield the same total shift factor as starting with the second variable in the first place. This equivalence may be expressed as follows:

$$\log[a_{(H1,T)}] + \log[a_{(H,To)}] = \log[a_{(H,T1)}] + \log[a_{(Ho,T)}] \qquad (5.1)$$

where

H_o, H_1 = reference and fixed moisture levels, respectively

T_o, T_1 = reference and fixed temperatures, respectively

H , T = variable moisture and temperature, respectively

In other words, through equation 5.1 it is possible to "transfer" a certain set of data at one set of hygrothermal service conditions to another, merely by knowing the corresponding shift factors. This procedure is schematically shown in Figure 5.192. Examples of the applications of equation 5.1 are also given in Figure 5.192. In this case, it is desired to transfer a set of data obtained under 91°C (196°F) and 1% moisture content, to the reference state of 22°C (72°F) and 0% moisture content by following two different paths. All necessary shift factors are given in Tables 5.2-5.3 for transverse tensile properties, Tables 5.5-5.6 for in-plane shear properties, and Tables 5.8-5.9 for longitudinal tensile properties. Equation 5.1 in this case becomes:

$$\log[a_{(1\%,\,T)}] + \log[a_{(H,\ 72^{o}F)}] = \log[a_{(H,\ 196^{o}F)}] + \log[a_{(0\%,\,T)}] \qquad (5.2)$$

Equation 5.2 states that shifting the data from

196°F & 1% C --to-- 72 °F & 1% C --to-- 72°F & 0% C

is the same as shifting the same data from

196°F & 1% C --to-- 196°F & 0% C --to-- 72°F & 0% C

In Figure 5.193, The appropriate shift factors were substituted in equation 5.2 for transverse, modulus (E_{22}), tensile strength (F_{2T}), ultimate strain (ε_{2T}), shear modulus (G_{12}) and shear strength (F_{12}), which are matrix dominated properties and thus most sensitive to service conditions. As seen in Figure 5.193, the two paths taken show shift factor agreement within 10% for all properties except for G_{12} which showed agreement within 18%. These are acceptable values, and better agreement was not expected since all shift factors have an inherent error of approximately 10% due to human error in shifting the data which also are subjected to an experimental deviation of the order of 10%.

From the above discussion, the validity of equation 5.1 is established, and concequently a new procedure for determining the HGTM behavior of graphite/epoxy composites has been introduced. This method shows excellent correlation with experimental data, and brings us one step closer in developing a complete theory for predicting material behavior under any set of service conditions.

Table 5.1. Average transverse tensile properties for unidirectional AS4/3501-6 Graphite/Epoxy.

PROPERTY	STRAIN RATE	0% MOISTURE			1% MOISTURE	
		22°C(72°F)	60°C(140°F)	91°C(196°F)	22°C(72°F)	91°C(196°F)
Transverse Modulus, E_{22}, GPa(Msi)	High	11.9(1.73)	11.0(1.60)	10.7(1.56)	11.9(1.72)	11.4(1.66)
	Low	10.0(1.45)	10.9(1.58)	10.1(1.47)	11.6(1.68)	9.2(1.33)
Transverse Tensile Strength, F_{2T}, MPa(Ksi)	High	59.3(8.60)	62.9(9.07)	60.7(8.80)	40.8(5.92)	37.7(5.46)
	Low	64.2(9.30)	59.0(8.55)	54.8(7.94)	47.9(6.95)	31.0(4.50)
Ultimate Transverse Tensile Strain, ε_{2T}, %	High	0.52	0.52	0.52	0.33	0.36
	Low	0.64	0.56	0.54	0.40	0.34
Minor Poisson's , Ratio, ν_{21}	High	0.014	0.017	0.014	0.011	0.015
	Low	0.012	0.015	0.015	0.020	

Table 5.2. Time-temperature shift functions, $\log a_T$, for transverse tensile properties of AS4/3501-6 Graphite/Epoxy at 0 % (Dry), and 1 % (Wet) moisture content.

Temperature °C (°F)	E_{2T}		F_{2T}		ε_{2T}	
	Wet	Dry	Wet	Dry	Wet	Dry
22 (72)	0.00	0.00	0.00	0.00	0.00	0.00
60 (140)		-1.20		-1.00		-1.66
91 (196)	-2.20	-3.20	-0.82	-1.60	-1.00	-2.91
128 (263)		-5.22		-4.30		-6.00

Table 5.3. Time-moisture shift functions, $\log a_H$, for transverse tensile properties of AS4/3501-6 Graphite/Epoxy at 22°C (72°F), and 91°C (196°F).

Moisture Content	E_{2T}		F_{2T}		ε_{2T}	
	72°F	196°F	72°F	196°F	72°F	196°F
0 %	0.00	0.00	0.00	0.00	0.00	0.00
1 %	0.00	1.00	3.50	4.00	3.34	5.14

Table 5.4. Average in-plane shear properties for unidirectional AS4/3501-6 Graphite/Epoxy.

PROPERTY	STRAIN RATE	0% MOISTURE			1% MOISTURE	
		22°C(72°F)	60°C(140°F)	91°C(196°F)	22°C(72°F)	91°C(196°F)
In-Plane Shear Modulus G_{12}, GPa(Msi)	High	8.9(1.29)	7.0(1.01)	7.6(1.10)	8.9(1.30)	6.1(0.88)
	Low	7.2(1.05)	6.3(0.92)	7.0(0.95)	8.6(1.25)	7.0(1.02)
In-Plane Shear Strength, F_{12}, MPa(Ksi)	High	83.(12.1)	93.(12.5)	85(12.3)	80(11.7)	67(9.7)
	Low	76.(11.0)	73.(10.6)	73(10.5)	76(11.0)	57(8.3)
Ultimate In-Plane Shear Strain, γ_{12}, %	High	1.14	1.38	1.48	1.15	2.20
	Low	1.15	1.39	1.50	1.14	1.49

Table 5.5. Time-temperature shift functions, $\log a_T$, for in-plane shear properties of AS4/3501-6 Graphite/Epoxy at 0 % (Dry), and 1 % (Wet) moisture content.

Temperature °C (°F)	G_{12}		F_{12}		γ_{12}	
	Wet	Dry	Wet	Dry	Wet	Dry
22 (72)	0.00	0.00	0.00	0.00	0.00	0.00
60 (140)		-1.20		-0.75		-2.50
91 (196)	-2.22	-1.80	-2.70	-1.75	5.68	-4.20
128 (263)		-4.30		-3.60		-6.50

Table 5.6. Time-moisture shift functions, $\log a_H$, for in-plane shear properties of AS4/3501-6 Graphite/Epoxy at 22°C (72°F), and 91°C (196°F).

Moisture Content	G_{12}		F_{12}		γ_{12}	
	72°F	196°F	72°F	196°F	72°F	196°F
0 %	0.00	0.00	0.00	0.00	0.00	0.00
1 %	0.75	0.00	-1.50	-2.60	0.00	1.14

Table 5.7. Average longitudinal tensile properties for unidirectional AS4/3501-6 Graphite/Epoxy.

PROPERTY	STRAIN RATE	0% MOISTURE			1% MOISTURE	
		22°C(72°F)	60°C(140°F)	91°C(196°F)	22°C(72°F)	91°C(196°F)
Longitudinal Modulus, E_{11}, GPa(Msi)	High	147(21.3)	152(22.1)	155(22.5)	148(21.6)	147(21.3)
	Low	143(21.8)	147(21.4)	142(20.7)	145(21.1)	153(22.5)
Longitudinal Tensile Strength, F_{1T}, MPa(Ksi)	High	2340(339)	2360(342)	2410(349)	2210(320)	2200(319)
	Low	2410(439)	2250(326)	2330(337)	2200(318)	2300(334)
Ultimate Longitudinal Tensile Strain, ε_{1T}, %	High	1.42	1.48	1.60	1.46	1.51
	Low	1.55	1.45	1.50	1.43	1.48
Major Poisson's, Ratio, v_{12}	High	0.26	0.27	0.30	0.29	0.27
	Low	0.27	0.32	0.35	0.28	0.33

Table 5.8. Time-temperature shift functions, $\log a_T$, for longitudinal tensile properties of AS4/3501-6 Graphite/Epoxy at 0 % (Dry), and 1 % (Wet) moisture content.

Temperature	E_{11}		F_{1T}		ε_{1T}		ν_{12}	
°C (°F)	Wet	Dry	Wet	Dry	Wet	Dry	Wet	Dry
22 (72)	0.00	0.00	0.00	0.00	0.00	0.00	0.00	0.00
60 (140)		1.20		0.00		0.35		0.25
91 (196)	2.22	2.00	-1.18	0.00	0.00	0.70	2.00	0.40
128 (263)		3.00		0.00		1.80		1.00

Table 5.9. Time-moisture shift functions, $\log a_H$, for longitudinal tensile properties of AS4/3501-6 Graphite/Epoxy at 22°C (72°F), and 91°C (196°F).

Temperature	E_{11}		F_{1T}		ε_{1T}		ν_{12}	
°C (°F)	72°F	196°F	72°F	196°F	72°F	196°F	72°F	196°F
0 %	0.00	0.00	0.00	0.00	0.00	0.00	0.00	0.00
1 %	0.76	1.25	4.00	3.00	0.00	0.00	0.00	0.00

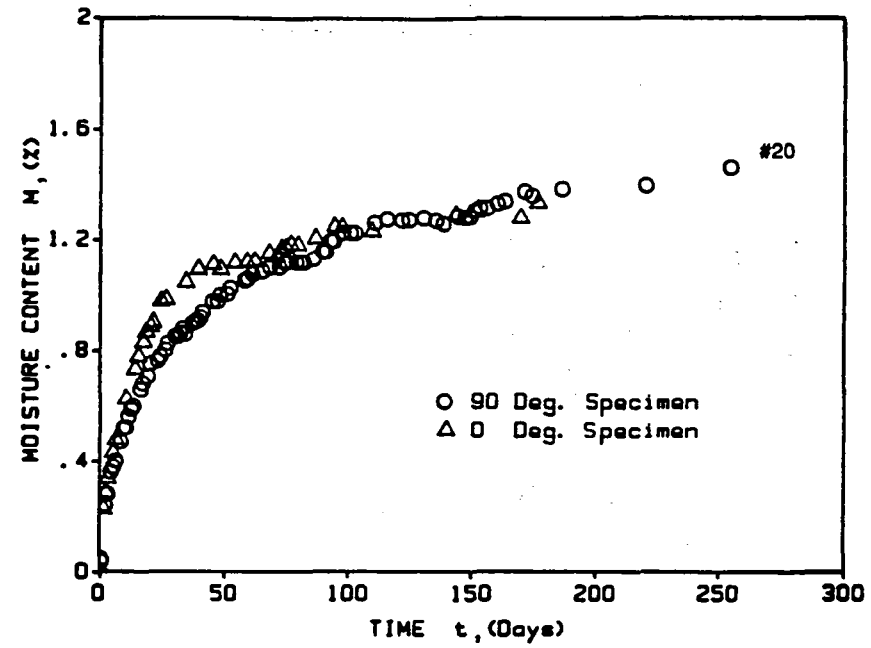

Figure 5.1 Moisture absorption for unidirectional AS4/3501-6 Graphite/Epoxy composite at 100% relative humidity and 49°C (120°F)

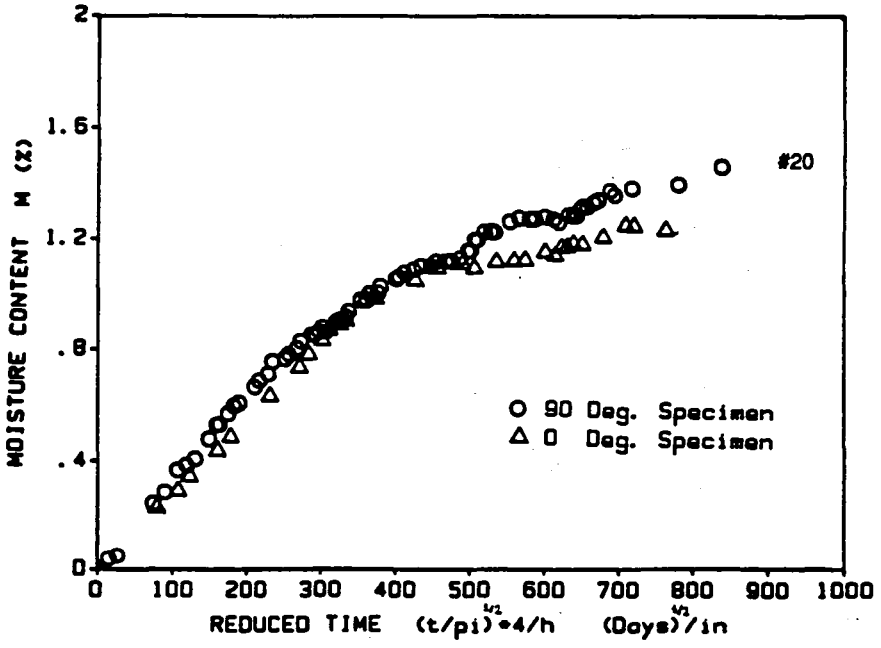

Figure 5.2 Reduced moisture absorption plot for unidirectional AS4/3501-6 Graphite/Epoxy

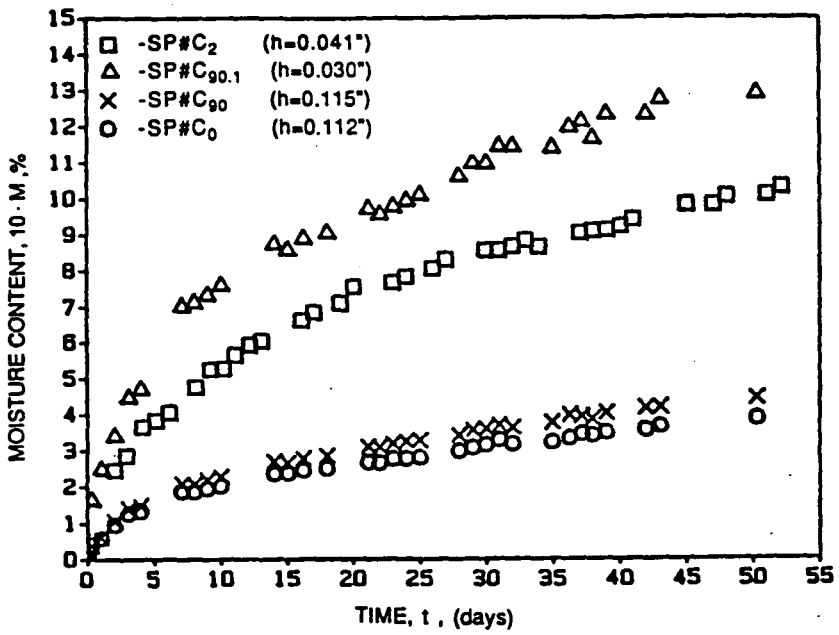

Figure 5.3 Moisture content as a function of time for unidirectional AS4/3501-6 Graphite/Epoxy

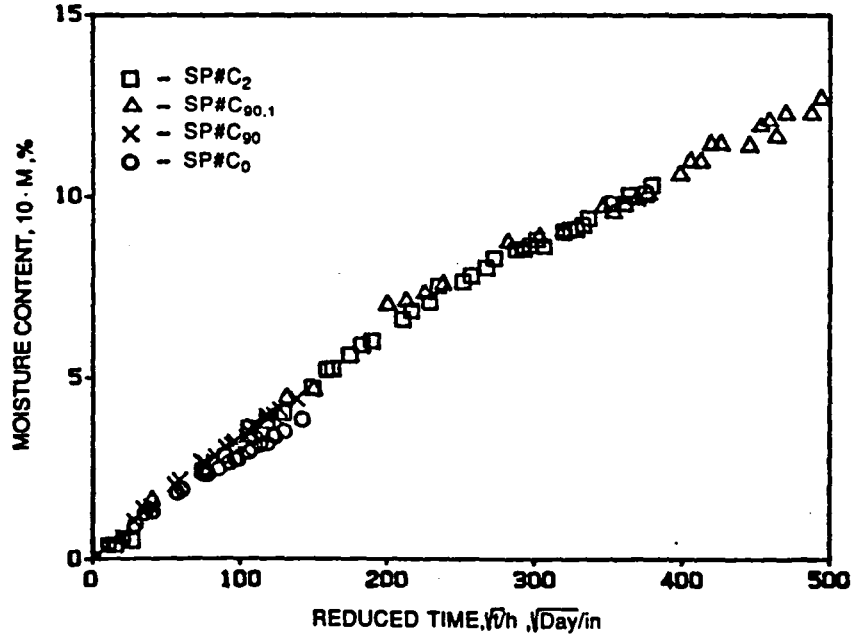

Figure 5.4 Moisture content as a function of reduced time for unidirectional AS4/3501-6 Graphite/Epoxy

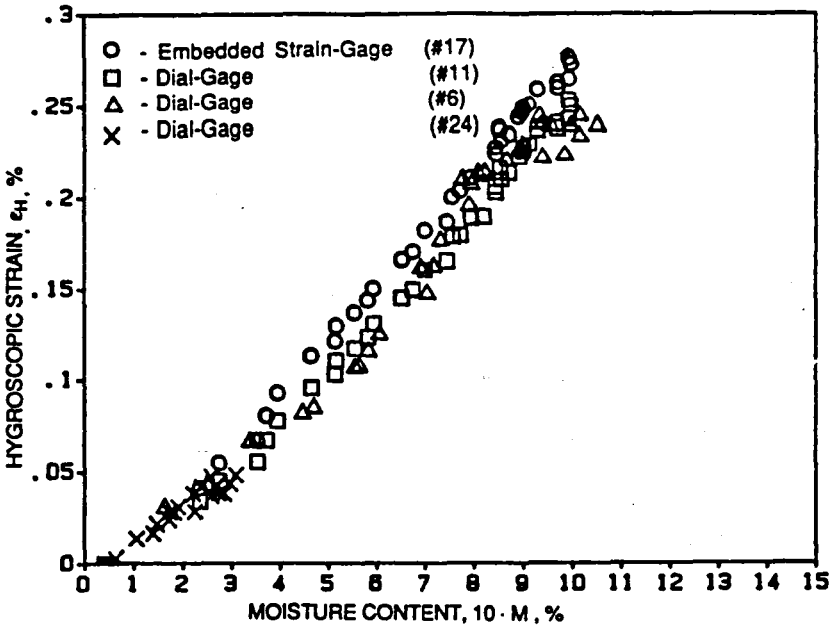

Figure 5.5 Transverse hygroscopic strain as a function of moisture content in unidirectional AS4/3501-6 Graphite/Epoxy

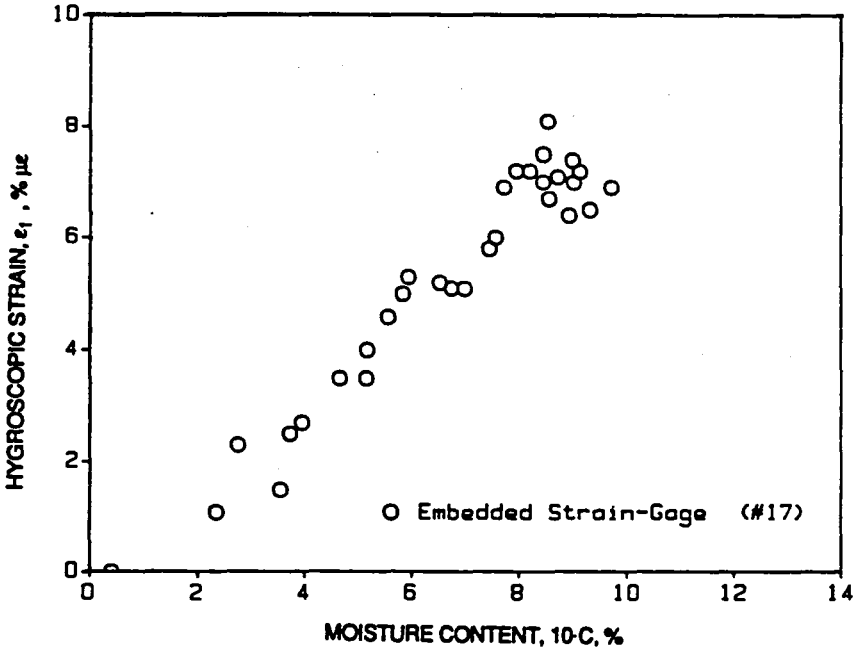

Figure 5.6 Longitudinal hygroscopic strain in $[90_8]$ AS4/3501-6 Graphite/Epoxy as a function of moisture content (C)

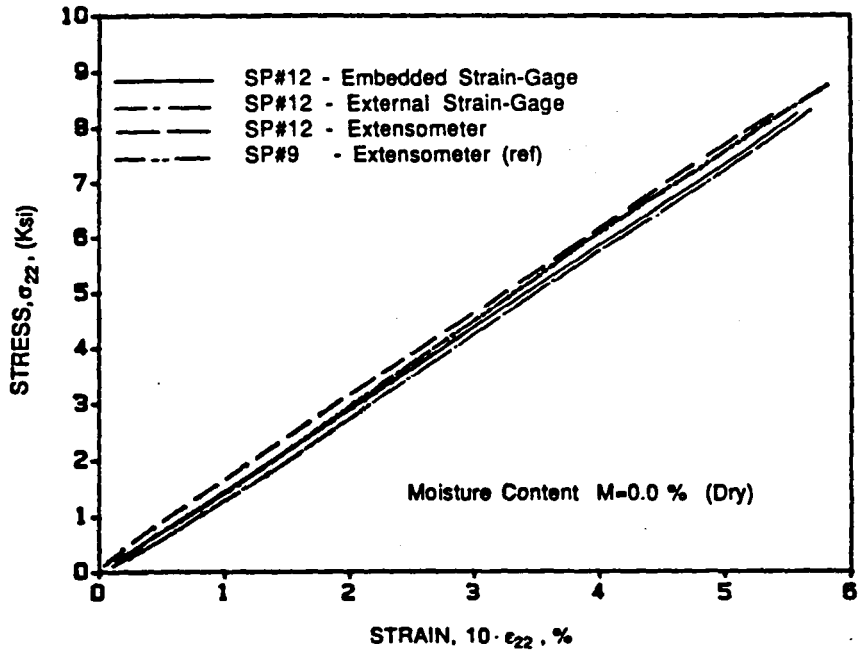

Figure 5.7 Stress-strain curves for $[90_8]$ Graphite/Epoxy specimens under uniaxial tensile loading with different strain measurement techniques (T=22°C (72°F), C=0%)

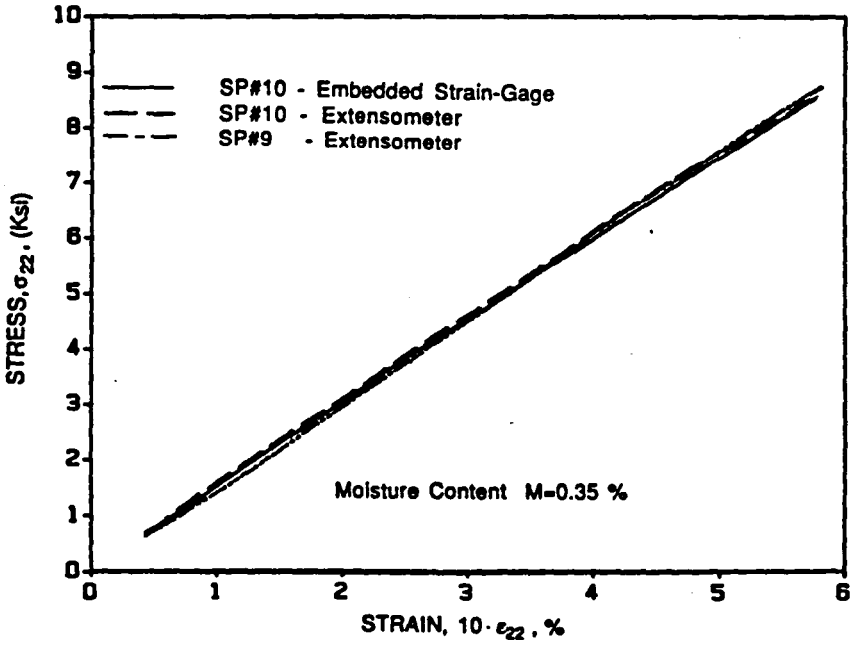

Figure 5.8 Stress-strain curves for $[90_8]$ AS4/3501-6 Graphite/Epoxy specimens conditioned to 0.35% moisture content under uniaxial tensile loading at a strain rate of $1.5 \cdot 10^{-5}$ s^{-1}

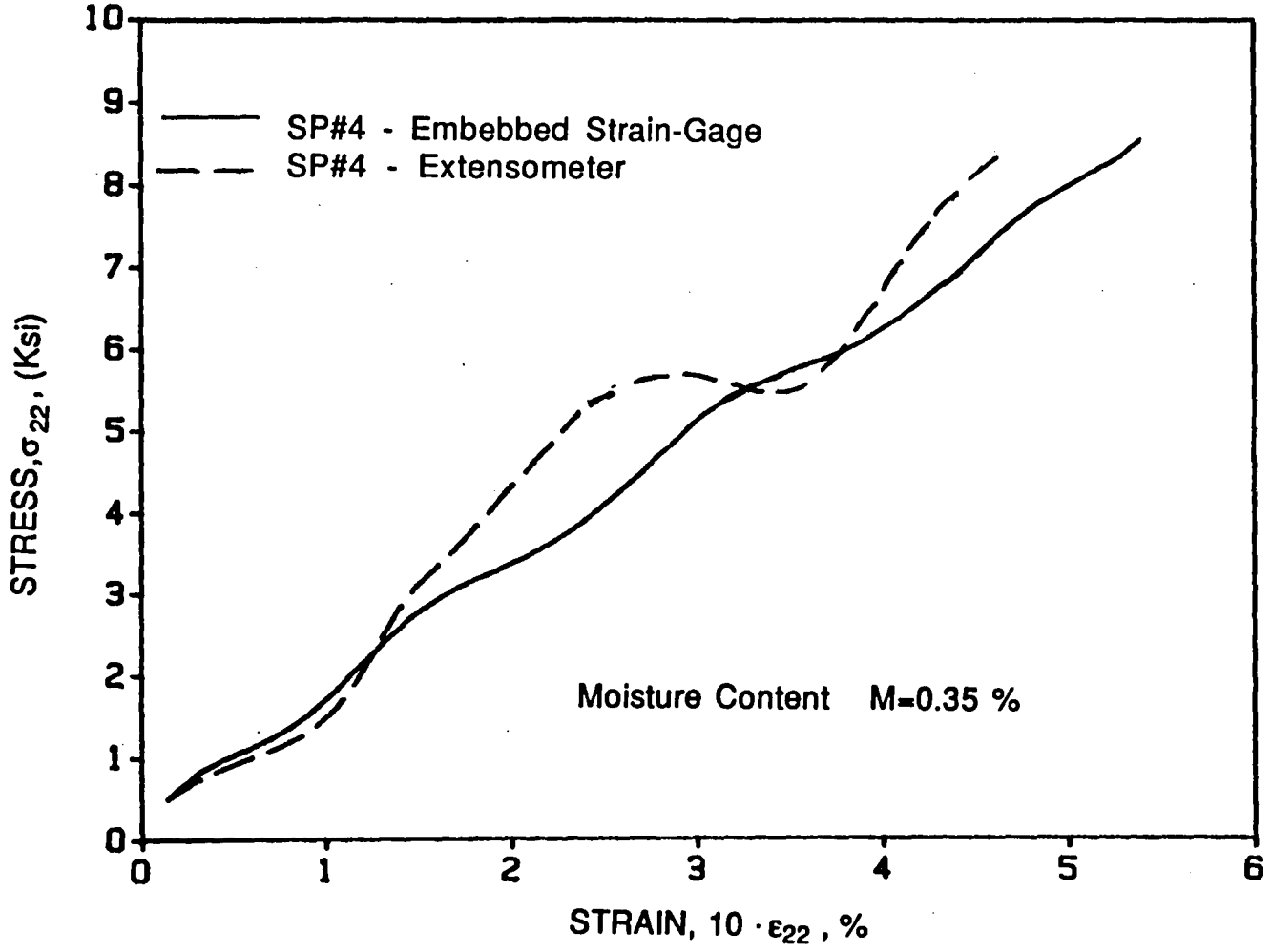

Figure 5.9 Stress-strain curves for $[90_8]$ Graphite/Epoxy conditioned to 0.35% moisture content under uniaxial tensile loading at a strain rate of 5 s^{-1}

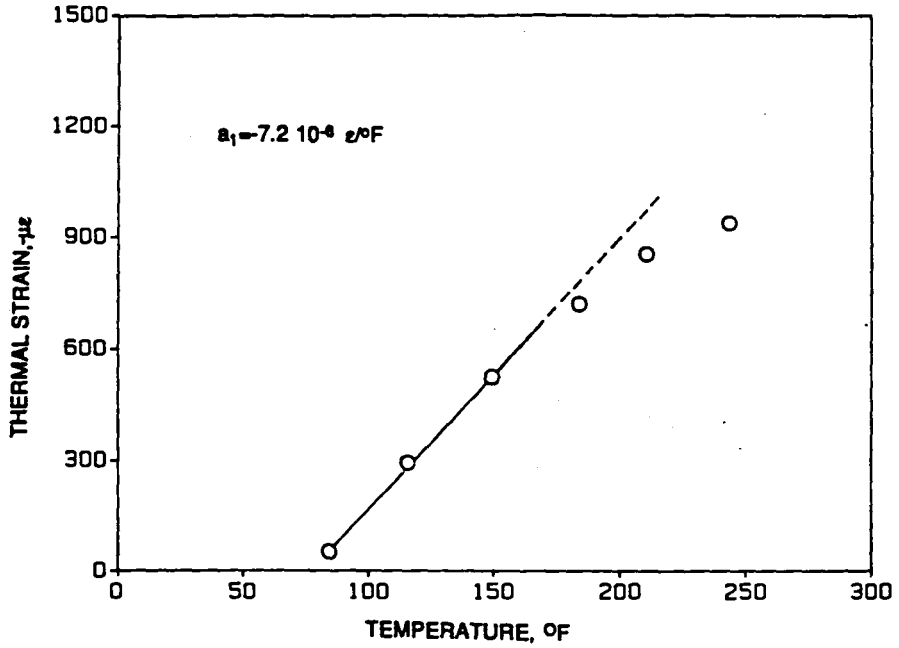

Figure 5.10 Thermal strain in unidirectional AS4/3501-6 Graphite/Epoxy along fibers

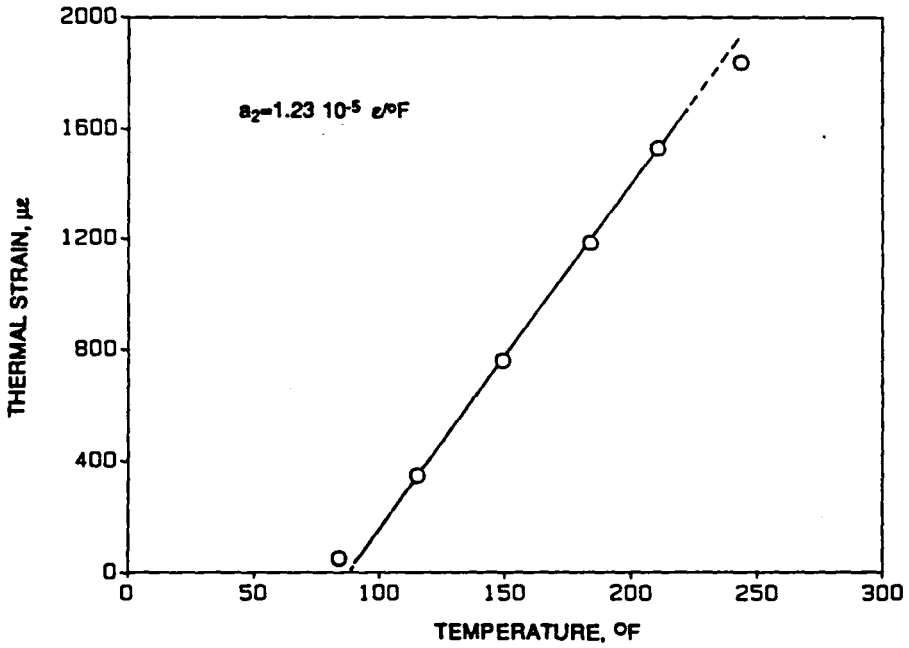

Figure 5.11 Thermal strain in unidirectional AS4/3501-6 Graphite/Epoxy in direction perpendicular to fibers

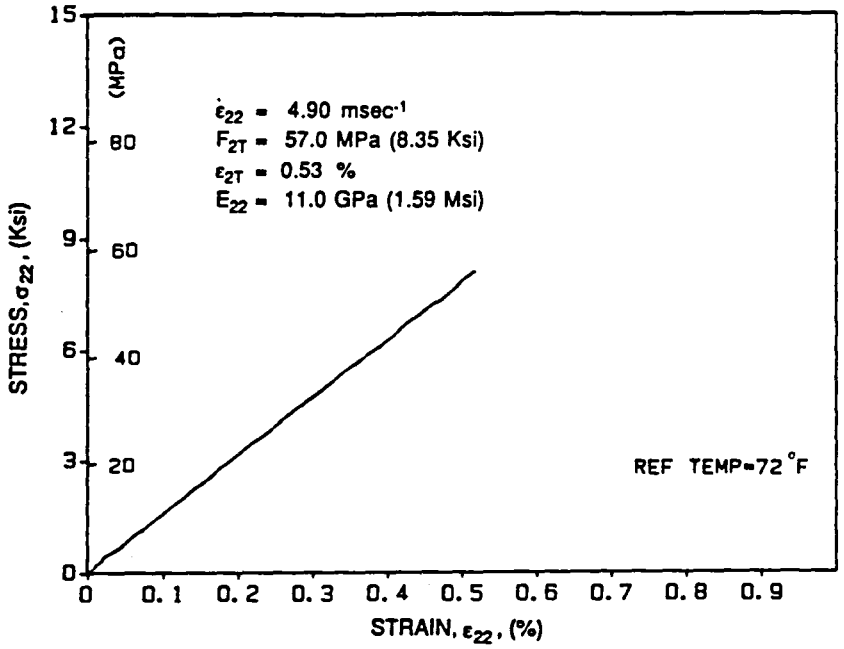

Figure 5.12 Typical stress-strain curve for $[90_8]$ AS4/3501-6 Graphite/Epoxy ($\dot{\varepsilon}_{22}$=4.9·10^{-3} s^{-1}, T=22°C (72°F), C=0%)

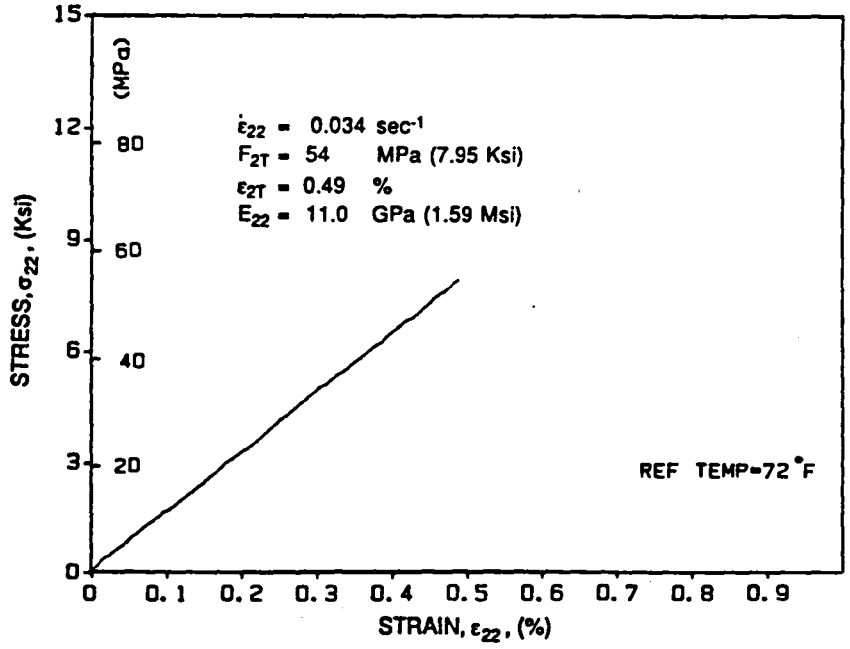

Figure 5.13 Typical stress-strain curve for $[90_8]$ AS4/3501-6 Graphite/Epoxy ($\dot{\varepsilon}_{22}$=3.4·10^{-2} s^{-1}, T=22°C (72°F), C=0%)

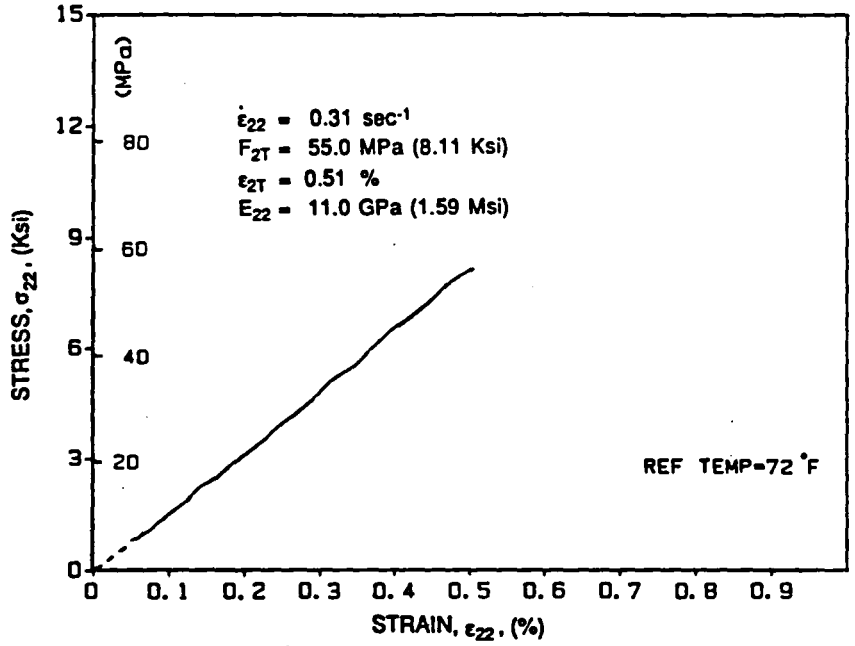

Figure 5.14 Typical stress-strain curve for [90_8] AS4/3501-6 Graphite/Epoxy ($\dot{\varepsilon}_{22}$=3.1·10^{-1} s^{-1}, T=22°C (72°F), C=0%)

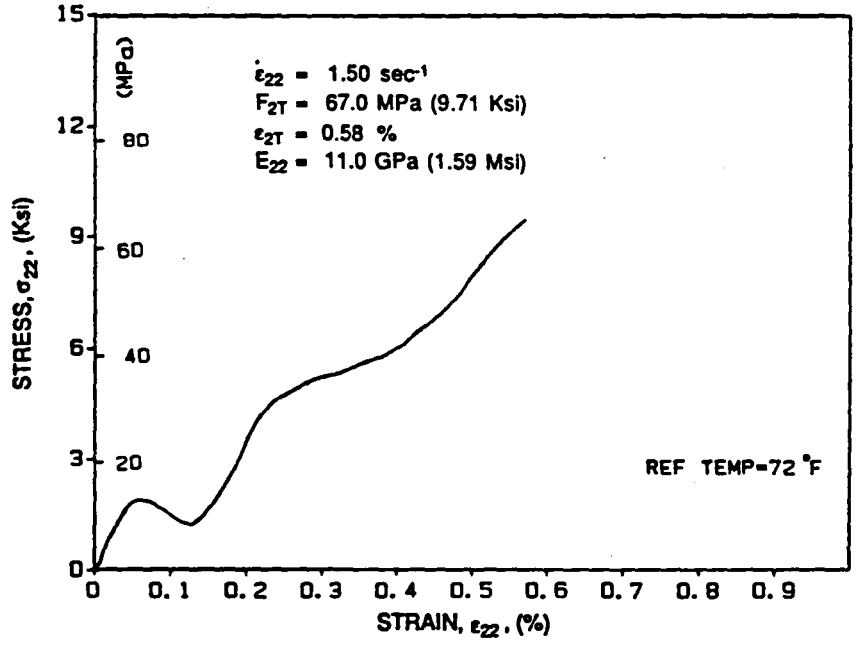

Figure 5.15 Typical stress-strain curve for [90_8] AS4/3501-Graphite/Epoxy ($\dot{\varepsilon}_{22}$=1.5 s^{-1}, T=22°C (72°F), C=0%)

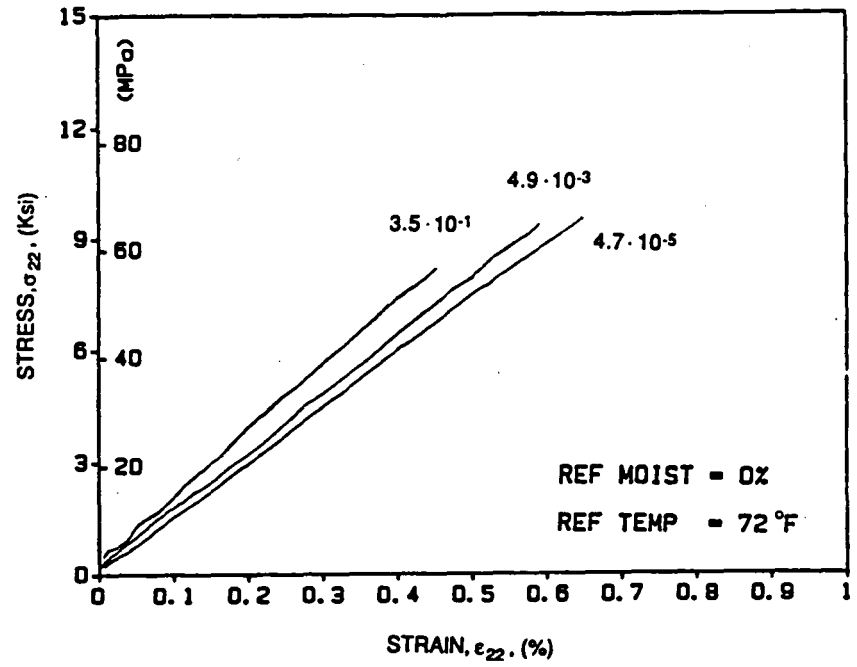

Figure 5.16 Transverse stress-strain curves for dry specimens at room temperature and various strain rates

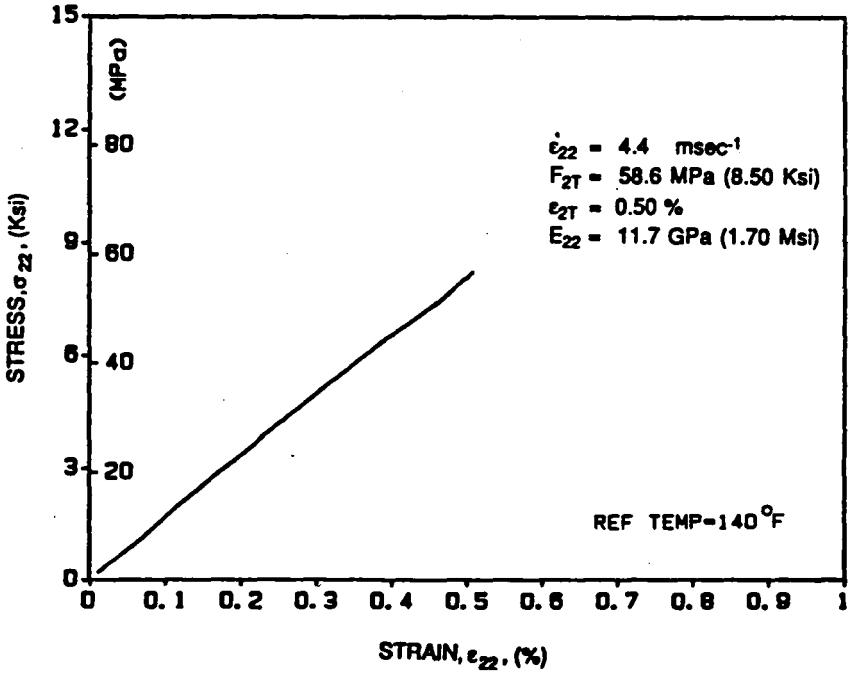

Figure 5.17 Typical stress-strain curve for $[90_8]$ AS4/3501-6 Graphite/Epoxy ($\dot{\varepsilon}_{22}$=4.4·10^{-3} s^{-1}, T=60°C (140°F), C=0%)

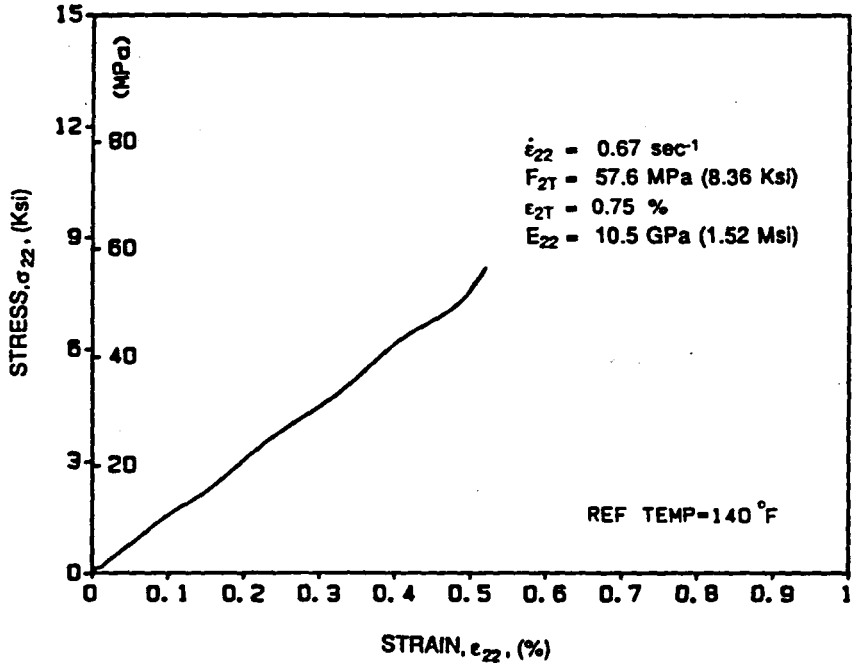

Figure 5.18 Typical stress-strain curve for [90_8] AS4/3501-6 Graphite/Epoxy ($\dot{\varepsilon}_{22}$=0.67 s^{-1}, T=60°C (140°F), C=0%)

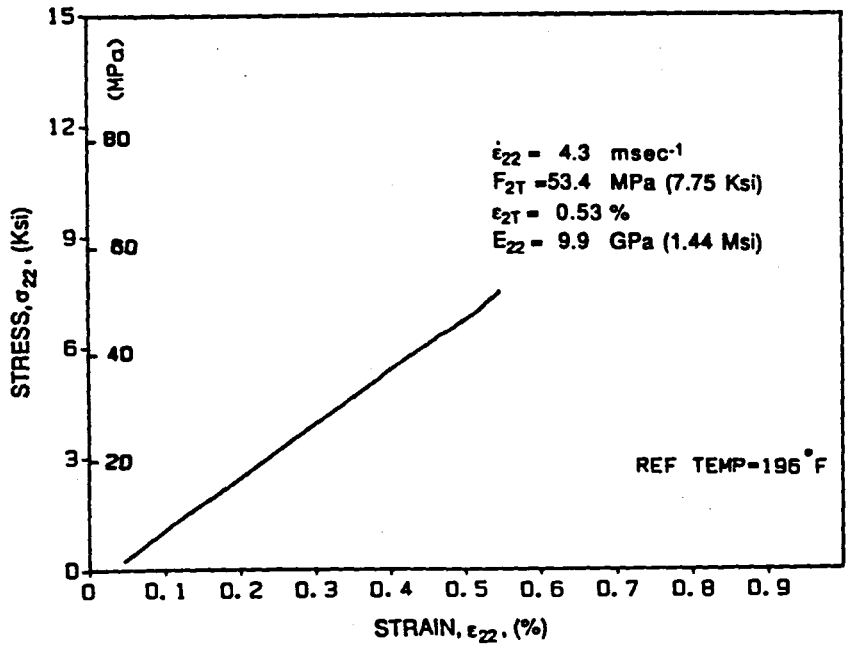

Figure 5.19 Typical stress-strain curve for [90_8] AS4/3501-6 Graphite/Epoxy ($\dot{\varepsilon}_{22}$=4.3·10^{-3} s^{-1}, T=91°C (196°F), C=0%)

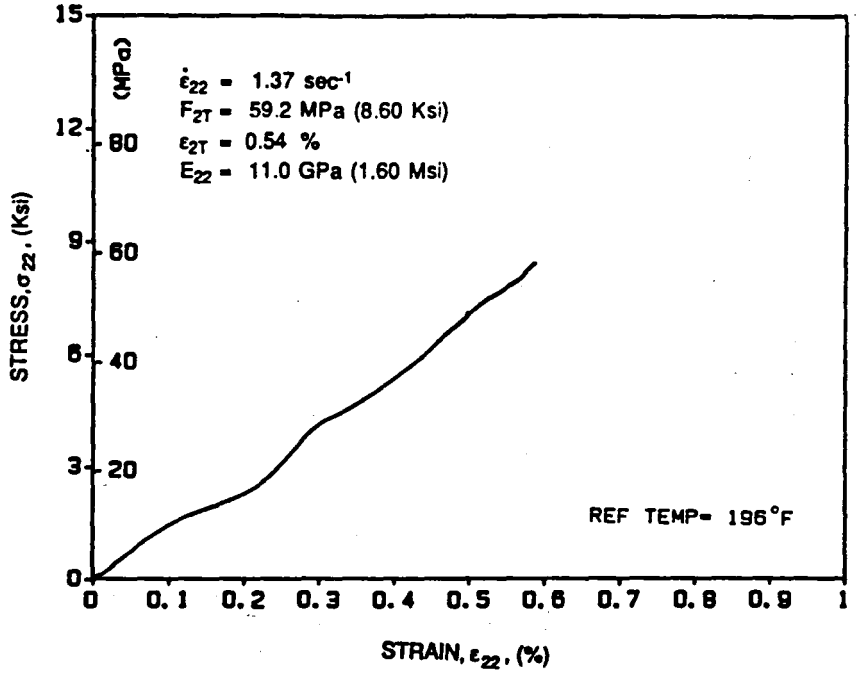

Figure 5.20 Typical stress-strain curve for [90_8] AS4/3501-6 Graphite/Epoxy ($\dot{\varepsilon}_{22}$=1.37 s^{-1}, T=91°C (196°F), C=0%)

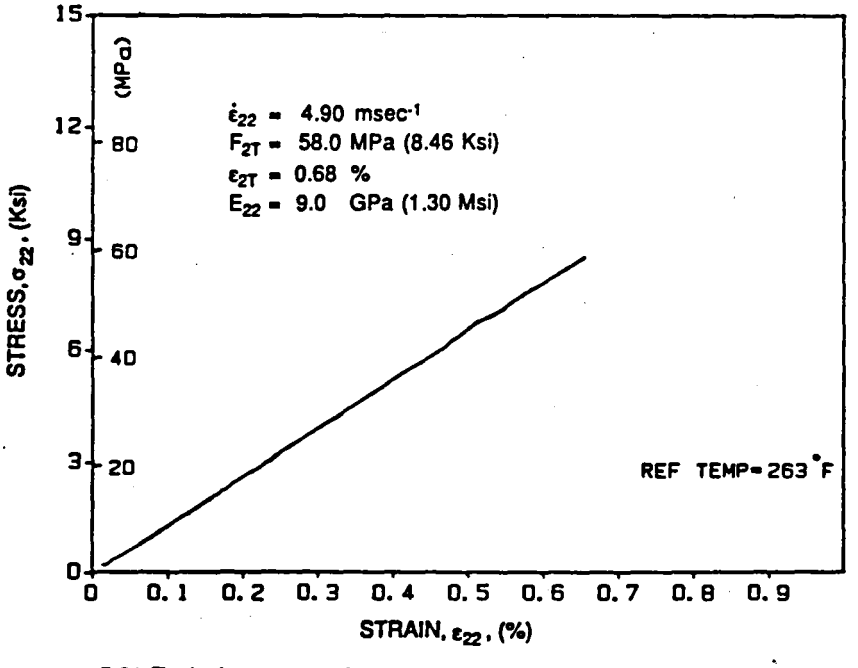

Figure 5.21 Typical stress-strain curve for [90_8] AS4/3501-6 Graphite/Epoxy ($\dot{\varepsilon}_{22}$=4.9·10^{-3} s^{-1}, T=128°C (263°F), C=0%)

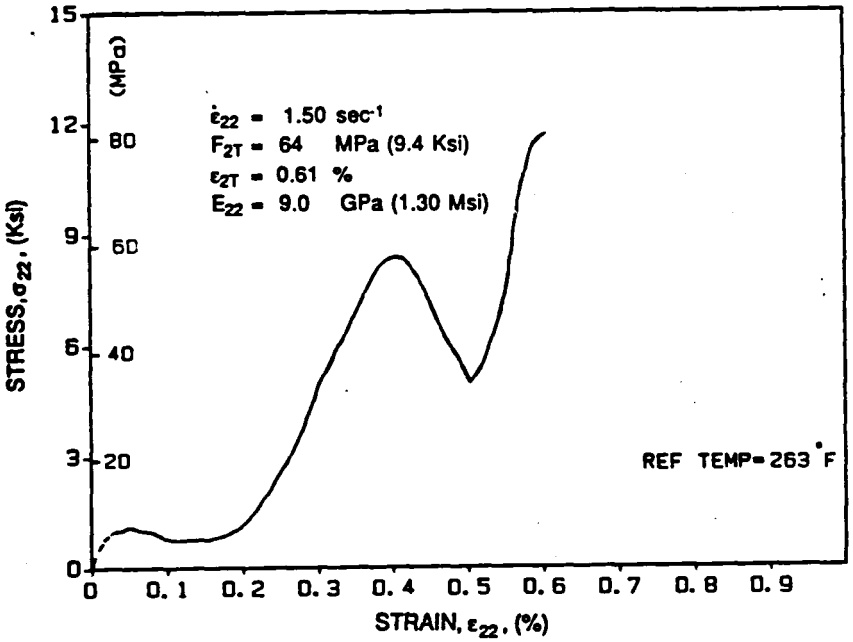

Figure 5.22 Typical stress-strain curve for [90_8] AS4/3501-6 Graphite/Epoxy ($\dot{\varepsilon}_{22}$=1.5 s^{-1}, T=128°C (263°F), C=0%)

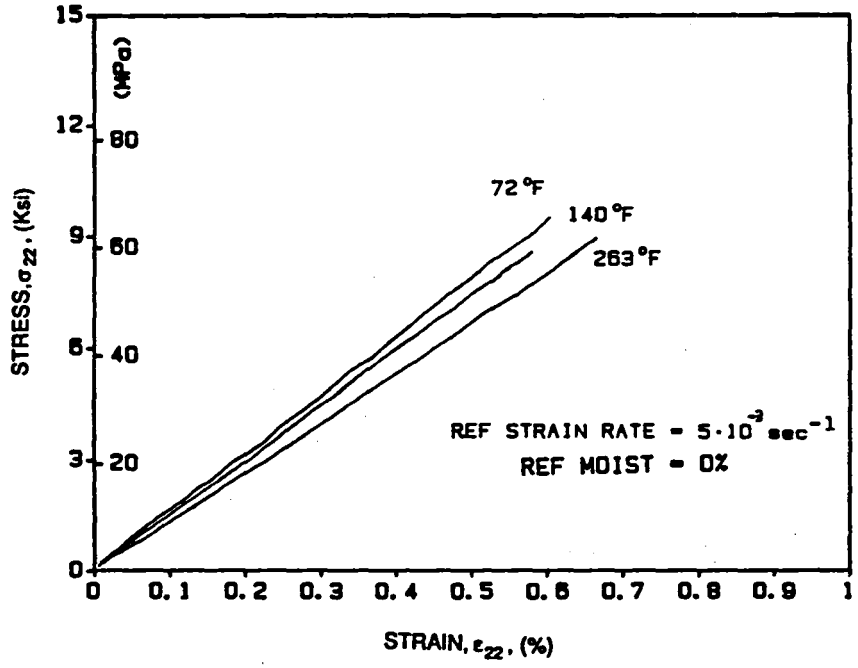

Figure 5.23 Transverse stress-strain curves for dry specimens at 5·10^{-3} s^{-1} strain rate at various temperatures

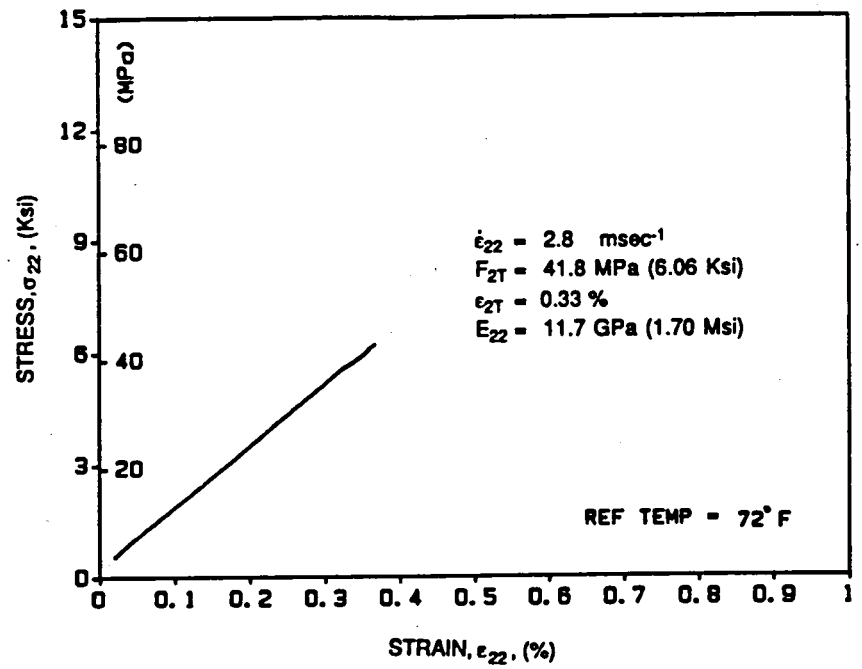

Figure 5.24 Typical stress-strain curve for $[90_8]$ AS4/3501-6 Graphite/Epoxy ($\dot{\epsilon}_{22}$=2.8·10^{-3} s^{-1}, T=22°C (72°F), C=1%)

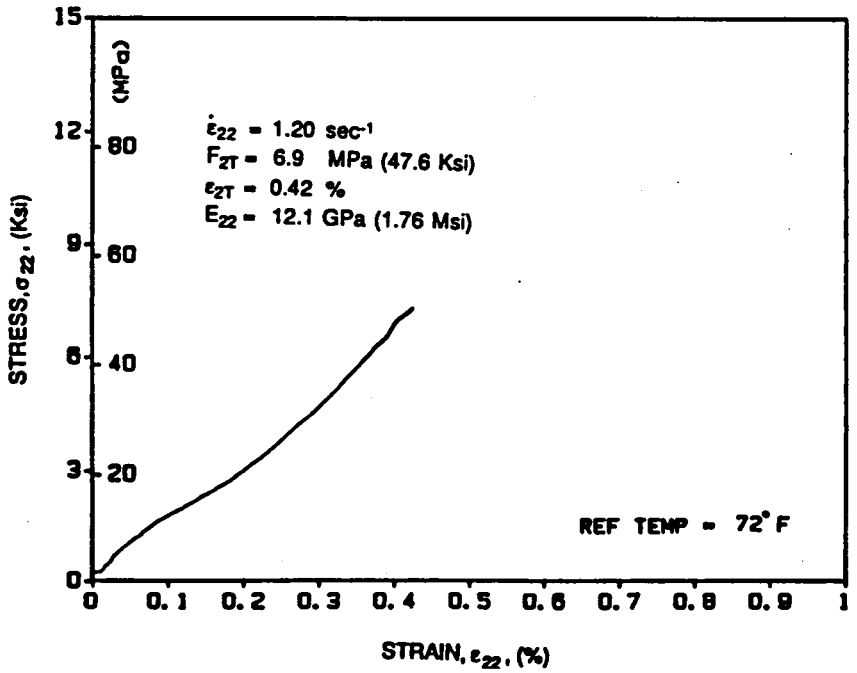

Figure 5.25 Typical stress-strain curve for $[90_8]$ AS4/3501-6 Graphite/Epoxy ($\dot{\epsilon}_{22}$=1.2 s^{-1}, T=22°C (72°F), C=1%)

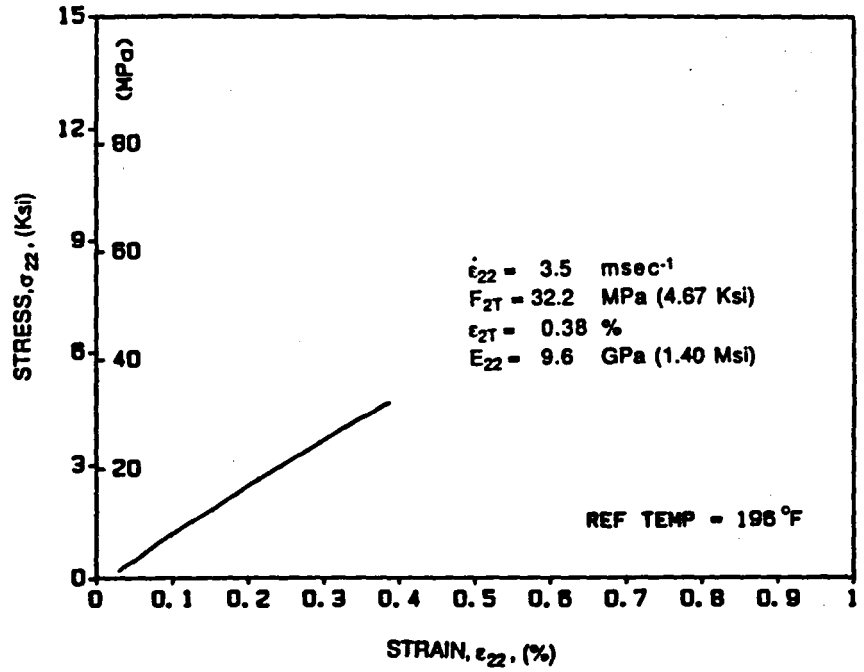

Figure 5.26 Typical stress-strain curve for [90_8] AS4/3501-6 Graphite/Epoxy ($\dot{\varepsilon}_{22}$=3.5$10^{-3}$ s^{-1}, T=91°C (196°F), C=1%)

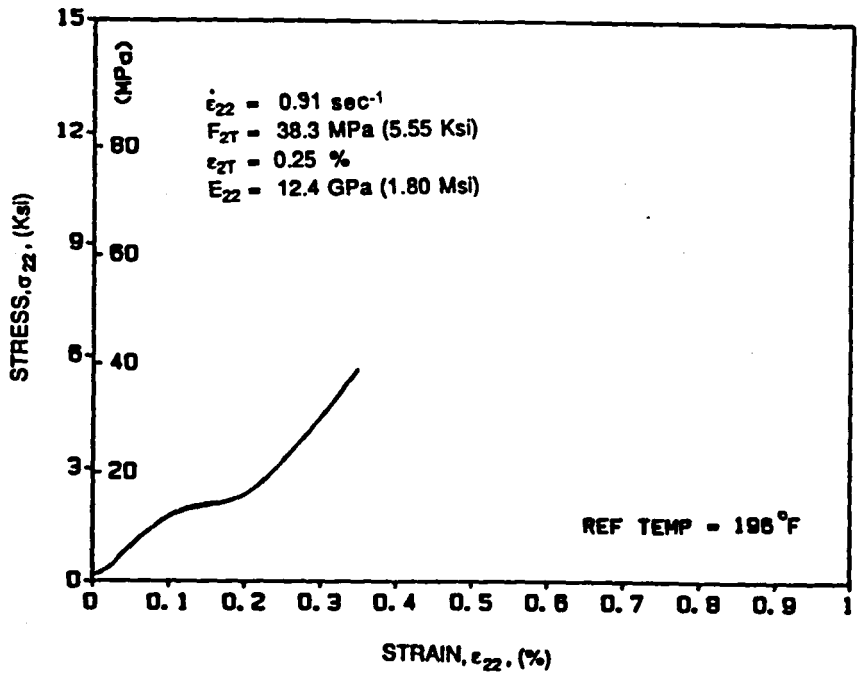

Figure 5.27 Typical stress-strain curve for [90_8] AS4/3501-6 Graphite/Epoxy ($\dot{\varepsilon}_{22}$=0.91 s^{-1}, T=91°C (196°F), C=1%)

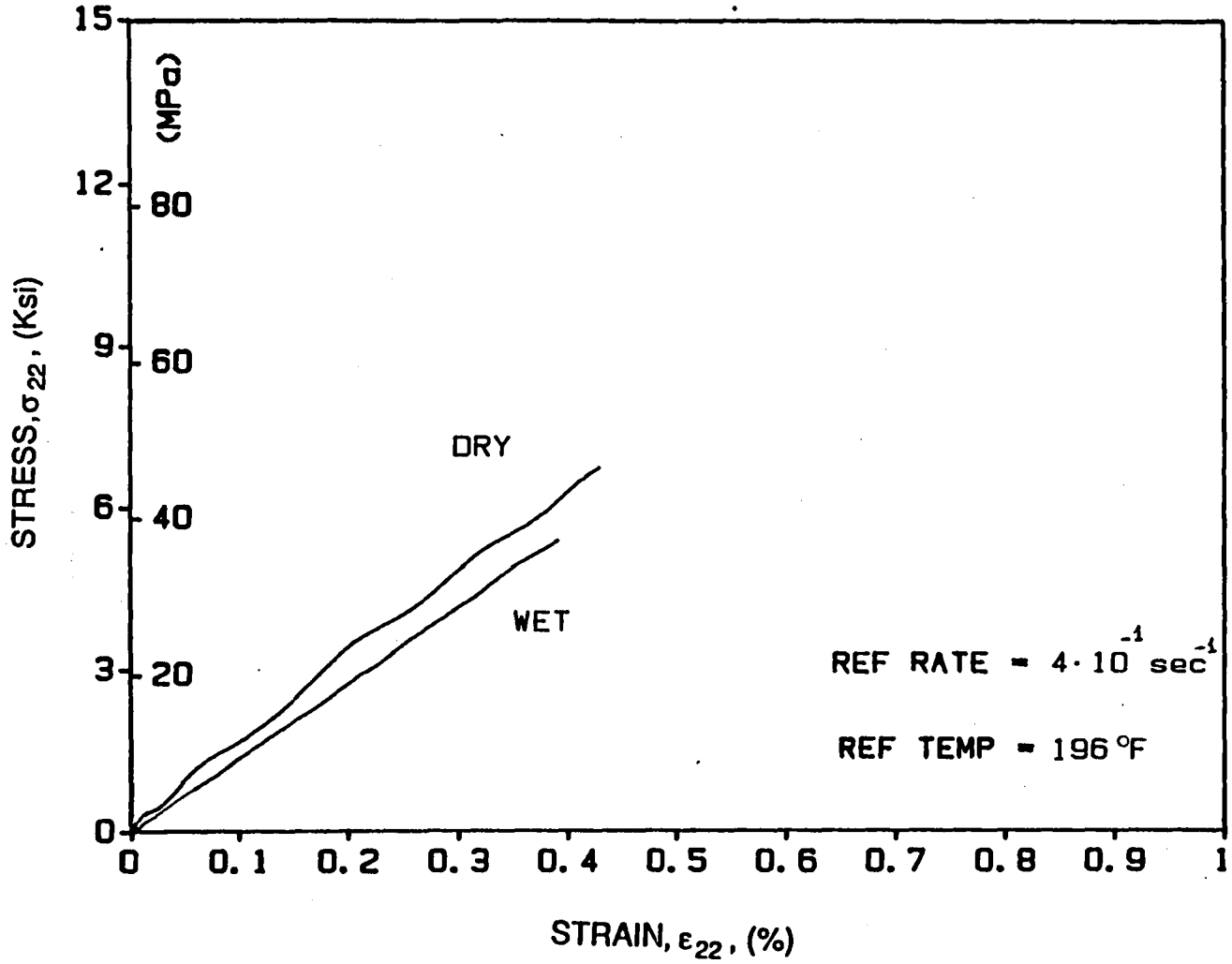

Figure 5.28 Transverse stress-strain curves for dry and wet specimens at 91°C (196°F) and a 4.10^{-1} s^{-1} strain rate

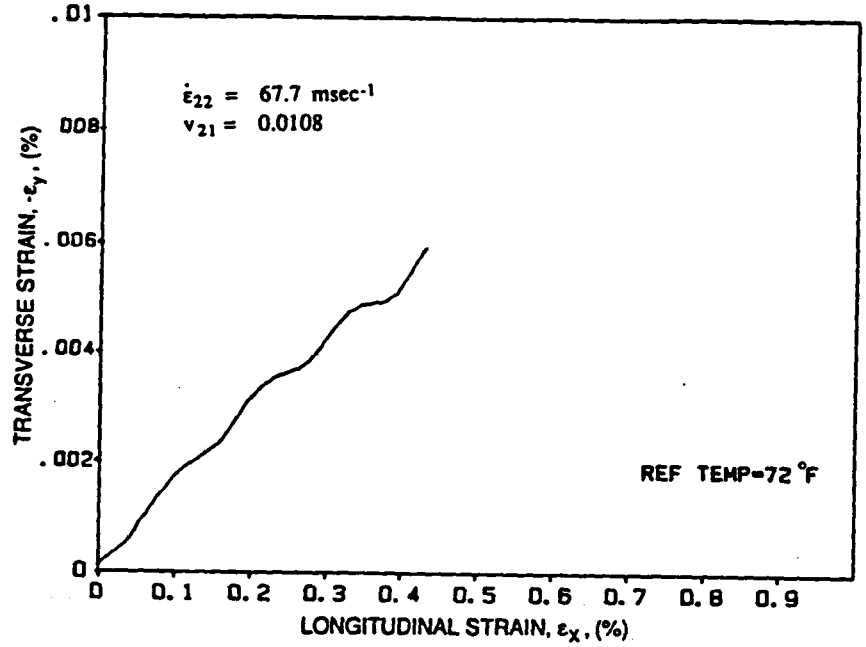

Figure 5.29 Typical transverse vs. longitudinal strain curve for [90_8] AS4/3501-6 Graphite/Epoxy ($\dot{\varepsilon}_{22}$=6.8$10^{-2}$ s^{-1}, T=22°C (72°F), C=0%)

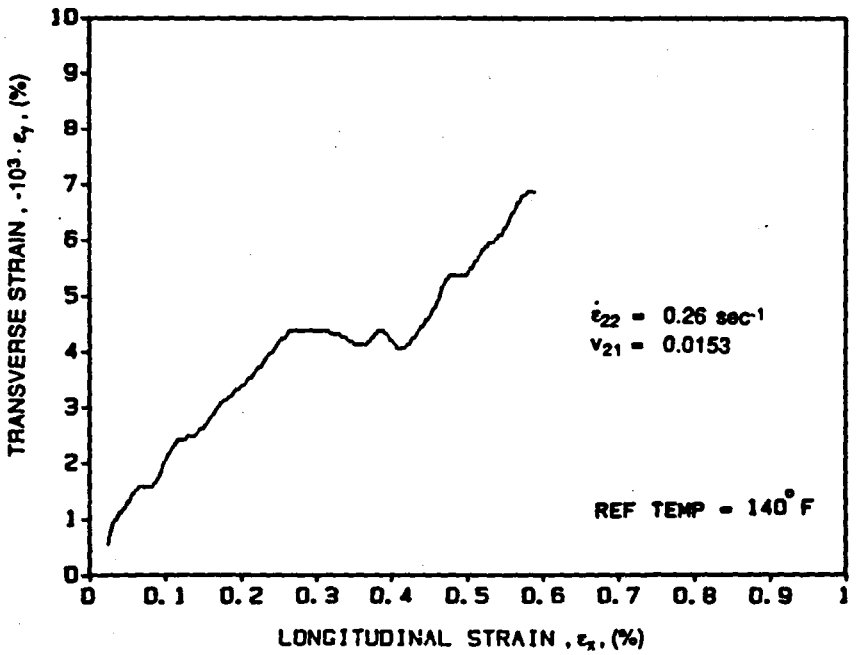

Figure 5.30 Typical transverse vs. longitudinal strain curve for [90_8] AS4/3501-6 Graphite/Epoxy ($\dot{\varepsilon}_{22}$=0.26 s^{-1}, T=60°C (140°F), C=0%)

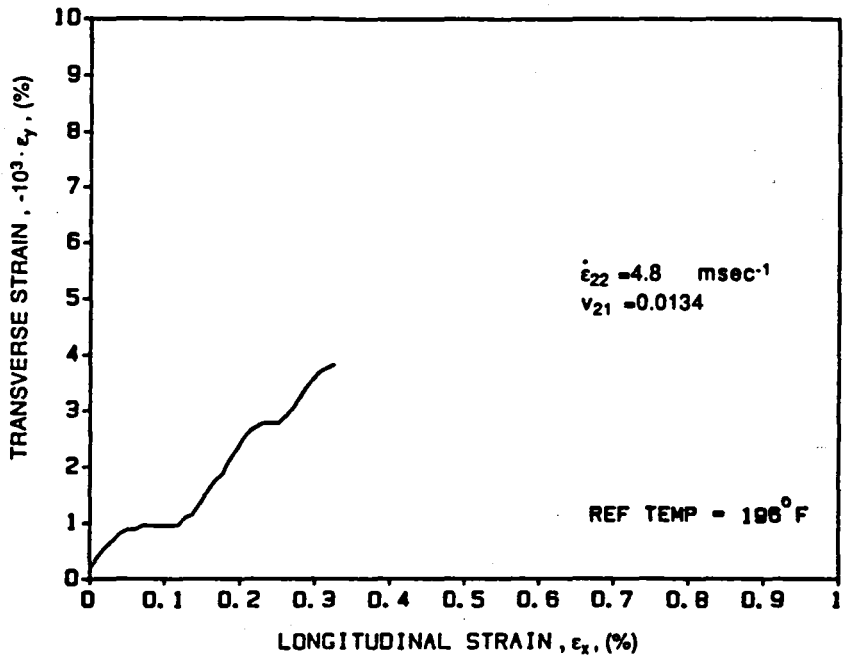

Figure 5.31 Typical transverse vs. longitudinal strain curve for $[90_8]$ AS4/3501-6 Graphite/Epoxy ($\dot{\varepsilon}_{22}$=4.8·10^{-3} s^{-1}, T=91°C (196°F), C=0%)

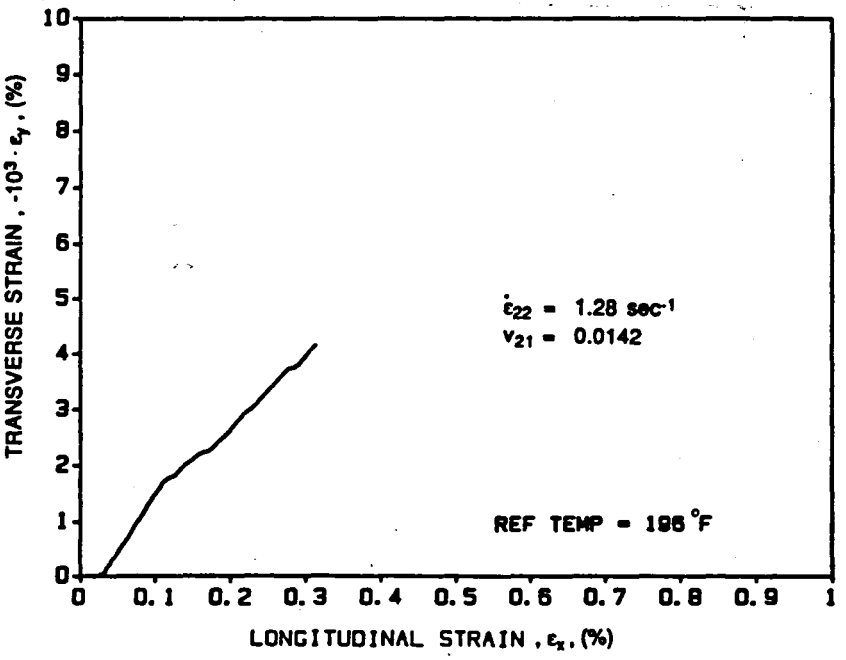

Figure 5.32 Typical transverse vs. longitudinal strain curve for $[90_8]$ AS4/3501-6 Graphite/Epoxy ($\dot{\varepsilon}_{22}$=1.28 s^{-1}, T=91°C (196°F), C=0%)

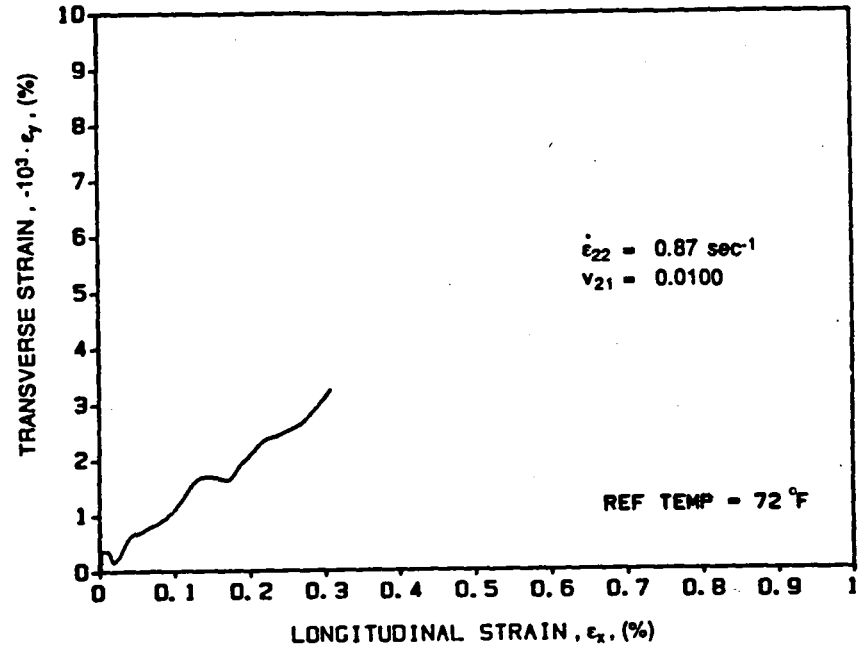

Figure 5.33 Typical transverse vs. longitudinal strain curve for [90_8] AS4/3501-6 Graphite/Epoxy ($\dot{\varepsilon}_{22}$=0.87 s^{-1}, T=22°C (72°F), C=1%)

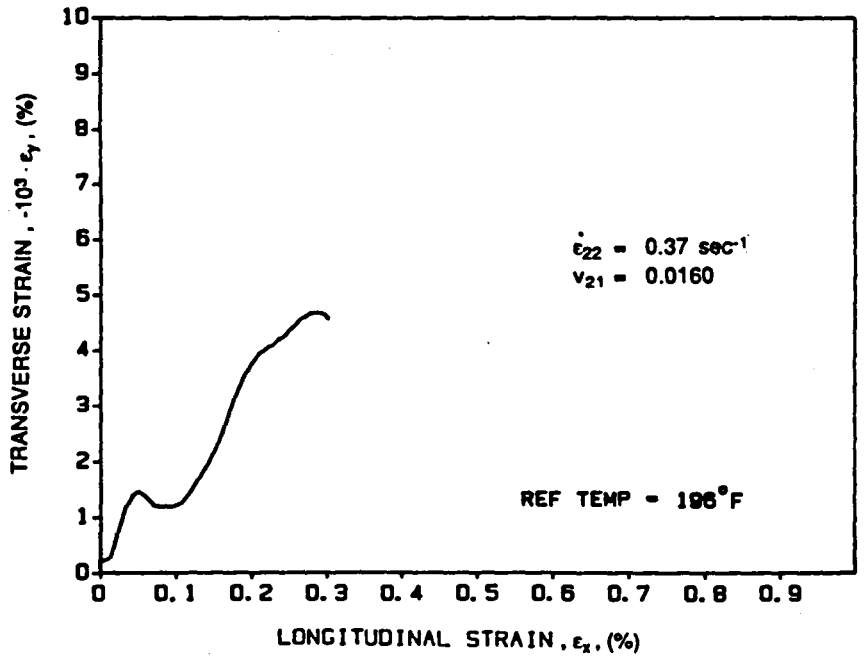

Figure 5.34 Typical transverse vs. longitudinal strain curve for [90_8] AS4/3501-6 Graphite/Epoxy ($\dot{\varepsilon}_{22}$=0.37 s^{-1}, T=91°C (196°F), C=1%)

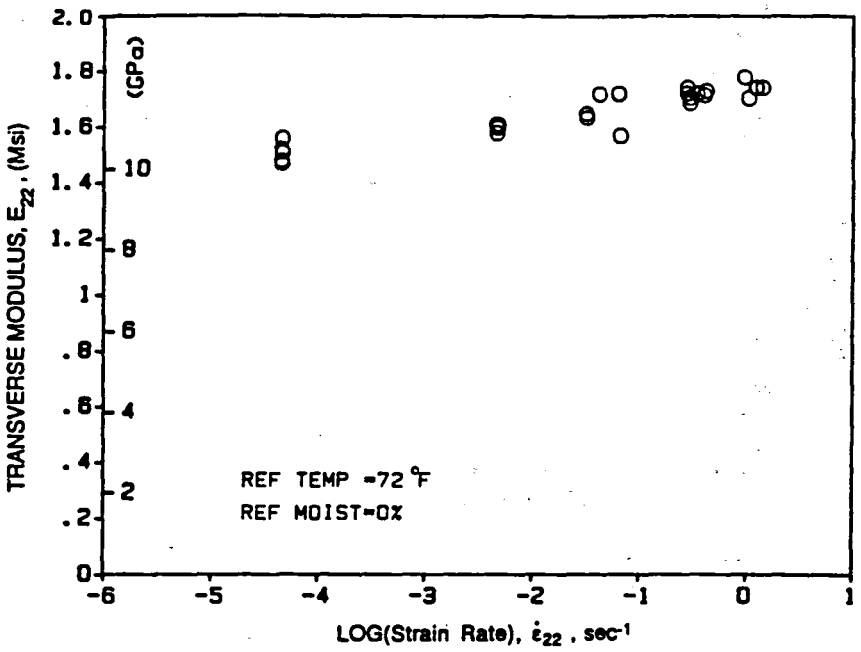

Figure 5.35 Transverse modulus vs. log(strain rate) curve for AS4/3501-6 Graphite/Epoxy, (T=22°C (72°F), C=0%)

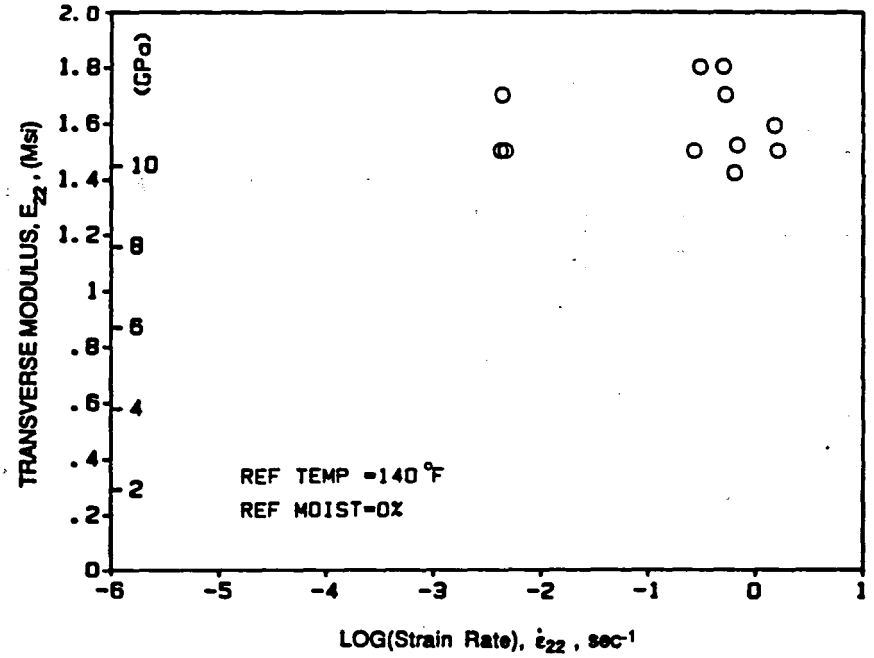

Figure 5.36 Transverse modulus vs. log(strain rate) curve for AS4/3501-6 Graphite/Epoxy, (T=60°C (140°F), C=0%)

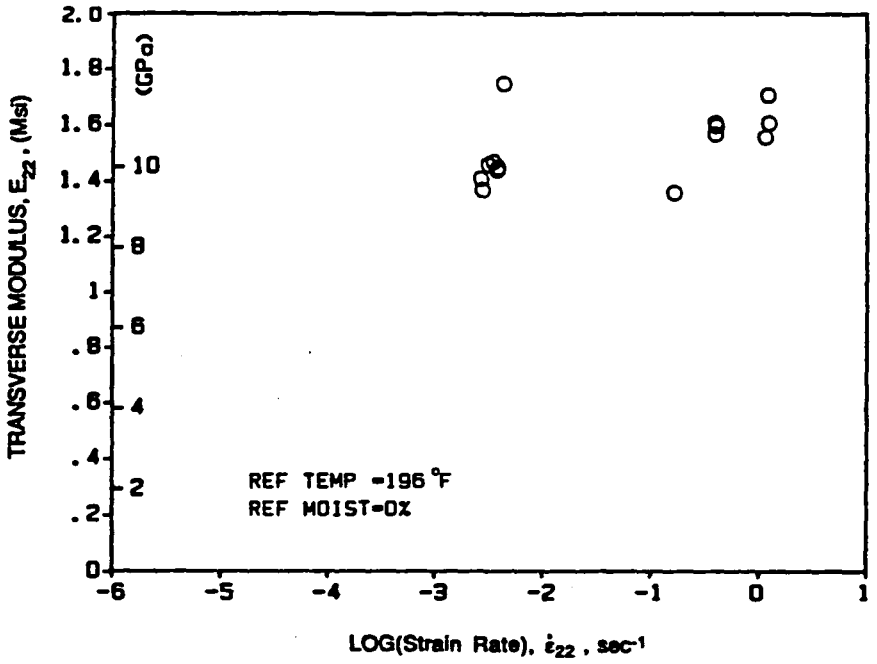

Figure 5.37 Transverse modulus vs. log(strain rate) curve for AS4/3501-6 Graphite/Epoxy, (T=91°C (196°F), C=0%)

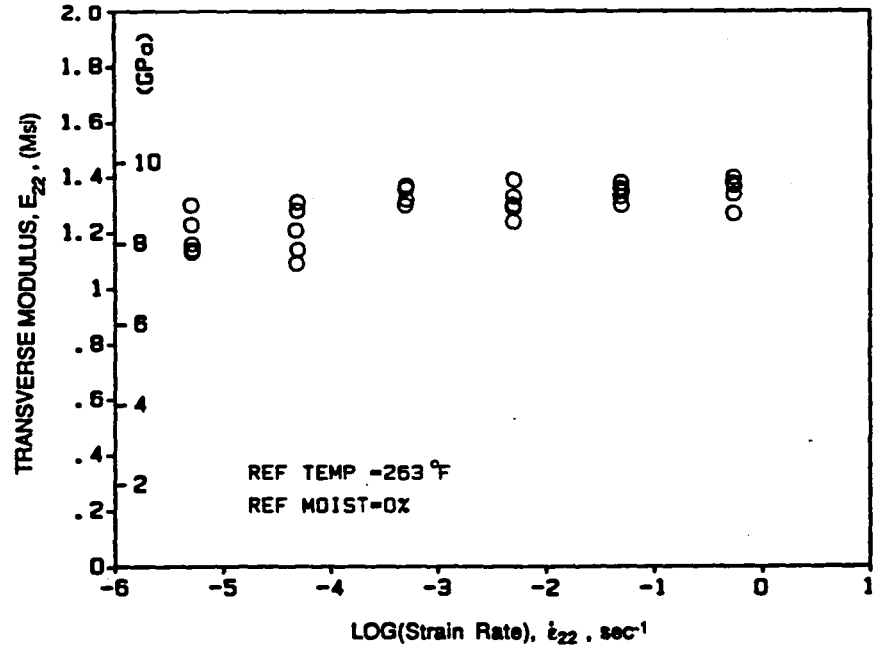

Figure 5.38 Transverse modulus vs. log(strain rate) curve for AS4/3501-6 Graphite/Epoxy, (T=128°C (263°F), C=0%)

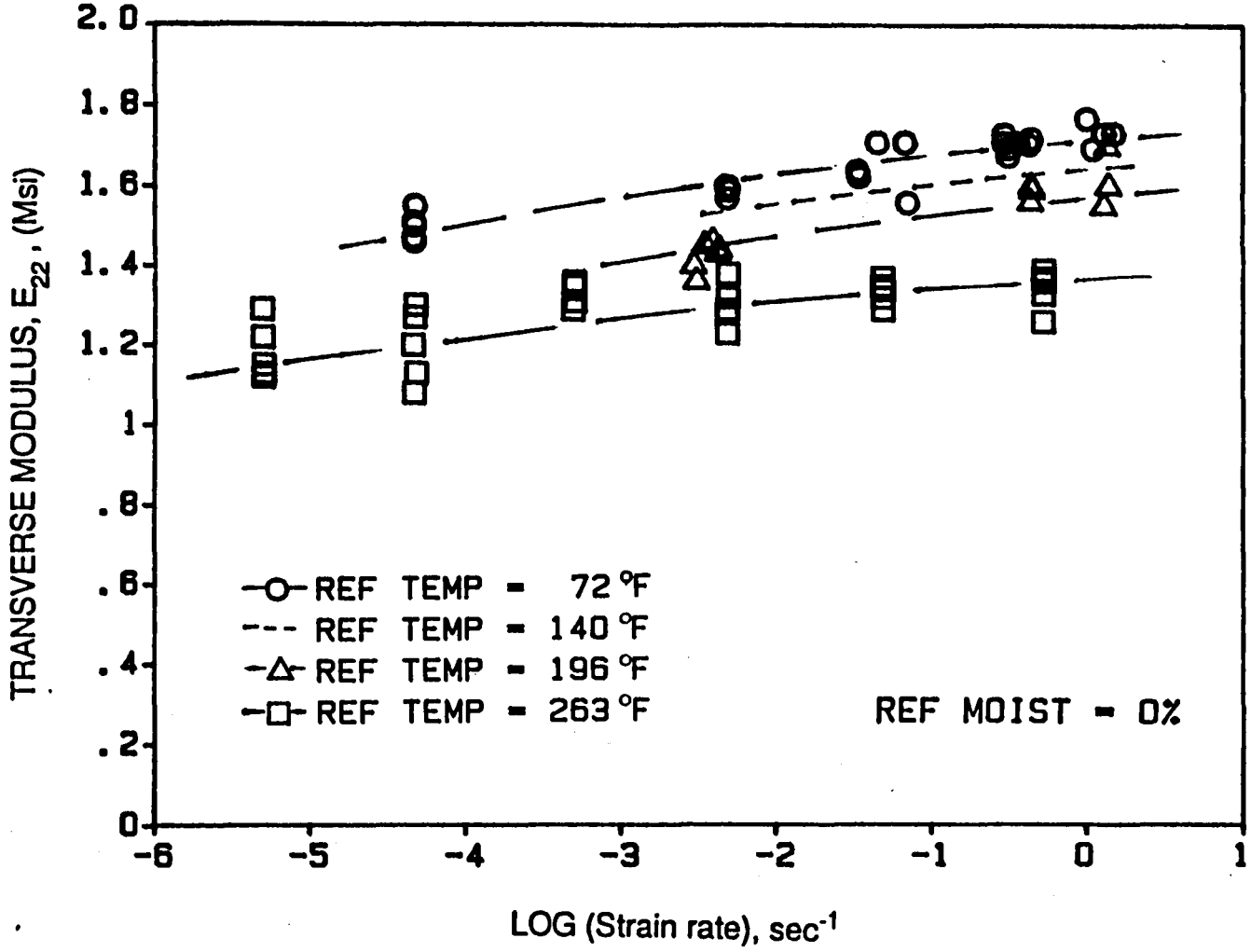

Figure 5.39 Transverse modulus as a function of strain rate at various temperatures for dry specimens

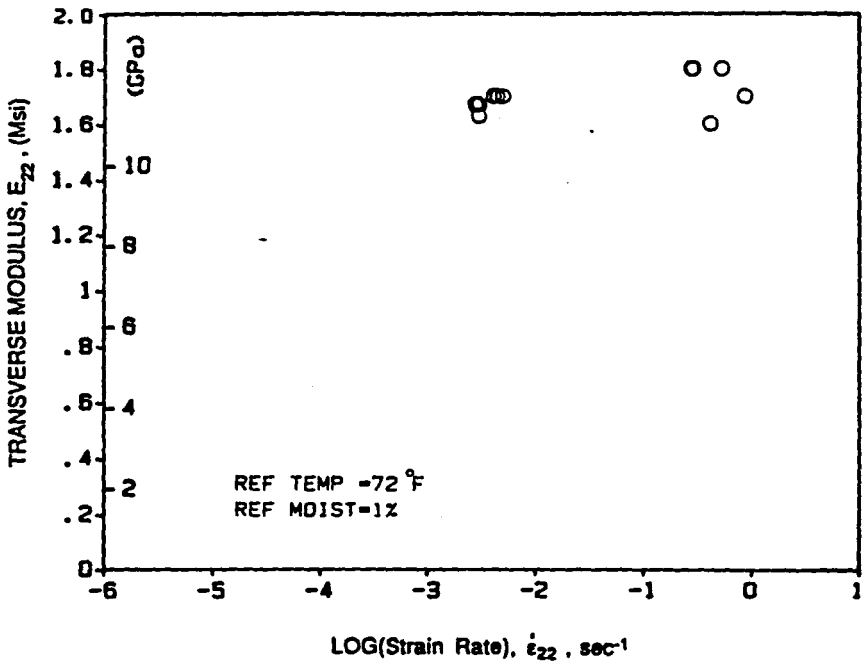

Figure 5.40 Transverse modulus vs. log(strain rate) curve for AS4/3501-6 Graphite/Epoxy, (T=22°C (72°F), C=1%)

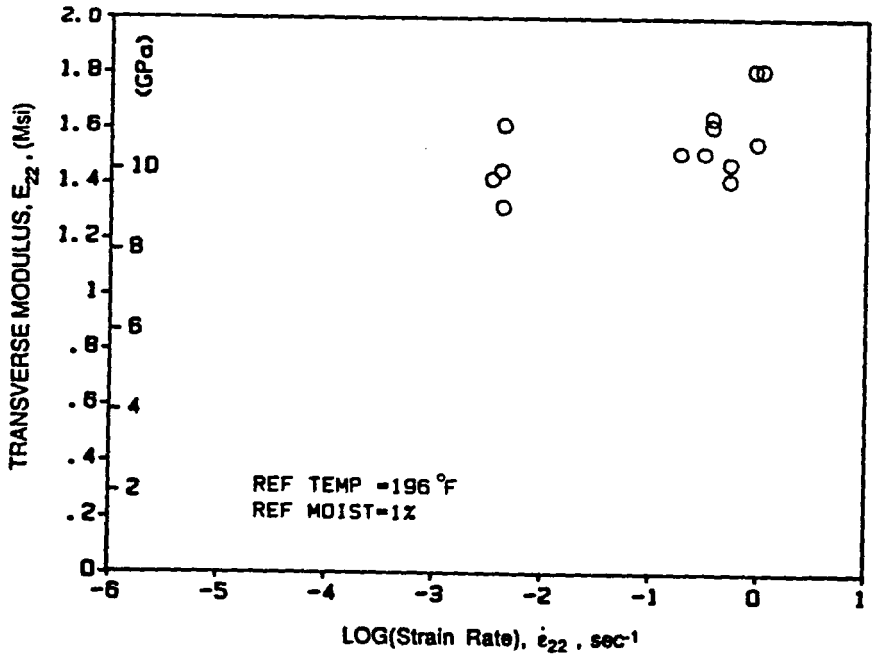

Figure 5.41 Transverse modulus vs. log(strain rate) curve for AS4/3501-6 Graphite/Epoxy, (T=91°C (196°F), C=1%)

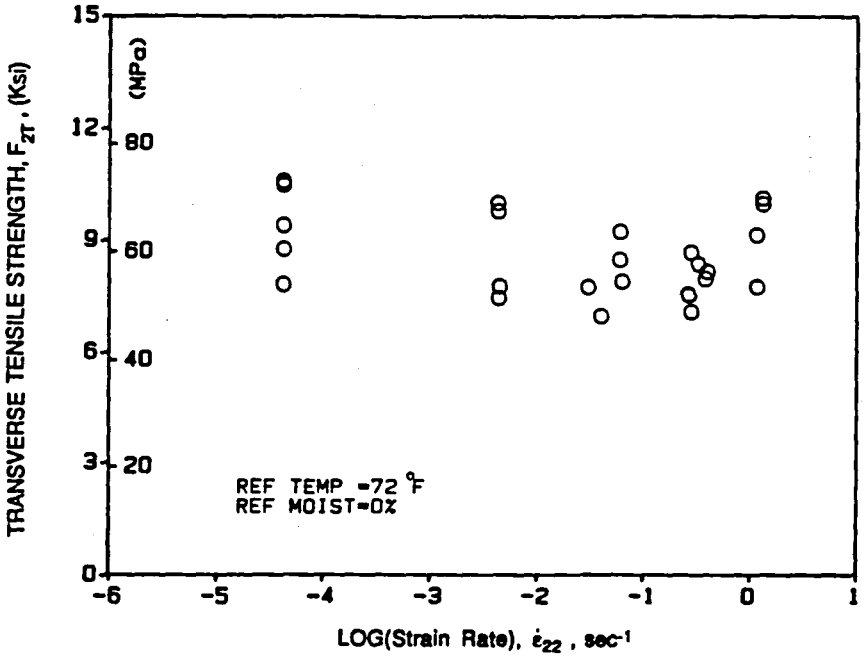

Figure 5.42 Transverse tensile strength vs. log(strain rate) curve for AS4/3501-6 Graphite/Epoxy, (T=22°C (72°F), C=0%)

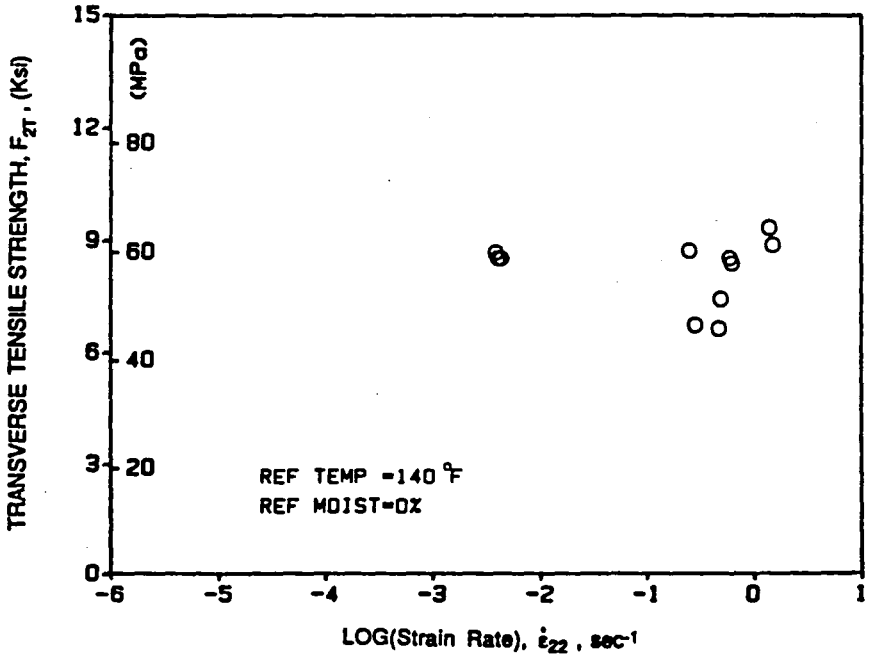

Figure 5.43 Transverse tensile strength vs. log(strain rate) curve for AS4/3501-6 Graphite/Epoxy, (T=60°C (140°F), C=0%)

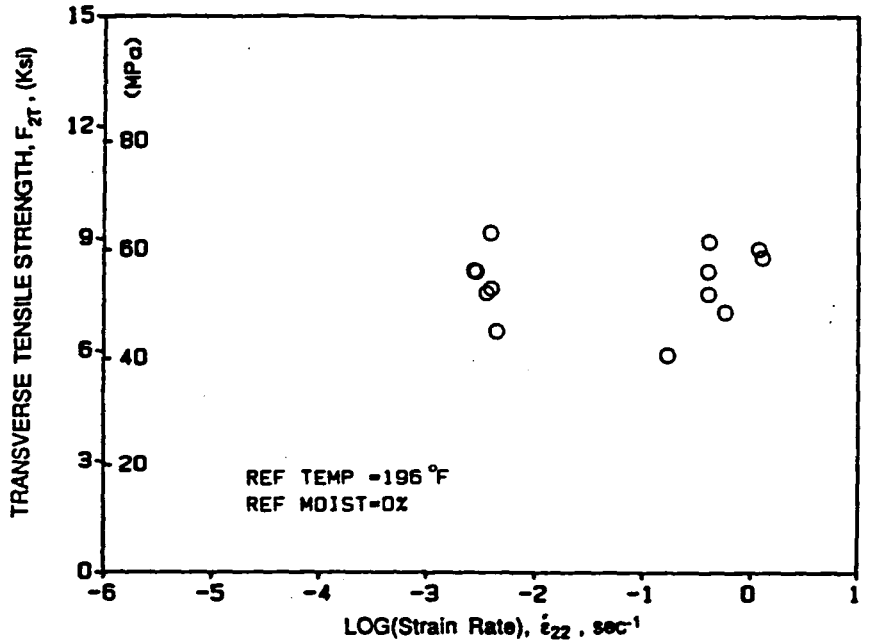

Figure 5.44 Transverse tensile strength vs. log(strain rate) curve for AS4/3501-6 Graphite/Epoxy, (T=91°C (196°F), C=0%)

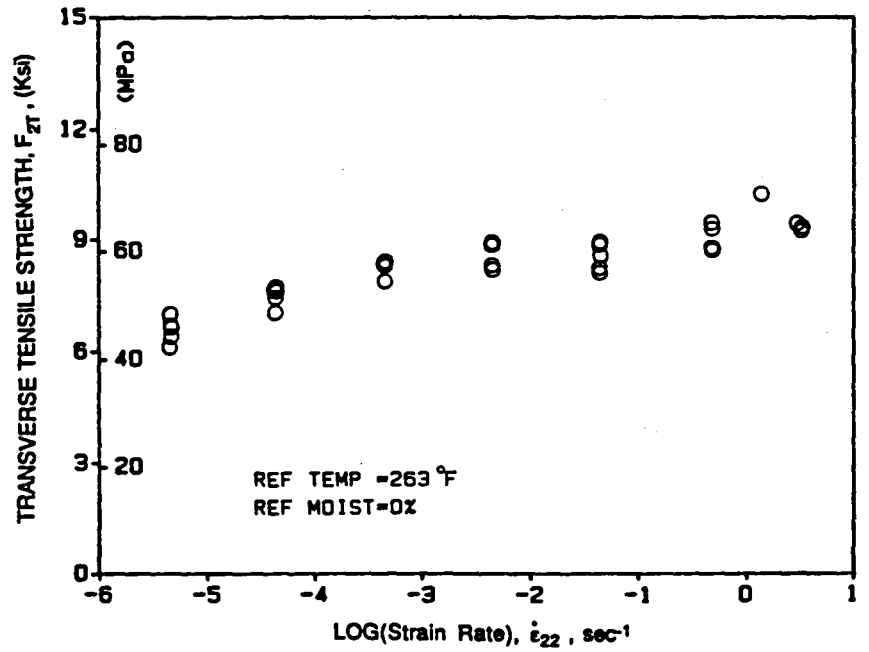

Figure 5.45 Transverse tensile strength vs. log(strain rate) curve for AS4/3501-6 Graphite/Epoxy, (T=128°C (263°F), C=0%)

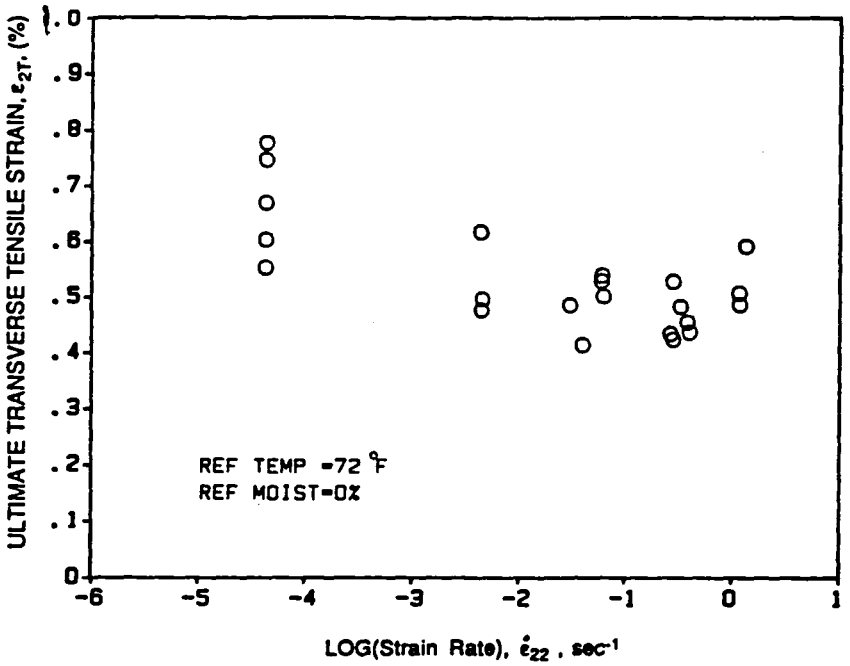

Figure 5.46 Ultimate transverse tensile strain vs. log(strain rate) curve for AS4/3501- 6 Graphite/Epoxy, (T=22°C (72°F, C=0%)

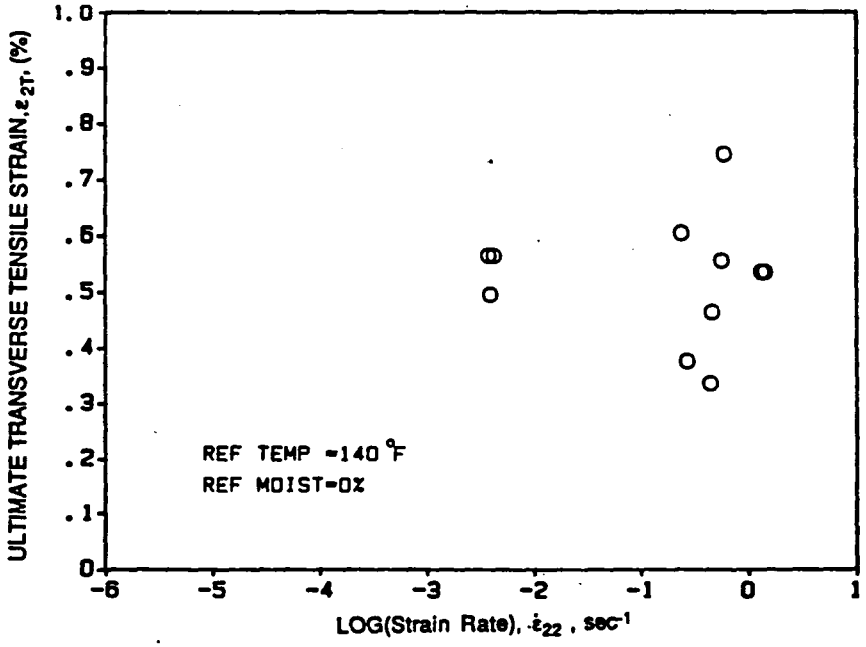

Figure 5.47 Ultimate transverse tensile strain vs. log(strain rate) curve for AS4/3501-6 Graphite/Epoxy, (T=60°C (140°F), C=0%)

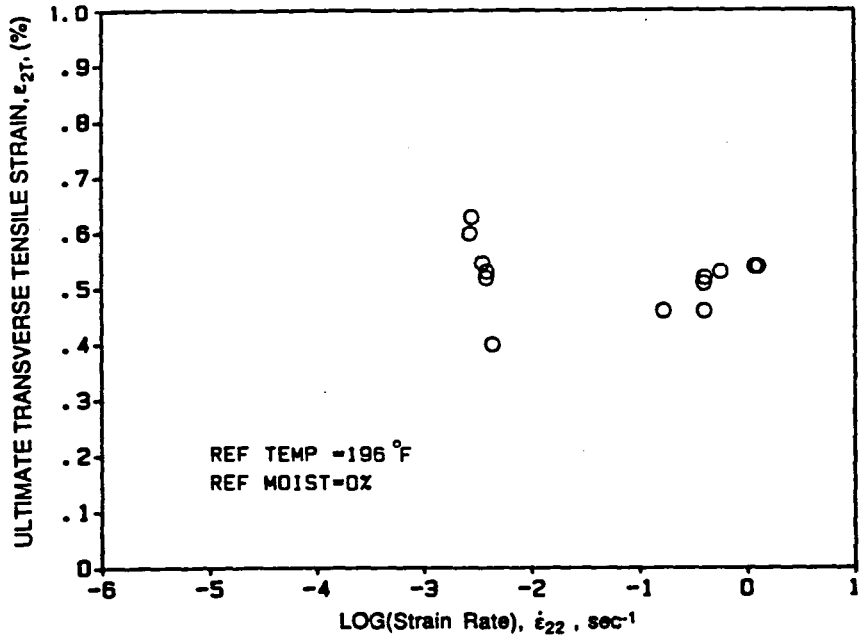

Figure 5.48 Ultimate transverse tensile strain vs. log(strain rate) curve for AS4/3501-6 Graphite/Epoxy, (T=91°C (196°F), C=0%)

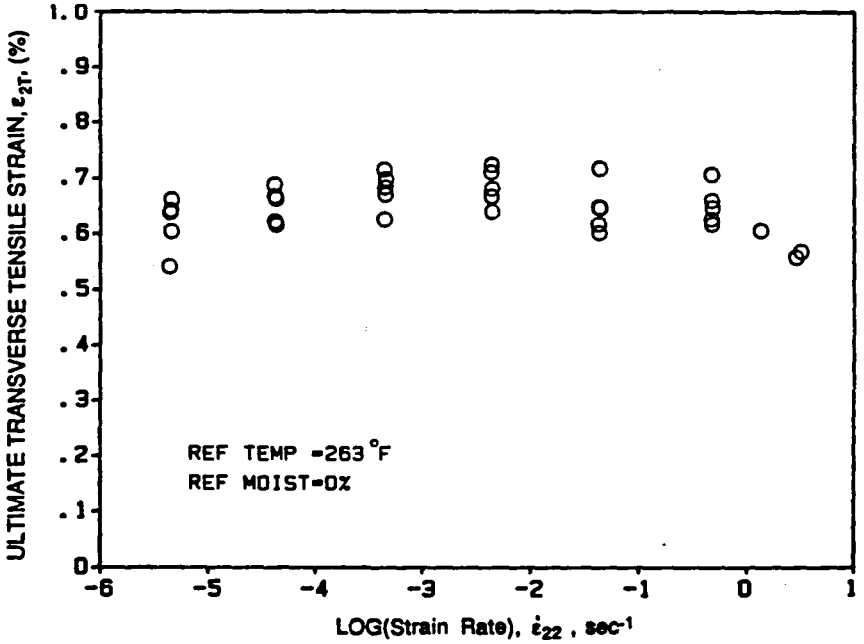

Figure 5.49 Ultimate transverse tensile strain vs. log(strain rate) curve for AS4/3501-6 Graphite/Epoxy, (T=128°C (263°F), C=0%)

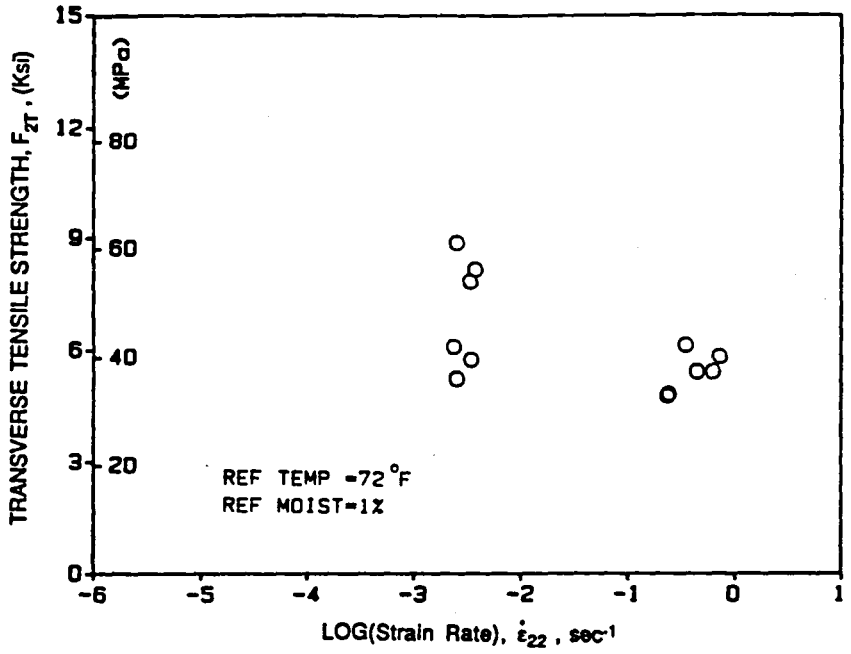

Figure 5.50 Transverse tensile strength vs. log(strain rate) curve for AS4/3501-6 Graphite/Epoxy, (T=22°C (72°F), C=1%)

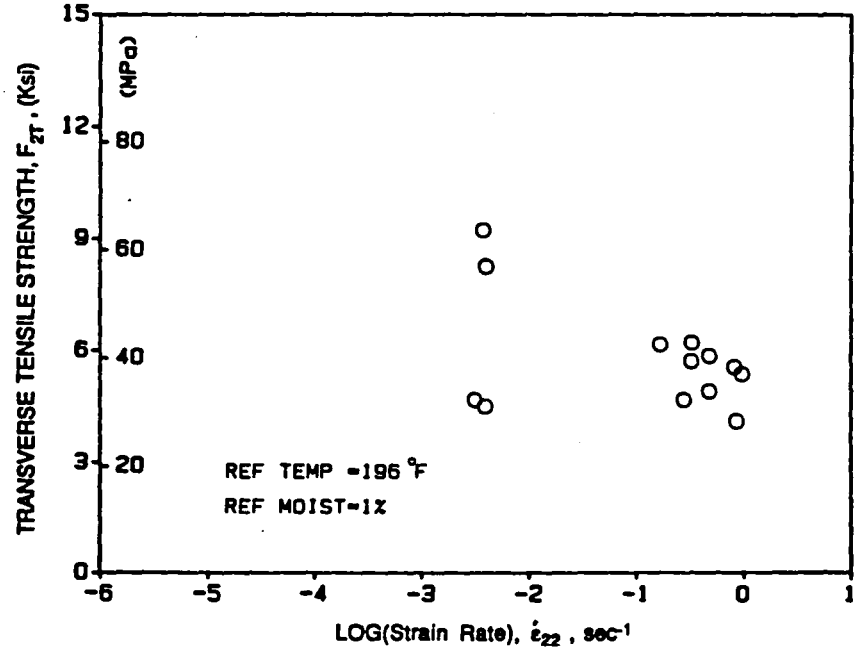

Figure 5.51 Transverse tensile strength vs. log(strain rate) curve for AS4/3501-6 Graphite/Epoxy, (T=91°C (196°F), C=1%)

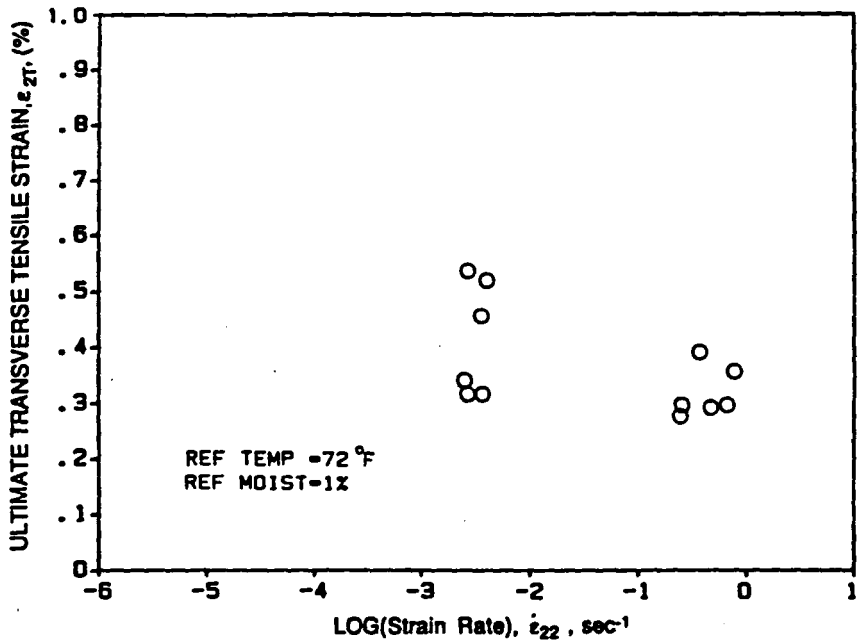

Figure 5.52 Ultimate transverse tensile strain vs. log(strain rate) curve for AS4/3501-6 Graphite/Epoxy, (T=22°C (72°F), C=1%)

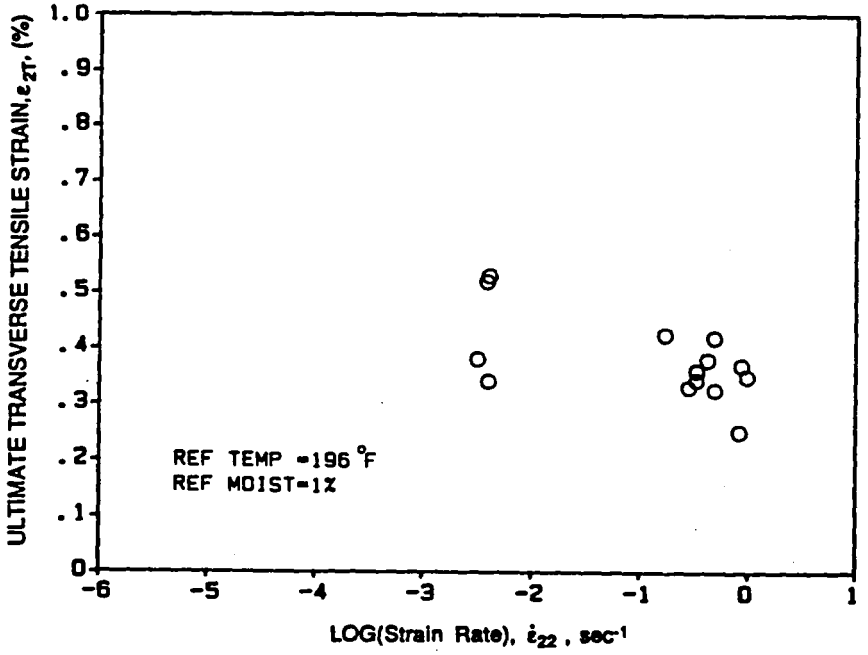

Figure 5.53 Ultimate transverse tensile strain vs. log(strain rate) curve for AS4/3501-6 Graphite/Epoxy, (T=91°C (196°F), C=1%)

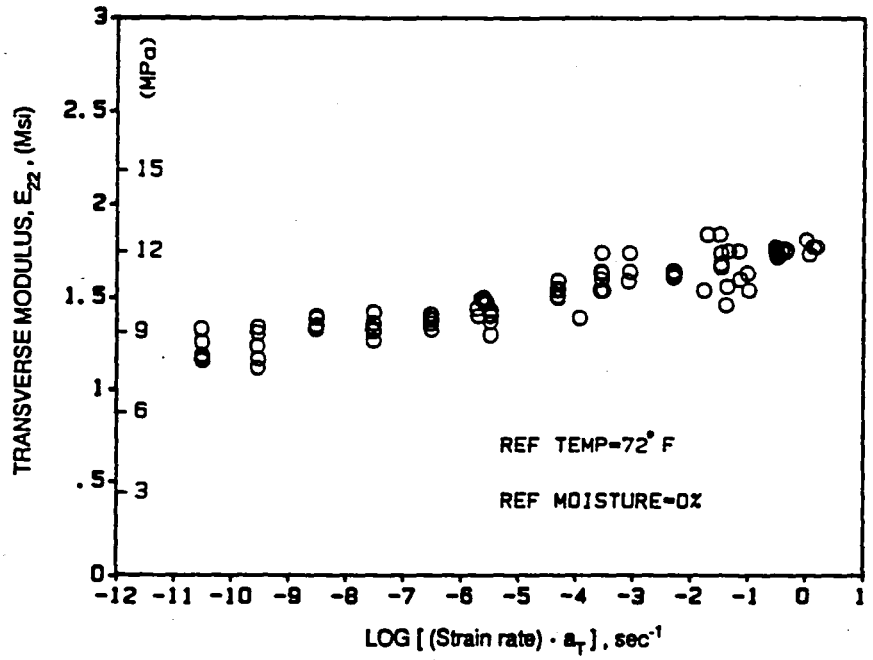

Figure 5.54 Time-temperature master curve for transverse modulus,(T=22°C (72°F), C=0%)

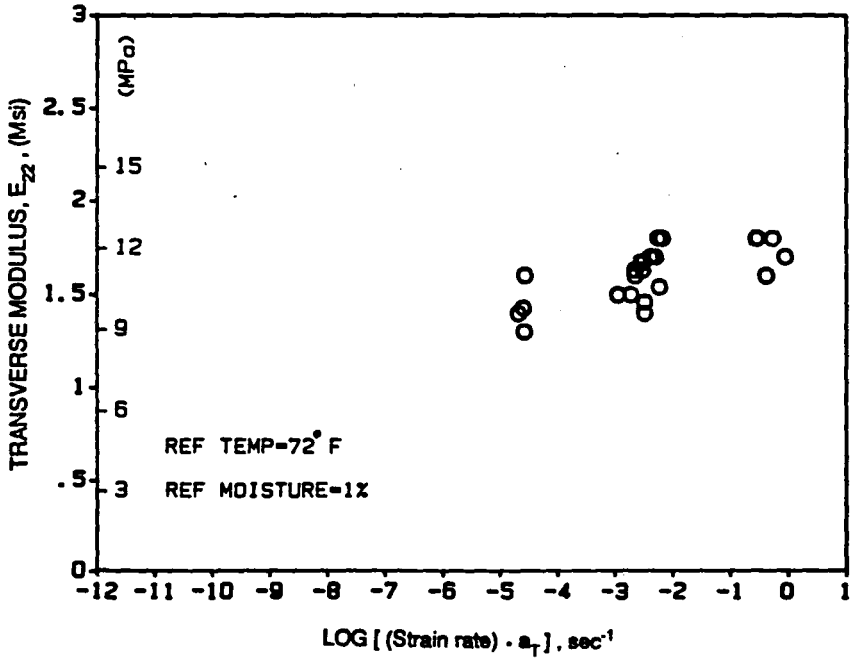

Figure 5.55 Time-temperature master curve for transverse modulus, (T=22°C (72°F), C=1%)

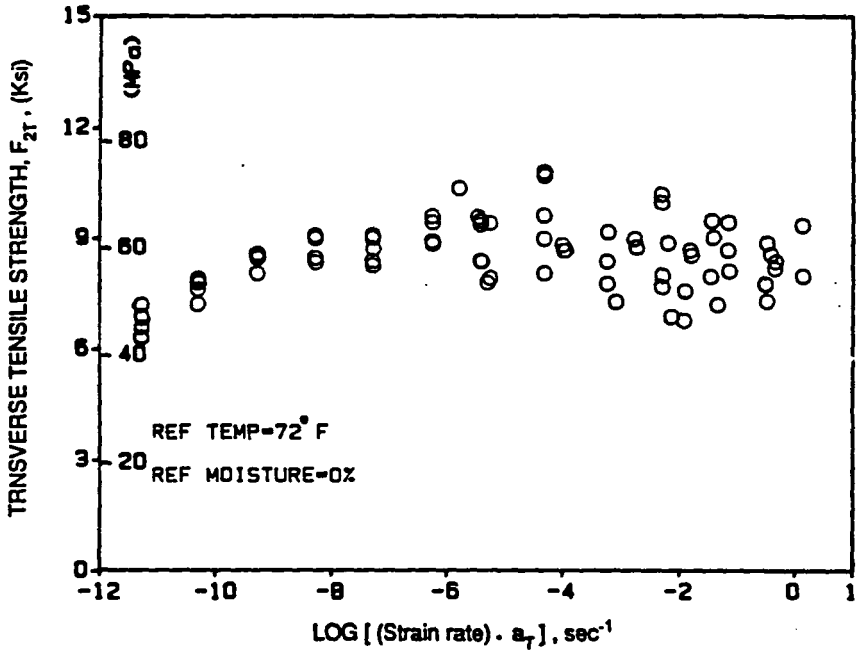

Figure 5.56 Time-temperature master curve for transverse tensile strength, (T=22°C (72°F), C=0%)

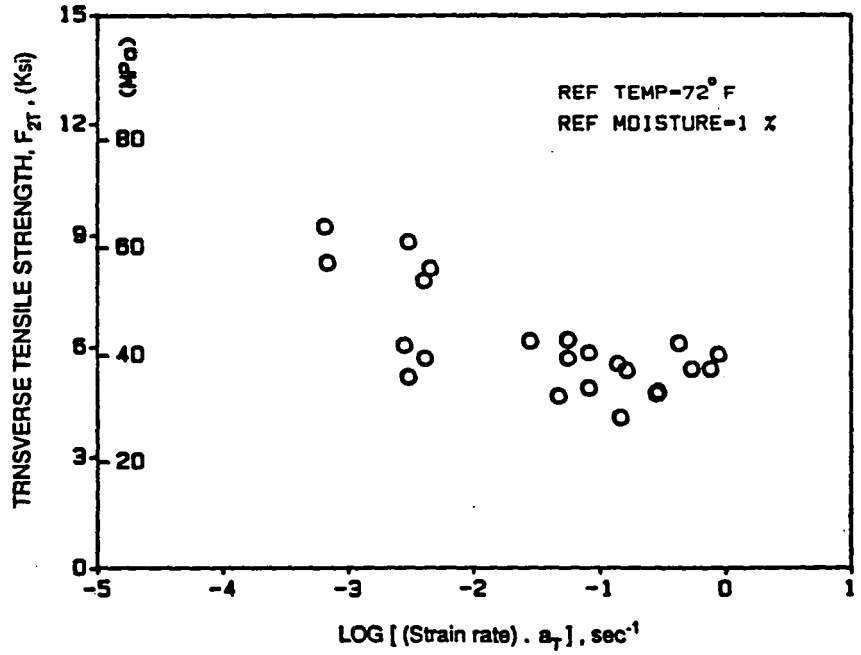

Figure 5.57 Time-temperature master curve for transverse tensile strength, (T=22°C (72°F), C=1%)

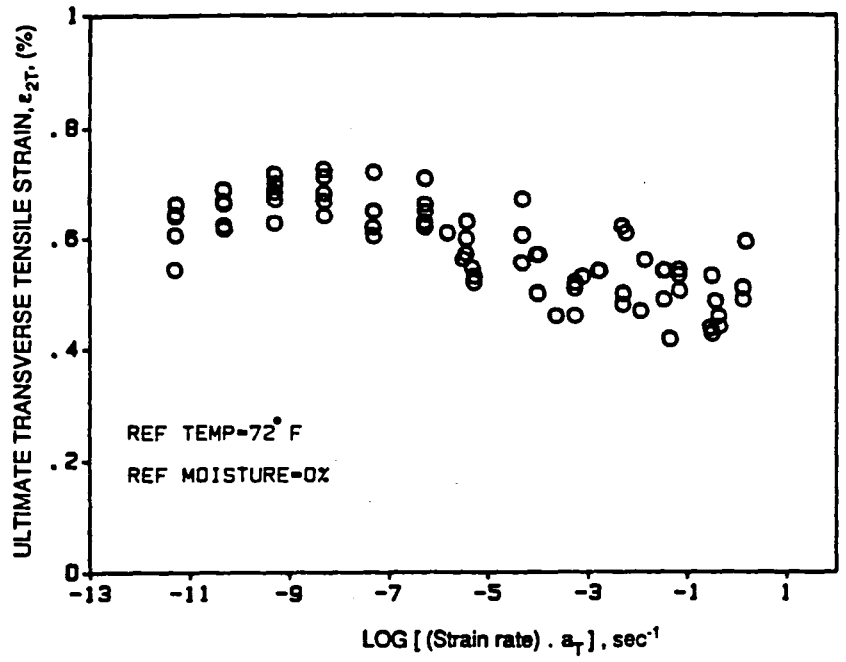

Figure 5.58 Time-temperature master curve for ultimate transverse tensile strain, (T=22°C (72°F), C=0%)

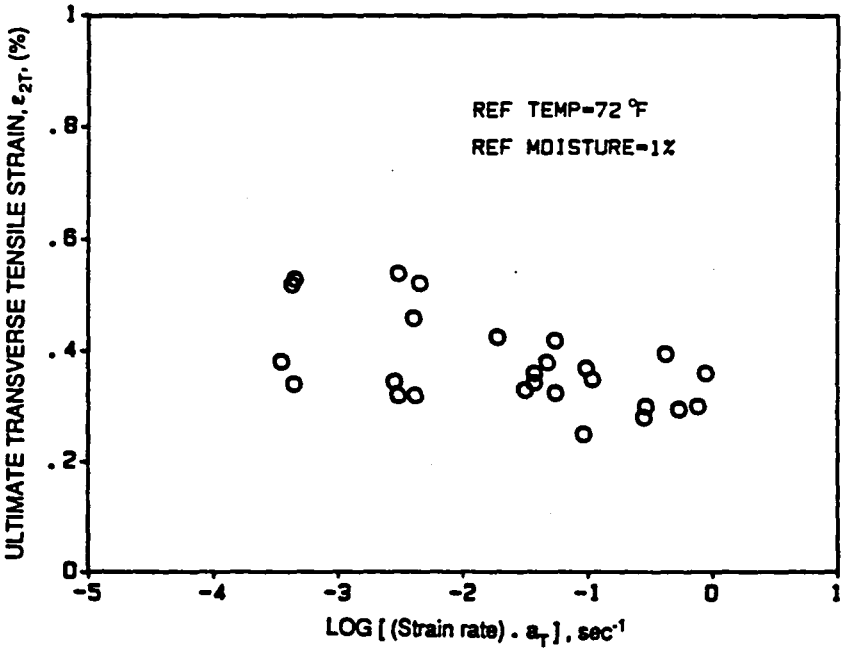

Figure 5.59 Time-temperature master curve for ultimate transverse tensile strain, (T=22°C (72°F), C=1%)

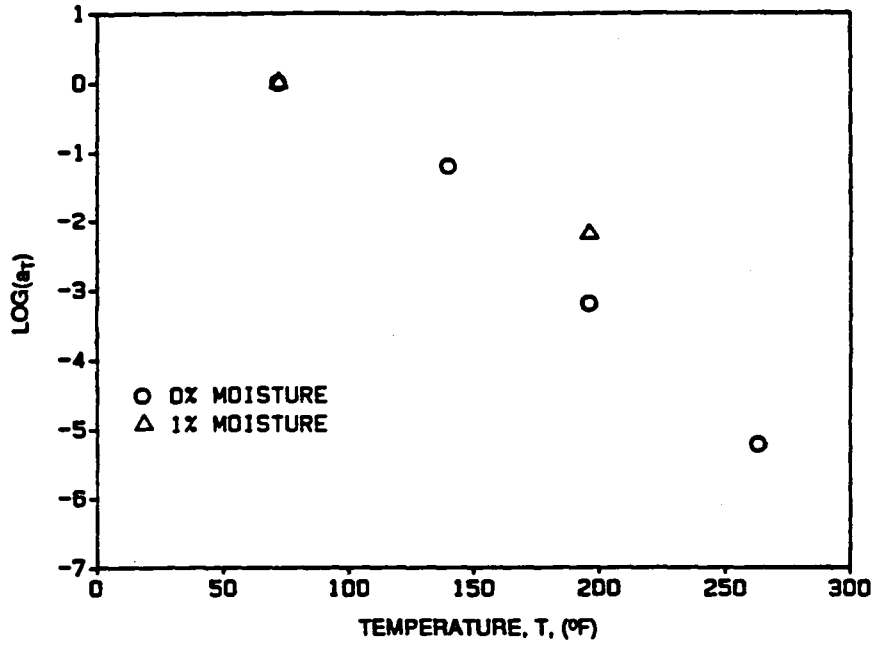

Figure 5.60 Log(Time-temperature shift factor) vs. temperature for transverse modulus under dry and wet (C=1%) conditions

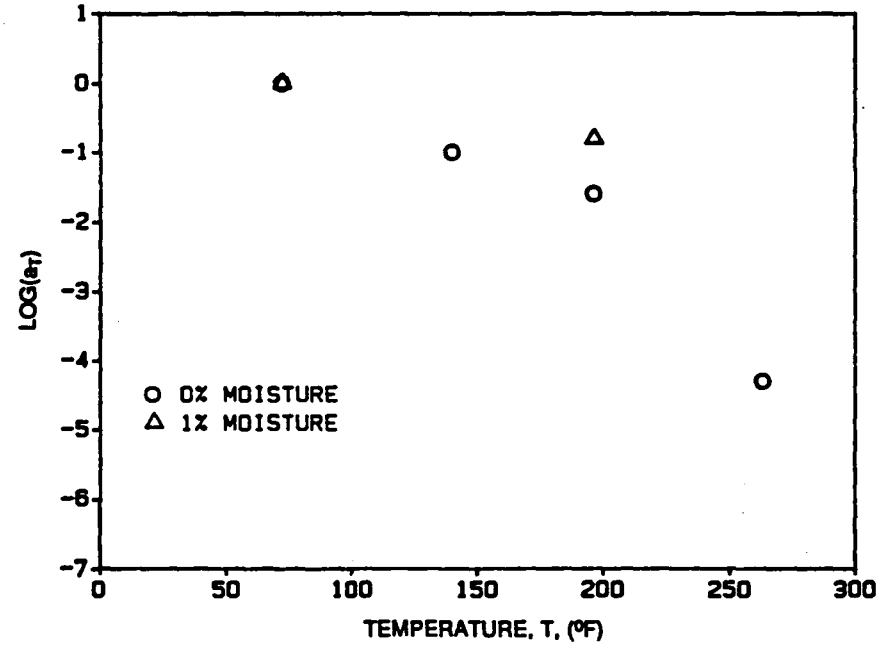

Figure 5.61 Log(Time-temperature shift factor) vs. temperature for transverse tensile strength under dry and wet (C=1%) conditions

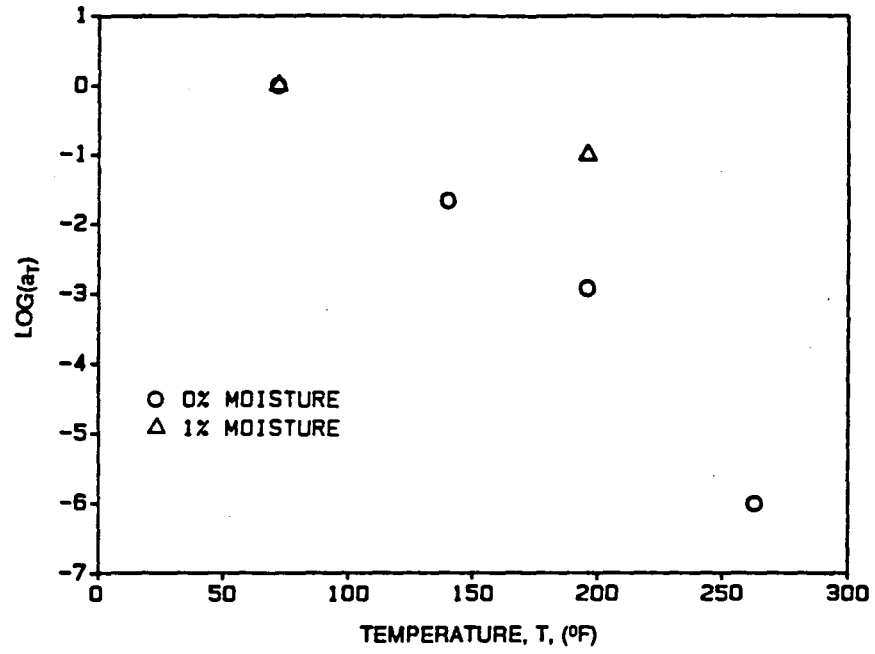

Figure 5.62 Log(Time-temperature shift factor) vs. temperature for transverse tensile strain under dry and wet (C=1%) conditions

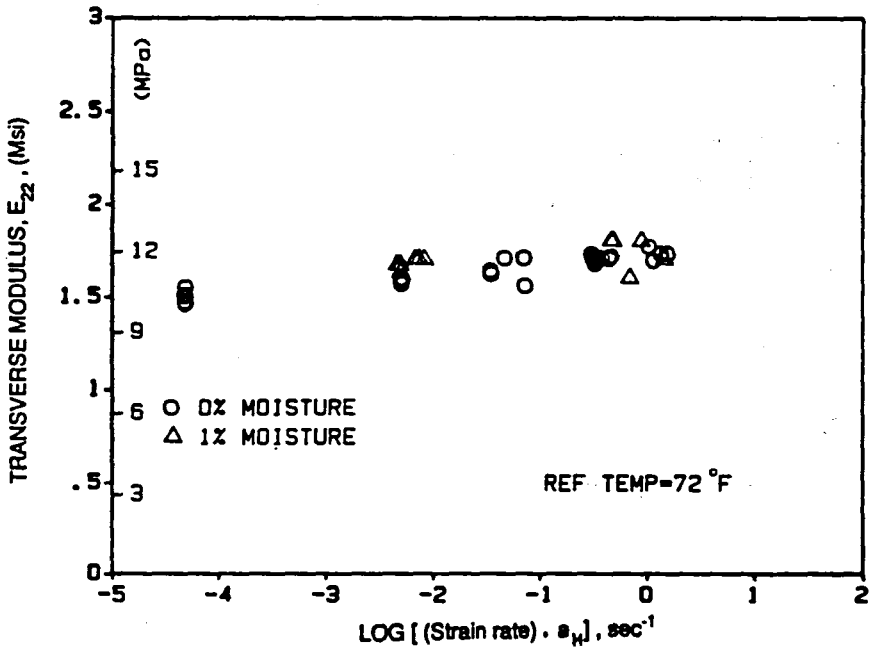

Figure 5.63 Time-moisture master curve for transverse modulus, (T=22°C (72°F), C=0%)

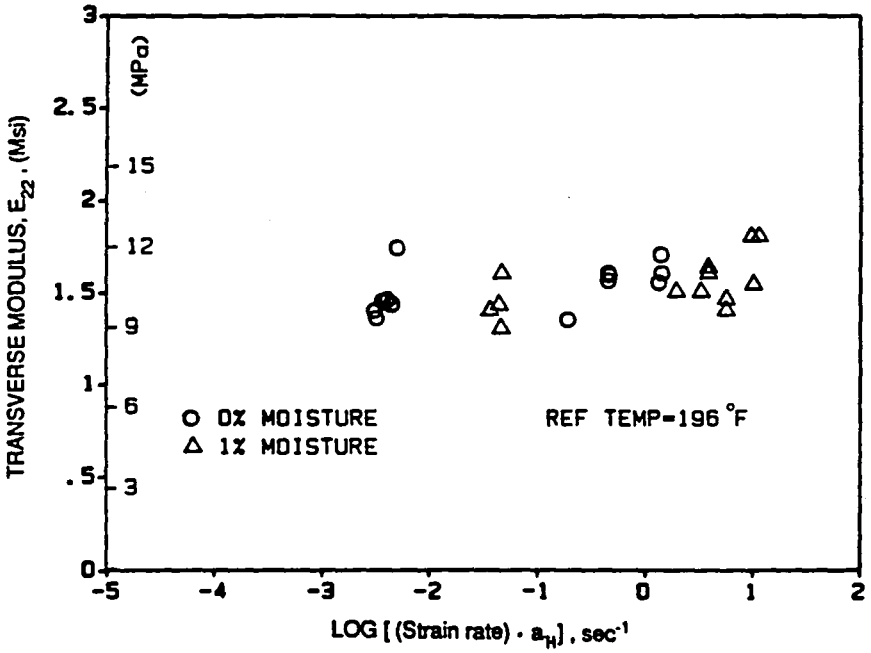

Figure 5.64 Time-moisture master curve for transverse modulus, (T=91°C 196°F), C=0%)

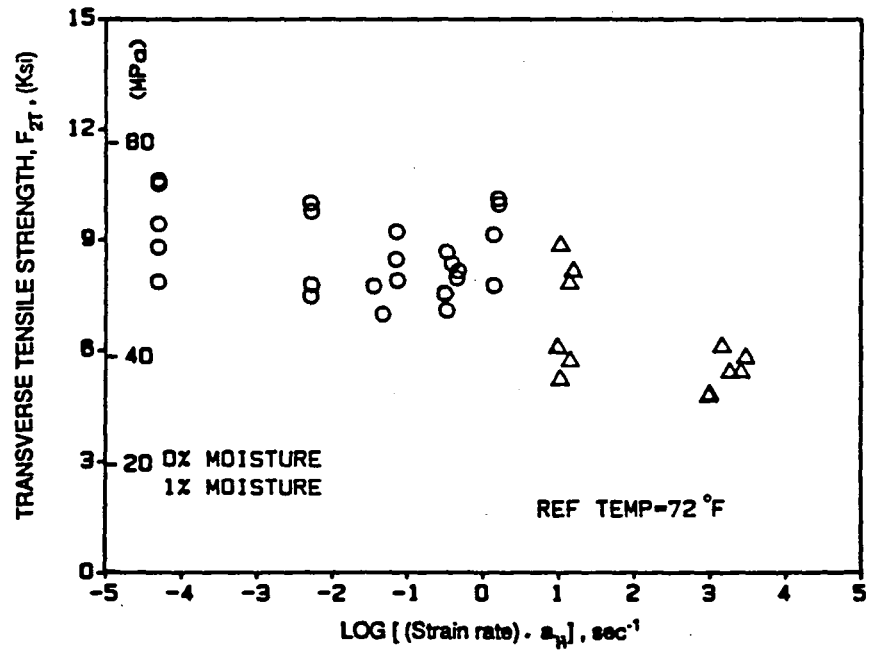

Figure 5.65 Time-moisture master curve for transverse tensile strength, (T=22°C (72°F), C=0%)

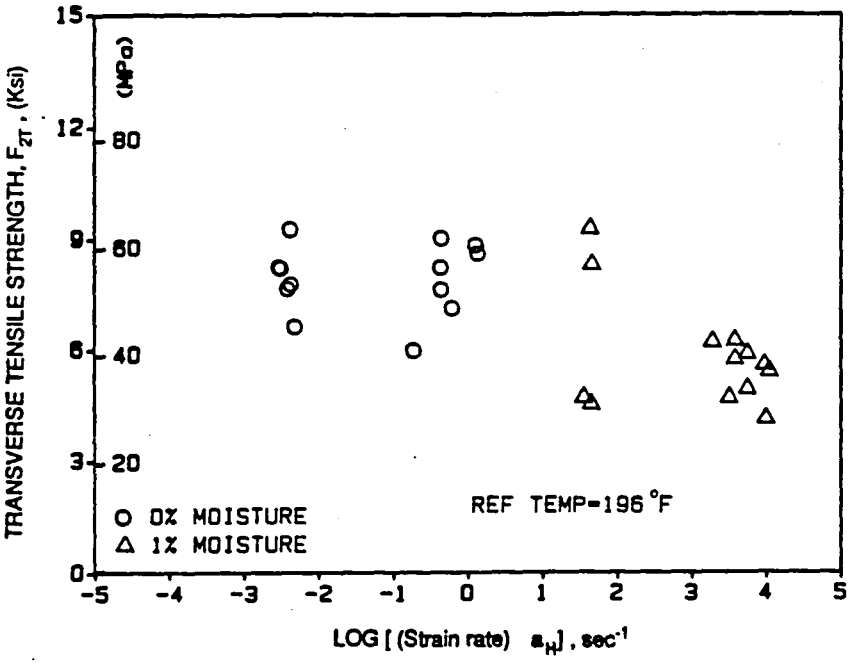

Figure 5.66 Time-moisture master curve for transverse tensile strength, (T=91°C (196°F), C=0%)

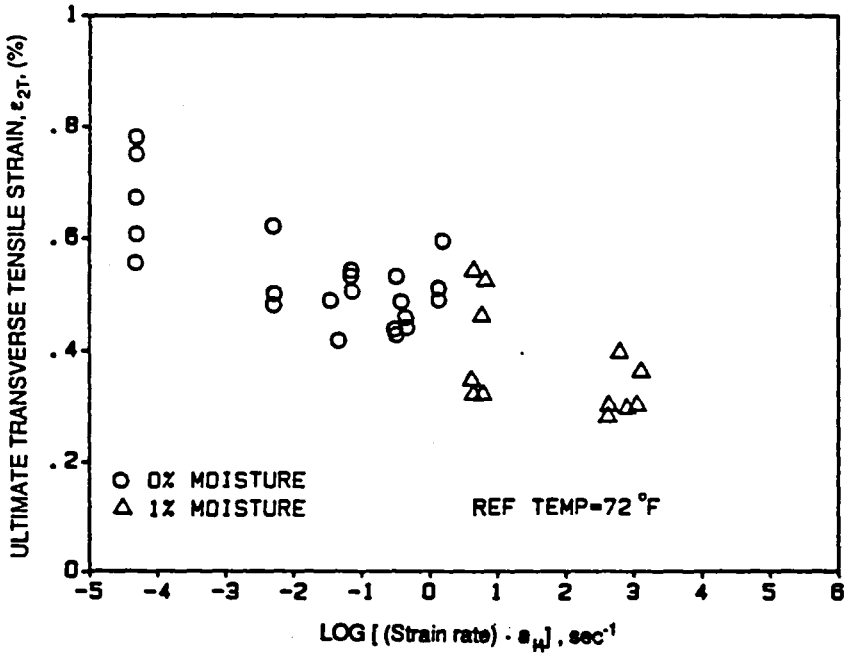

Figure 5.67 Time-moisture master curve for ultimate transverse tensile strain, (T=22°C (72°F), C=0%)

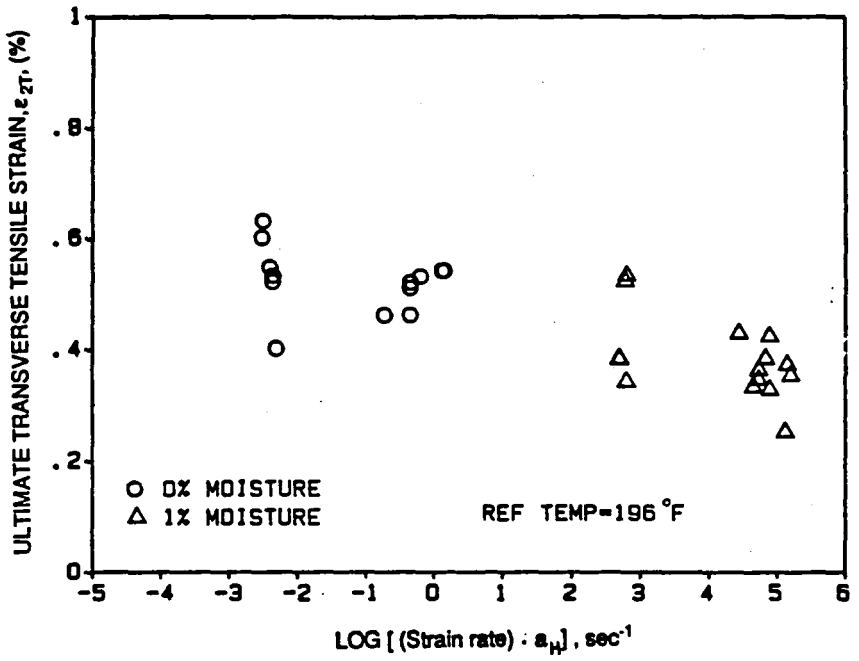

Figure 5.68 Time-moisture master curve for ultimate transverse tensile strain, (T=91°C (196°F), C=0%)

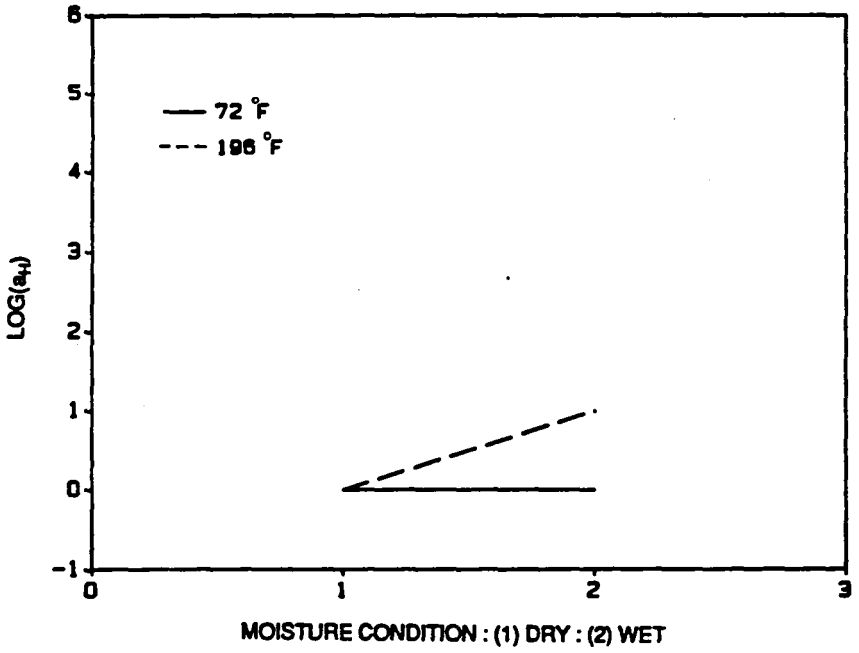

Figure 5.69 Log(Time-moisture shift factor) vs. moisture condition for transverse modulus, (T=22°C (72°F) and T=91°C (196°F)

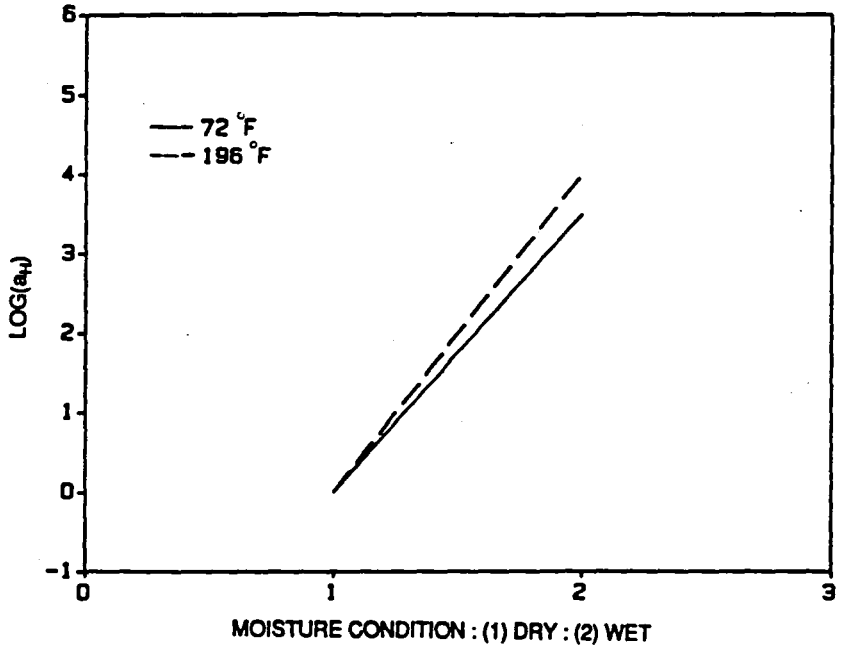

Figure 5.70 Log(Time-moisture shift factor) vs. moisture condition for transverse tensile strength, (T=22°C (72°F) and T=91°C (196°F)

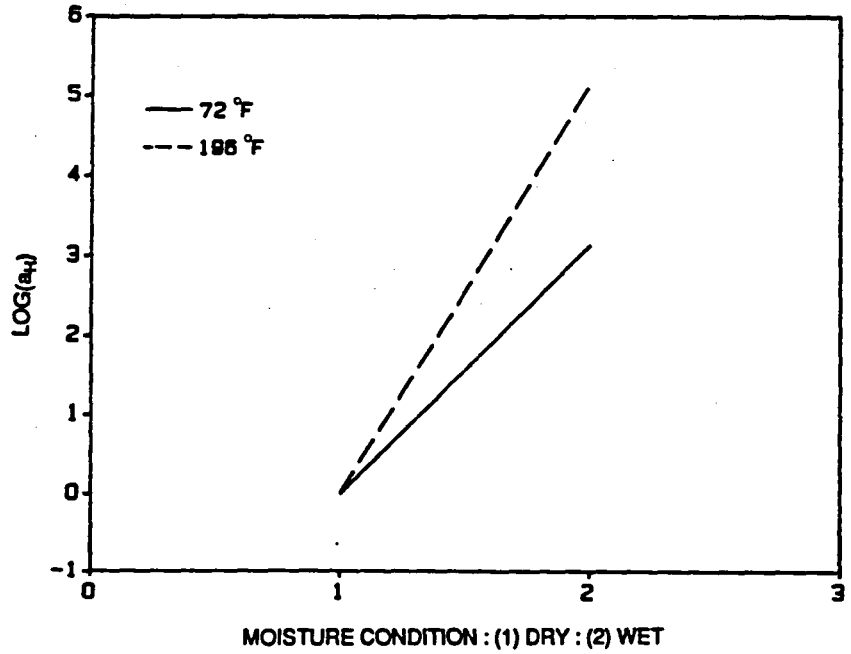

Figure 5.71 Log(Time-moisture shift factor) vs. moisture condition for transverse tensile strain, (T=22°C (72°F) and T=91°C (196°F)

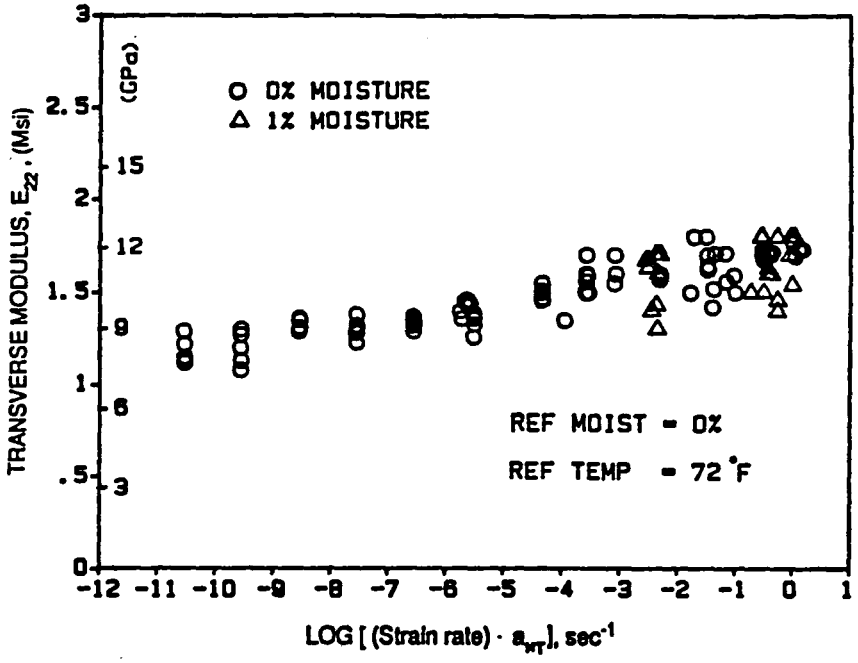

Figure 5.72 Time-Temperature-moisture master curve for transverse modulus

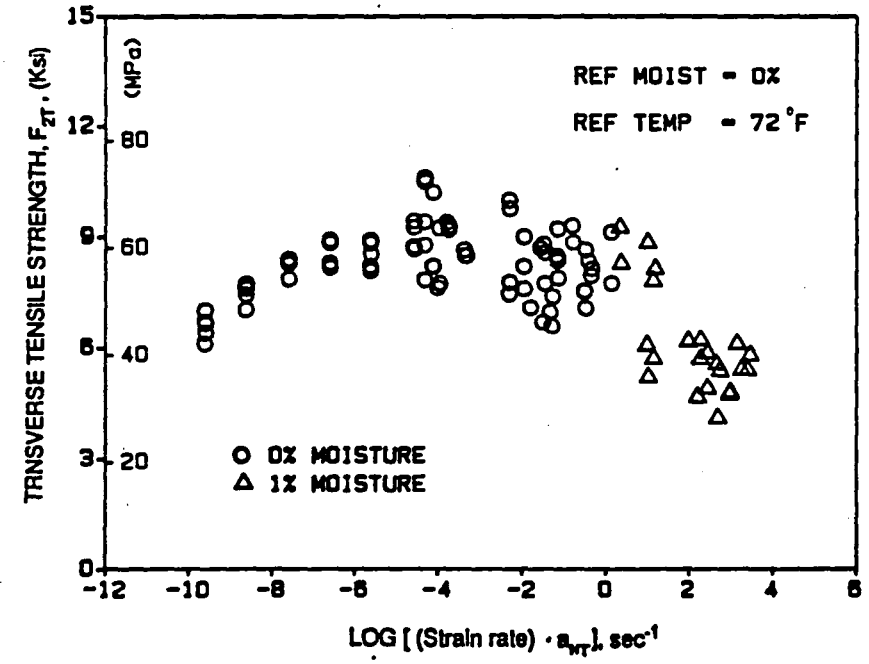

Figure 5.73 Time-Temperature-moisture master curve for transverse, tensile strength

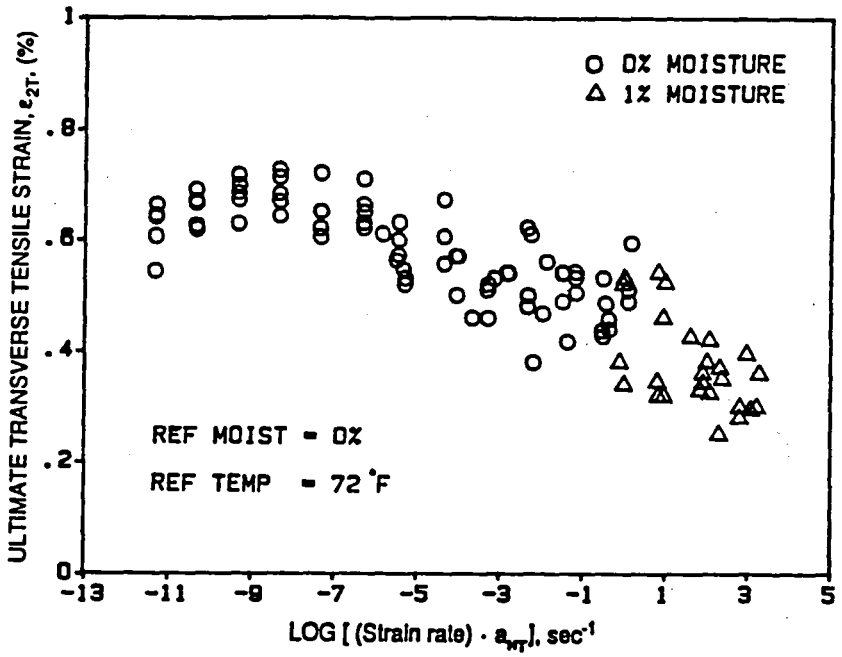

Figure 5.74 Time-Temperature-moisture master curve for transverse tensile strain

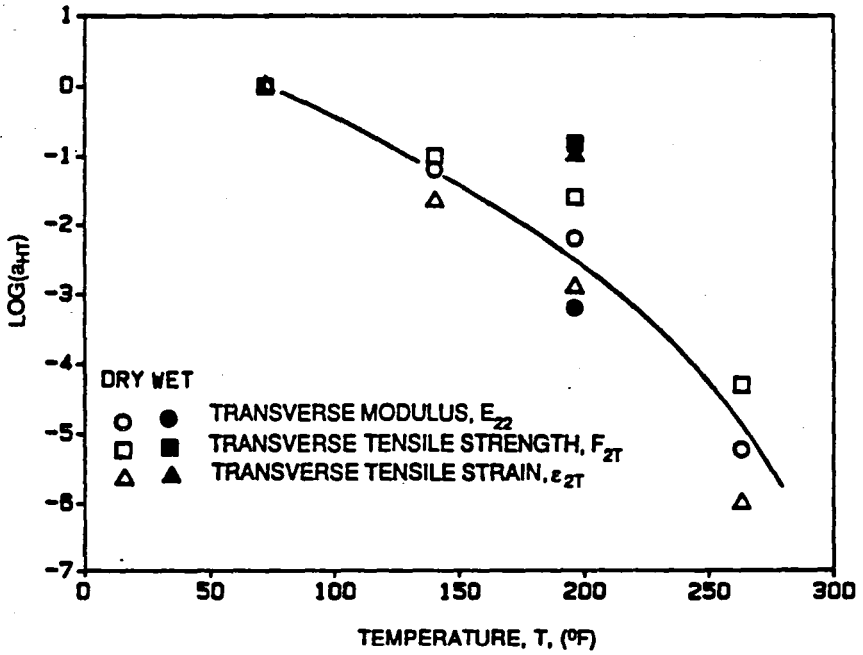

Figure 5.75 Time-temperature shift function for transverse tensile properties under dry and wet (C=1%) conditions

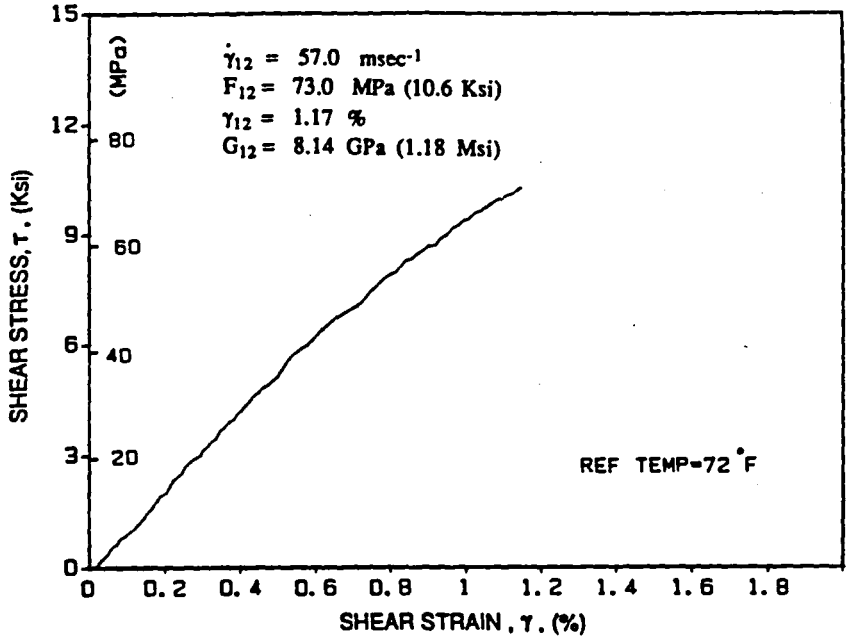

Figure 5.76 Typical shear stress-strain curve for [10_8] AS4/3501-6 Graphite/Epoxy, ($\dot{\gamma}$=5.7·10^{-2} s^{-1}, T=22°C (72°F), C=0%)

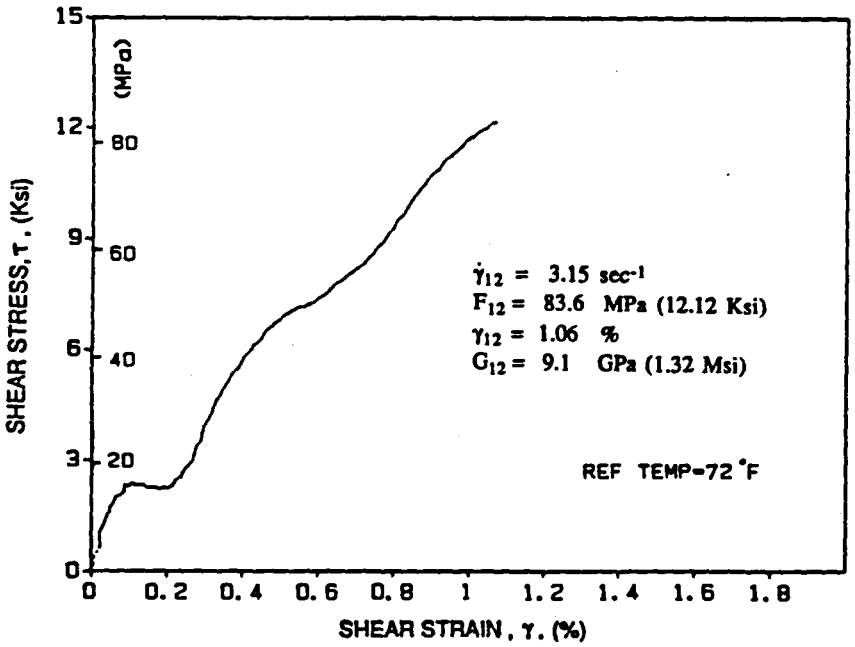

Figure 5.77 Typical shear stress-strain curve for [10_8] AS4/3501-6 Graphite/Epoxy, ($\dot{\gamma}$=3.15 s^{-1}, T=22°C (72°F), C=0%)

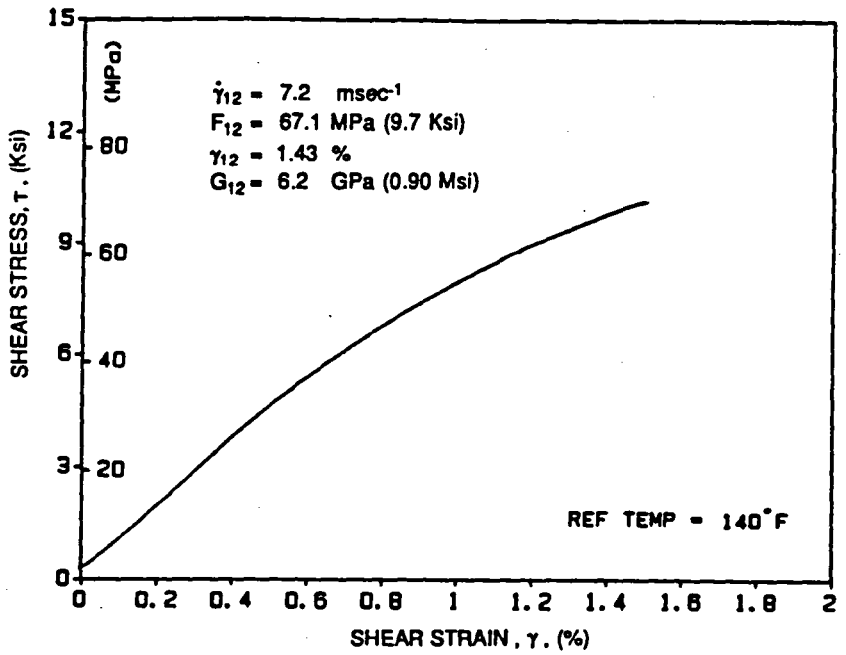

Figure 5.78 Typical shear stress-strain curve for [10_6] AS4/3501-6 Graphite/Epoxy, ($\dot{\gamma}$=7.2$10^{-3}$ s^{-1}, T=60°C (140°F), C=0%)

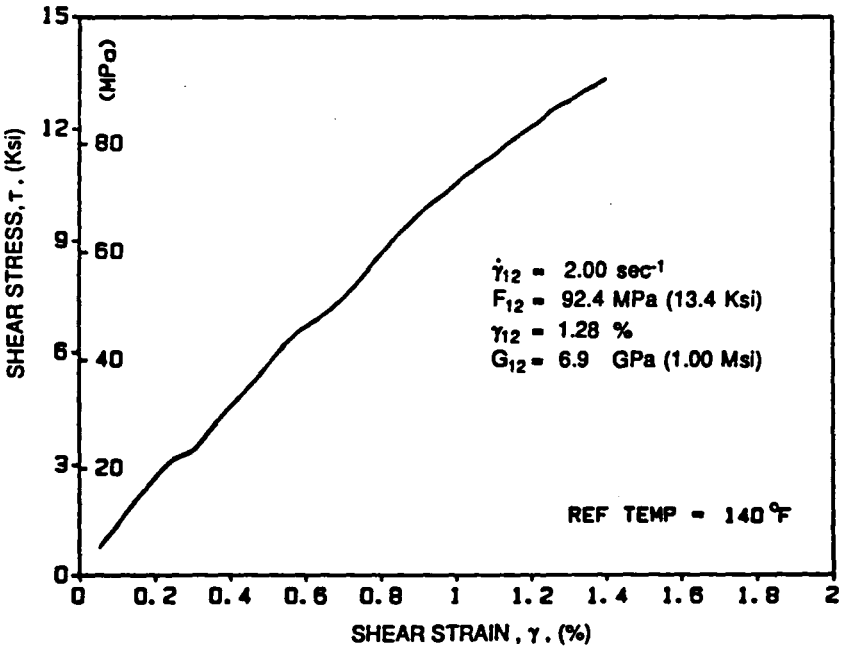

Figure 5.79 Typical shear stress-strain curve for [10_6] AS4/3501-6 Graphite/Epoxy, ($\dot{\gamma}$=2.0 s^{-1}, T=60°C (140°F), C=0%)

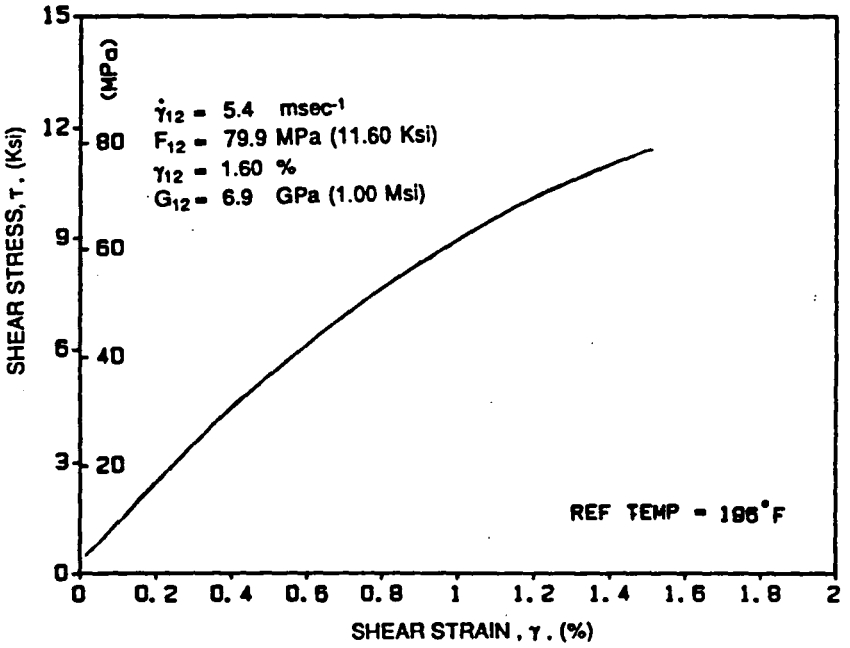

Figure 5.80 Typical shear stress-strain curve for [10_6] AS4/3501-6 Graphite/Epoxy, ($\dot{\gamma}$=5.4·10^{-3} s^{-1}, T=91°C (196°F), C=0%)

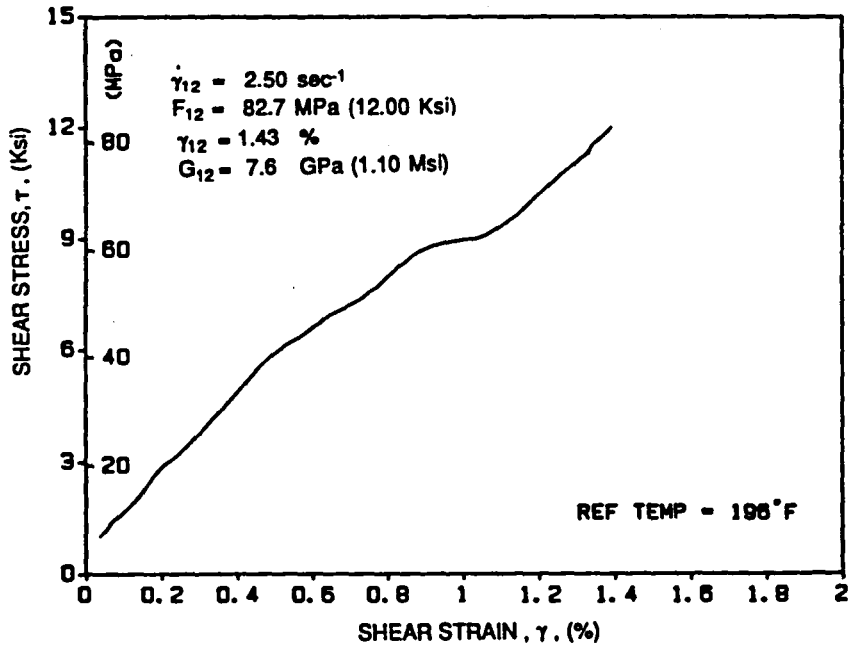

Figure 5.81 Typical shear stress-strain curve for [10_6] AS4/3501-6 Graphite/Epoxy, ($\dot{\gamma}$=2.5s^{-1}, T=91°C (196°F), C=0%)

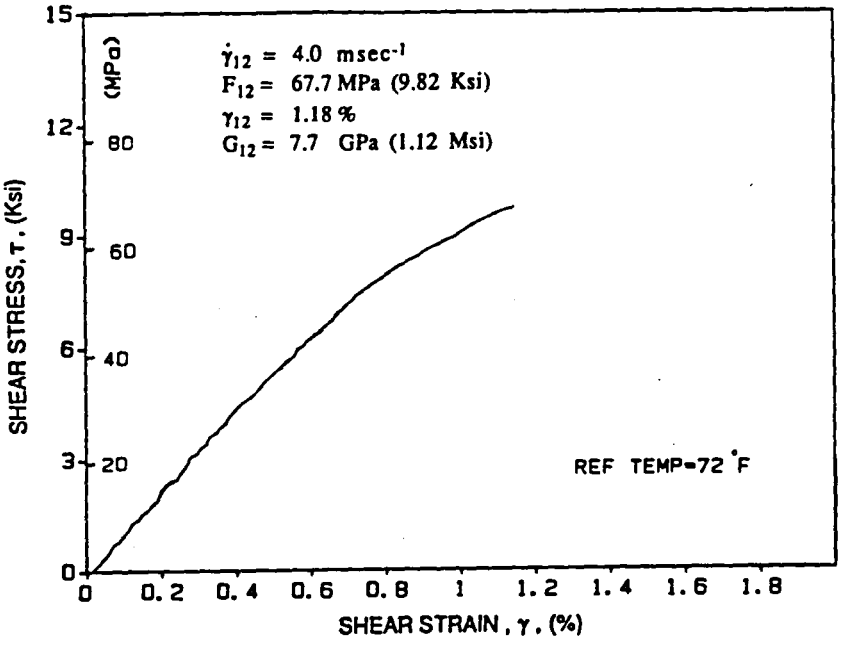

Figure 5.82 Typical shear stress-strain curve for [10_6] AS4/3501-6 Graphite/Epoxy, ($\dot{\gamma}$=4.0·10^{-3} s^{-1}, T=22°C (72°F), C=0%)

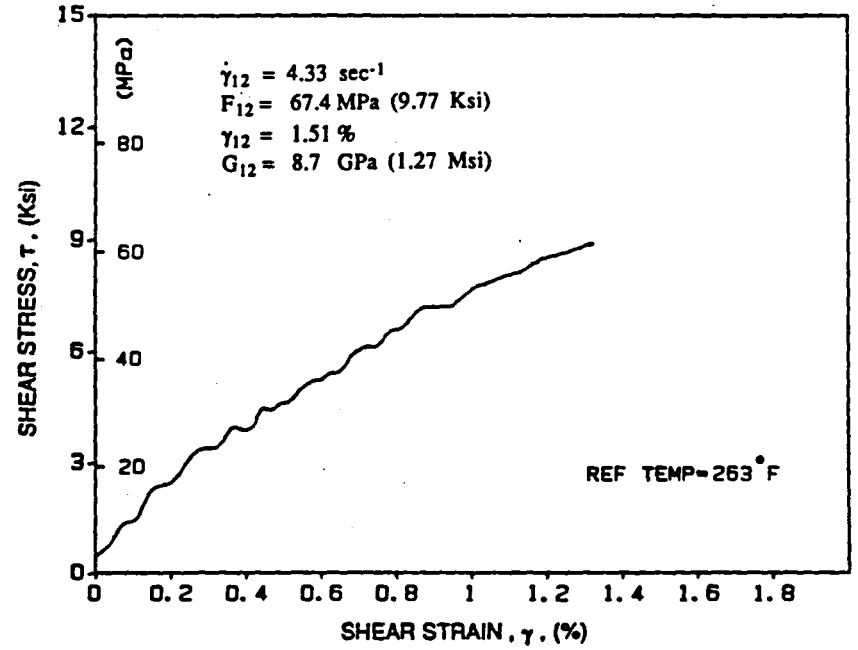

Figure 5.83 Typical shear stress-strain curve for [10_6] AS4/3501Graphite/Epoxy, ($\dot{\gamma}$=4.33 s^{-1}, T128°C (263°F), C=0%)

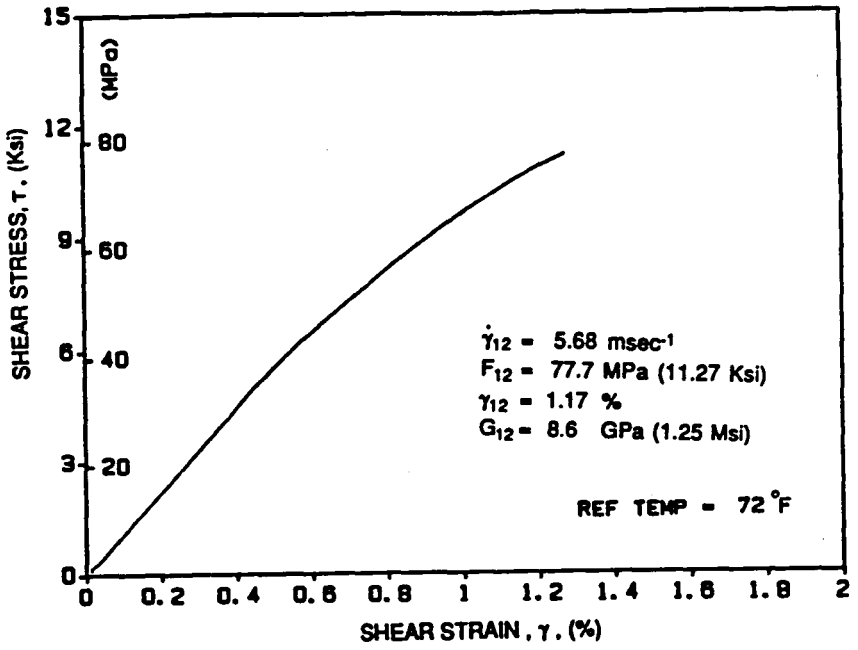

Figure 5.84 Typical shear stress-strain curve for [10_6] AS4/3501-6 Graphite/Epoxy, ($\dot{\gamma}$=5.6$10^{-3}$ s^{-1}, T=22°C (72°F), C=1%)

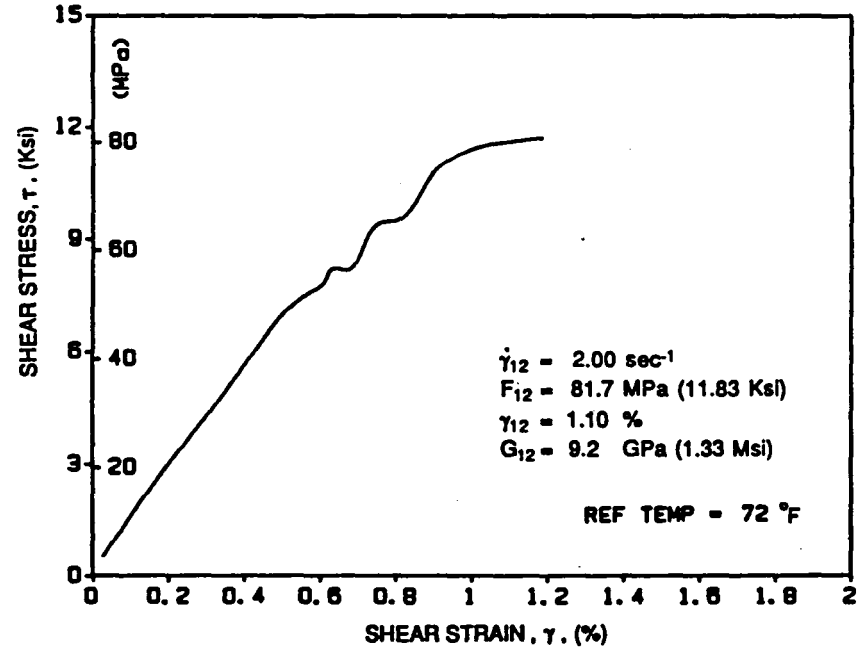

Figure 5.85 Typical shear stress-strain curve for [10_6] AS4/3501-6 Graphite/Epoxy, ($\dot{\gamma}$=2.0 s^{-1}, T=22°C (72°F), C=1%)

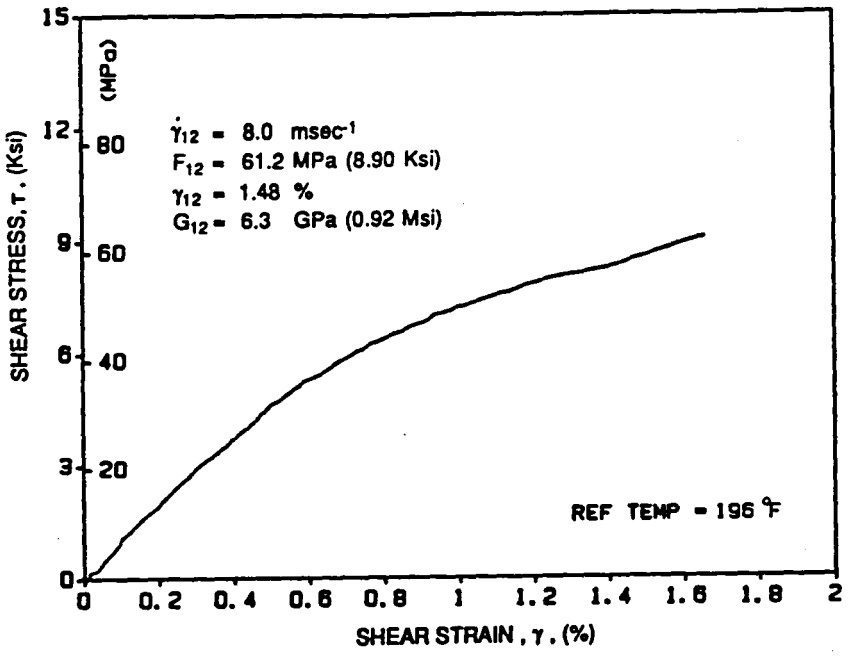

Figure 5.86 Typical shear stress-strain curve for [10_6] AS4/3501-6 Graphite/Epoxy, ($\dot{\gamma}$=8.0·10^{-3} s^{-1}, T=91°C (196°F), C=1%)

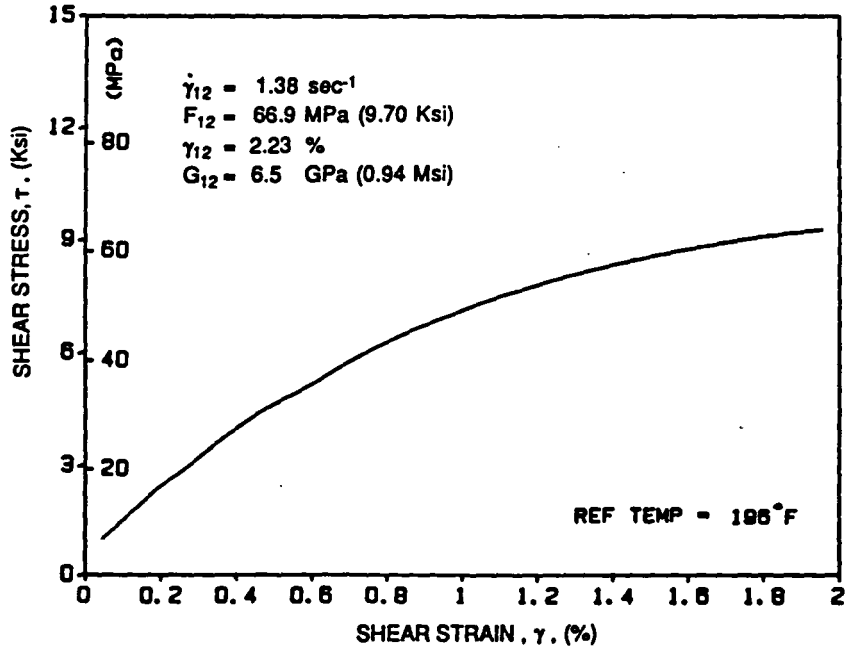

Figure 5.87 Typical shear stress-strain curve for [10_6] AS4/3501-6 Graphite/Epoxy, ($\dot{\gamma}$=1.38s^{-1}, T=91°C (196°F), C=1%)

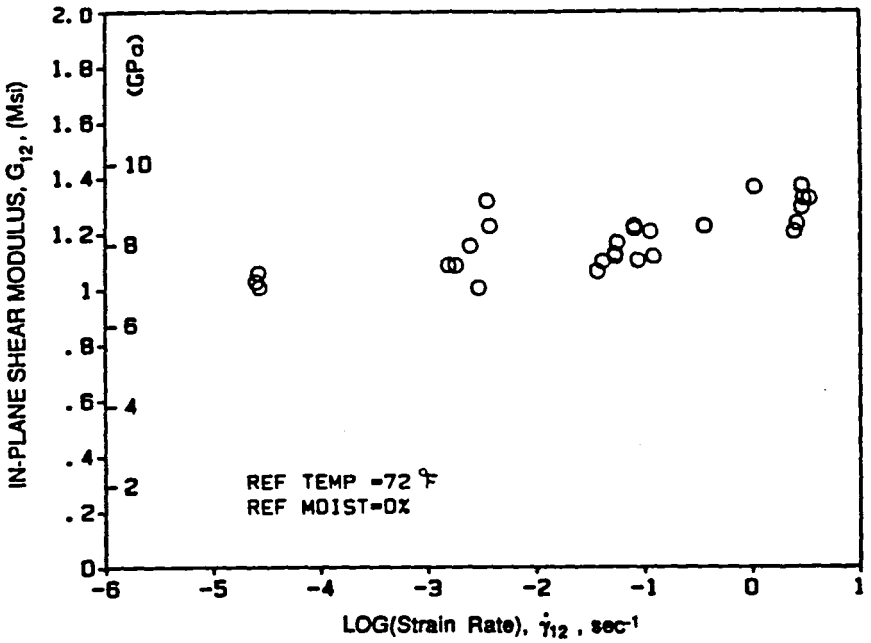

Figure 5.88 In-plane shear modulus vs. log(strain rate) curve for AS4/3501-6 Graphite/Epoxy, (T=22°C (72°F), C=0%)

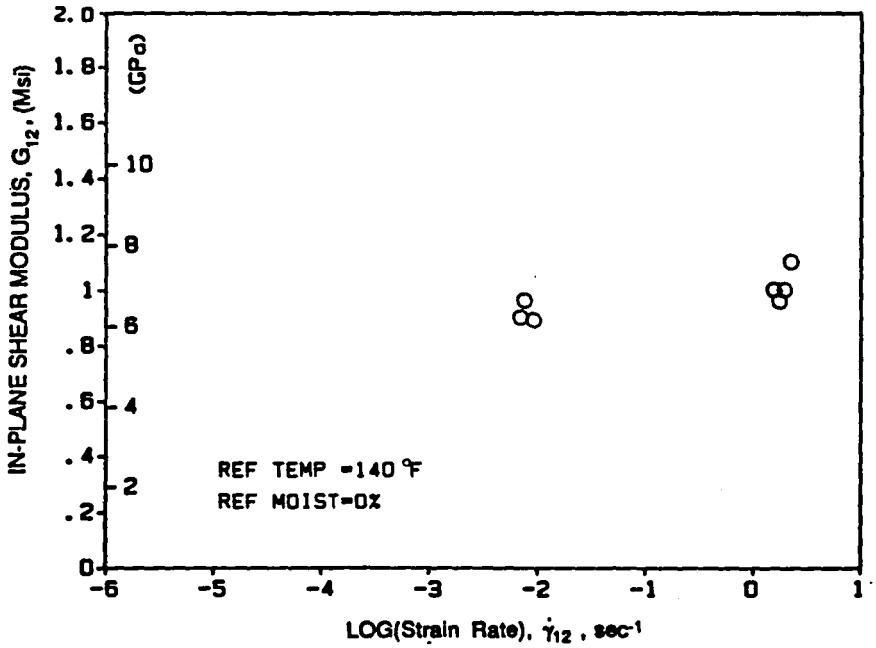

Figure 5.89 In-plane shear modulus vs. log(strain rate) curve for AS4/3501-6 Graphite/Epoxy, (T=60°C (140°F), C=0%)

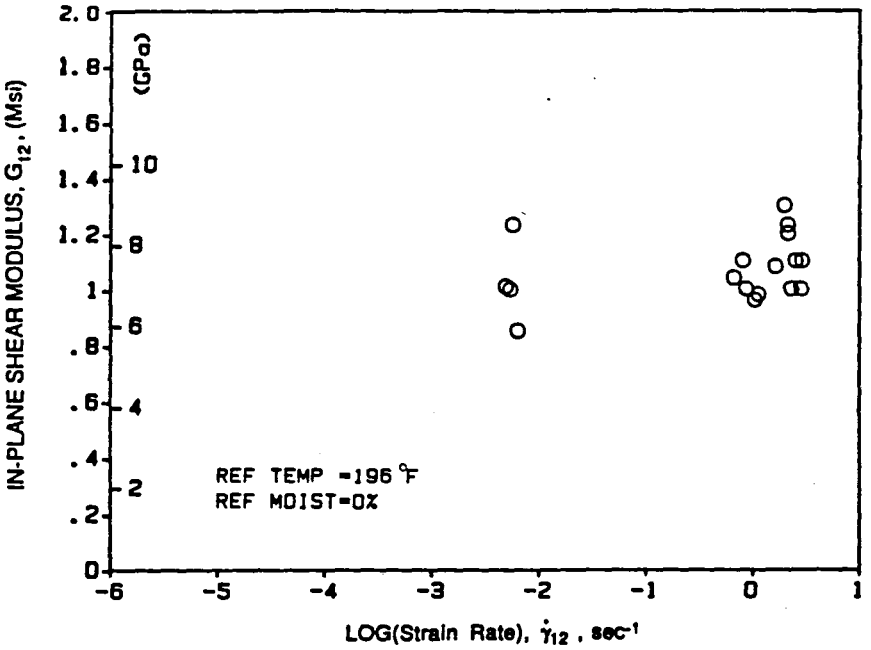

Figure 5.90 In-plane shear modulus vs. log(strain rate) curve for AS4/3501-6 Graphite/Epoxy, (T=91°C (196°F), C=0%)

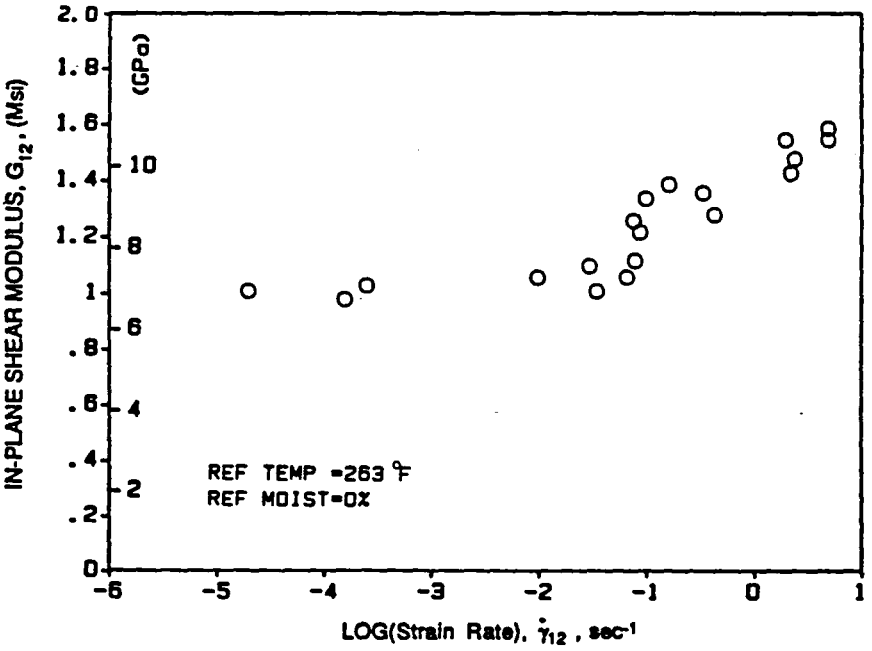

Figure 5.91 In-plane shear modulus vs. log(strain rate) curve for AS4/3501-6 Graphite/Epoxy, (T=128°C (263°F), C=0%)

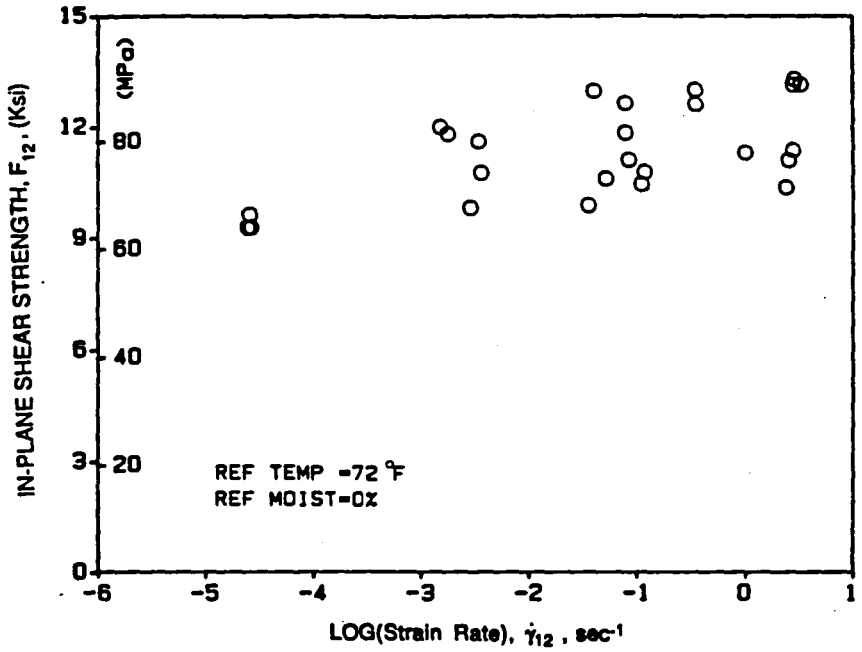

Figure 5.92 In-plane shear strength vs. log(strain rate) curve for AS4/3501-6 Graphite/Epoxy, (T=22°C (72°F), C=0%)

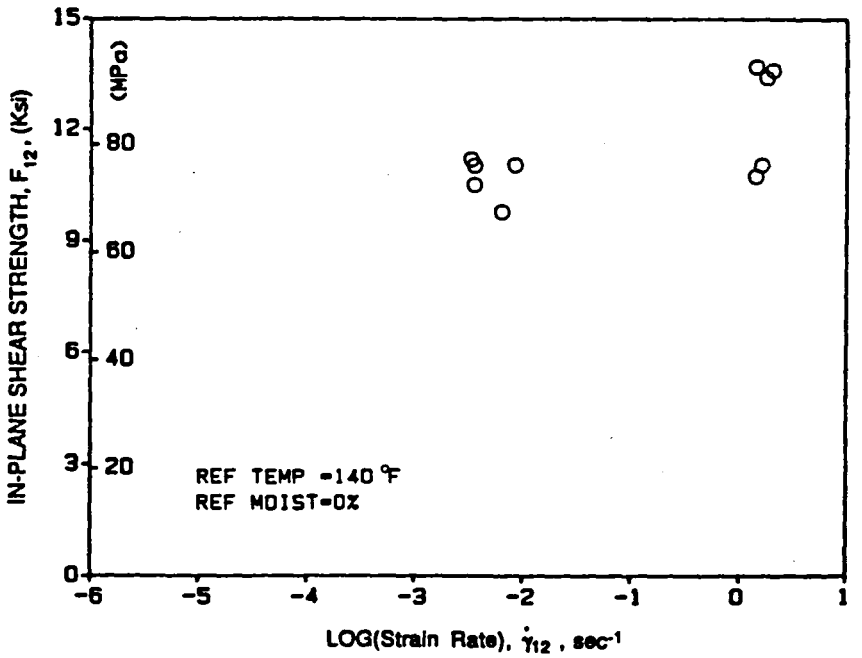

Figure 5.93 In-plane shear strength vs. log(strain rate) curve for AS4/3501-6 Graphite/Epoxy, (T=60°C (140°F), C=0%)

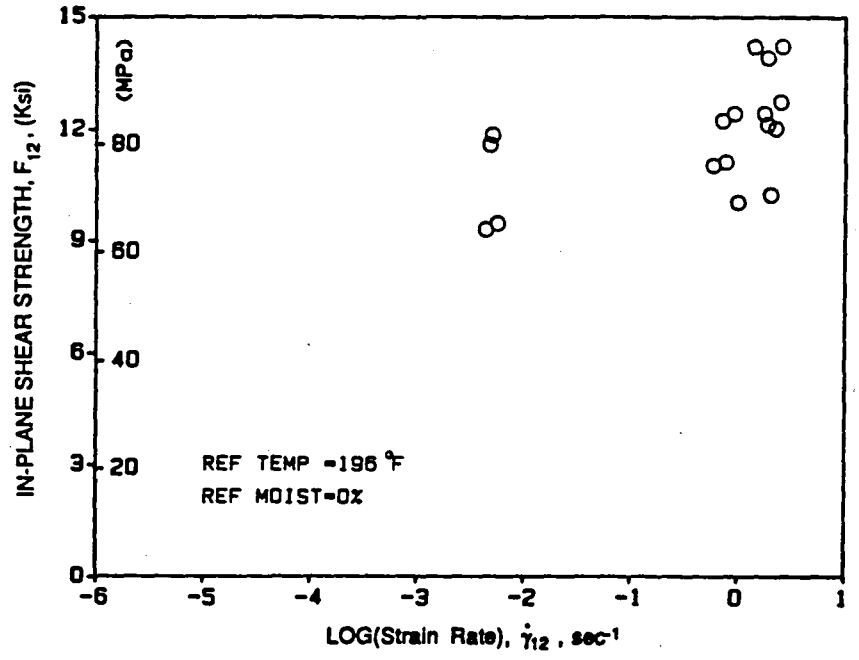

Figure 5.94 In-plane shear strength vs. log(strain rate) curve for AS4/3501-6 Graphite/Epoxy, (T=91°C (196°F), C=0%)

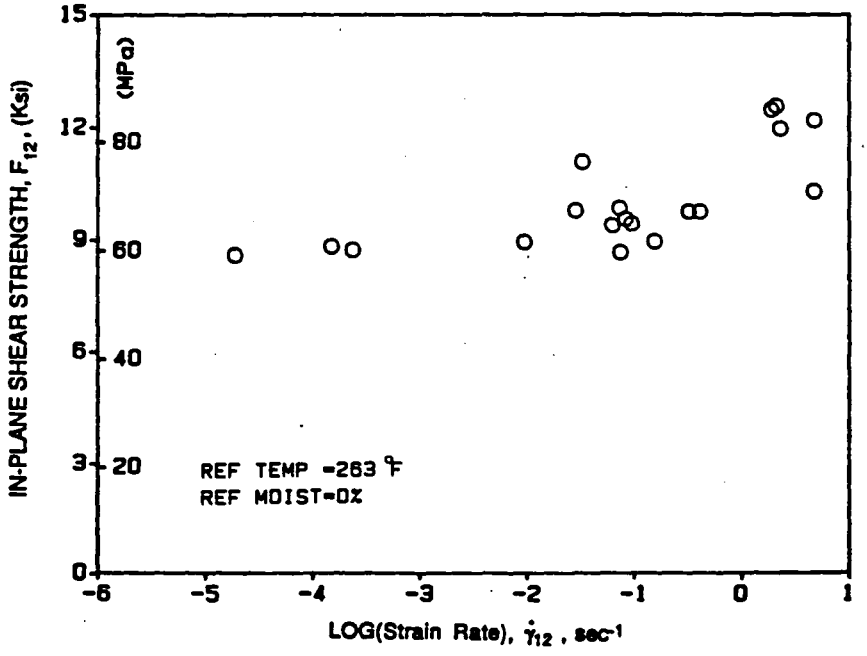

Figure 5.95 In-plane shear strength vs. log(strain rate) curve for AS4/3501-6 Graphite/Epoxy, (T=128°C (263°F), C=0%)

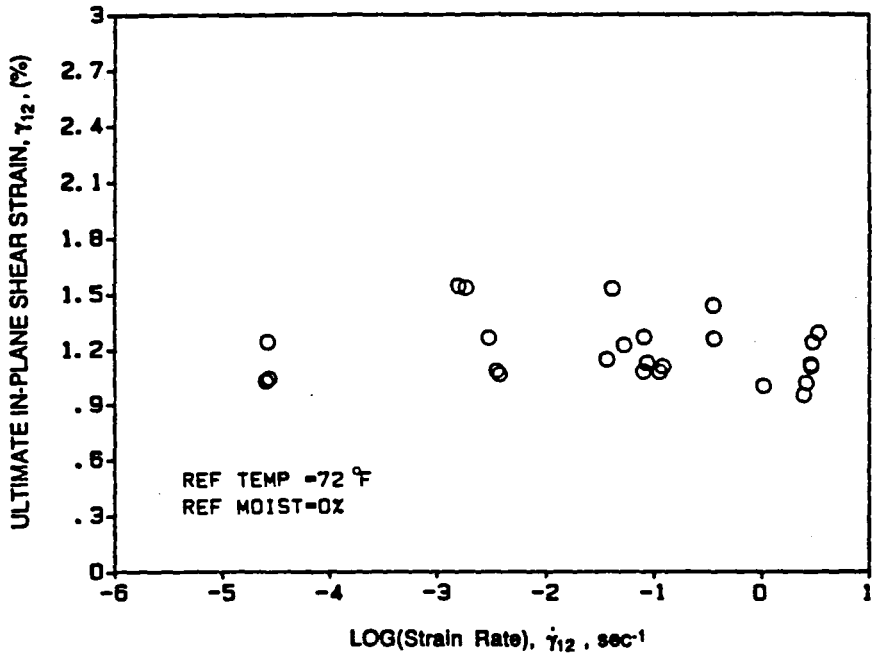

Figure 5.96 Ultimate in-plane shear strain vs. log(strain rate) curve for AS4/3501-6 Graphite/Epoxy, (T=22°C (72°F), C=0%)

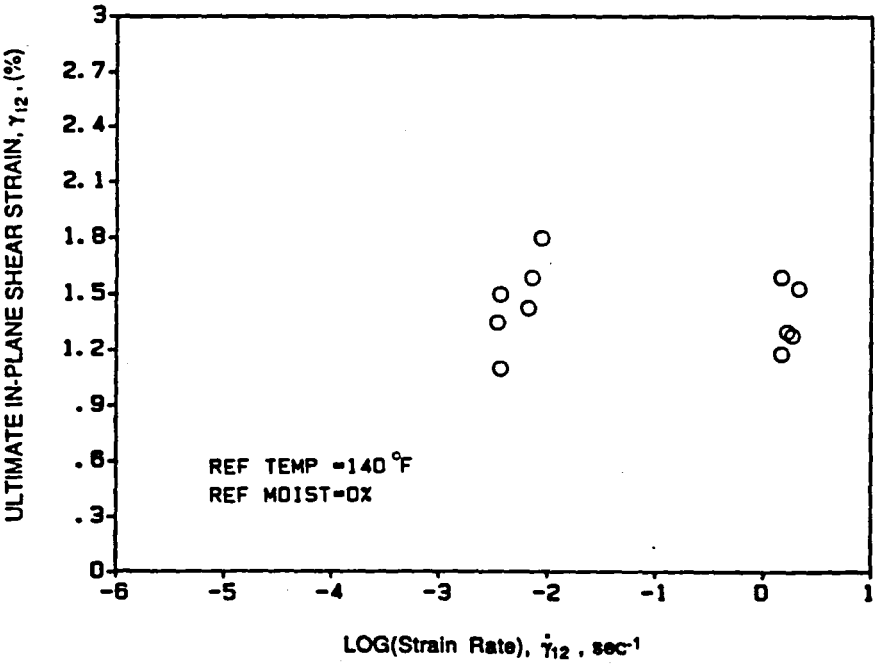

Figure 5.97 Ultimate in-plane shear strain vs. log(strain rate) curve for AS4/3501-6 Graphite/Epoxy, (T=60°C (140°F), C=0%)

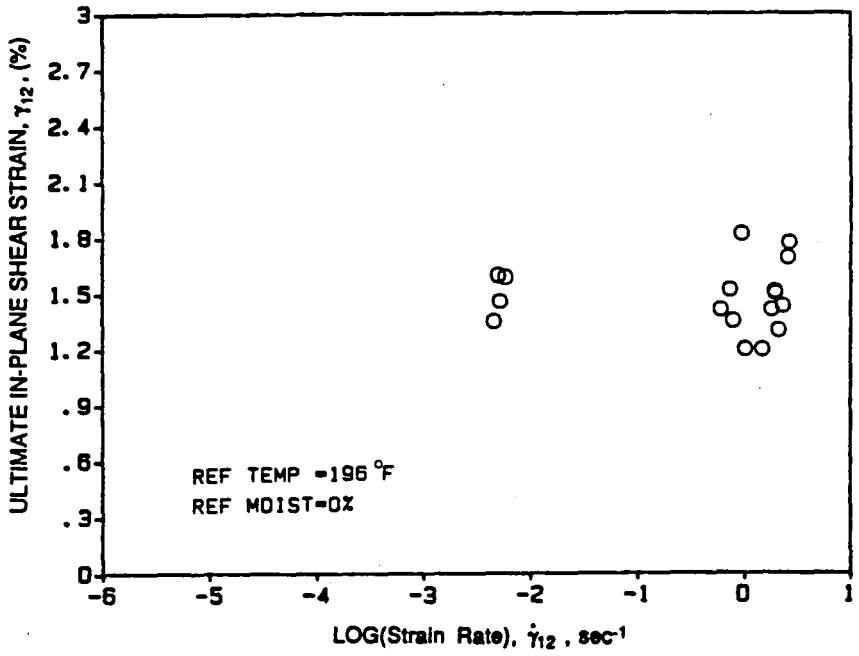

Figure 5.98 Ultimate in-plane shear strain vs. log(strain rate) curve forAS4/3501-6 Graphite/Epoxy, (T=91°C (196°F), C=0%)

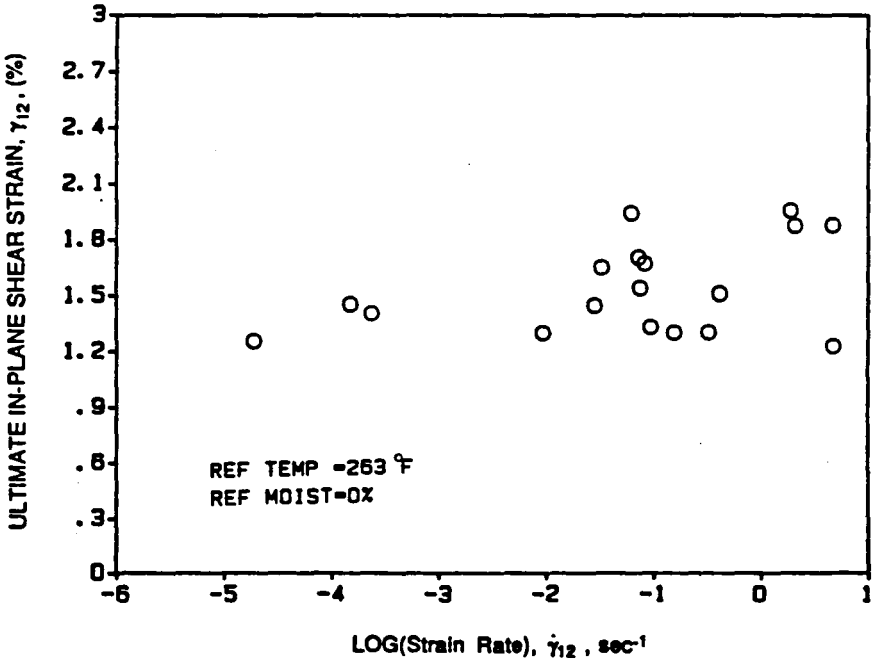

Figure 5.99 Ultimate in-plane shear strain vs. log(strain rate) curve for AS4/3501-6 Graphite/Epoxy, (T=128°C (263°F), C=0%)

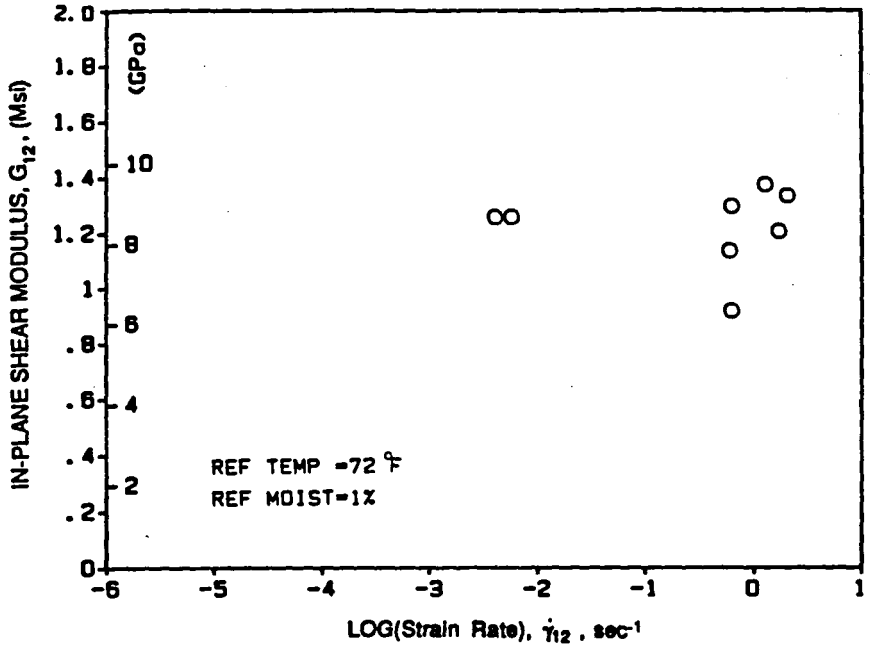

Figure 5.100 In-plane shear modulus vs. log(strain rate) curve for AS4/3501-6 Graphite/Epoxy, (T=22°C (72°F), C=1%)

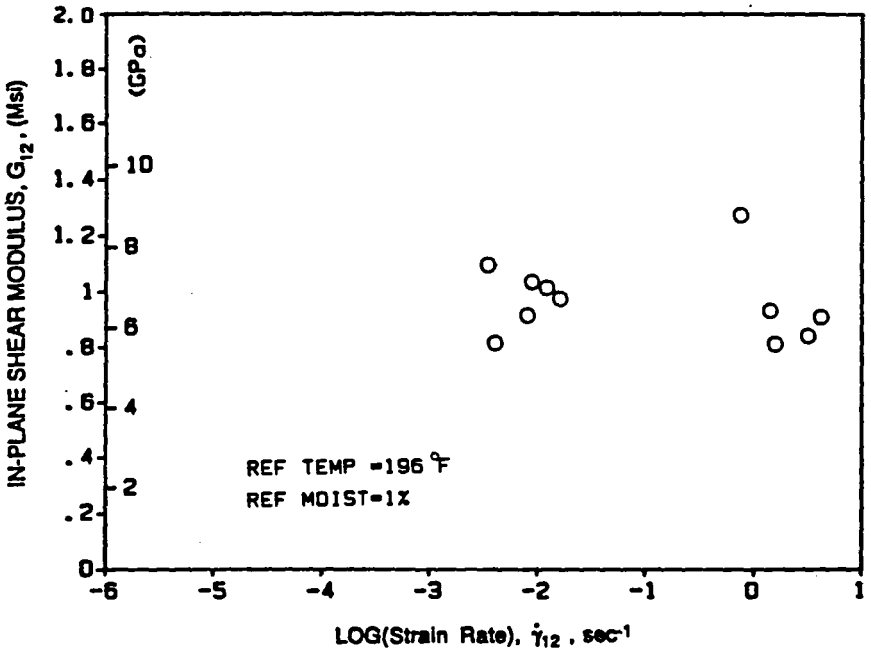

Figure 5.101 In-plane shear modulus vs. log(strain rate) curve for AS4/3501-6 Graphite/Epoxy, (T=91°C (196°F), C=1%)

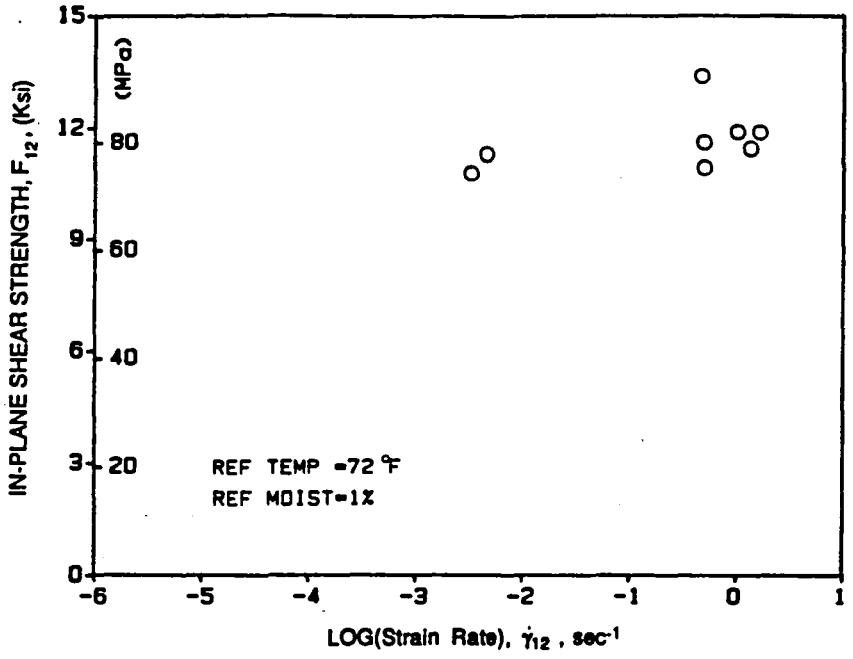

Figure 5.102 In-plane shear strength vs. log(strain rate) curve for AS4/3501-6 Graphite/Epoxy, (T=22°C (72°F), C=1%)

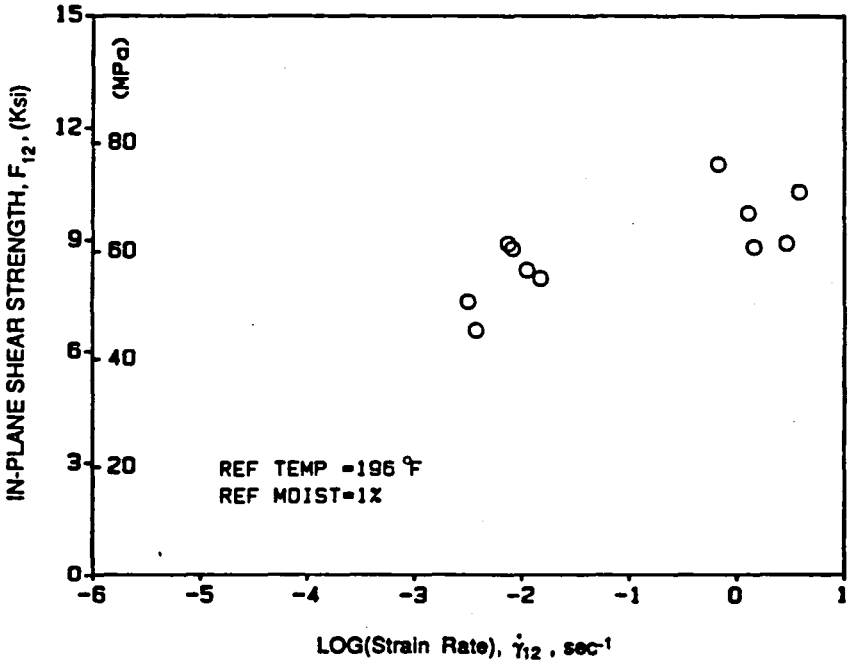

Figure 5.103 In-plane shear strength vs. log(strain rate) curve for AS4/3501-6 Graphite/Epoxy, (T=91°C (196°F), C=1%)

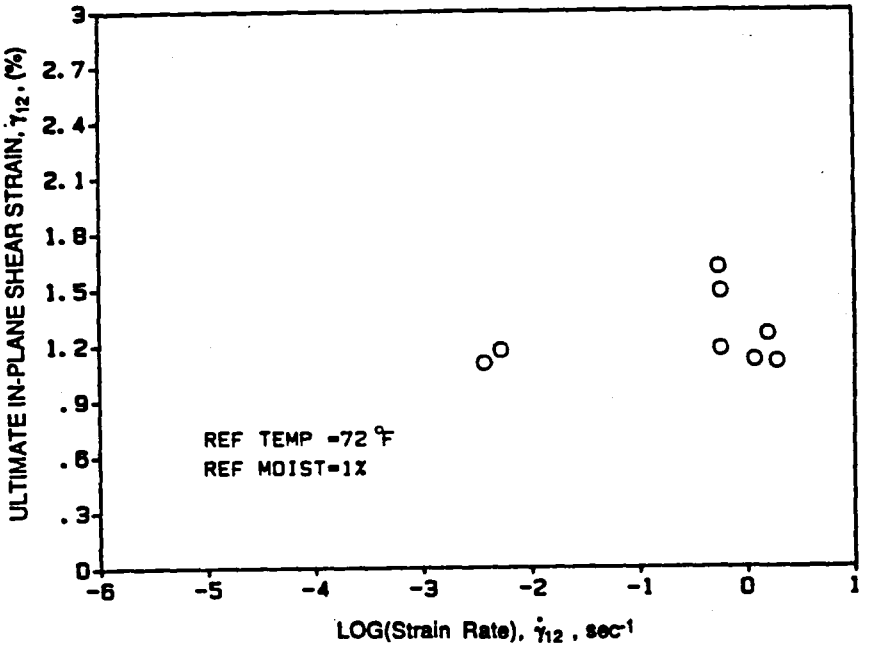

Figure 5.104 Ultimate in-plane shear strain vs. log(strain rate) curve for AS4/3501-6 Graphite/Epoxy, (T=22°C (72°F), C=1%)

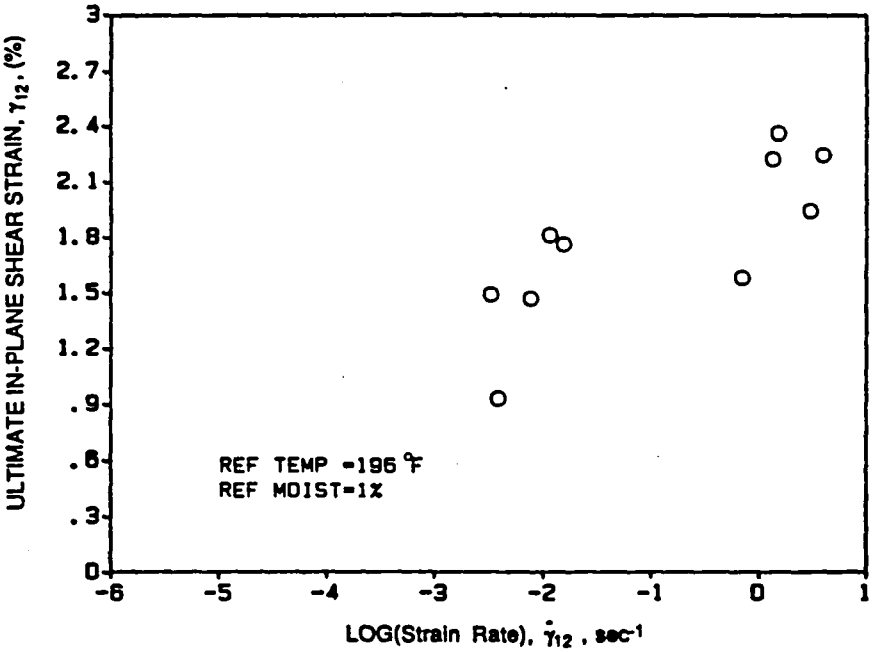

Figure 5.105 Ultimate in-plane shear strain vs. log(strain rate) curve for AS4/3501-6 Graphite/Epoxy, (T=91°C (196°F), C=1%)

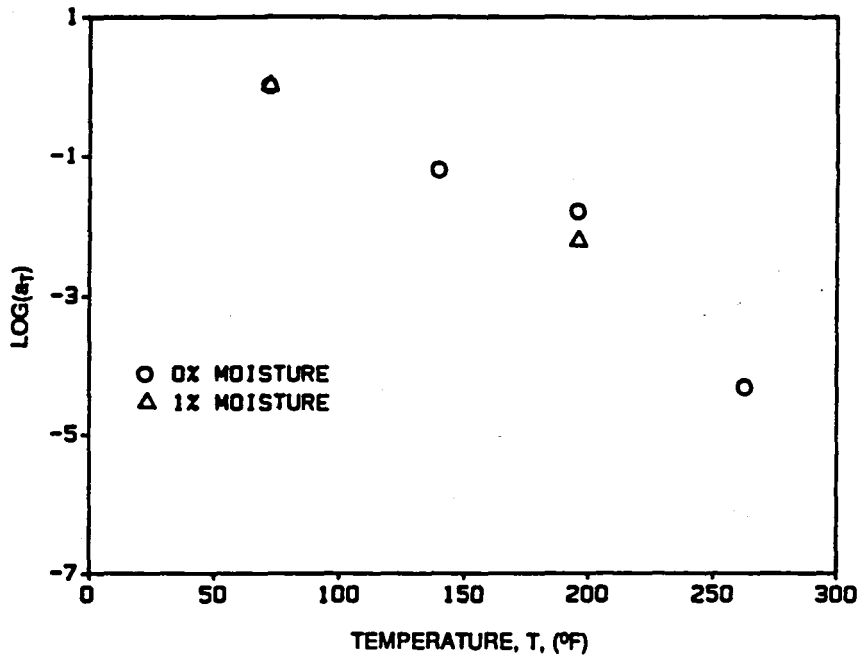

Figure 5.106 Log(Time-temperature shift factor) vs. temperature for in-plane shear modulus under dry and wet (C=1%) conditions

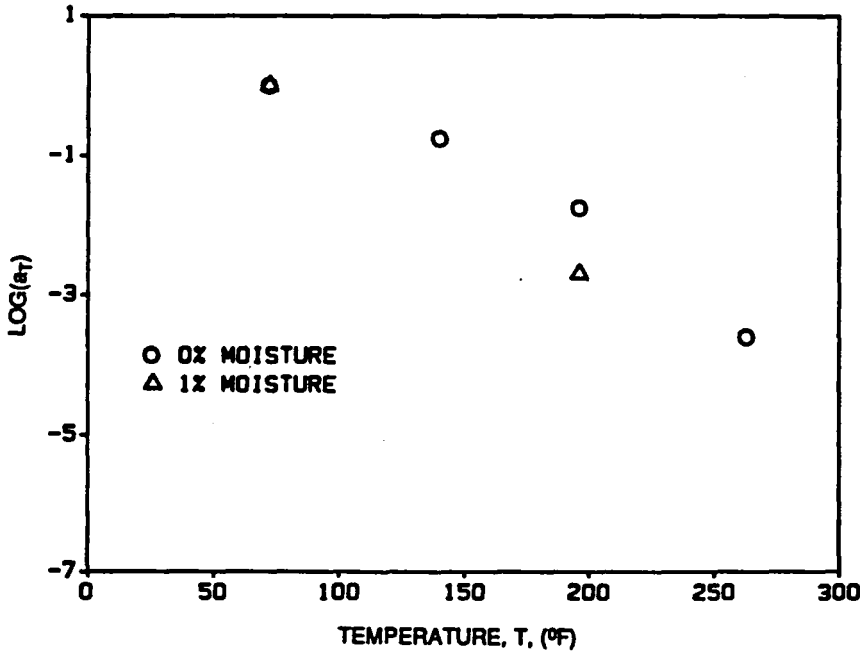

Figure 5.107 Log(Time-temperature shift factor) vs. temperature for in-plane shear strength under dry and wet (C=1%) conditions

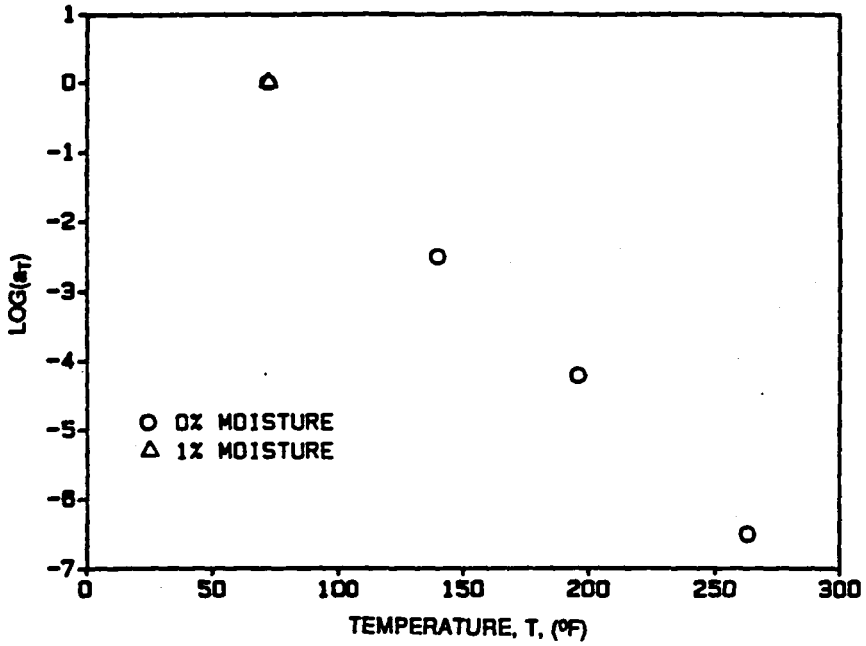

Figure 5.108 Log(Time-temperature shift factor) vs. temperature for ultimate in-plane shear strain under dry and wet (C=1%) conditions

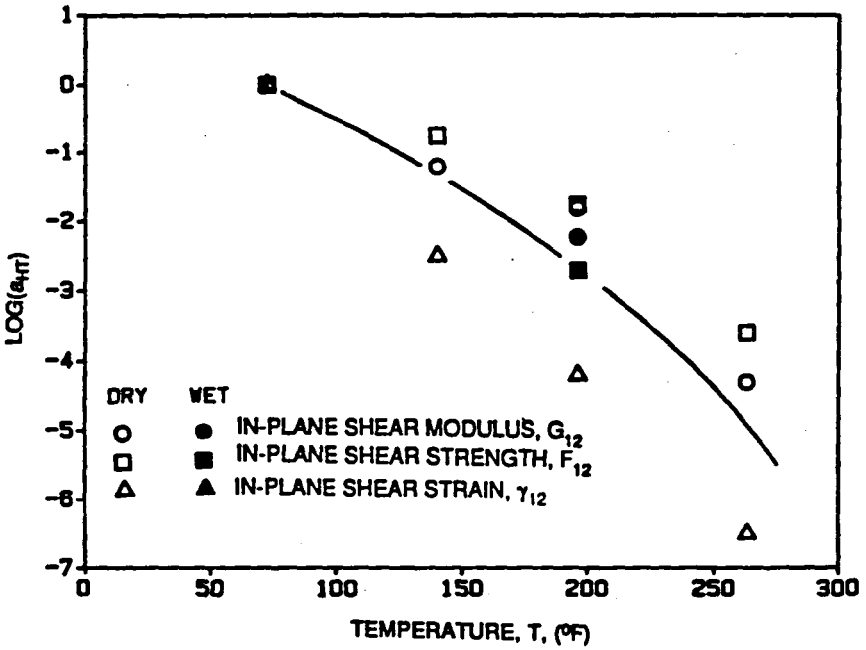

Figure 5.109 Log(Time-temperature shift factor) vs. temperature for in-plane shear properties under dry and wet (C=1%) conditions

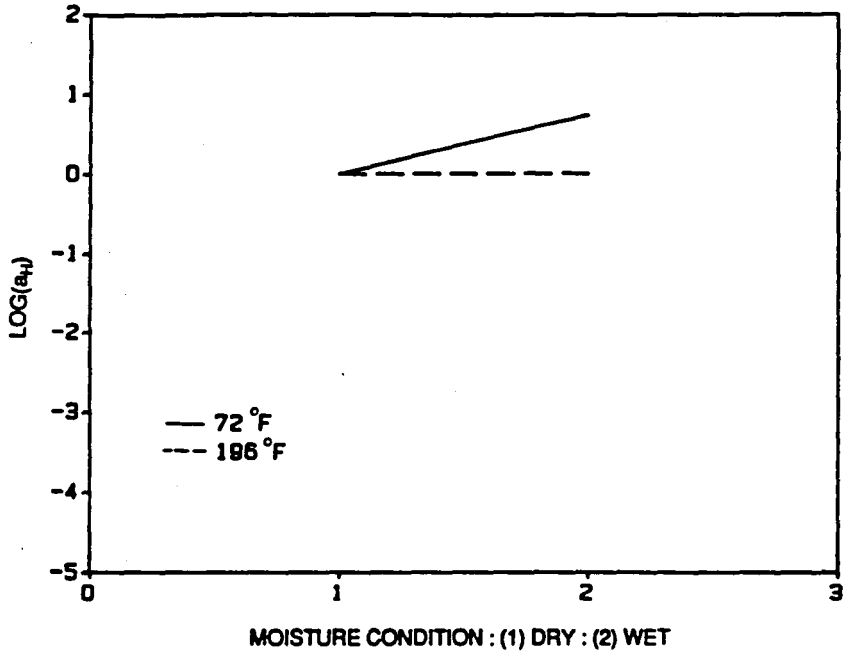

Figure 5.110 Log(Time-moisture shift factor) vs. moisture condition for in-plane shear modulus, (T=22°F (72°F) and T=91°C (196°F))

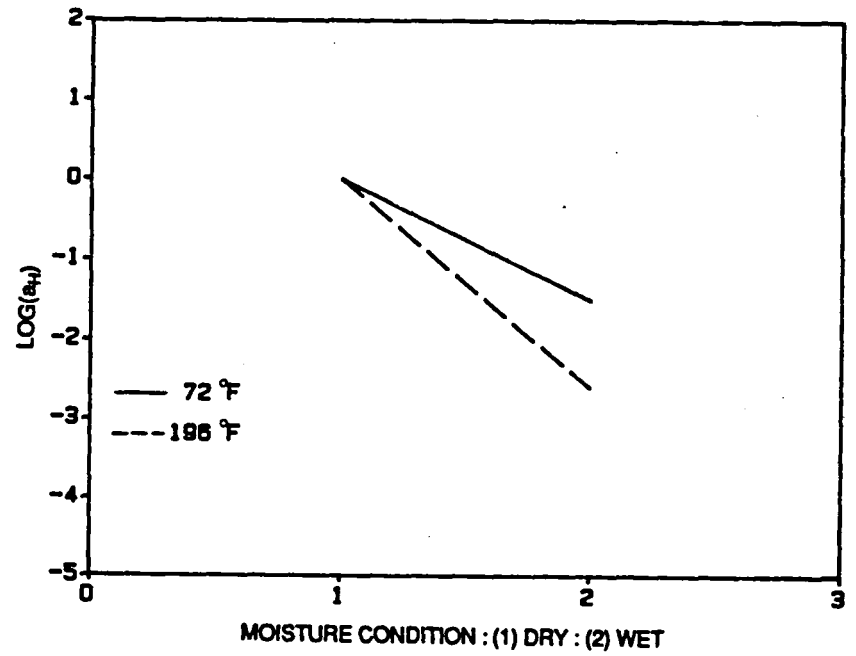

Figure 5.111 Log(Time-moisture shift factor) vs. moisture condition for in-plane shear strength, (T=22°F (72°F) and T=91°C (196°F))

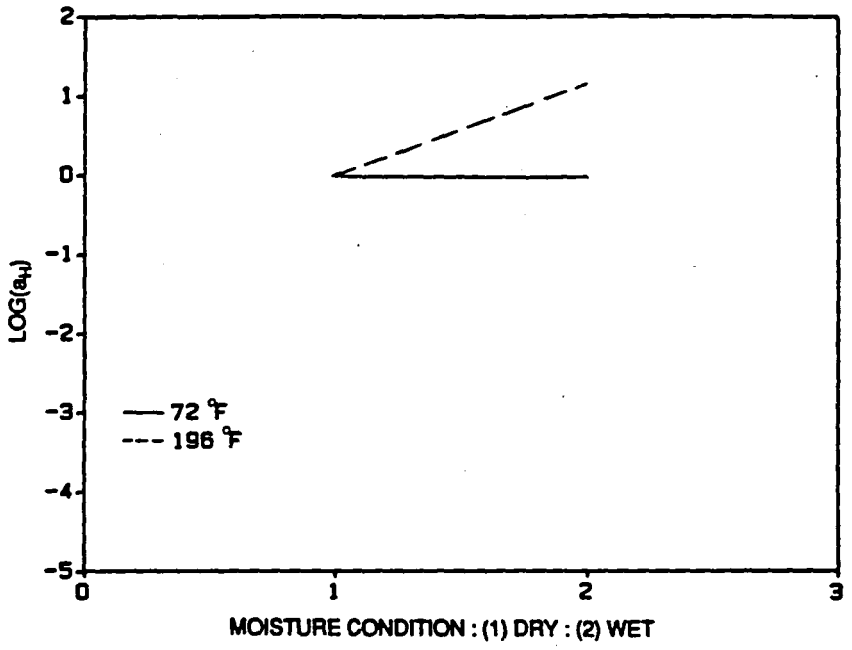

Figure 5.112 Log(Time-moisture shift factor) vs. moisture condition for in-plane shear strain, (T=22°F (72°F) and T=91°C (196°F))

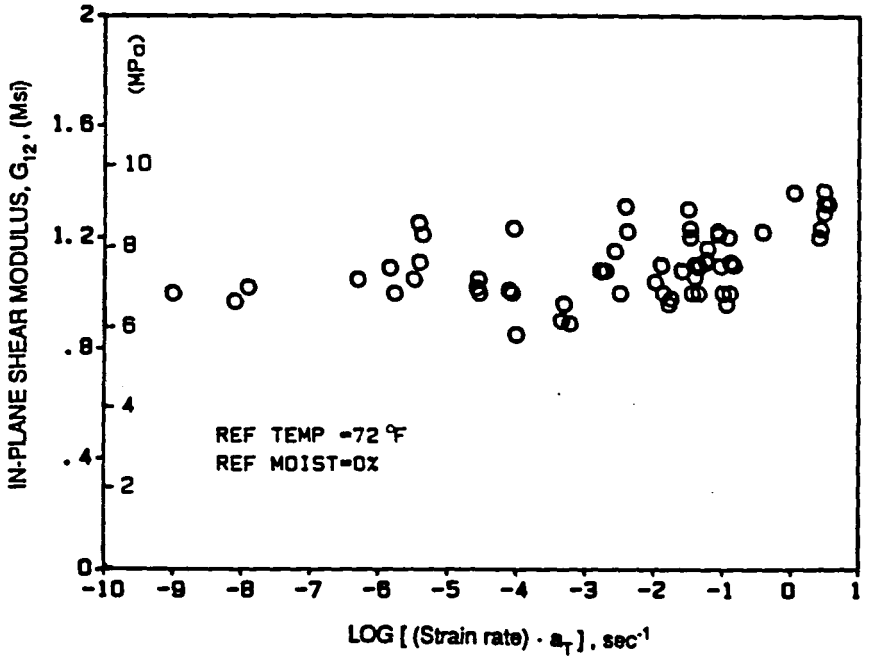

Figure 5.113 Time-temperature master curve for in-plane shear modulus, (T=22°C (72°F), C=0%)

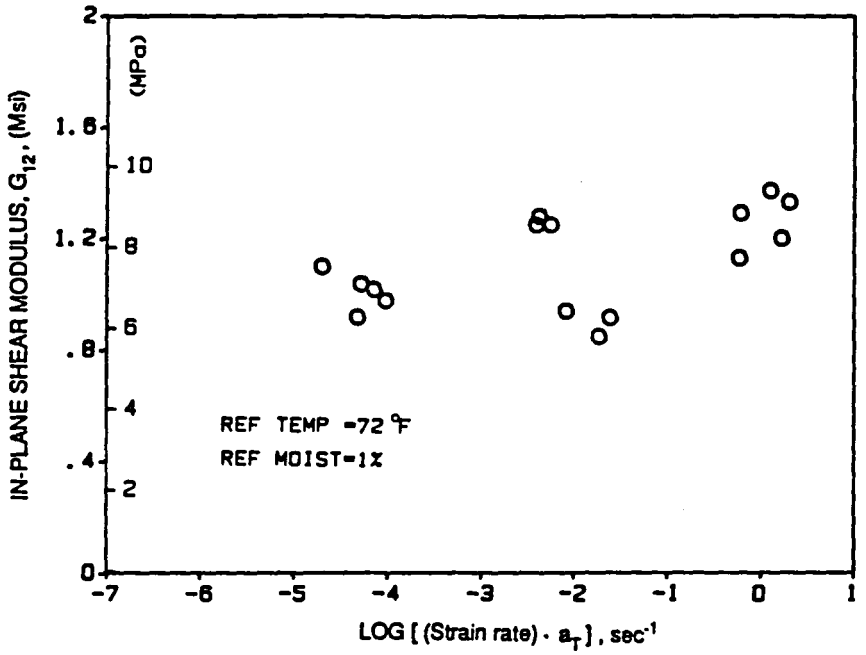

Figure 5.114 Time-temperature master curve for in-plane shear modulus, (T=22°C (72°F), C=1%)

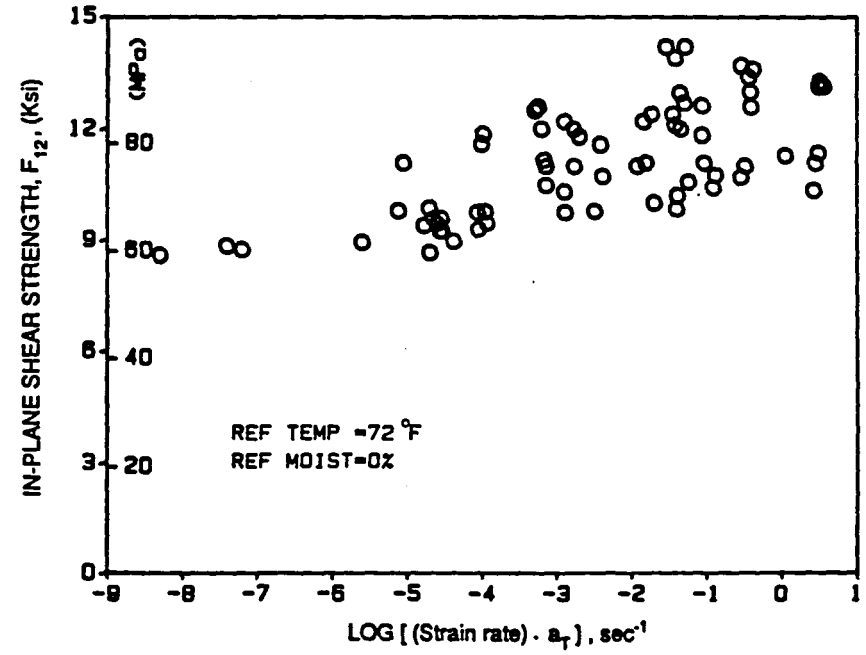

Figure 5.115 Time-temperature master curve for in-plane shear strength, (T=22°C (72°F), C=0%)

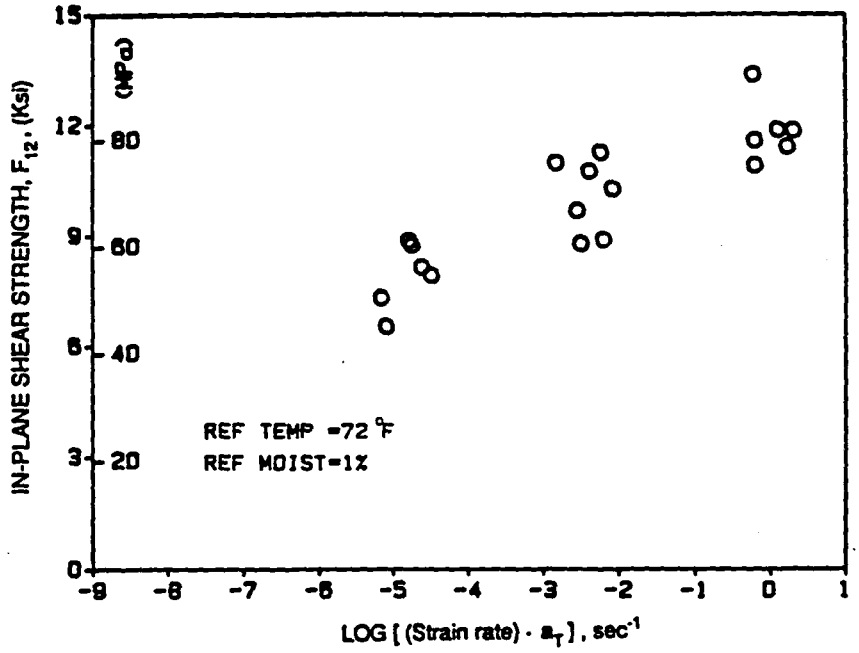

Figure 5.116 Time-temperature master curve for in-plane shear strength, (T=22°C (72°F), C=1%)

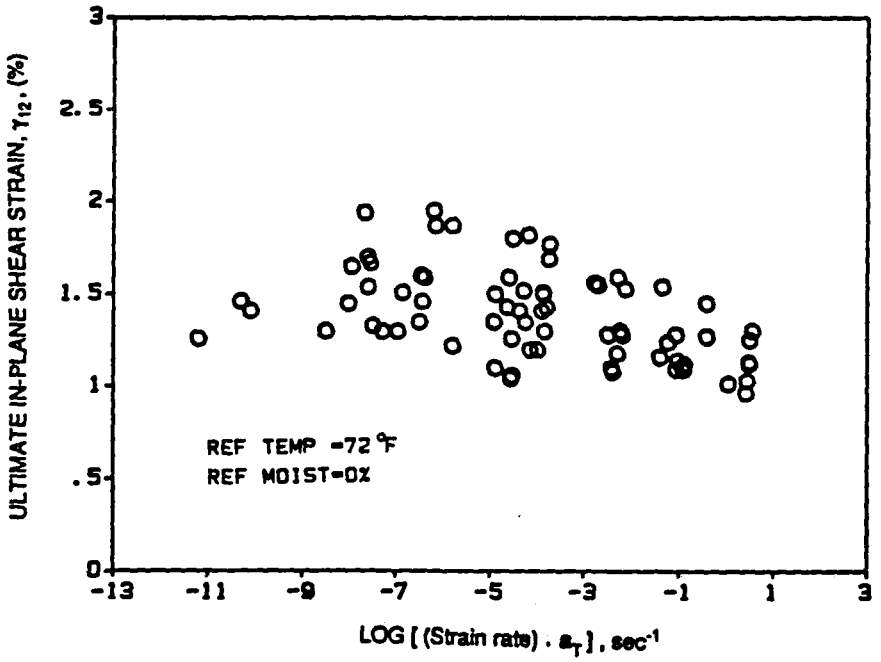

Figure 5.117 Time-temperature master curve for ultimate in-plane shear strain, (T=22°C (72°F), C=0%)

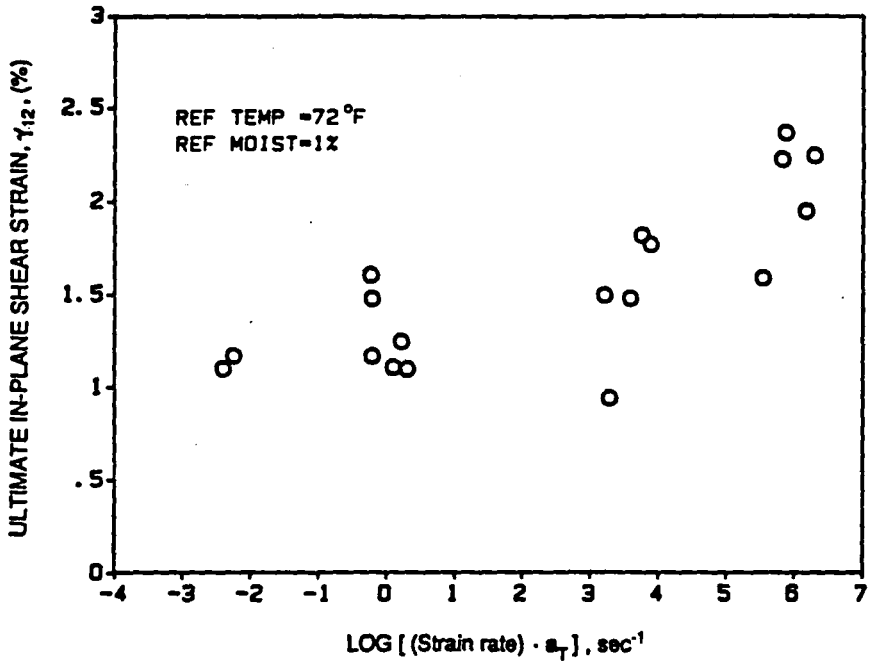

Figure 5.118 Time-temperature master curve for ultimate in-plane shear strain, (T=22°C (72°F), C=1%)

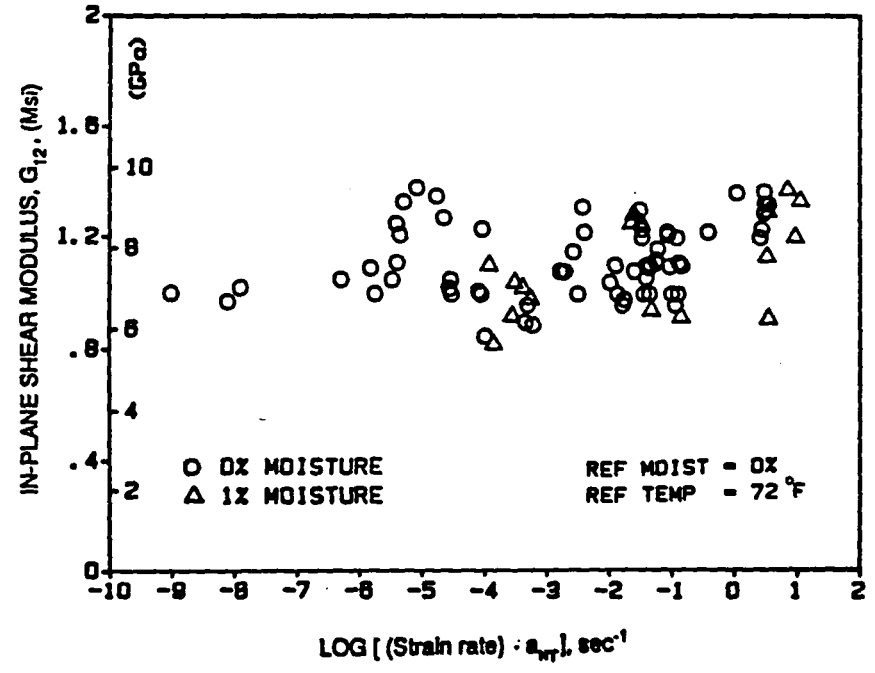

Figure 5.119 Time-temperature-moisture master curve for in-plane shear modulus

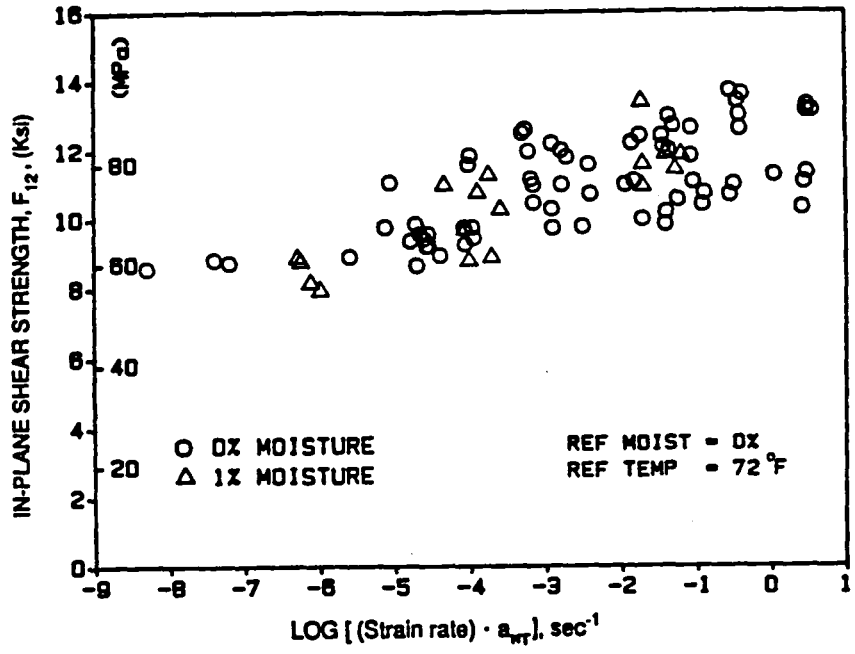

Figure 5.120 Time-temperature-moisture master curve for in-plane shear strength

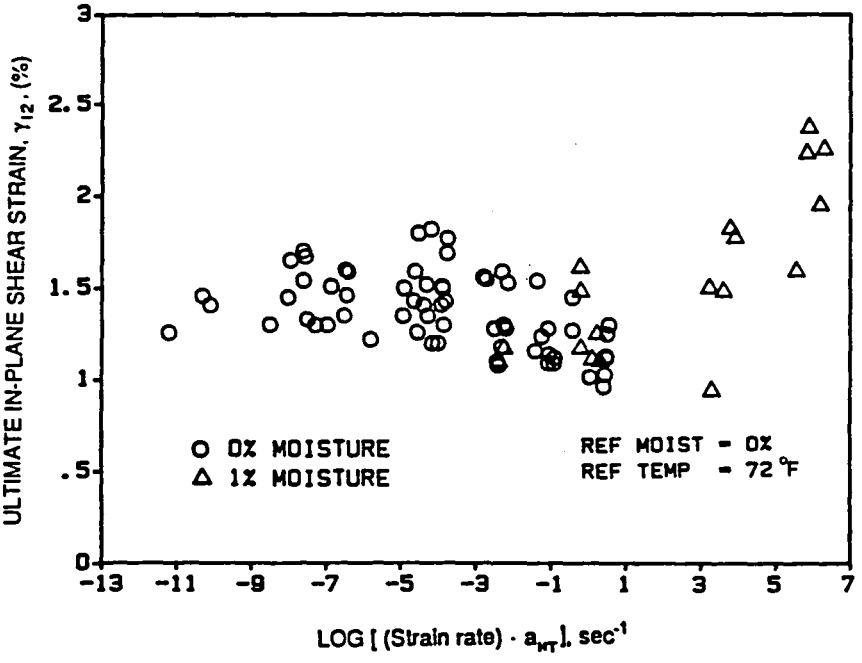

Figure 5.121 Time-temperature-moisture master curve for ultimate in-plane shear strain

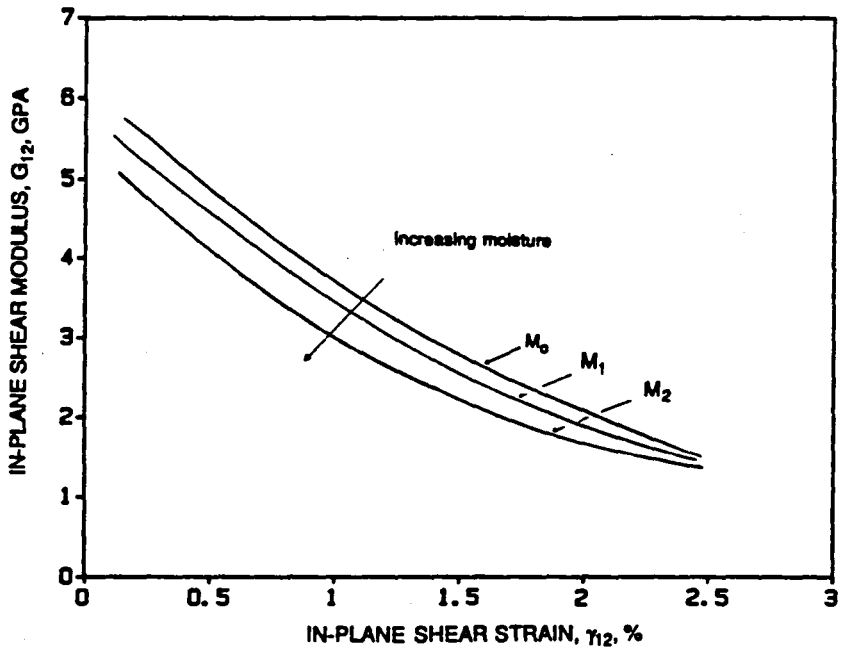

Figure 5.122 Moisture effects on in-plane shear modulus of a typical Graphite/Epox material [11]

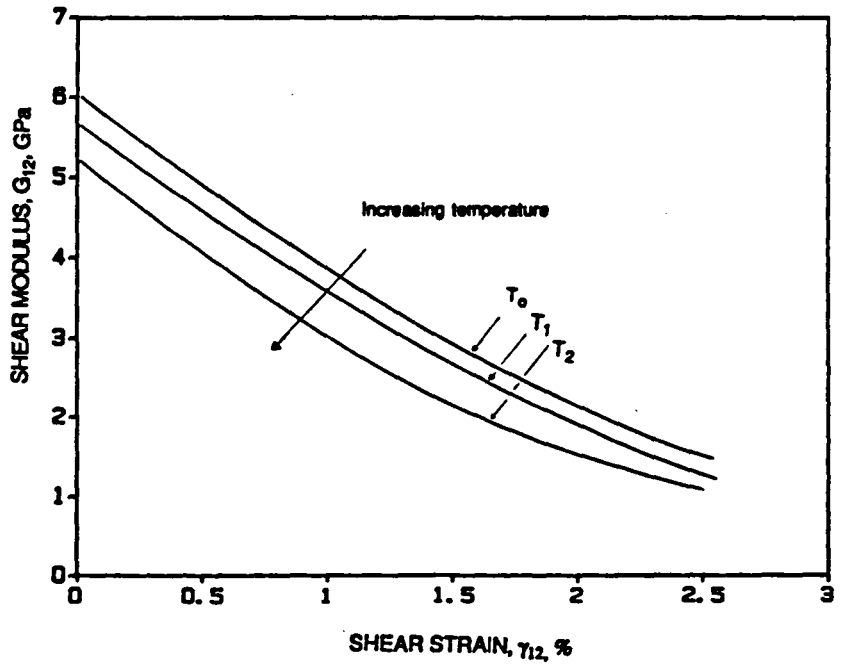

Figure 5.123 Temperature effects on in-plane shear modulus of a typical Graphite/Epoxy material [11]

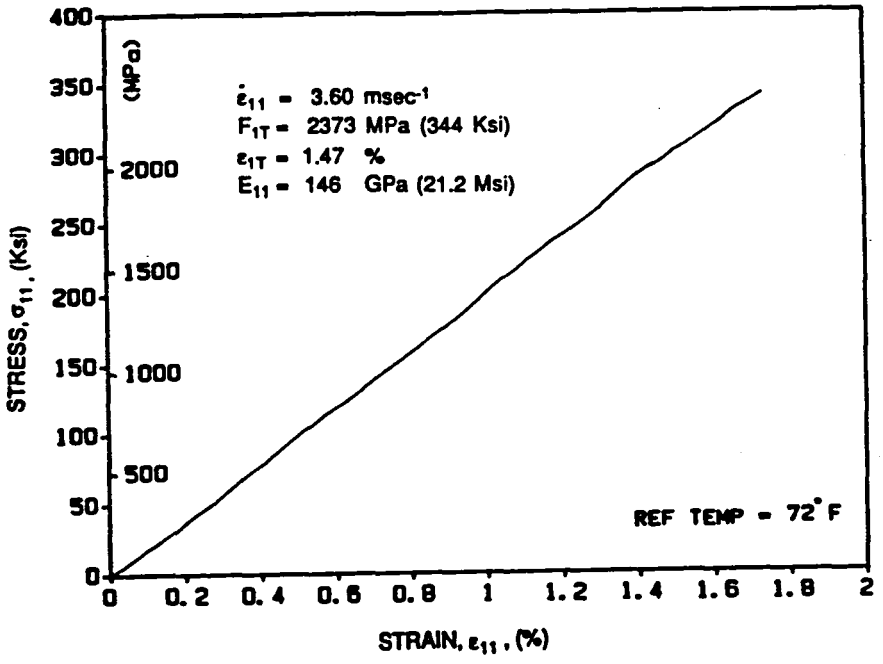

Figure 5.124 Typical stress-strain curve for $[0_8]$ AS4/3501-6 Graphite/Epoxy ($\dot{\varepsilon}_{11}$=3.6$10^{-3}$ s^{-1}, T=22°C (72°F), C=0%)

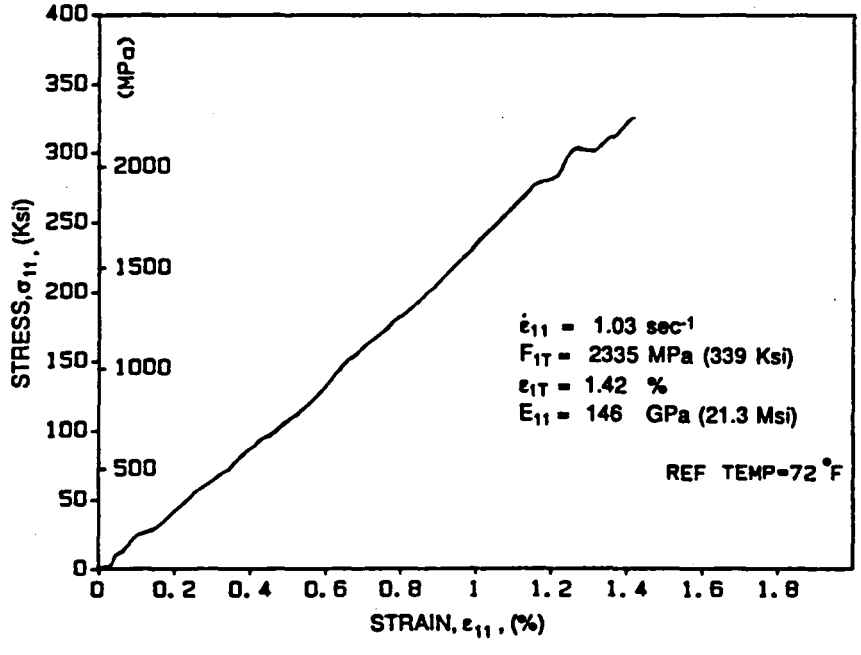

Figure 5.125 Typical stress-strain curve for $[0_8]$ AS4/3501-6 Graphite/Epoxy ($\dot{\varepsilon}_{11}$= 1.0 s^{-1}, T=22°C (72°F), C=0%)

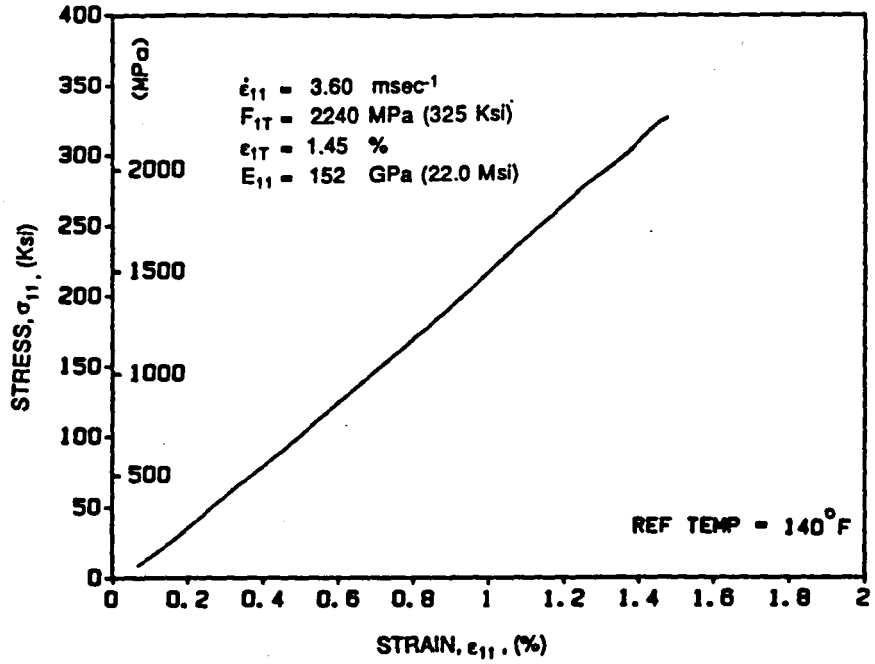

Figure 5.126 Typical stress-strain curve for $[0_6]$ AS4/3501-6 Graphite/Epoxy ($\dot{\varepsilon}_{11}$=3.6·10^{-3} s^{-1}, T=60°C (140°F), C=0%)

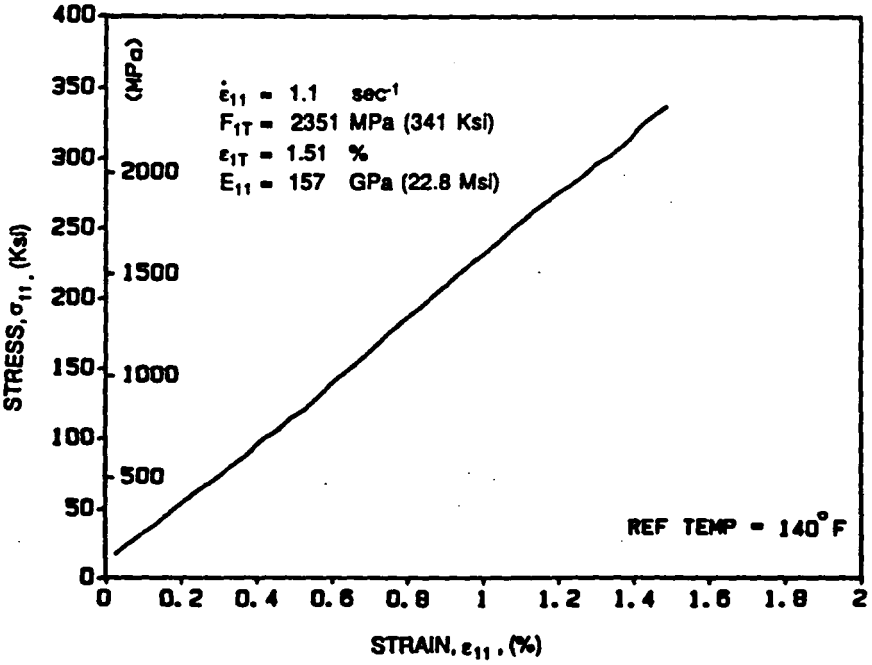

Figure 5.127 Typical stress-strain curve for $[0_6]$ AS4/3501-6 Graphite/Epoxy ($\dot{\varepsilon}_{11}$=1.1 s^{-1}, T=60°C (140°F), C=0%)

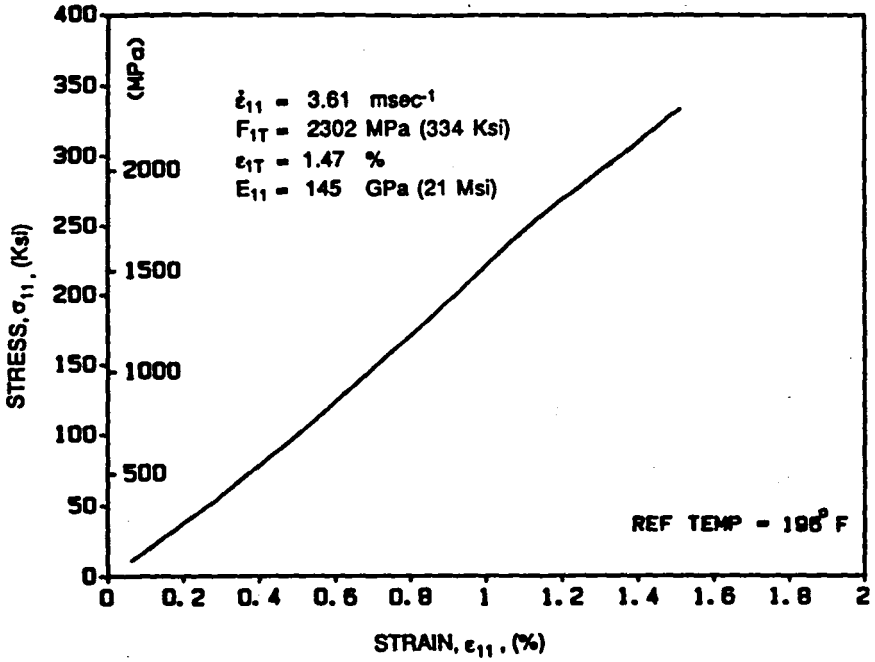

Figure 5.128 Typical stress-strain curve for $[0_6]$ AS4/3501-6 Graphite/Epoxy ($\dot{\varepsilon}_{11}$=3.6·10^{-3} s^{-1}, T=91°C (196°F), C=0%)

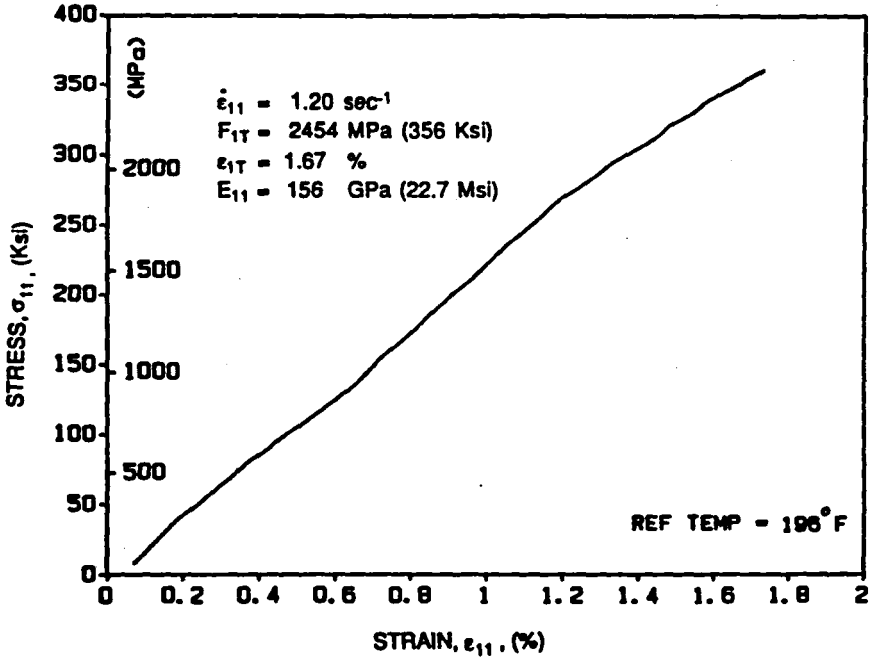

Figure 5.129 Typical stress-strain curve for $[0_6]$ AS4/3501-6 Graphite/Epoxy ($\dot{\varepsilon}_{11}$=1.2·s^{-1} T=91°C (196°F), C=0%)

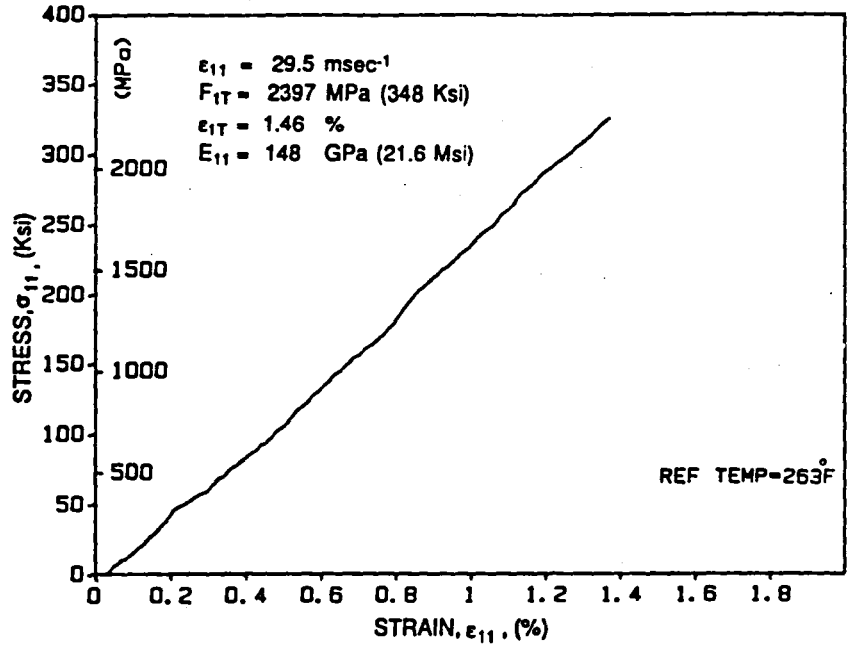

Figure 5.130 Typical stress-strain curve for $[0_6]$ AS4/3501-6 Graphite/Epoxy ($\dot{\varepsilon}_{11}$=2.9·10^{-4} s^{-1}, T=128°C (263°F), C=0%)

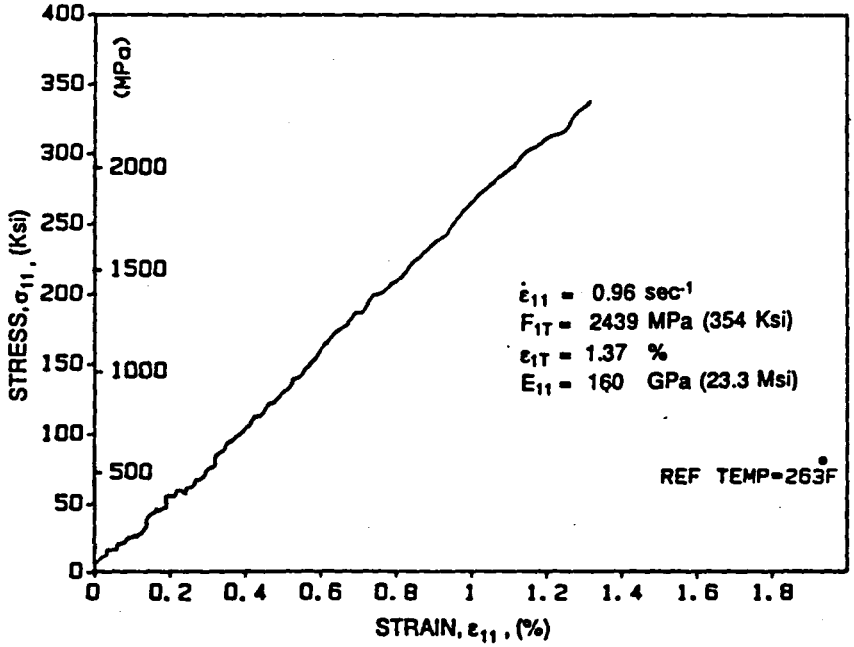

Figure 5.131 Typical stress-strain curve for $[0_6]$ AS4/3501-6 Graphite/Epoxy ($\dot{\varepsilon}_{11}$=0.95· s^{-1}, T=128°C (263°F), C=0%)

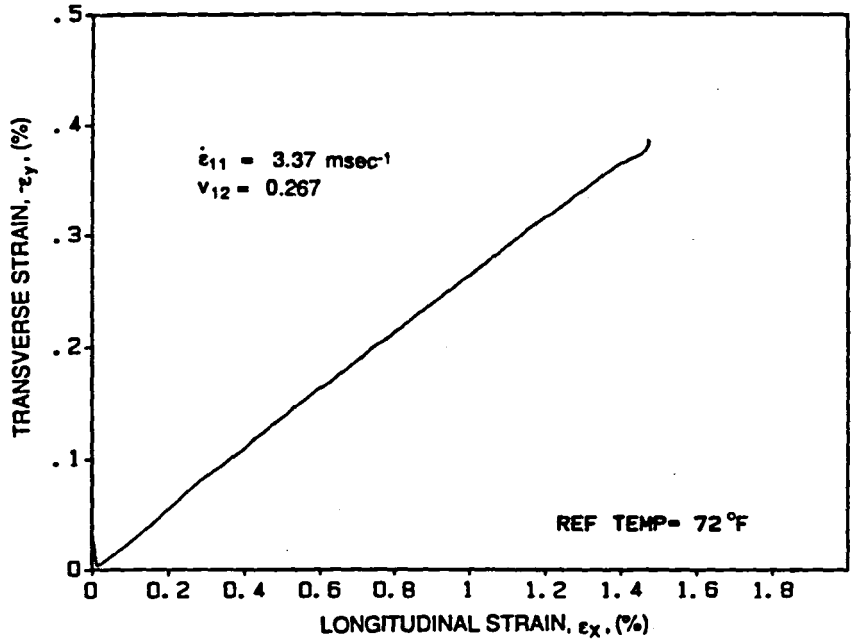

Figure 5.132 Typical transverse vs. longitudinal strain curve for $[0_6]$ AS4/3501-6 Graphite/Epoxy ($\dot{\varepsilon}_{11}$=3.37·10^{-3} s^{-1}, T=22°C (72°F), C=0%)

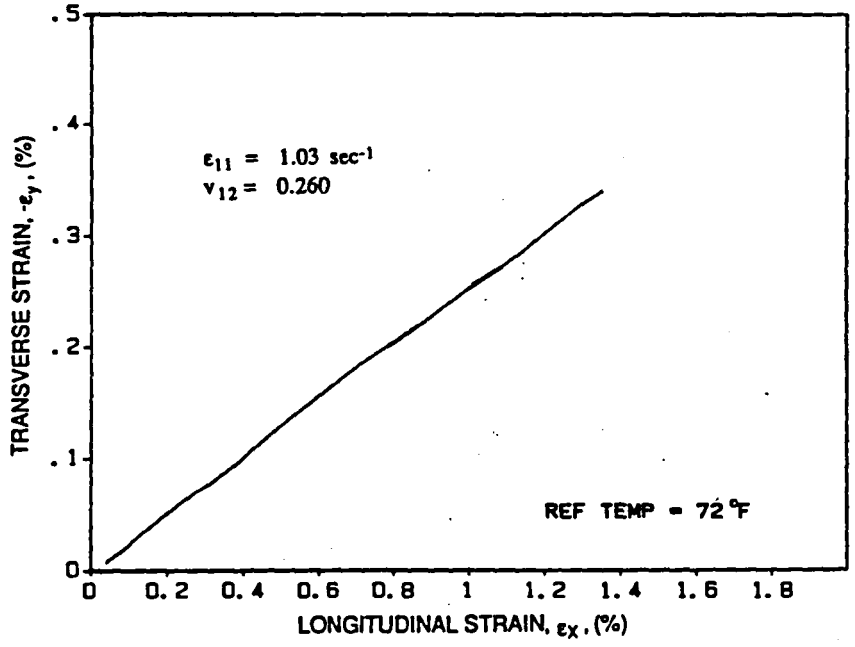

Figure 5.133 Typical transverse vs. longitudinal strain curve for $[0_6]$ AS4/3501-6 Graphite/Epoxy ($\dot{\varepsilon}_{11}$=1.03 s^{-1}, T=22°C (72°F), C=0%)

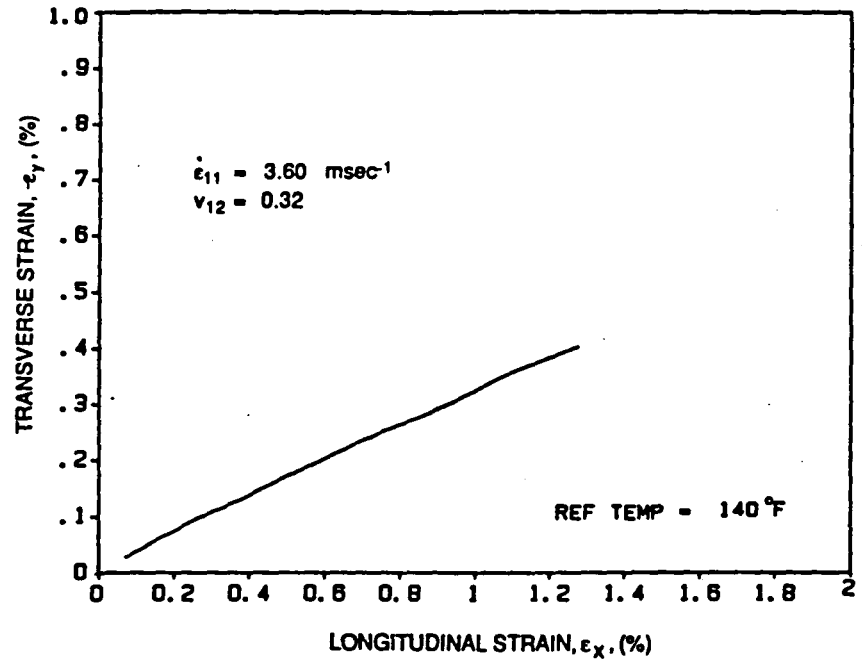

Figure 5.134 Typical transverse vs. longitudinal strain curve for $[0_8]$ AS4/3501-6 Graphite/Epoxy ($\dot{\varepsilon}_{11}$=3.60·10^{-3} s^{-1}, T=60°C (140°F), C=0%)

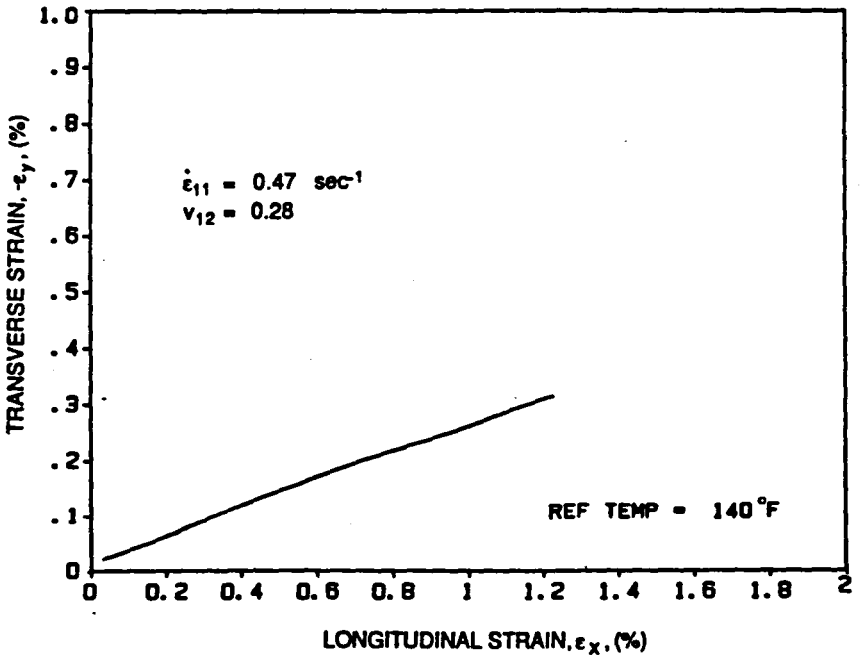

Figure 5.135 Typical transverse vs. longitudinal strain curve for $[0_8]$ AS4/3501-6 Graphite/Epoxy ($\dot{\varepsilon}_{11}$=0.47 s^{-1}, T=60°C (140°F), C=0%)

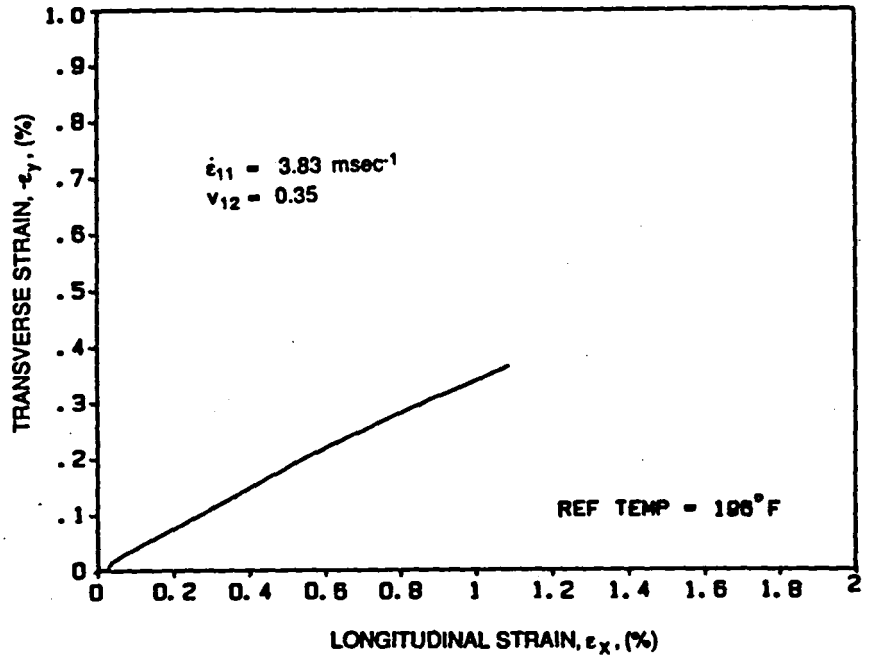

Figure 5.136 Typical transverse vs. longitudinal strain curve for $[0_8]$ AS4/3501-6 Graphite/Epoxy ($\dot{\varepsilon}_{11}$=3.38$10^{-3}$ s^{-1}, T=91°C (196°F), C=0%)

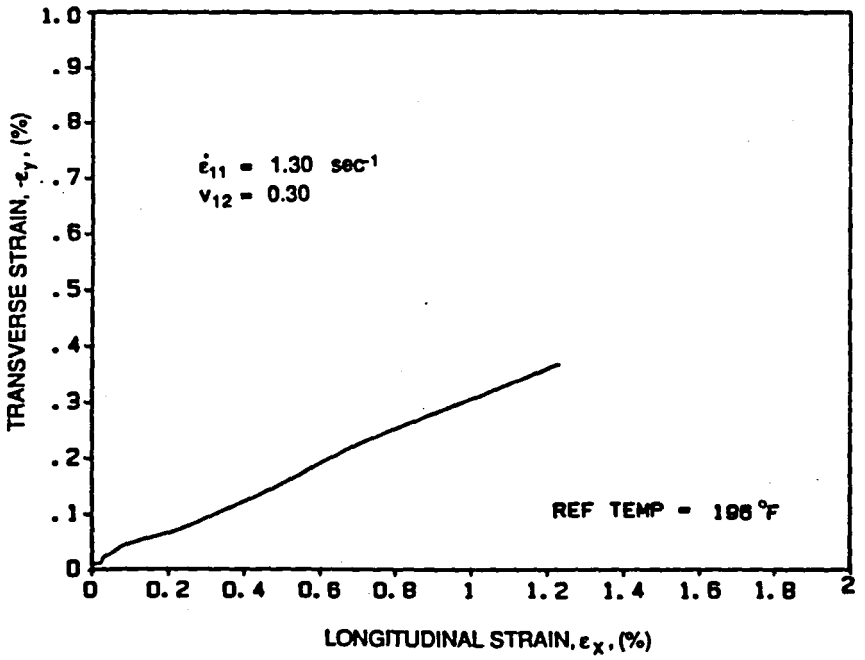

Figure 5.137 Typical transverse vs. longitudinal strain curve for $[0_8]$ AS4/3501-6 Graphite/Epoxy ($\dot{\varepsilon}_{11}$=1.30$10^{-3}$ s^{-1}, T=91°C (196°F), C=0%)

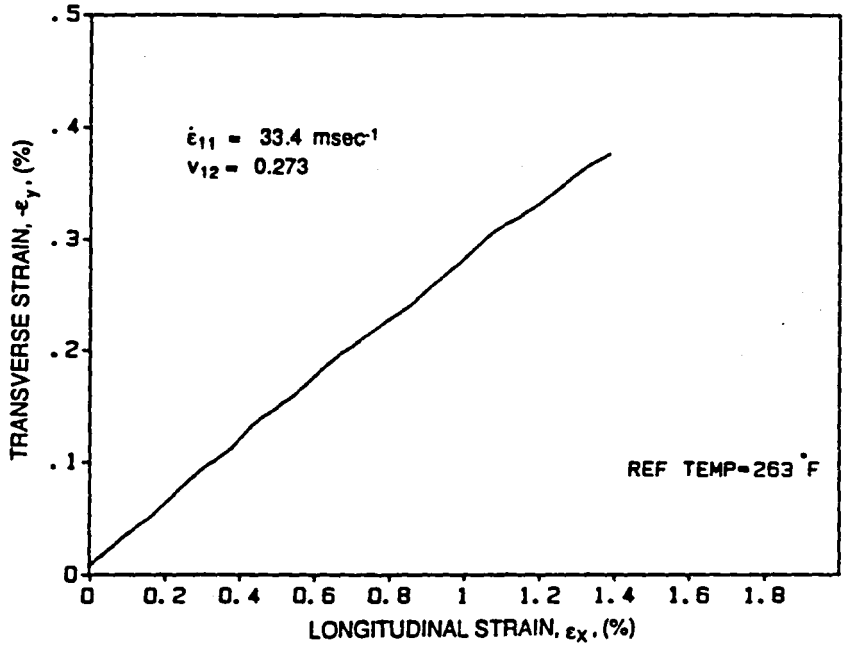

Figure 5.138 Typical transverse vs. longitudinal strain curve for $[0_6]$ AS4/3501-6 Graphite/Epoxy ($\dot{\varepsilon}_{11}$=3.24$10^{-4}$ s^{-1}, T=128°C (163°F), C=0%)

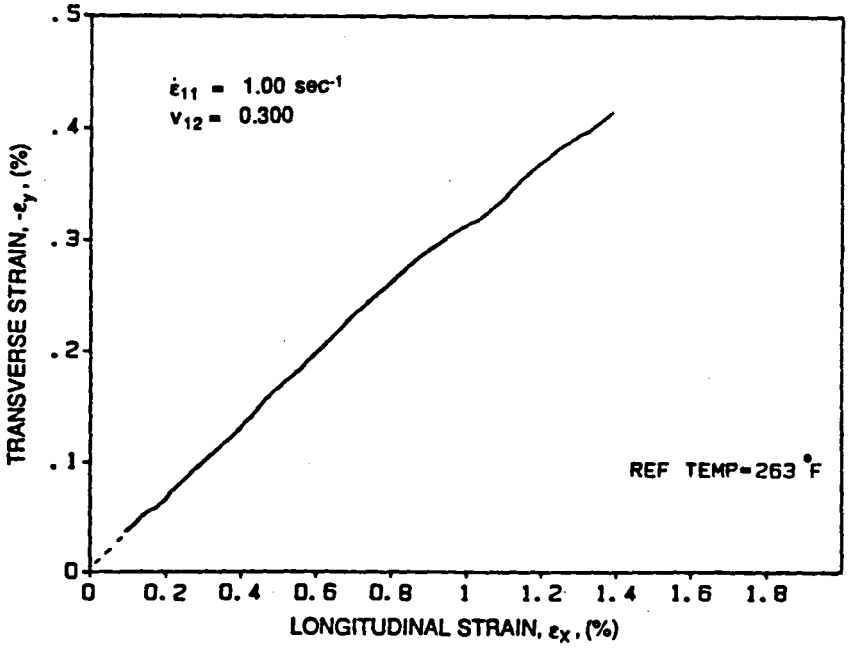

Figure 5.139 Typical transverse vs. longitudinal strain curve for $[0_6]$ AS4/3501-6 Graphite/Epoxy ($\dot{\varepsilon}_{11}$=1.0$10^{-3}$ s^{-1}, T=128°C (263°F), C=0%)

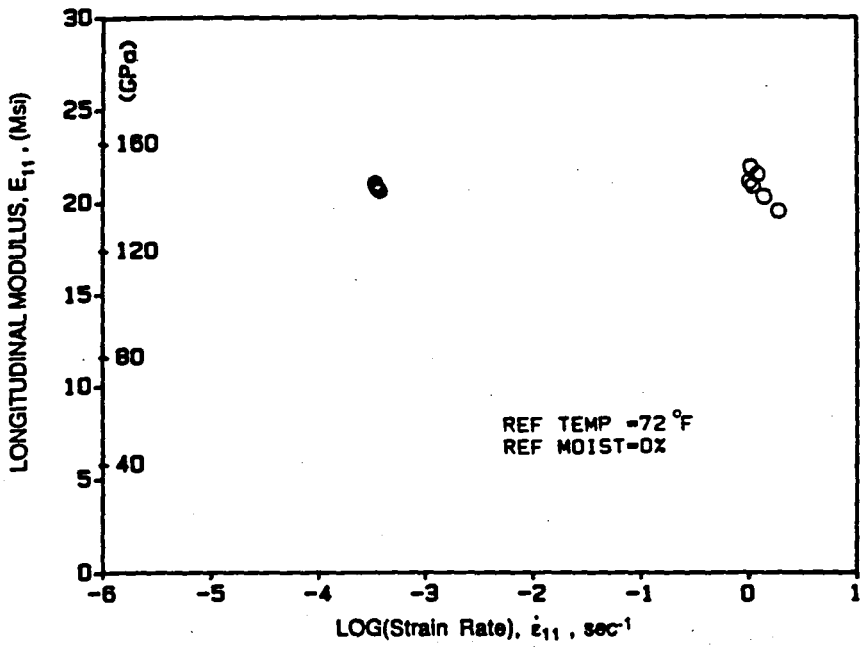

Figure 5.140 Longitudinal modulus vs. log(strain rate) curve for AS4/3501-6 Graphite/Epoxy, (T=22°C (72°F), C=0%)

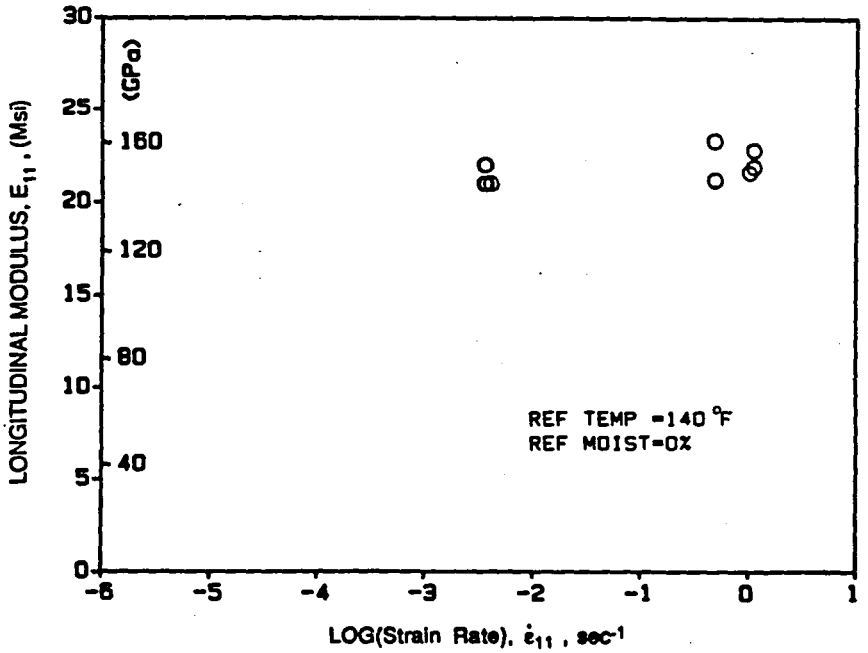

Figure 5.141 Longitudinal modulus vs. log(strain rate) curve for AS4/3501-6 Graphite/Epoxy, (T=60°C (140°F), C=0%)

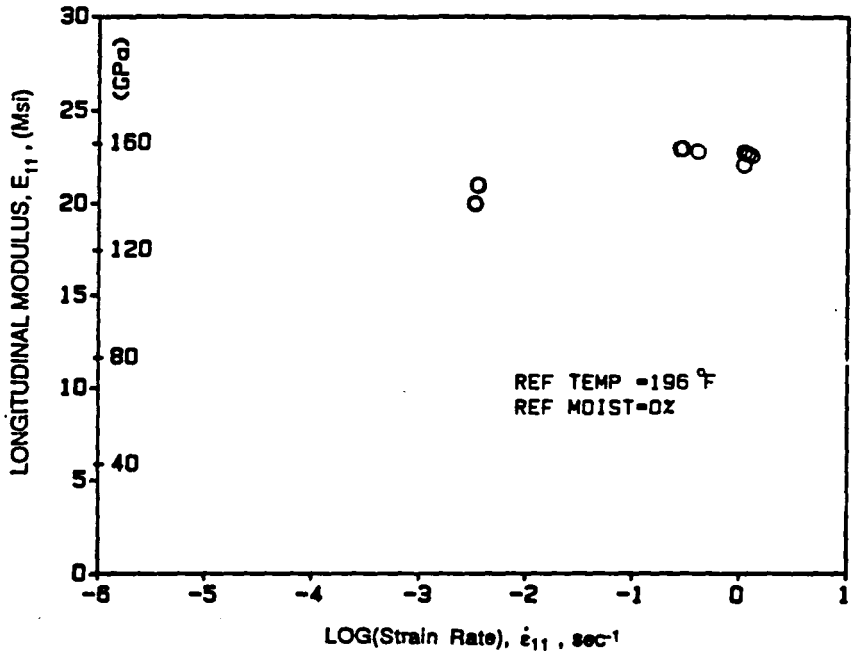

Figure 5.142 Longitudinal modulus vs. log(strain rate) curve for AS4/3501-6 Graphite/Epoxy, (T=91°C (196°F), C=0%)

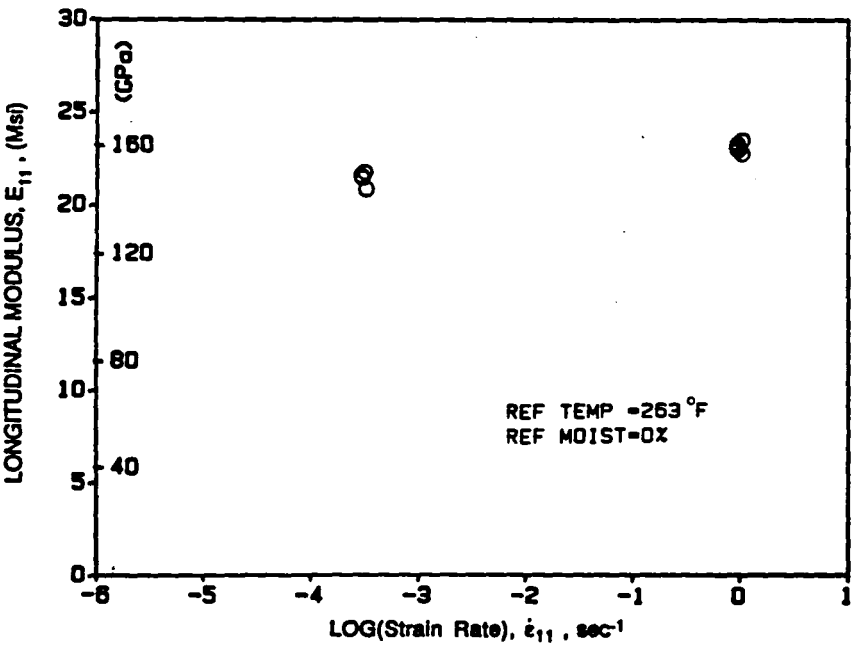

Figure 5.143 Longitudinal modulus vs. log(strain rate) curve for AS4/3501-6 Graphite/Epoxy, (T=128°C (263°F), C=0%)

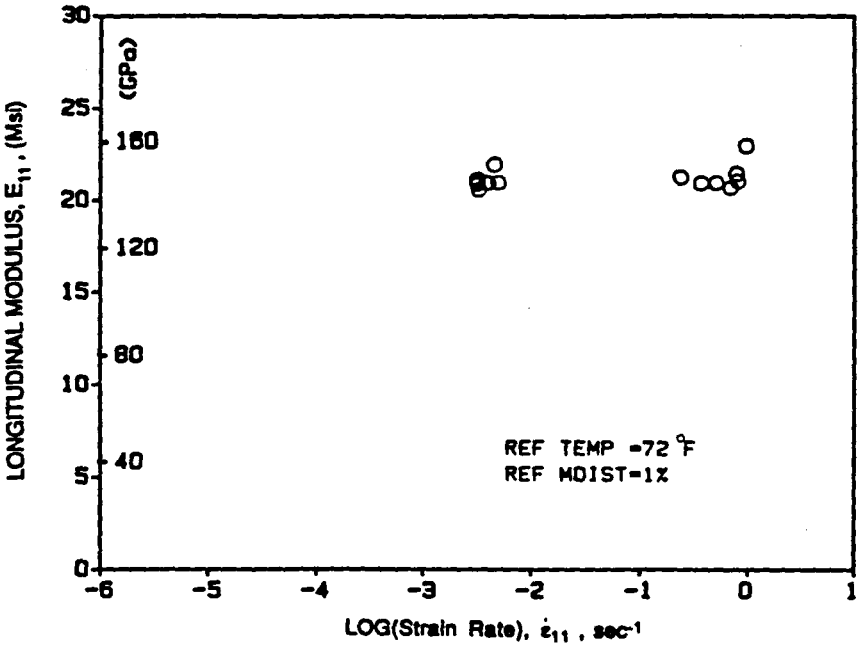

Figure 5.144 Longitudinal modulus vs. log(strain rate) curve for AS4/3501-6 Graphite/Epoxy, (T=22°C (72°F), C=1%)

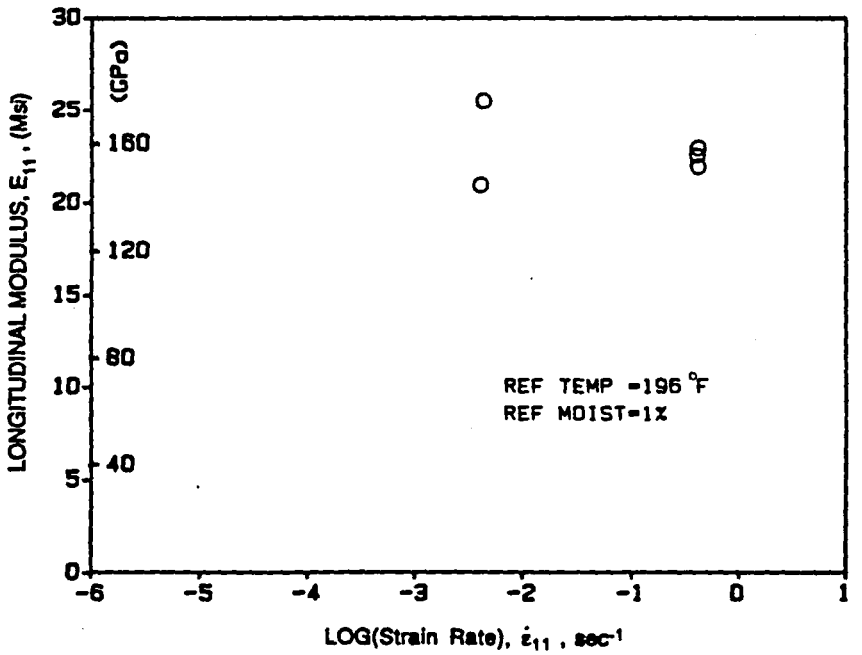

Figure 5.145 Longitudinal modulus vs. log(strain rate) curve for AS4/3501-6 Graphite/Epoxy, (T=91°C (196°F), C=1%)

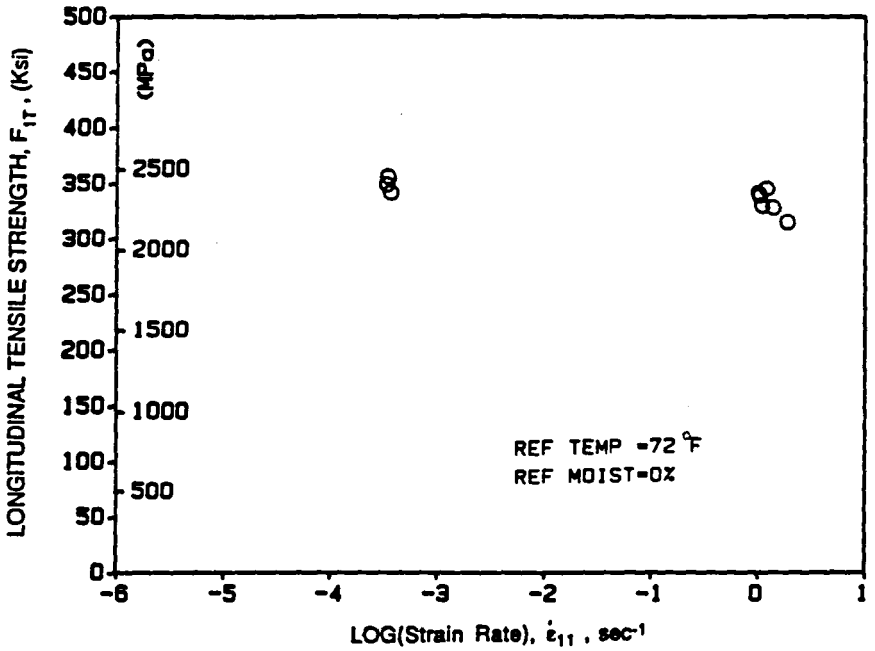

Figure 5.146 Longitudinal tensile strength vs. log(strain rate) curve for AS4/3501-6 Graphite/Epoxy, (T=22°C (72°F), C=0%)

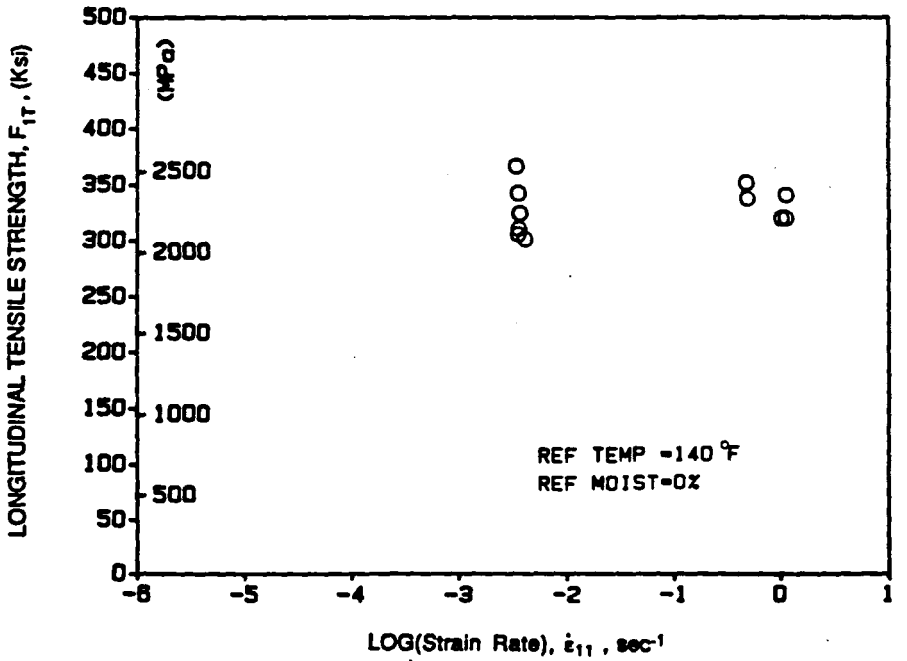

Figure 5.147 Longitudinal tensile strength vs. log(strain rate) curve for AS4/3501-6 Graphite/Epoxy, (T=60°C (140°F), C=0%)

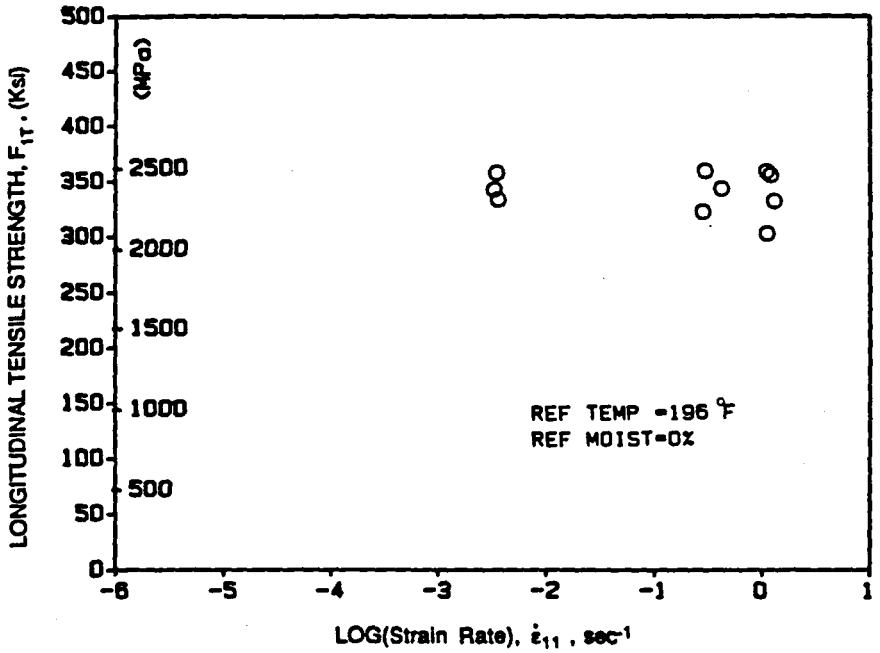

Figure 5.148 Longitudinal tensile strength vs. log(strain rate) curve for AS4/3501-6 Graphite/Epoxy, (T=91°C (196°F), C=0%)

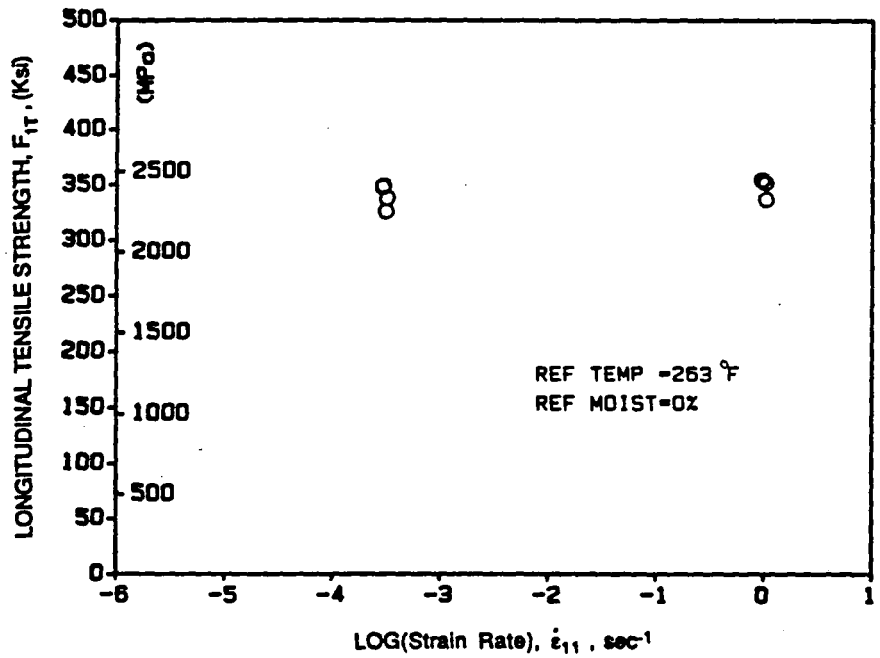

Figure 5.149 Longitudinal tensile strength vs. log(strain rate) curve for AS4/3501-6 Graphite/Epoxy, (T=128°C (263°F), C=0%)

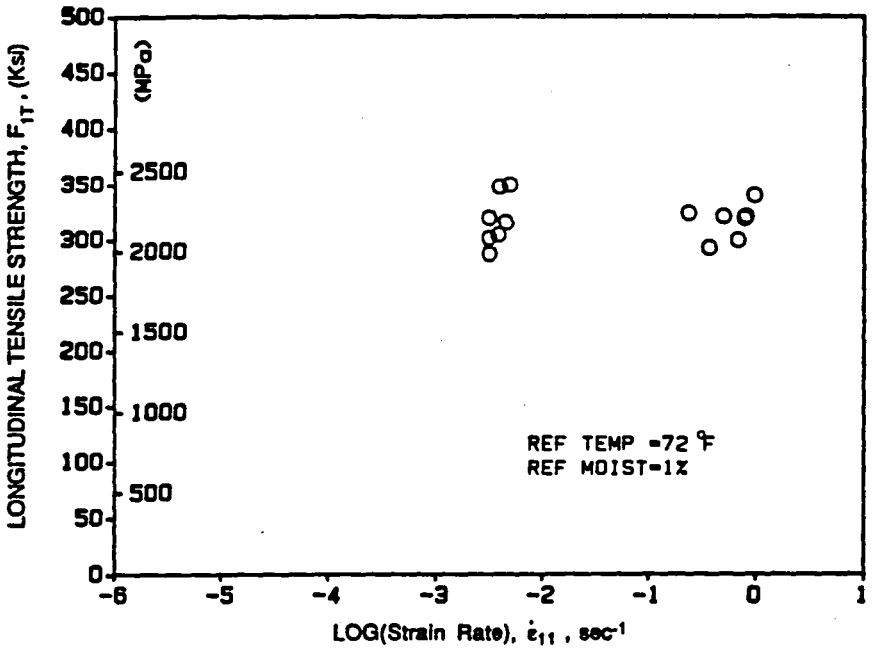

Figure 5.150 Longitudinal tensile strength vs. log(strain rate) curve for AS4/3501-6 Graphite/Epoxy, (T=22°C (72°F), C=1%)

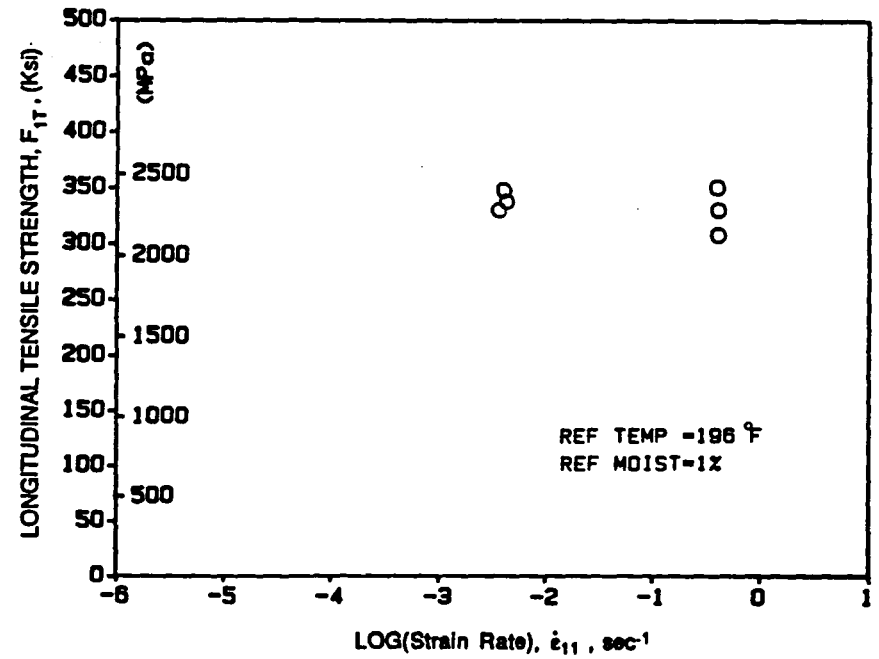

Figure 5.151 Longitudinal tensile strength vs. log(strain rate) curve for AS4/3501-6 Graphite/Epoxy, (T=91C (196°F), C=1%)

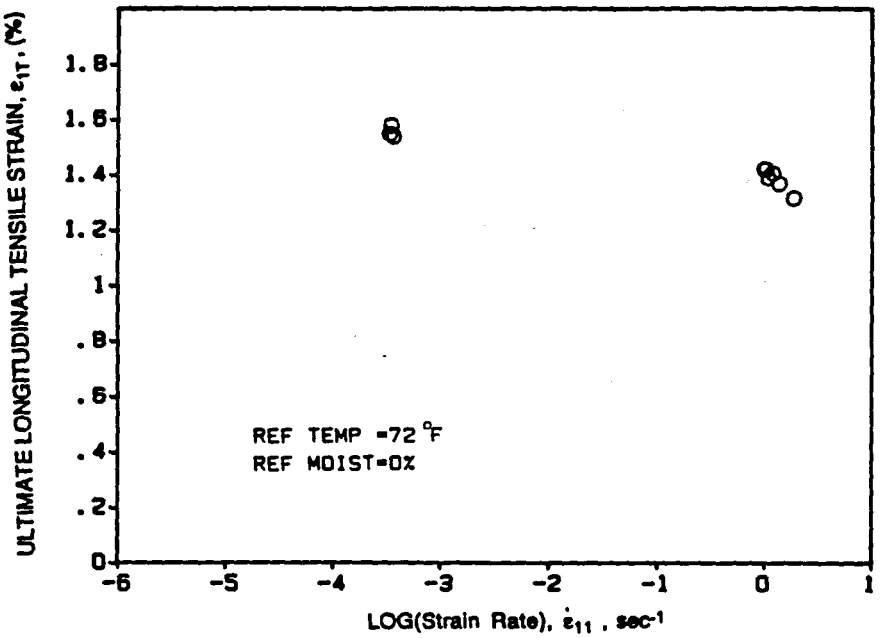

Figure 5.152 Ultimate longitudinal tensile strain vs. log(strain rate) curve for AS4/3501-6 Graphite/Epoxy, (T=22°C (72°F), C=0%)

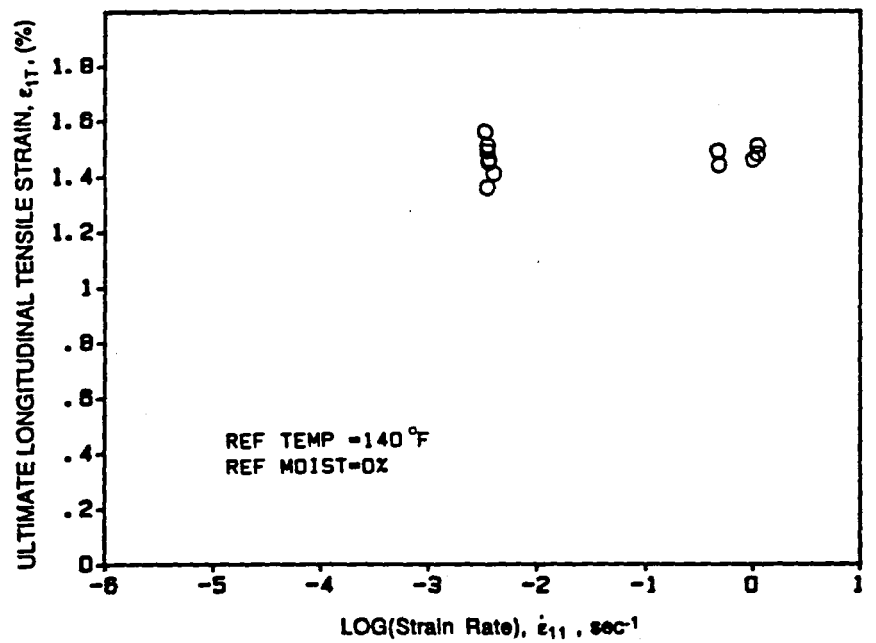

Figure 5.153 Ultimate longitudinal tensile strain vs. log(strain rate) curve for AS4/3501-6 Graphite/Epoxy, (T=60°C (140°F), C=0%)

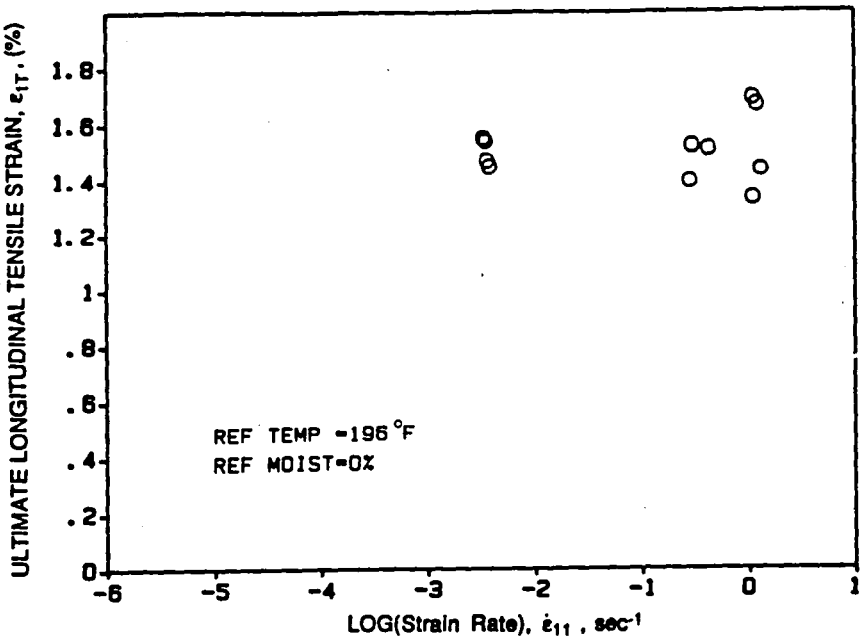

Figure 5.154 Ultimate longitudinal tensile strain vs. log(strain rate) curve for AS4/3501-6 Graphite/Epoxy, (T=91°C (196°F), C=0%)

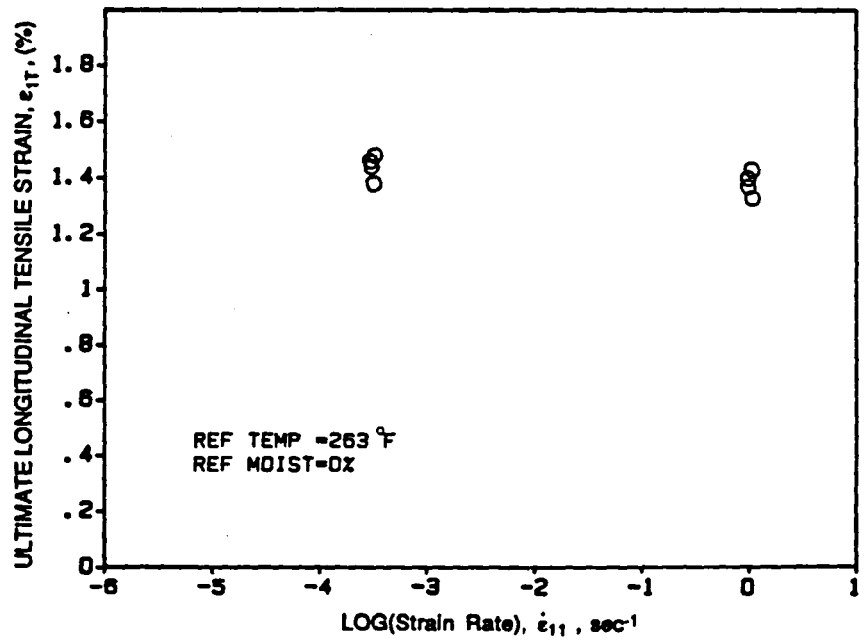

Figure 5.155 Ultimate longitudinal tensile strain vs. log(strain rate) curve for AS4/3501-6 Graphite/Epoxy, (T=128°C (263°F), C=0%)

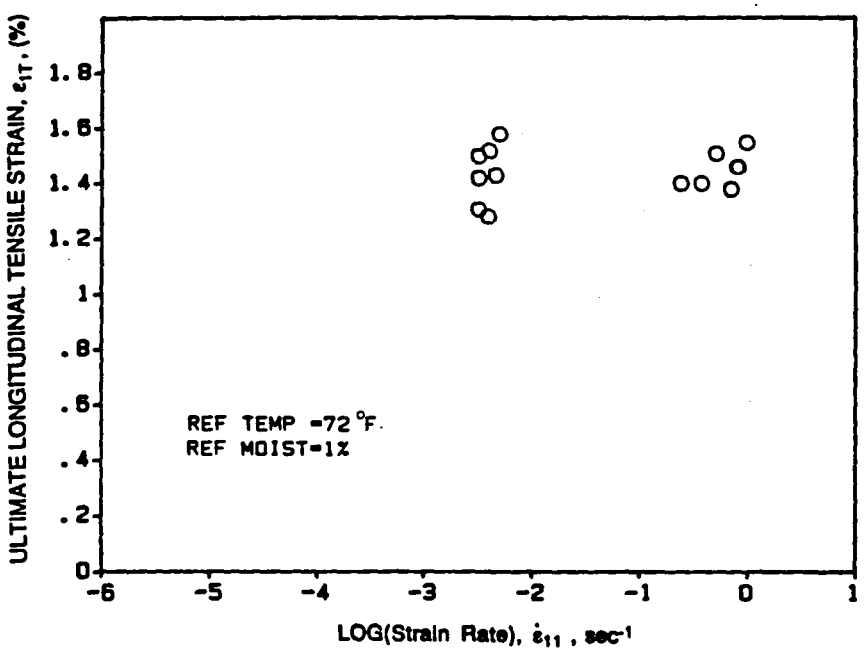

Figure 5.156 Ultimate longitudinal tensile strain vs. log(strain rate) curve for AS4/3501-6 Graphite/Epoxy, (T=22°C (72°F), C=1%)

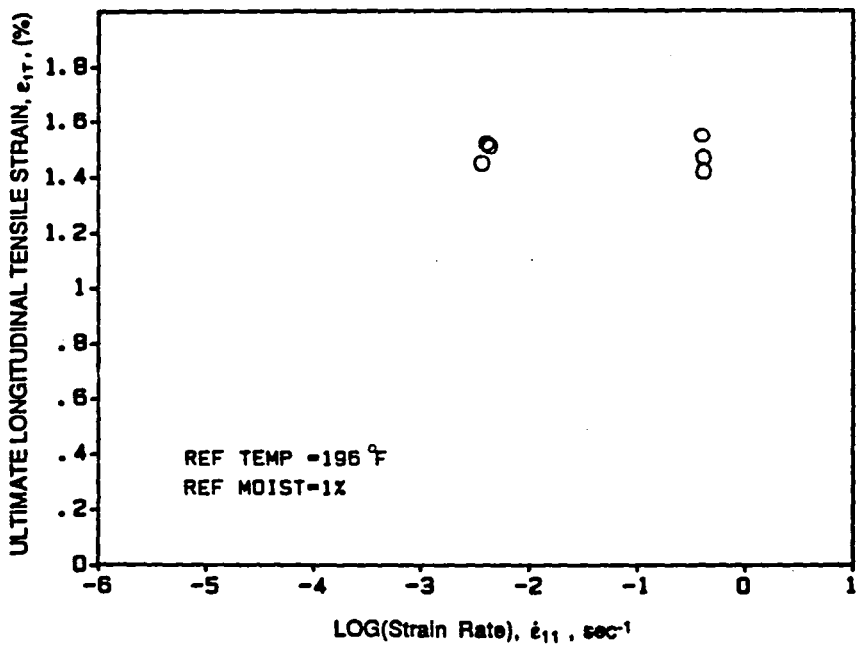

Figure 5.157 Ultimate longitudinal tensile strain vs. log(strain rate) curve for AS4/3501-6 Graphite/Epoxy, (T=91°C (196°F), C=1%)

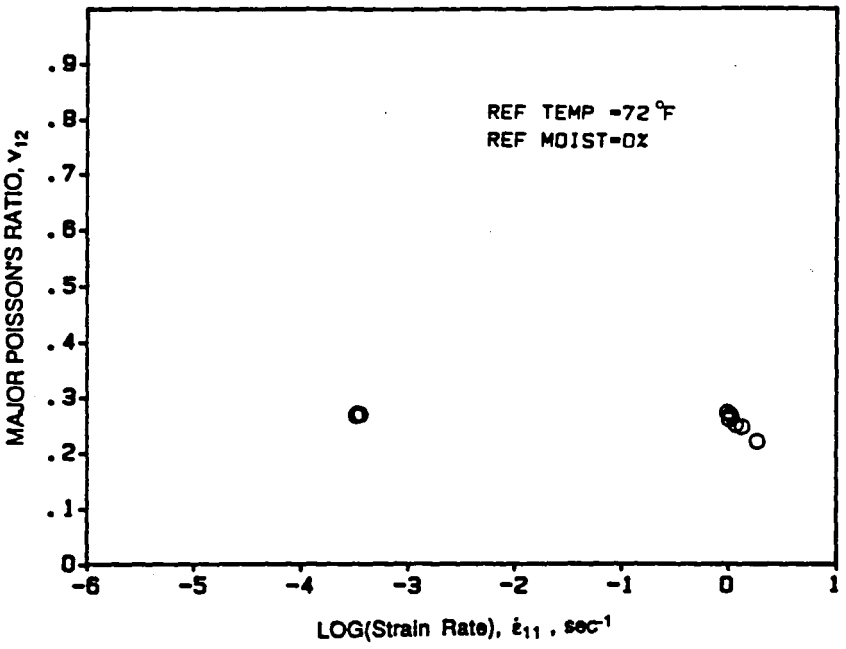

Figure 5.158 Major Poisson's ratio vs. log(strain rate) curve for AS4/3501-6 Graphite/Epoxy, (T=22°C (72°F), C=0%)

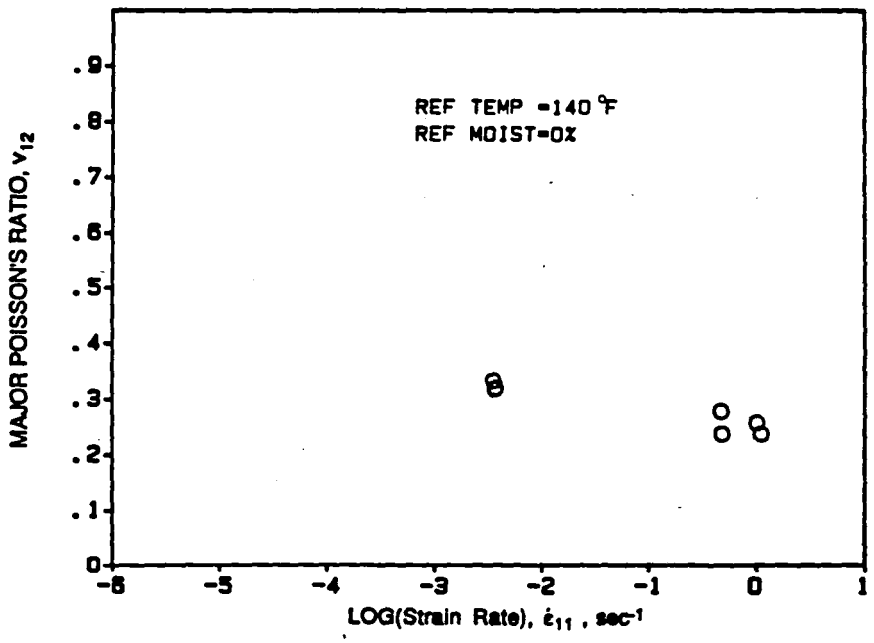

Figure 5.159 Major Poisson's ratio vs. log(strain rate) curve for AS4/3501-6 Graphite/Epoxy, (T=60°C (140°F), C=0%)

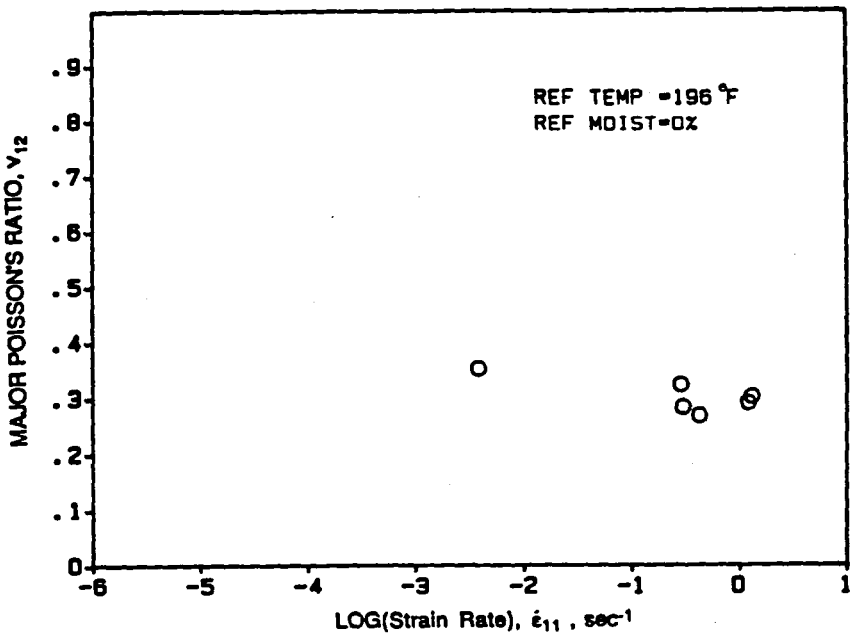

Figure 5.160 Major Poisson's ratio vs. log(strain rate) curve for AS4/3501-6 Graphite/Epoxy, (T=91°C (196°F), C=0%)

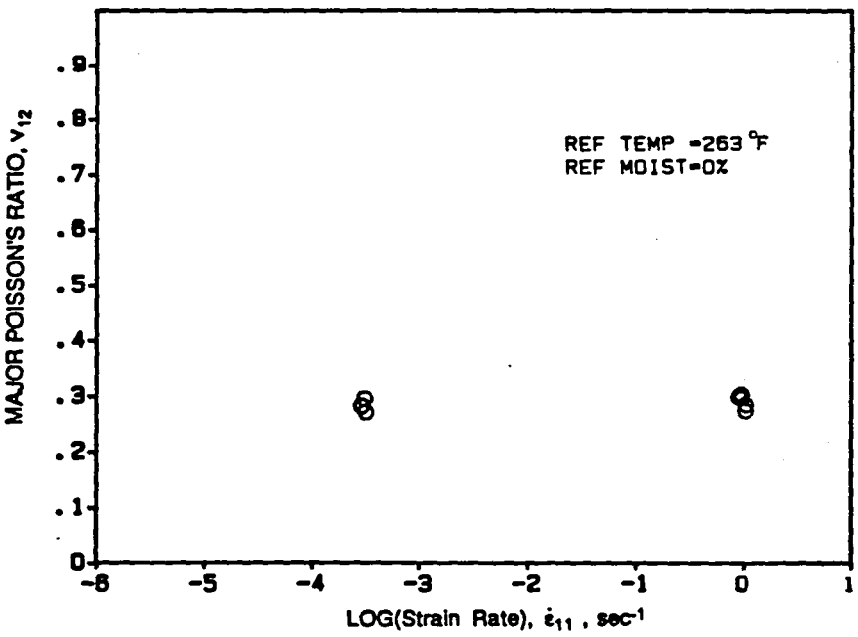

Figure 5.161 Major Poisson's ratio vs. log(strain rate) curve for AS4/3501-6 Graphite/Epoxy, (T=128°C (263°F), C=0%)

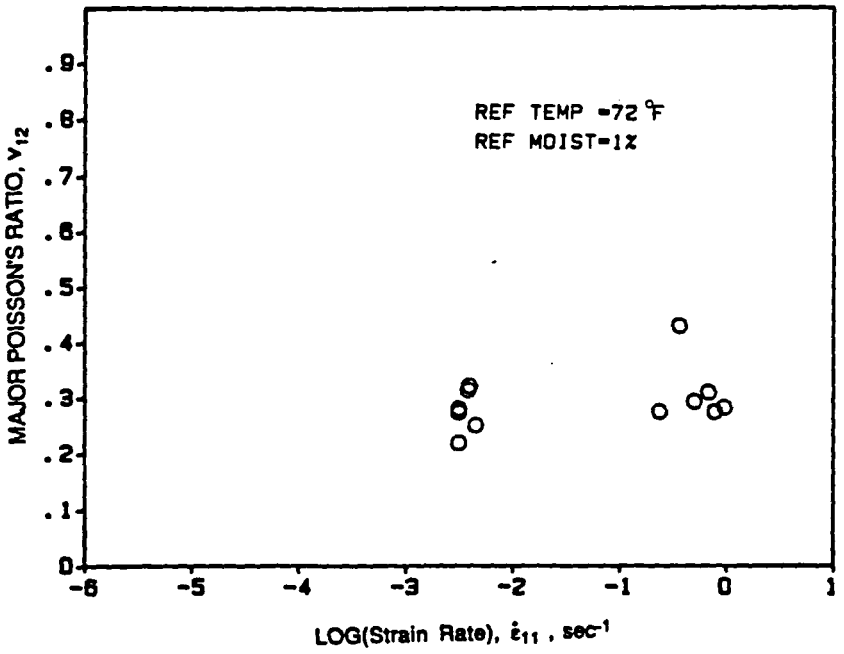

Figure 5.162 Major Poisson's ratio vs. log(strain rate) curve for AS4/3501-6 Graphite/Epoxy, (T=22°C (72°F), C=1%)

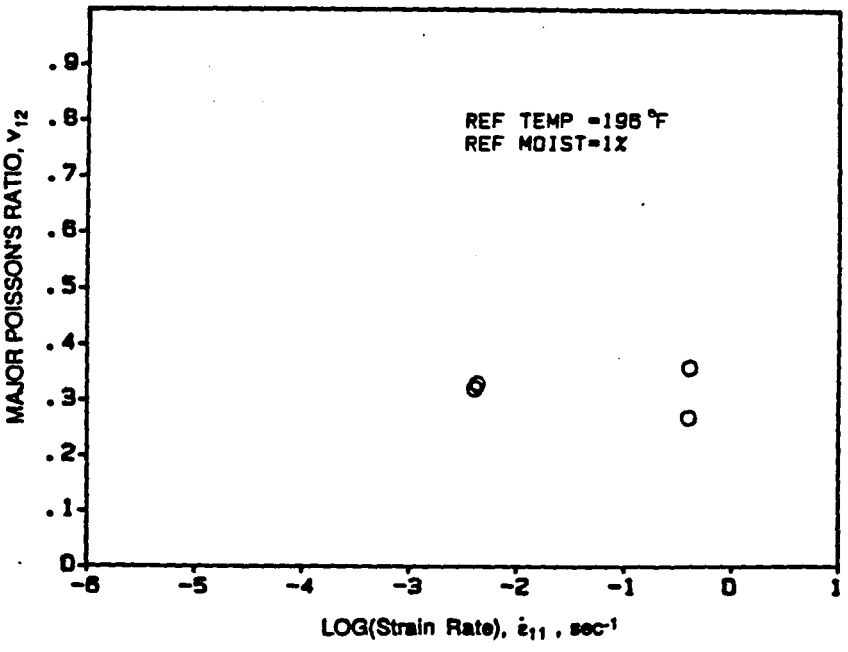

Figure 5.163 Major Poisson's ratio vs. log(strain rate) curve for AS4/3501-6 Graphite/Epoxy, (T=22°C (72°F), C=1%)

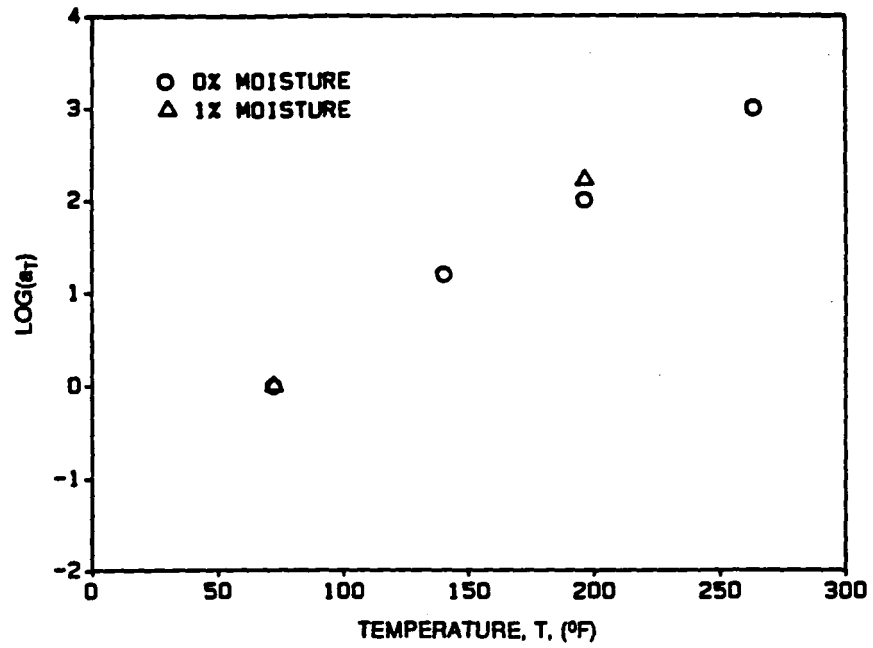

Figure 5.164 Log(Time-temperature shift factor) vs. temperature for longitudinal modulus under dry and wet (C=1%) conditions

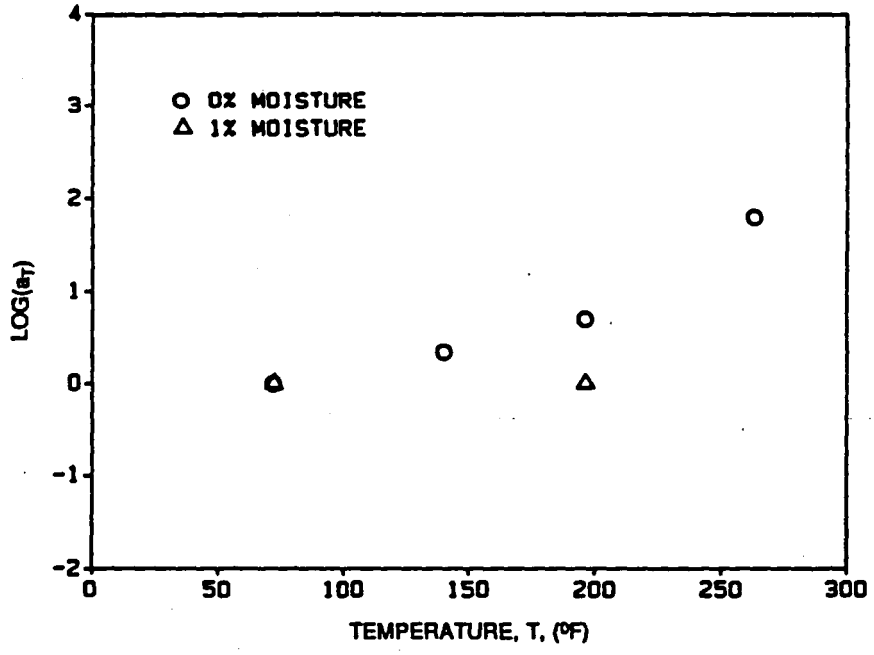

Figure 5.165 Log(Time-temperature shift factor) vs. temperature for longitudinal tensile strain under dry and wet (C=1%) conditions

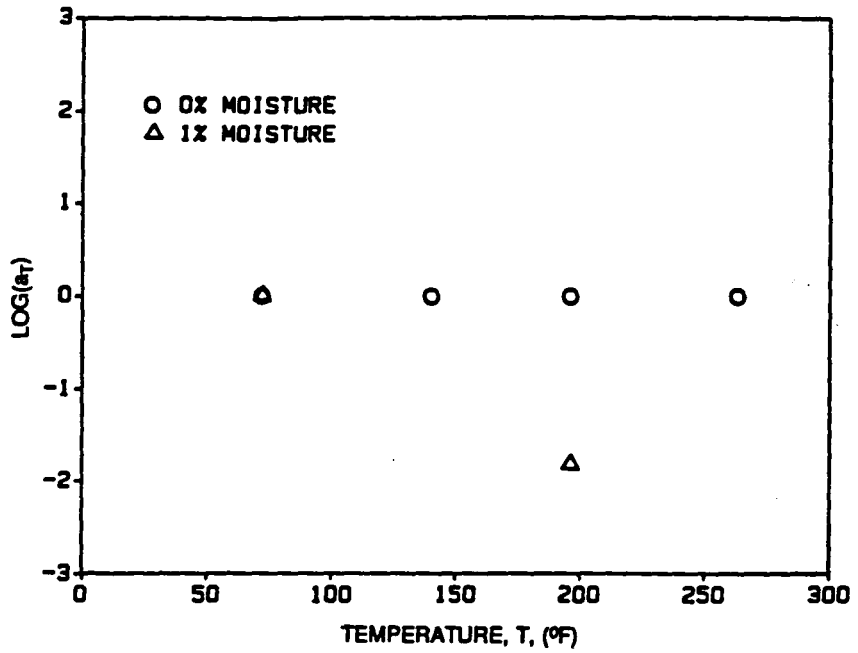

Figure 5.166 Log(Time-temperature shift factor) vs. temperature for ultimate longitudinal tensile strength under dry and wet (C=1%) conditions

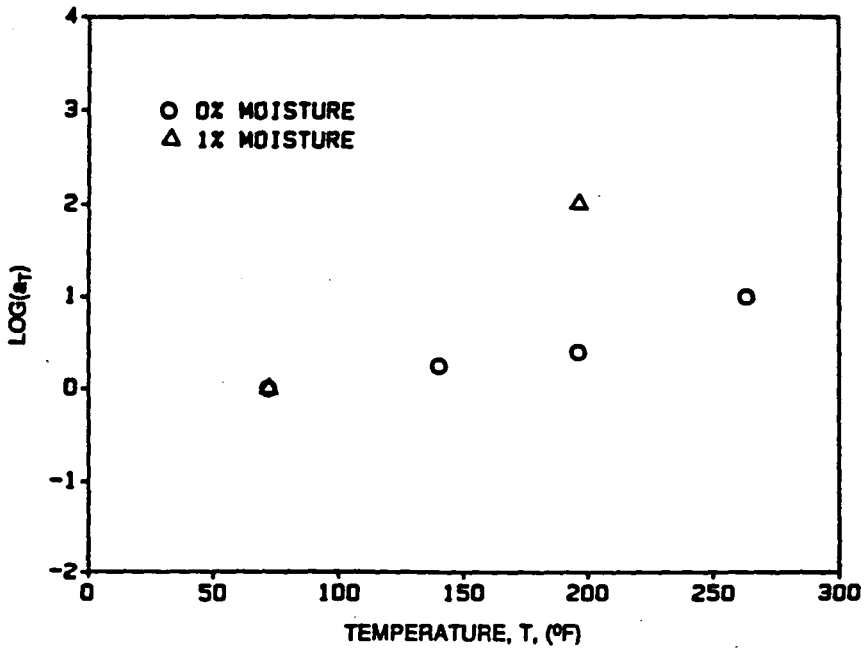

Figure 5.167 Log(Time-temperature shift factor) vs. temperature for major Poisson's ratio under dry and wet (C=1%) conditions

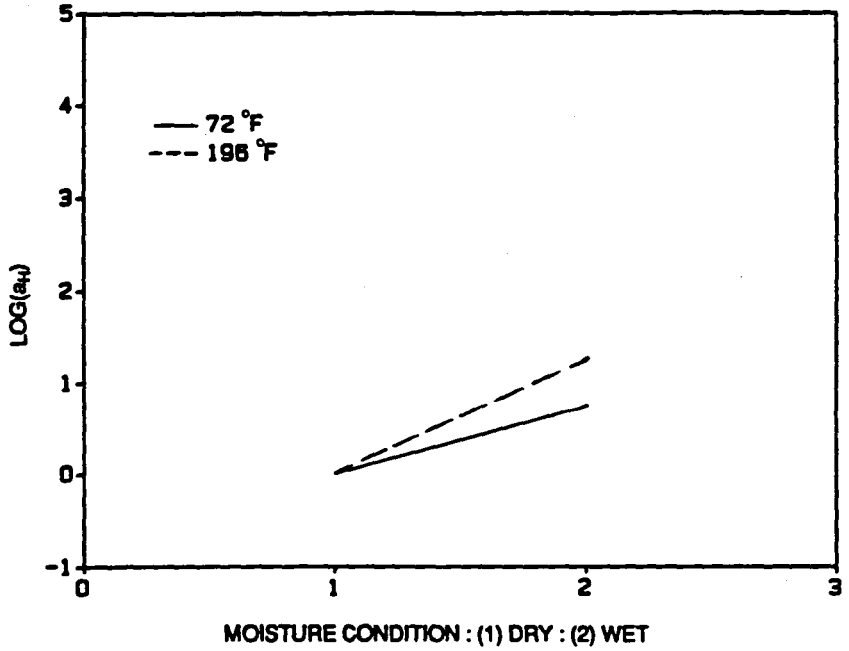

Figure 5.168 Log(Time-temperature shift factor) vs. moisture for longitudinal modulus, (T=22°C, (72°F) and T=91°C (196°F)

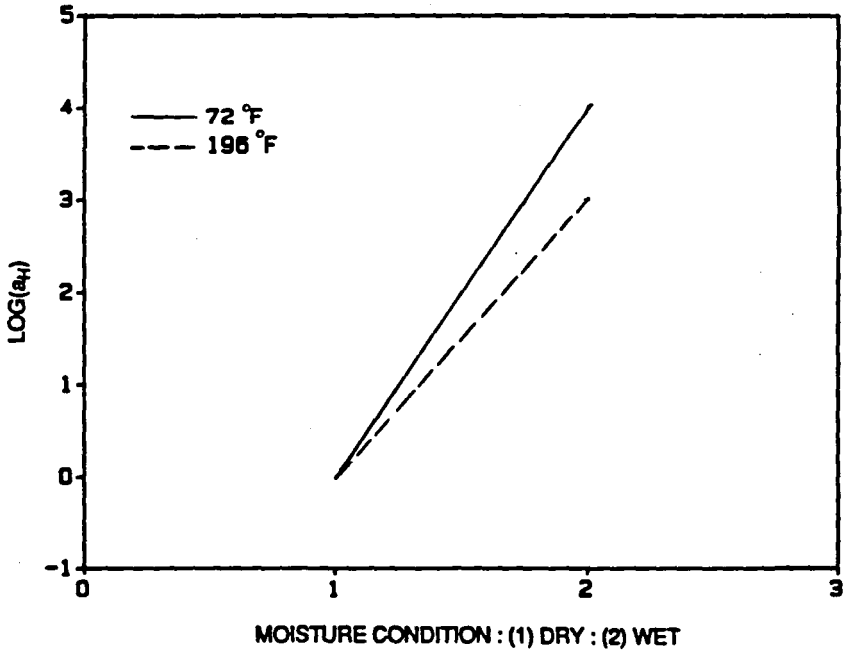

Figure 5.169 Log(Time-temperature shift factor) vs. moisture for longitudinal tensile strength, (T=22°C, (72°F) and T=91°C (196°F)

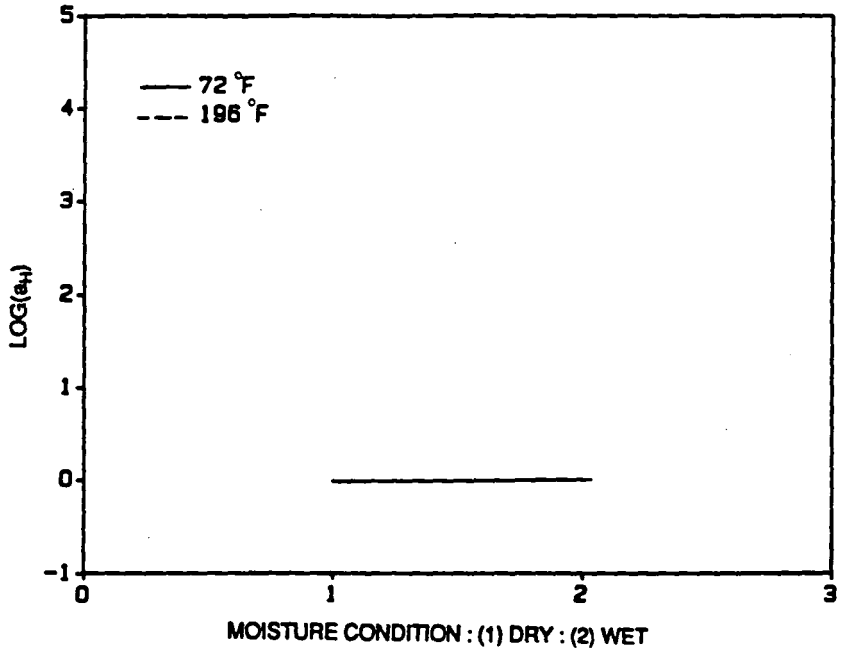

Figure 5.170 Log(Time-temperature shift factor) vs. moisture for longitudinal tensile strain, (T=22°C, (72°F) and T=91°C (196°F)

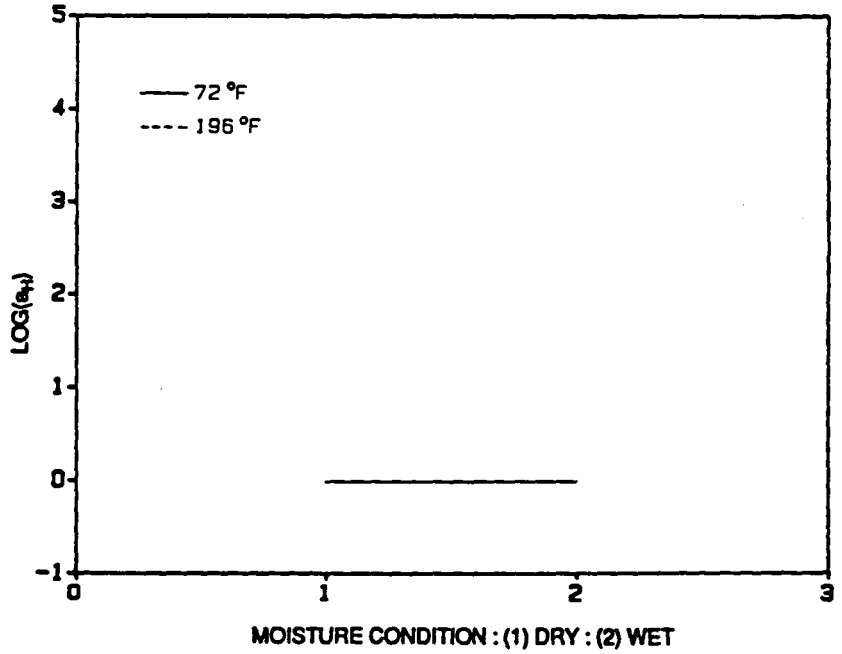

Figure 5.171 Log(Time-temperature shift factor) vs. moisture for major Poisson's ratio, (T=22°C, (72°F) and T=91°C (196°F)

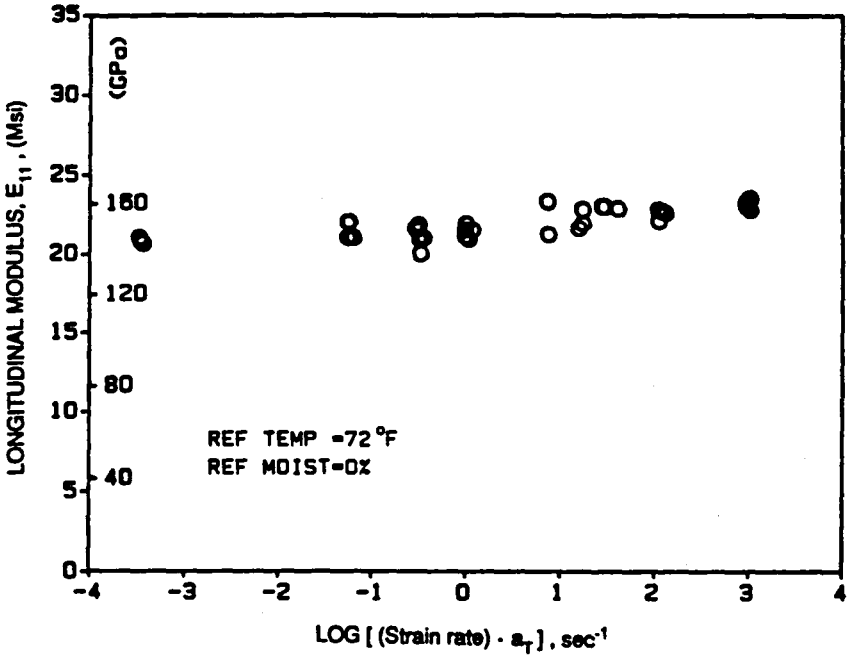

Figure 5.172 Time-temperature master curve for longitudinal modulus, (T=22°C (72°F), C=0%)

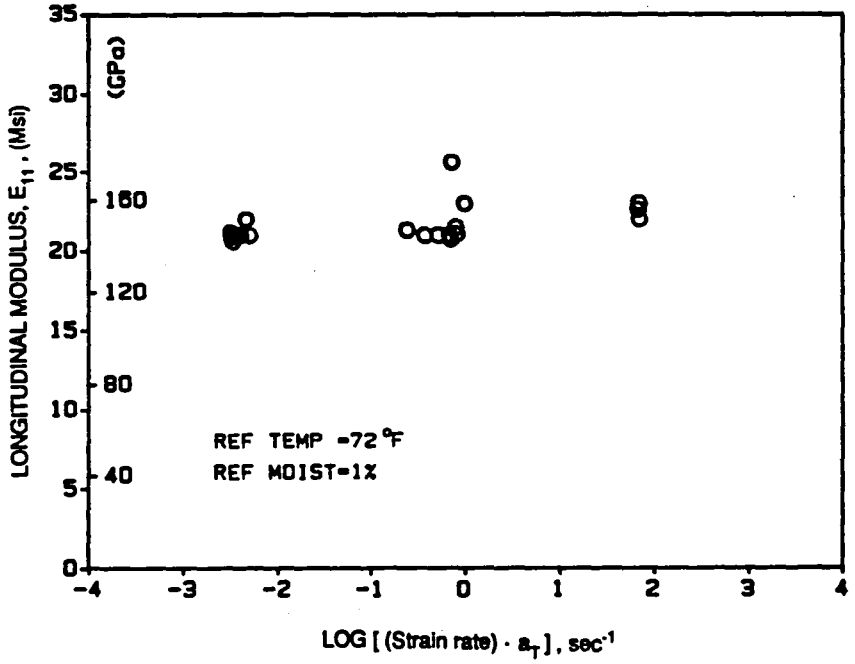

Figure 5.173 Time-temperature master curve for longitudinal modulus, (T=22°C (72°F), C=1%)

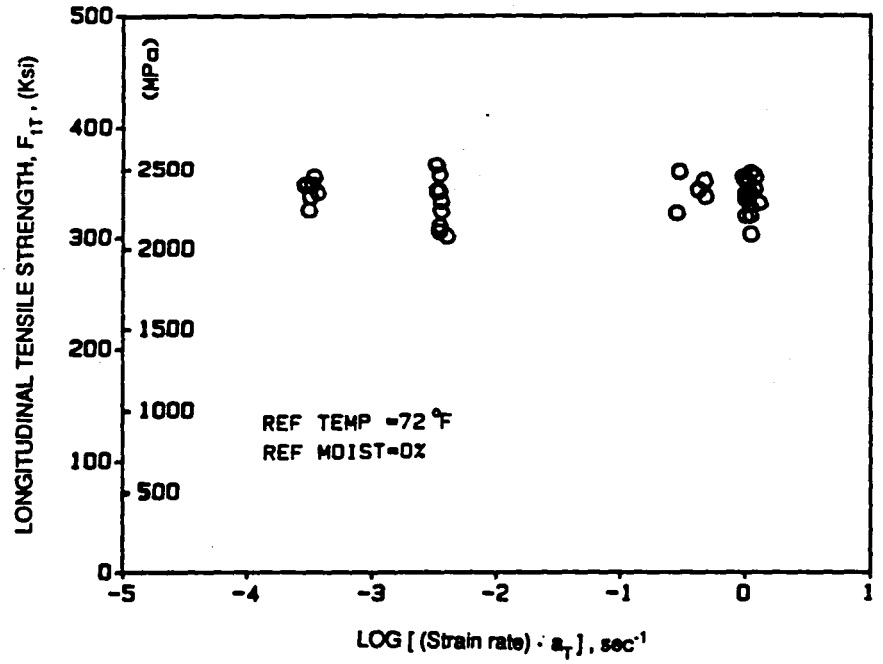

Figure 5.174 Time-temperature master curve for longitudinal tensile strength, (T=22°C (72°F), C=0%)

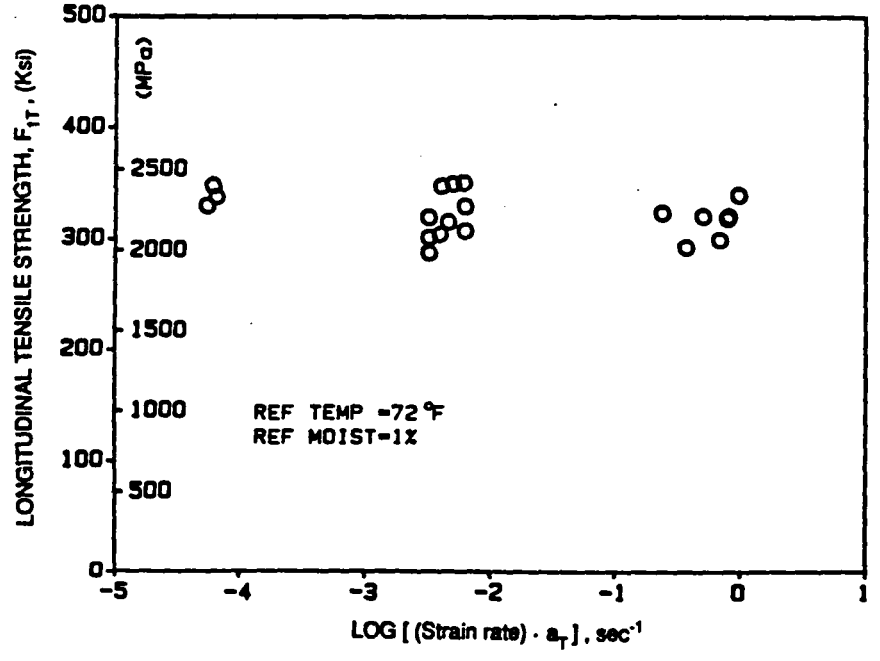

Figure 5.175 Time-temperature master curve for longitudinal tensile strength, (T=22°C (72°F), C=1%)

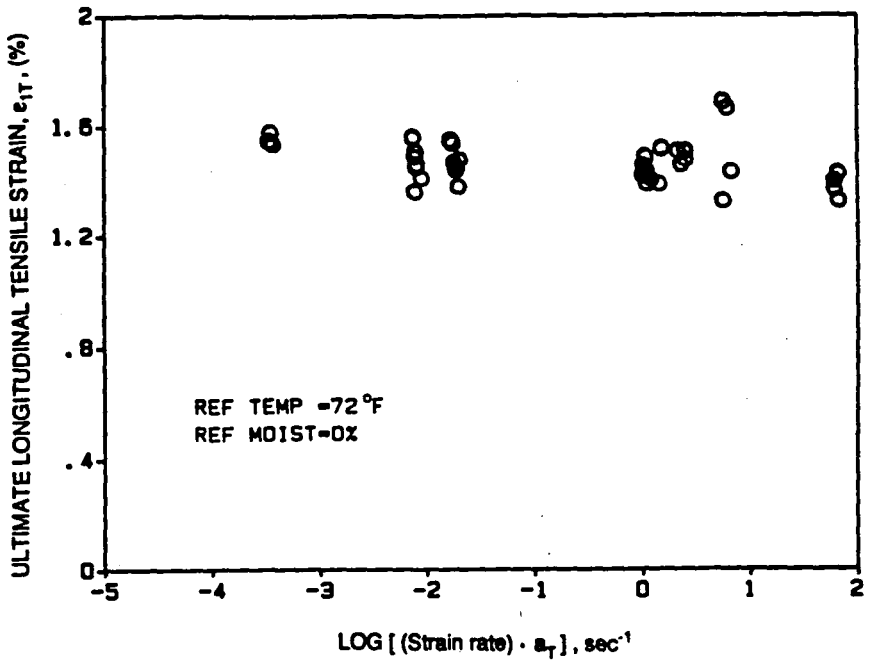

Figure 5.176 Time-temperature master curve for longitudinal tensile strain, (T=22°C (72°F), C=0%)

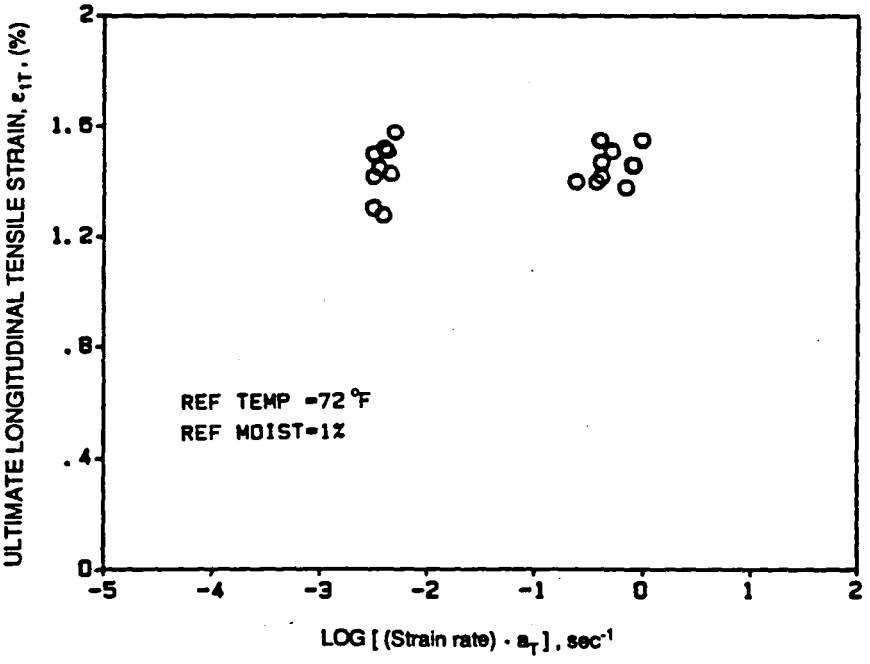

Figure 5.177 Time-temperature master curve for longitudinal tensile strain, (T=22°C (72°F), C=1%)

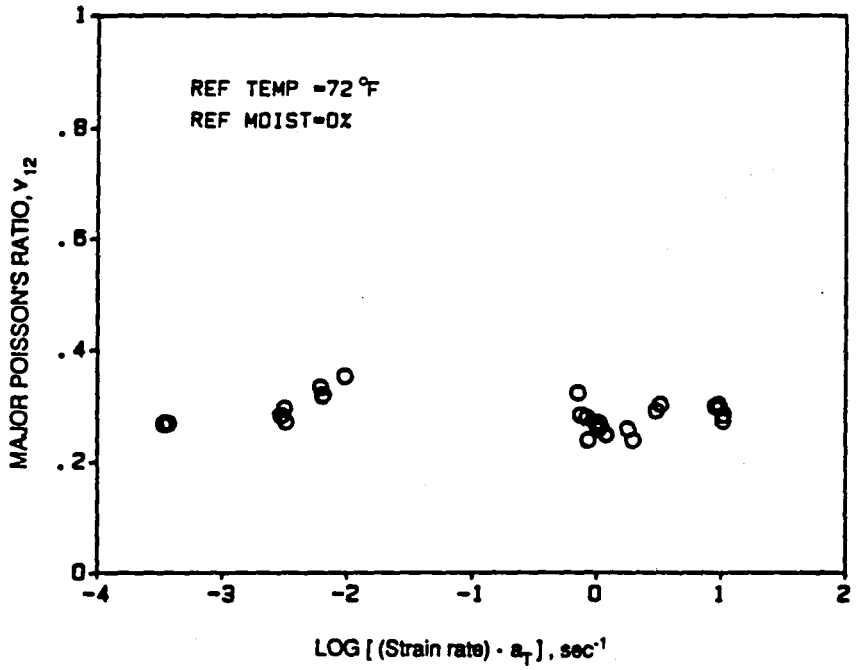

Figure 5.178 Time-temperature master curve for major Poisson's ratio, (T=22°C (72°F), C=0%)

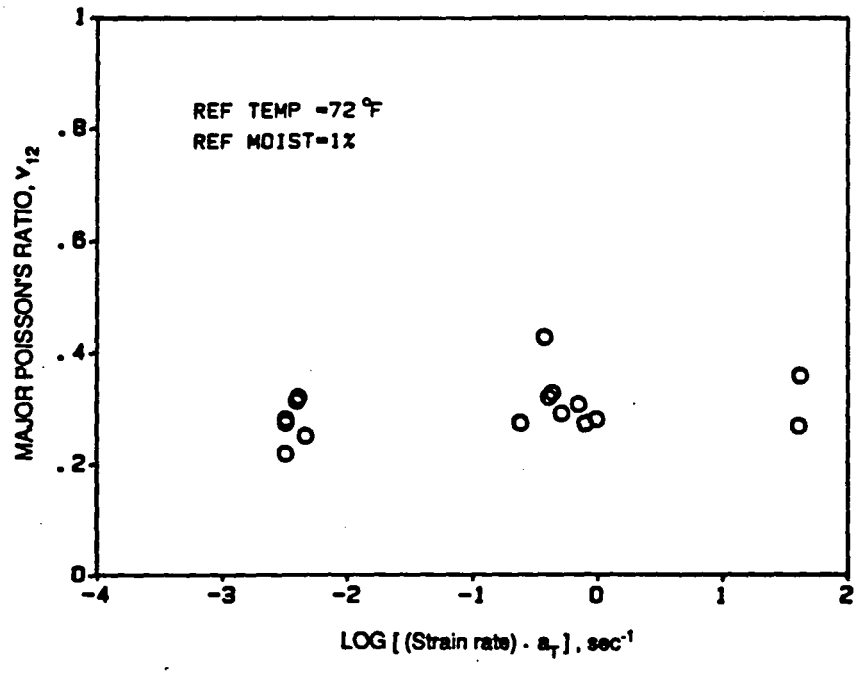

Figure 5.179 Time-temperature master curve for major Poisson's ratio, (T=22°C (72°F), C=1%)

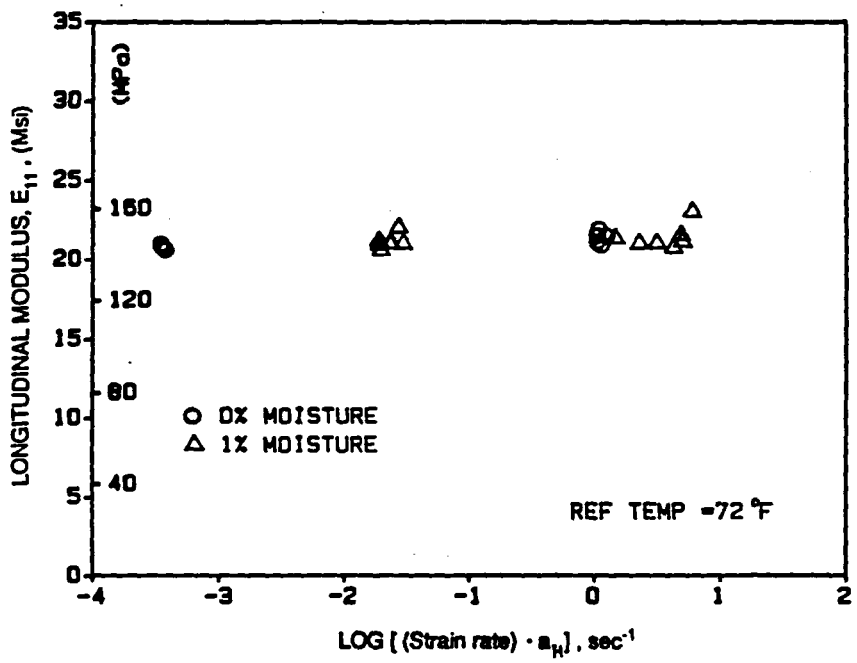

Figure 5.180 Time-moisture master curve for longitudinal modulus, (T=22°C (72°F), C=0%)

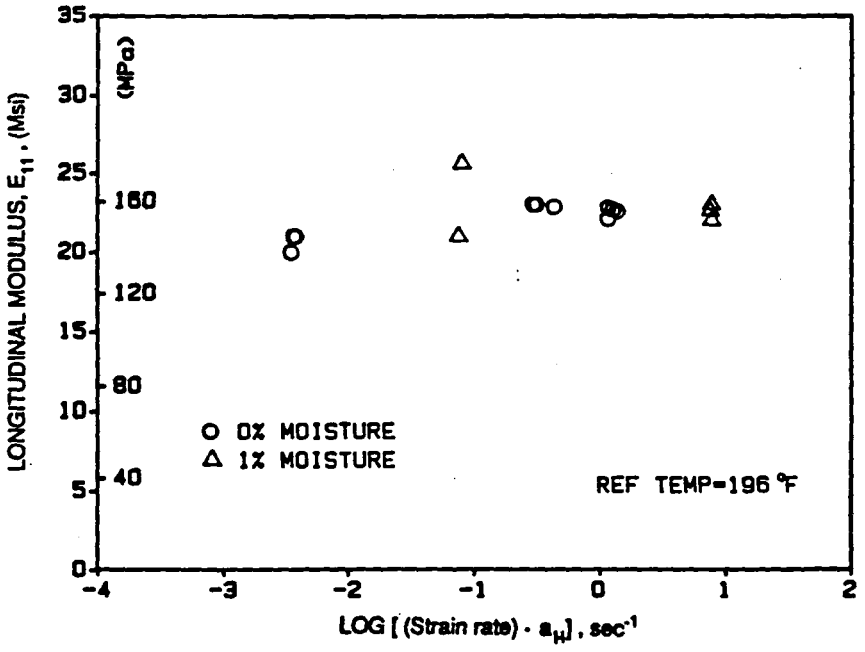

Figure 5.181 Time-moisture master curve for longitudinal modulus, (T=91°C (196°F), C=0%)

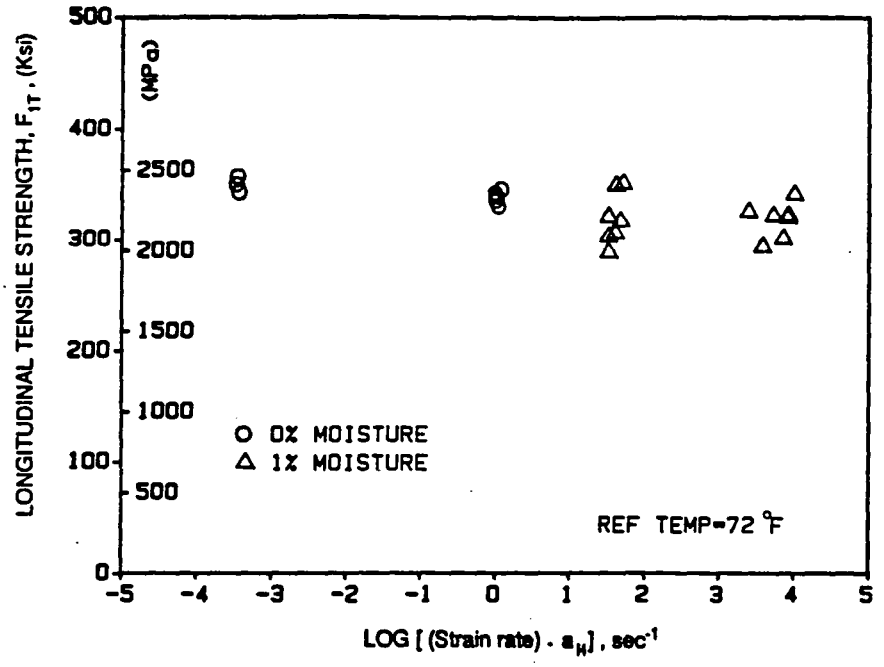

Figure 5.182 Time-moisture master curve for longitudinal tensile strength, (T=22°C (72°F), C=0%)

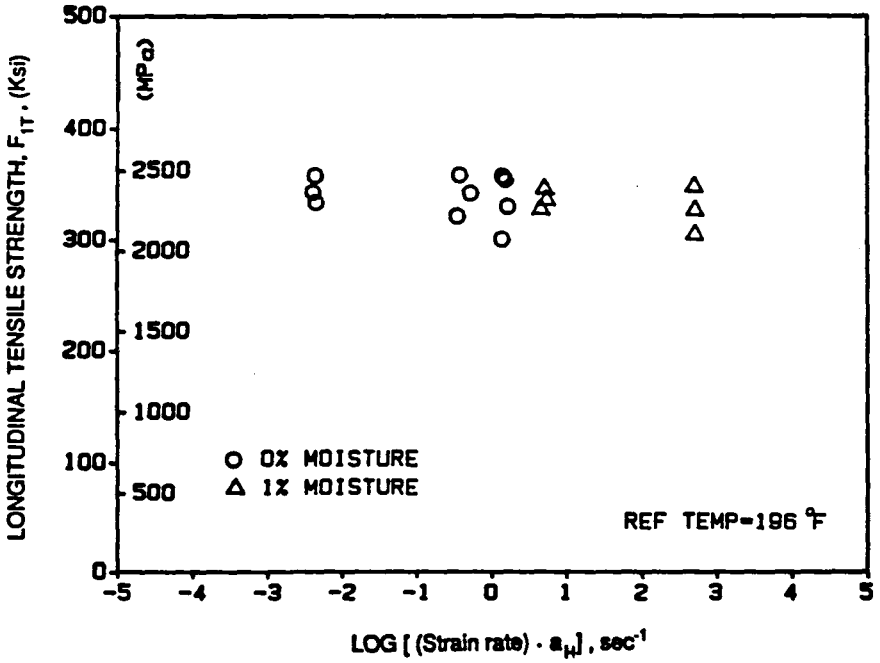

Figure 5.183 Time-moisture master curve for longitudinal tensile strength, (T=91°C (196°F), C=0%)

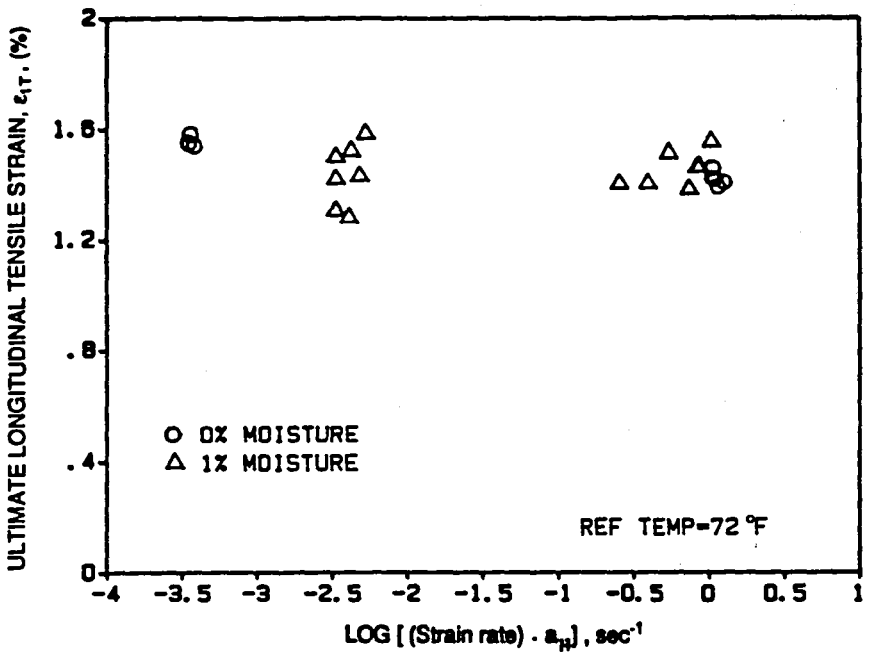

Figure 5.184 Time-moisture master curve for ultimate longitudinal tensile strain, (T=22°C (72°F), C=0%)

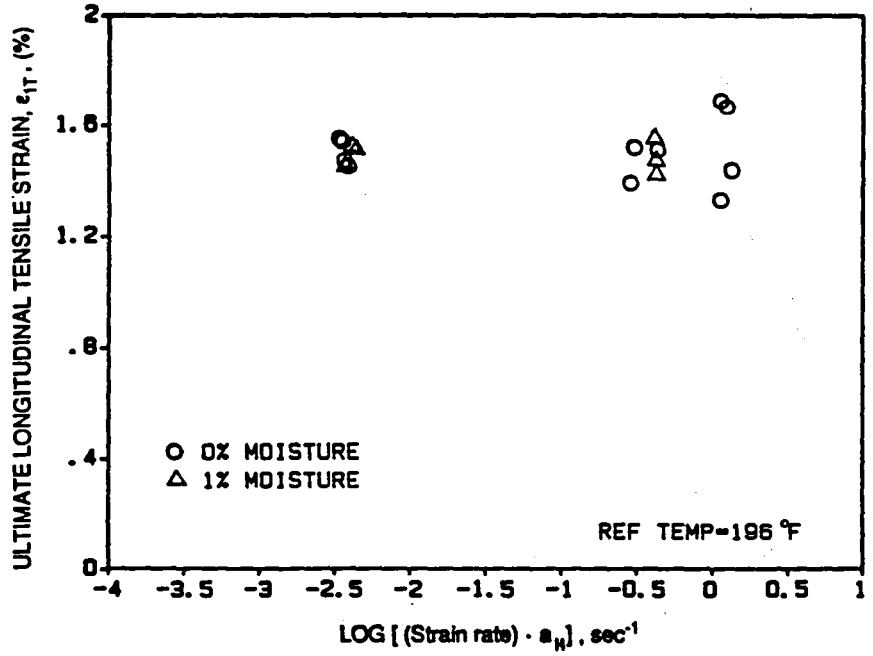

Figure 5.185 Time-moisture master curve for ultimate longitudinal tensile strain, (T=91°C (196°F), C=0%)

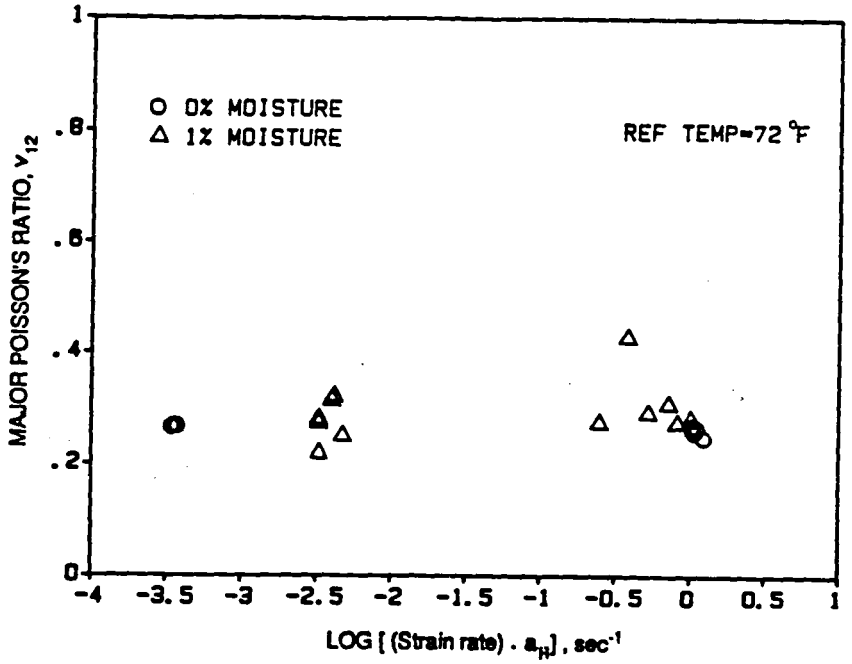

Figure 5.186 Time-moisture master curve for major Poisson's ratio, (T=22°C (72°F), C=0%)

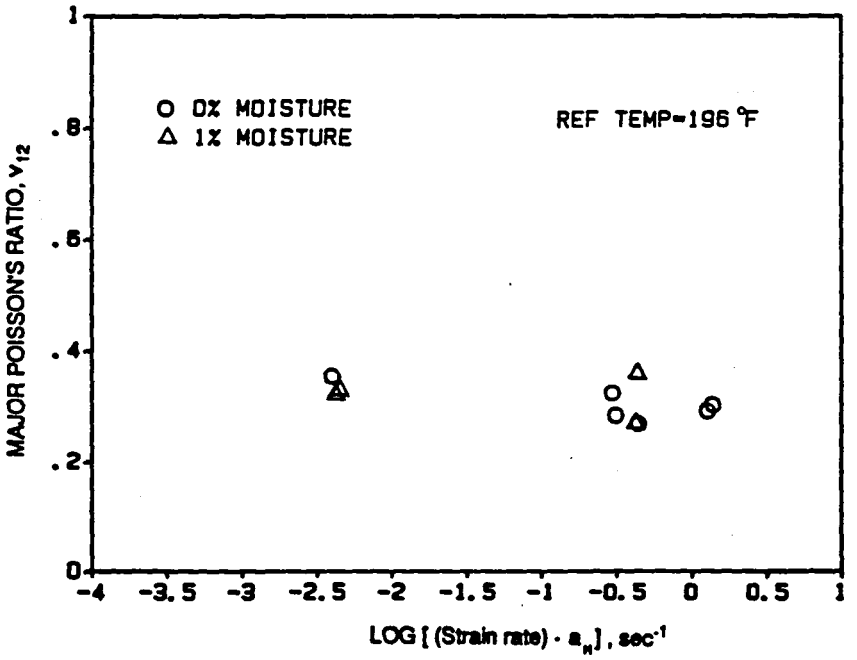

Figure 5.187 Time-moisture master curve for major Poisson's ratio, (T=91°C (196°F), C=0%)

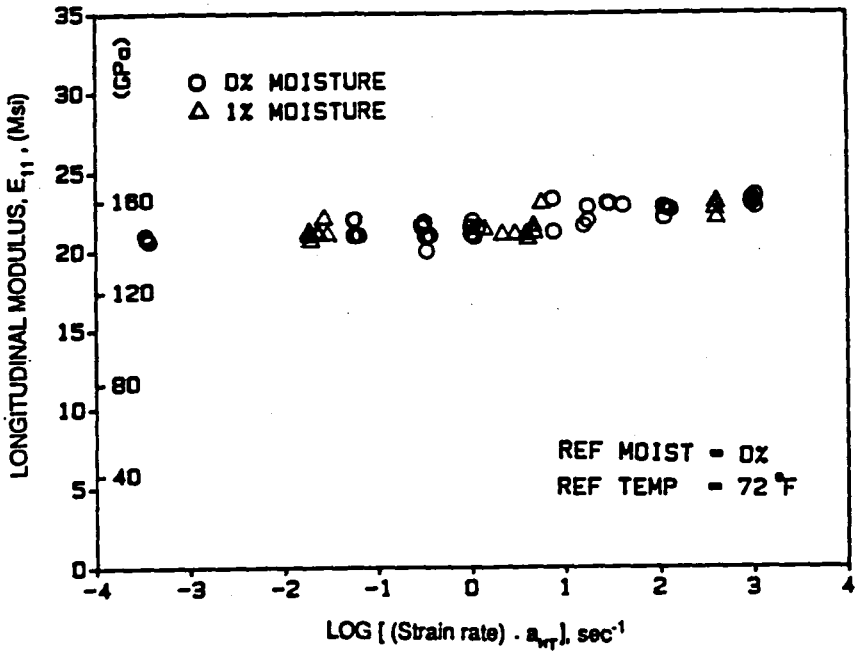

Figure 5.188 Time-temperature-moisture master curve for longitudinal modulus

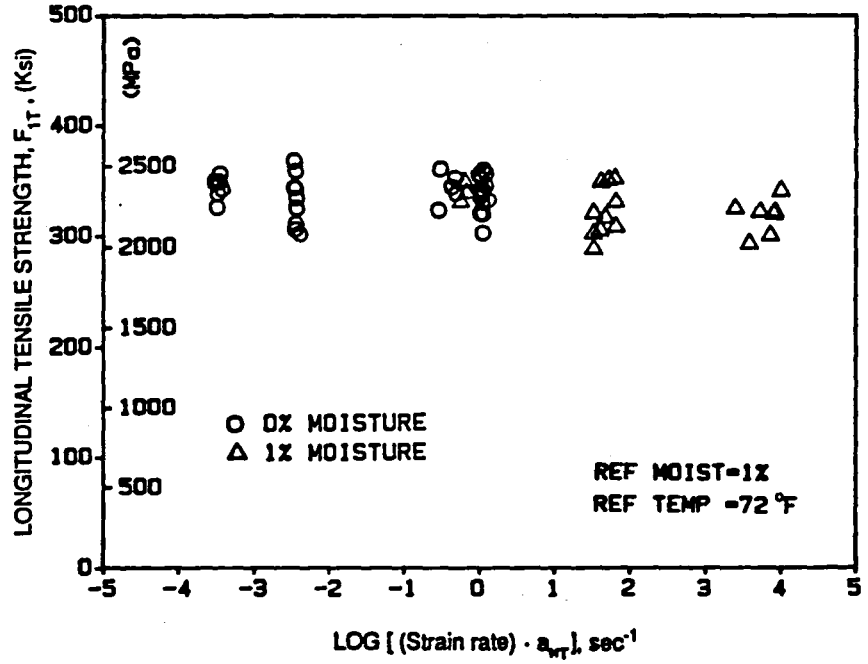

Figure 5.189 Time-temperature-moisture master curve for longitudinal tensile strength

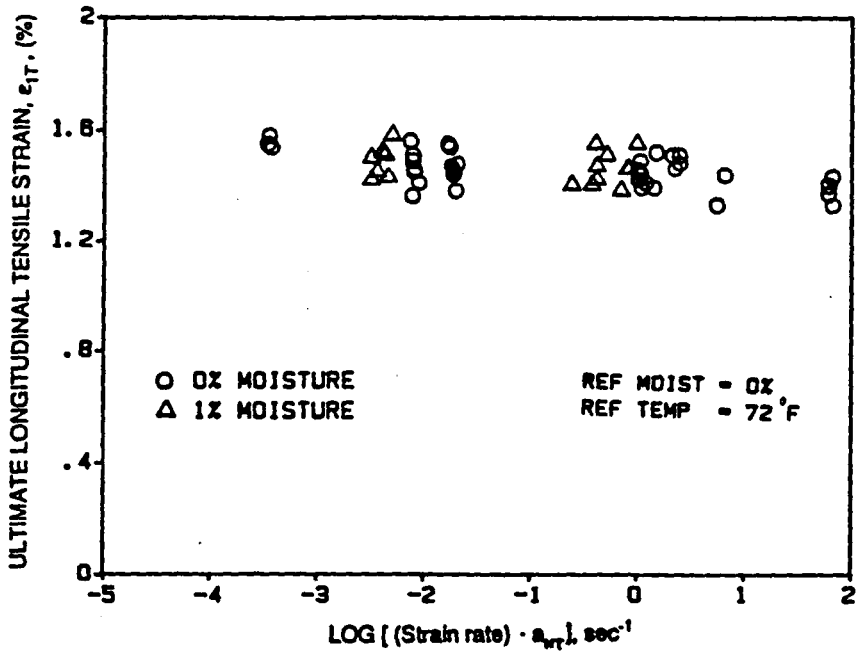

Figure 5.190 Time-temperature-moisture master curve for longitudinal tensile strain

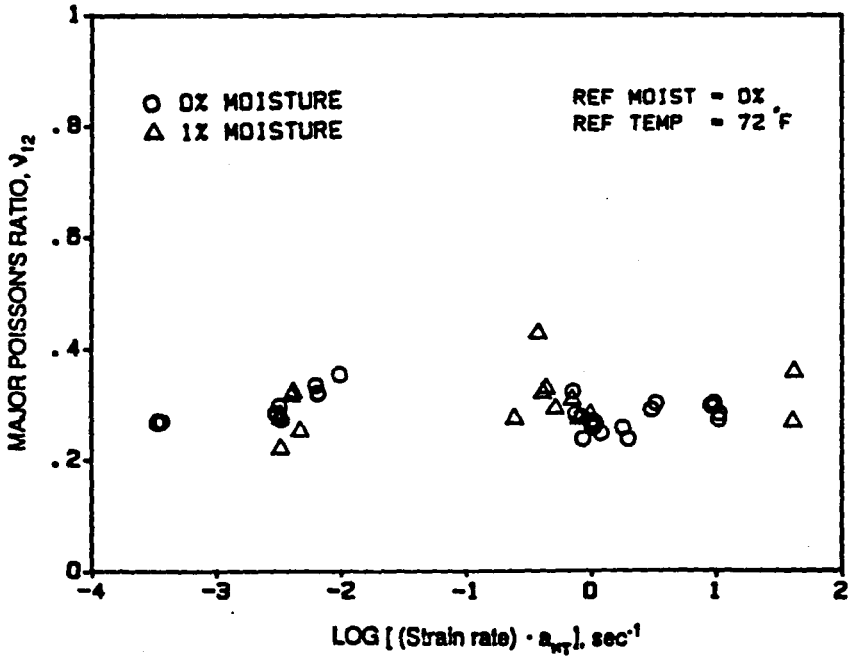

Figure 5.191 Time-temperature-moisture master curve for major Poisson's ratio

TIME - TEMPERATURE - MOISTURE SHIFT FACTOR

$$\log[a_T(H_n,T)] + \log[a_H(T_0,H)] = \log[a_H(T_n,H)] + \log[a_T(H_0,T)]$$

H_n , T_n = Fixed level of moisture and temperature

H_0 , T_0 = Reference point of moisture and temperature

H , T = Variable moisture and temperature

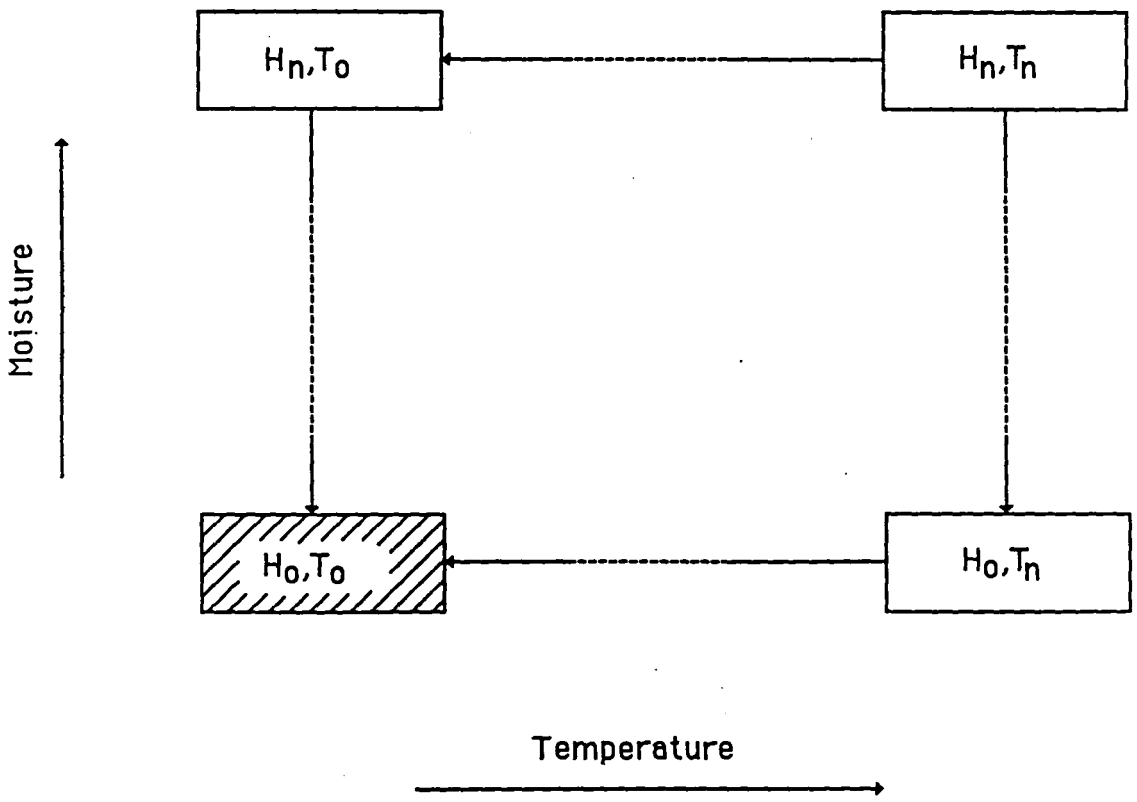

Figure 5.192 Time-temperature-moisture superposition.

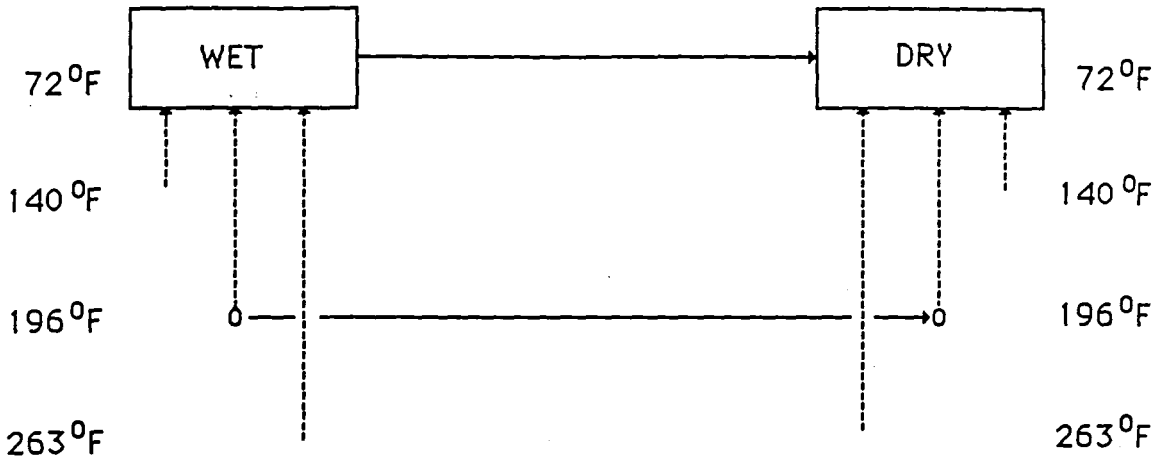

$$\log[a_{(1\%,T)}] + \log[a_{(H,72^{o}F)}] = \log[a_{(H,196^{o}F)}] + \log[a_{(0\%,T)}]$$

PROPERTY

E_{22}	-2.2 + 0.0 = 1.0 - 3.2 = -2.2 = -2.2
F_{22}	-0.8 + 3.5 = 4.0 - 1.6 = 2.7 = 2.4
ε_{2T}	-1.0 + 3.3 = 5.1 - 2.9 = 2.3 = 2.2
G_{12}	-2.2 +0.75 = 0.0 -1.8 = -1.5 = -1.8
F_{12}	-2.7 - 1.5 = -2.6-1.7 = -4.3 = -4.3

Figure 5.193 Examples of shifting data to different hygrothermal reference conditions with the use of shift factors and equation 5.1.

VI. SUMMARY, CONCLUSIONS AND RECOMMENDATIONS FOR FUTURE WORK.

In this work, the mechanical properties of AS4/3501-6 Graphite/Epoxy were evaluated at strain rates ranging from $5 \cdot 10^{-6}$ s^{-1} to 5 s^{-1}, four different temperature levels of 22°C (72°F), 60°C (140°F), 91°C (196°F), 128°C (263°F), and two moisture levels of 0% and 1%. From the data obtained, time-temperature, time-moisture, and time-temperature-moisture constitutive relations were established for the composite, and a hygrothermomechanical (HGTM) procedure for predicting material response under any set of environmental conditions has been proposed.

The main conclusions drawn from the results of all tests performed and the accompanying data analyses are as follows:

1. The embedded gage technique was thoroughly examined and found to be appropriate for both hygrothermal expansion and mechanical strain measurements. For high strain rate tests of wet specimens, the method was found to be more reliable than that of surface gages and the conventional extensometer.
2. All transverse properties were found to decrease with increasing temperature and moisture content.
3. Ultimate transverse properties were found to increase with strain rate at low temperatures and follow an opposite trend at high temperatures, for dry specimens. For wet specimens, those properties showed a slight decrease with temperature.

4. Transverse modulus tends to increase with increasing strain rate for all specimens tested.
5. In-plane shear properties are reduced at high moisture content and elevated temperatures at a given strain rate.
6. The effect of moisture and temperature, at the various strain rates tested, on the longitudinal tensile properties was found to be insignificant.
7. Time-temperature shift functions were obtained for the all properties. These functions tend to follow second order curves when plotted on semi-log coordinates, and cover a wider range of temperature than the traditional straight line fit.
8. Time-temperature-moisture master curves were constructed for all mechanical properties. However, the combined shift function has not been established yet.
9. The values of the time-temperature-moisture shift factor were found to be path independent only when one of the variables is held constant.
10. Thus, it is possible to transfer a set of material property data from on hygrothermal testing state to another, if the corresponding shift factors are known.

Although the work presented here touched almost every aspect of characterization and prediction of composite material properties under various HGTM conditions, there is a lot more to be done before this subject may be considered as fully investigated. It is recommended that the following work be done:

1. More tests at various moisture levels in order to obtain more complete time-temperature-moisture super-master curves, and to enable the

formulation of the combined time-temperature-moisture shift function. The same data would also establish the time-moisture shift functions.

2. Curve fit the time-temperature shift factor versus temperature data available in this report and obtain a time-temperature shift function.
3. Expand the strain rate range to simulate impact and/or examine the effect of various hygrothermal histories on the impact response of the material,
4. Investigate the influence of defects, such as holes, cracks, and embedded inclusions on the high strain rate properties, under different moisture contents and temperatures.

APPENDIX A

AS4/3501-6 GRAPHITE/EPOXY PROPERTY TABLES

Table A-1. Tensile Properties of [90_8] AS4/3501-6 Graphite/Epoxy at Low Strain Rates, 22°C (72°F) and 0% Moisture.

Initial Properties

Specimen Number	Strain Rate ($\dot{\varepsilon}_{22}$), ms^{-1}	Modulus (E_{22}) GPa (Msi)	Poisson's Ratio ν_{21}
90/-5L1	0.047	10.0(1.46)	-
90/-5L2	0.047	10.4(1.51)	-
90/-5L3	0.047	10.3(1.50)	-
90/-5L4	0.047	10.1(1.47)	-
90/-5L5	0.047	10.7(1.55)	-

Ultimate Properties

Specimen Number	Time to Failure (t_f), s	Strength (F_{2T}) MPa (Ksi)	Strain (ε_{2T}), %
90/-5L1	140	64(9.42)	0.67
90/-5L2	124	60(8.79)	0.61
90/-5L3	151	73(10.60)	0.75
90/-5L4	121	54(7.85)	0.55
90/-5L5	158	72(10.50)	0.78

Table A-2. Tensile Properties of [90_8] AS4/3501-6 Graphite/Epoxy at Intermediate Strain Rates, 22°C (72°F) and 0% Moisture.

Initial Properties

Specimen Number	Strain Rate ($\dot{\varepsilon}_{22}$), m s^{-1}	Modulus (E_{22}) GPa (Msi)	Poisson's Ratio ν_{21}
90/-3L1	4.94	10.9(1.46)	-
90/-3L2	4.90	10.8(1.57)	-
90/-3L3	4.90	10.9(1.59)	-
90/-3L4	4.90	11.0(1.60)	-
90/-3L5	4.90	11.0(1.60)	-

Ultimate Properties

Specimen Number	Time to Failure (t_f), s	Strength (F_{2T}) MPa (Ksi)	Strain (ε_{2T}), %
90/-3L1	0.95	51 (7.48)	0.48
90/-3L2	1.31	67 (9.77)	0.62
90/-3L3	1.39	76(11.10)	0.71
90/-3L4	1.28	68 (9.99)	0.62
90/-3L5	1.03	53 (7.78)	0.50

Table A-3. Tensile Properties of [90_8] AS4/3501-6 Graphite/Epoxy at High Strain Rates, 22°C (72°F) and 0% Moisture.

Initial Properties

Specimen Number	Strain Rate ($\dot{\varepsilon}_{22}$), s^{-1}	Modulus (E_{22}) GPa (Msi)	Poisson's Ratio ν_{21}
90/-1L1	0.295	11.9(1.73)	0.0120
90/-1L2	0.313	11.7(1.70)	0.0118
90/-1L3	0.313	11.6(1.68)	0.0135
90/-1L4	0.295	11.8(1.71)	0.0115
90/-1L5	0.365	11.8(1.71)	0.0120
90/-1L6	0.443	11.8(1.72)	0.0111
90/-1L7	0.426	11.7(1.70)	0.0117

Ultimate Properties

Specimen Number	Time to Failure (t_f), ms	Strength (F_{2T}) MPa (Ksi)	Strain (ε_{2T}), %
90/-1L1	19	51(7.53)	0.44
90/-1L2	18	59(8.66)	0.53
90/-1L3	17	48(7.08)	0.43
90/-1L4	18	52(7.55)	0.44
90/-1L5	15	57(8.35)	0.49
90/-1L6	15	56(8.15)	0.44
90/-1L7	14	54(7.96)	0.46

Table A-4. Tensile Properties of [90_8] AS4/3501-6 Graphite/Epoxy at Low Strain Rates , 22°C (72°F) and 1% Moisture.

Initial Properties

Specimen Number	Strain Rate ($\dot{\varepsilon}_{22}$) , ms^{-1}	Modulus (E_{22}) GPa (Msi)	Poisson's Ratio ν_{21}
E5	3.0	11.2 (1.63)	–
E6	4.0	–	–
E7	3.0	11.5 (1.67)	0.02
E8	2.8	11.7 (1.70)	–
		11.4 (1.65) x	
R6	4.5	11.7 (1.70)	–
V2	5.0	11.7 (1.70)	–
W4	4.1	11.7 (1.70)	–
Q7	3.3	10.3 (1.50)	–
R2	4.4	11.0 (1.60)	–

Ultimate Properties

Specimen Number	Time to Failure (t_f) , s	Strength (F_{2T}) MPa (Ksi)	Strain (ε_{2T}) , %
E5	1.8	60.9 (8.83)	0.54
E6	–	53.8 (7.80)	0.46
E7	1.1	35.8 (5.20)	0.33
			0.31 x
E8	1.1	41.8 (6.06)	0.34
			0.35
R6	1.1	55.9 (8.12)	0.52
V2	0.45	19.9 (2.90)	0.21
W4	0.82	39.3 (5.70)	0.32
Q7	0.92	33.1 (4.80)	0.31
R2	1.20	57.1 (8.27)	0.53

Table A-5. Tensile Properties of [90_8] AS4/3501-6 Graphite/Epoxy at Intermediate Strain Rates , 22°C (72°F) and 1% Moisture.

Initial Properties

Specimen Number	Strain Rate ($\dot{\varepsilon}_{22}$) , s^{-1}	Modulus (E_{22}) GPa (Msi)	Poisson's Ratio ν_{21}
V4	0.42	11.0 (1.60)	0.0120
V7	0.87	11.7 (1.70)	0.0100
Q1	0.53	12.4 (1.80)	
Q5	0.29	12.4 (1.80)	0.0108
Q6	0.28	12.4 (1.80)	0.0113

Ultimate Properties

Specimen Number	Time to Failure (t_f) , ms	Strength (F_{2T}) MPa (Ksi)	Strain (ε_{2T}) , %
V4	9.9	42.1 (6.10)	0.39
V7	4.9	39.9 (5.80)	0.36
Q1	4.0	37.2 (5.40)	0.30
Q5	8.8	33.0 (4.80)	0.30
Q6	11.7	32.7 (4.70)	0.28

Table A-6. Tensile Properties of [90_8] AS4/3501-6 Graphite/Epoxy at High Strain Rates , 22°C (72°F) and 1% Moisture.

Initial Properties

Specimen Number	Strain Rate ($\dot{\varepsilon}_{22}$) , s^{-1}	Modulus (E_{22}) GPa (Msi)	Poisson's Ratio ν_{21}
AA1	1.61	12.1 (1.76)	—
Q4	1.85	10.9 (1.58)	—
AA2		12.6 (1.82)	0.0286
V5	1.67		
V6	1.33	— —	—
W3	1.56	11.0 (1.60)	0.0667

Ultimate Properties

Specimen Number	Time to Failure (t_f) , ms	Strength (F_{2T}) MPa (Ksi)	Strain (ε_{2T}) , %
AA1	4.0	47 (6.9)	0.42
Q4	3.5	29 (4.2)	0.62
V5	4.6	46 (6.7)	0.44
V6	2.0	23 (3.4)	0.23
W3	3.5	42 (6.1)	0.38

Table A-7. Tensile Properties of [90_8] AS4/3501-6 Graphite/Epoxy at Low Strain Rates , 60°C (140°F) and 0% Moisture.

Initial Properties

Specimen Number	Strain Rate ($\dot{\varepsilon}_{22}$) ,m s^{-1}	Modulus (E_{22}) GPa (Msi)	Poisson's Ratio ν_{21}
J6	4.7	10.3 (1.50)	-
J7	4.2	10.3 (1.50)	-
J10	4.4	11.7 (1.70)	0.0152

Ultimate Properties

Specimen Number	Time to Failure (t_f) , s	Strength (F_{2T}) MPa (Ksi)	Strain (ε_{2T}) , %
J6	1.5	58.6 (8.50)	0.57
J7	2.1	59.6 (8.65)	0.57
J10	1.2	58.6 (8.50)	0.50

Table A-8. Tensile Properties of $[90_8]$ AS4/3501-6 Graphite/Epoxy at Intermediate Strain Rates , 60°C (140°F) and 0% Moisture.

Initial Properties

Specimen Number	Strain Rate $(\dot{\varepsilon}_{22})$, s^{-1}	Modulus (E_{22}) GPa (Msi)	Poisson's Ratio ν_{21}
M5	0.52	11.7 (1.70)	0.0308
R5	0.67	10.5 (1.52)	0.0080
R9	0.64	9.8 (1.42)	0.0114
Q9	0.40	10.0 (1.45)	—
Q2	0.26	10.3 (1.50)	0.0153
Q8	0.50	12.4 (1.80)	—
Q11	—	— —	—
CC6	0.30	12.4 (1.80)	0.0217
Q10	0.48	11.7 (1.70)	0.0300

Ultimate Properties

Specimen Number	Time to Failure (t_f) , ms	Strength (F_{2T}) MPa (Ksi)	Strain (ε_{2T}) , %
M5	9.6	51.0 (7.40)	0.47
R5	13.0	57.6 (8.36)	0.75
R9	8.3	58.6 (8.50)	0.56
Q9	7.1	34.4 (4.91)	0.29
Q2	24.0	59.9 (8.70)	0.61
Q8	8.2	45.5 (6.60)	0.34
CC6	14.0	46.2 (6.70)	0.38
Q10	7.5	42.8 (6.20)	0.32

Table A-9. Tensile Properties of $[90_8]$ AS4/3501-6 Graphite/Epoxy at High Strain Rates , 60°C (140°F) and 0% Moisture.

Initial Properties

Specimen Number	Strain Rate ($\dot{\varepsilon}_{22}$) , s^{-1}	Modulus (E_{22}) GPa (Msi)	Poisson's Ratio ν_{21}
J8	1.6	10.3 (1.50)	0.0175
J9	1.5	10.9 (1.59)	0.0114
AA8	1.3	12.2 (1.76)	—
AA6	1.2	10.7 (1.55)	—
AA9	1.5	11.0 (1.59)	—

Ultimate Properties

Specimen Number	Time to Failure (t_f) , ms	Strength (F_{2T}) MPa (Ksi)	Strain (ε_{2T}) , %
J8	4.4	61.0 (8.85)	0.54
J9	4.7	64.1 (9.30)	0.54
AA8	5.2	58.9 (8.53)	0.45
AA6	5.0	62.1 (9.00)	5.00
AA9	5.2	58.9 (8.53)	0.45

Table A-10 Tensile Properties of [90_8] AS4/3501-6 Graphite/Epoxy at Low Strain Rates , 91°C (196°F) and 0% Moisture.

Initial Properties

Specimen Number	Strain Rate ($\dot{\varepsilon}_{22}$) , ms^{-1}	Modulus (E_{22}) GPa (Msi)	Poisson's Ratio ν_{21}
J2	3.9	10.1 (1.46)	—
AA10	3.1	9.4 (1.36)	—
J3	4.3	9.9 (1.44)	—
J4	4.2	9.9 (1.43)	—
V1	3.5	10.0 (1.45)	0.0176
V10	4.8	12.0 (1.74)	0.0134
AA4	2.9	9.6 (1.40)	

Ultimate Properties

Specimen Number	Time to Failure (t_f) , s	Strength (F_{2T}) MPa (Ksi)	Strain (ε_{2T}) , %
J2	1.4	52.6 (76.3)	0.55
AA10	2.0	56.5 (8.20)	0.63
J3	1.4	53.4 (7.75)	0.53
J4	1.4	63.7 (9.24)	0.52
V1	0.8	29.0 (4.21)	0.29
V10	0.8	45.5 (6.60)	0.40
AA4	2.0	56.7 (8.22)	0.60

Table A-11. Tensile Properties of $[90_8]$ AS4/3501-6 Graphite/Epoxy at Intermediate Strain Rates , 91°C (196°F) and 0% Moisture.

Initial Properties

Specimen Number	Strain Rate $(\dot{\varepsilon}_{22})$, s^{-1}	Modulus (E_{22}) GPa (Msi)	Poisson's Ratio ν_{21}
M7	0.43	10.8 (1.56)	0.0136
M8	0.44	10.9 (1.59)	0.0132
M10	0.44	11.0 (1.60)	0.0172
J1	0.60	— —	—
CC1	0.18	9.3 (1.35)	—
R7	0.31	10.3 (1.50)	—

Ultimate Properties

Specimen Number	Time to Failure (t_f) , ms	Strength (F_{2T}) MPa (Ksi)	Strain (ε_{2T}) , %
M7	13.2	56.5 (8.20)	0.51
M8	13.3	62.0 (9.00)	0.52
M10	13.1	52.4 (7.60)	0.46
J1	8.5	48.9 (7.10)	0.53
CC1	27.1	41.1 (5.96)	0.46
R7	10.0	32.2 (4.67)	0.33

Table A-12. Tensile Properties of [90_8] AS4/3501-6 Graphite/Epoxy at High Strain Rates , 91°C (196°F) and 0% Moisture.

Initial Properties

Specimen Number	Strain Rate ($\dot{\varepsilon}_{22}$) , s^{-1}	Modulus (E_{22}) GPa (Msi)	Poisson's Ratio ν_{21}
M4	—	10.3 (1.50)	—
M9	—	11.4 (1.65)	—
W5	—	11.6 (1.69)	0.0197
CC3	1.34	11.7 (1.70)	0.0156
CC7	1.28	10.7 (1.55)	0.0142
CC10	1.37	11.0 (1.60)	0.0065

Ultimate Properties

Specimen Number	Time to Failure (t_f) , ms	Strength (F_{2T}) MPa (Ksi)	Strain (ε_{2T}) , %
M4	4.3	62.0 (9.00)	0.55
M9	4.5	60.7 (8.80)	0.47
W5	3.2	43.3 (6.30)	0.26
CC3	5.0	— —	—
CC7	3.7	60.7 (8.80)	0.54
CC10	4.8	59.2 (8.60)	0.54

Table A-13. Tensile Properties of $[90_8]$ AS4/3501-6 Graphite/Epoxy at Low Strain Rates , 91°C (196°F) and 1% Moisture.

Initial Properties

Specimen Number	Strain Rate ($\dot{\varepsilon}_{22}$) , ms^{-1}	Modulus (E_{22}) GPa (Msi)	Poisson's Ratio ν_{21}
R4	3.5	9.0 (1.30)	–
R10	4.4	8.9 (1.30)	–
R11	3.5	9.6 (1.40)	–

Ultimate Properties

Specimen Number	Time to Failure (t_f) , s	Strength (F_{2T}) MPa (Ksi)	Strain (ε_{2T}) , %
R4	1.2	29.0 (4.20)	0.30
R10	0.9	31.0 (4.50)	0.34
R11	1.1	32.2 (4.67)	0.38

Table A-14. Tensile Properties of $[90_8]$ AS4/3501-6 Graphite/Epoxy at Intermediale Strain Rates , 91°C (196°F) and 1% Moisture.

Initial Properties

Specimen Number	Strain Rate $(\dot{\varepsilon}_{22})$, s^{-1}	Modulus (E_{22}) GPa (Msi)	Poisson's Ratio ν_{21}
P3	0.37	11.2 (1.63)	0.0160
P8	0.54	10.1 (1.46)	—
P5	0.46	— —	0.0173
P4	0.37	11.0 (1.60)	—
DD2	0.19	10.3 (1.50)	0.0118
DD3	0.54	9.6 (1.40)	—
R7	0.31	10.3 (1.50)	—

Ultimate Properties

Specimen Number	Time to Failure (t_f) , ms	Strength (F_{2T}) MPa (Ksi)	Strain (ε_{2T}) , %
P3	7.2	39.3 (5.70)	0.34
P8	6.9	33.8 (4.90)	0.32
P5	6.7	— —	0.38
P4	6.9	42.7 (6.20)	0.36
DD2	21.0	42.5 (6.17)	0.42
DD3	5.0	40.3 (5.85)	0.42
R7	10.0	32.2 (4.77)	0.33

Table A-15. Tensile Properties of $[90_8]$ AS4/3501-6 Graphite/Epoxy at High Strain Rates , 91°C (196°F) and 1% Moisture.

Initial Properties

Specimen Number	Strain Rate ($\dot{\varepsilon}_{22}$) , s^{-1}	Modulus (E_{22}) GPa (Msi)	Poisson's Ratio ν_{21}
P7	0.91	12.4 (1.80)	
W7	1.07	12.4 (1.80)	
DD4	0.95	10.6 (1.54)	

Ultimate Properties

Specimen Number	Time to Failure (t_f) , ms	Strength (F_{2T}) MPa (Ksi)	Strain (ε_{2T}) , %
P7	3.55	38.3 (5.55)	0.25
W7	3.2	37.0 (5.37)	0.35
DD4	3.9	28.3 (4.10)	0.37

Table A-16. Tensile Properties of [90_8] AS4/3501-6 Graphite/Epoxy at Low Strain Rates, 128°C (263°F) and 0% Moisture.

Initial Properties

Specimen Number	Strain Rate ($\dot{\varepsilon}_{22}$), ms^{-1}	Modulus (E_{22}) GPa (Msi)	Poisson's Ratio ν_{21}
90/-4H1	0.50	9.3(1.35)	-
90/-4H2	0.50	8.9(1.29)	-
90/-4H3	0.50	9.0(1.31)	-
90/-4H4	0.50	9.3(1.35)	-
90/-4H5	0.50	9.4(1.36)	-

Ultimate Properties

Specimen Number	Time to Failure (t_f), s	Strength (F_{2T}) MPa (Ksi)	Strain (ε_{2T}), %
90/-4H1	11	54(7.87)	0.63
90/-4H2	14	57(8.37)	0.72
90/-4H3	13	57(8.40)	0.70
90/-4H4	12	57(8.29)	0.69
90/-4H5	12	57(8.35)	0.67

Table A-17. Tensile Properties of [90_8] AS4/3501-6 Graphite/Epoxy at Intermediate Strain Rates, 128°C (263°F) and 0% Moisture.

Initial Properties

Specimen Number	Strain Rate ($\dot{\varepsilon}_{22}$), s^{-1}	Modulus (E_{22}) GPa (Msi)	Poisson's Ratio ν_{21}
90/-1H1	0.53	9.5(1.38)	-
90/-1H2	0.53	9.4(1.37)	-
90/-1H3	0.53	9.4(1.36)	-
90/-1H4	0.53	8.7(1.26)	-
90/-1H5	0.53	9.2(1.33)	-

Ultimate Properties

Specimen Number	Time to Failure (t_f), ms	Strength (F_{2T}) MPa (Ksi)	Strain (ε_{2T}), %
90/-1H1	13	63(9.28)	0.68
90/-1H2	11	60(8.74)	0.63
90/-1H3	11	60(8.73)	0.65
90/-1H4	12	64(9.42)	0.71
90/-1H5	11	59(8.68)	0.62

Table A-18. Tensile Properties of [90_8] AS4/3501-6 Graphite/Epoxy at High Strain Rates, 128°C (263°F) and 0% Moisture.

Initial Properties

Specimen Number	Strain Rate ($\dot{\varepsilon}_{22}$), s^{-1}	Modulus (E_{22}) GPa (Msi)	Poisson's Ratio ν_{21}
90/0H1	1.52	11.4(1.65)	0.0156
90/0H2	3.27	11.5(1.67)	0.0161
90/0H3	3.54	11.7(1.70)	0.0159
90/OH4	3.64	11.2(1.63)	0.0154

Ultimate Properties

Specimen Number	Time to Failure (t_f), ms	Strength (F_{2T}) MPa (Ksi)	Strain (ε_{2T}), %
90/OH1	4.1	70(10.2)	0.61
90/0H2	1.8	64 (9.4)	0.56
90/OH3	2.4	63 (9.2)	0.53
90/0H4	1.9	64 (9.3)	

Table A-19. Shear Properties of [10_6] AS4/3501-6 Graphite/Epoxy at Low Strain Rates, 22°C (72°F) and 0% Moisture.

Initial Properties

Specimen Number	Strain Rate ($\dot{\gamma}_{12}$), ms^{-1}	Modulus (G_{12}) GPa (Msi)
10/-3L1	3.17	6.5(0.94)
10/-3L2	2.65	7.9(1.15)
10/-3L3	4.00	8.4(1.22)
10/-3L4	3.78	9.0(1.31)
10/-3L5	1.66	7.4(1.08)
10/-3L6	1.95	7.4(1.08)
10/-3L7	1.81	7.4(1.08)

Ultimate Properties

Specimen Number	Time to Failure (t_f) ,ms	Strength (F_{12}) MPa (Ksi)	Strain (γ_{12}) , %
10/-3L1	3.6	67 (9.78)	1.28
10/-3L2	3.1	59 (8.62)	0.96
10/-3L3	2.4	73(10.73)	1.08
10/-3L4	2.5	79(11.59)	1.10
10/-3L5	-	83(12.00)	1.56
10/-3L6	-	81(11.80)	1.55
10/-3L7	-	82(11.90)	1.55

Table A-20. Shear Properties of [10_6] AS4/3501-6 Graphite/Epoxy at Intermediate Strain Rates , 22°C (72°F) and 0% Moisture.

Initial Properties

Specimen Number	Strain Rate ($\dot{\gamma}_{12}$) , s^{-1}	Modulus (G_{12}) GPa (Msi)
10/-1L1	0.12	8.3(1.20)
10/-1L2	0.13	7.6(1.11)
10/-1L3	0.38	8.4(1.22)
10/-1L4	0.39	8.4(1.22)
10/-1L5	0.38	8.4(1.22)

Ultimate Properties

Specimen Number	Time to Failure (t_f) ,ms	Strength (F_{12}) MPa (Ksi)	Strain (γ_{12}) , %
10/-1L1	80	71(10.4)	1.09
10/-1L2	88	74(10.7)	1.12
10/-1L3	-	90(13.0)	1.45
10/-1L4	-	87(12.6)	1.27
10/-1L5	-	88(12.8)	1.36

Table A-21. Shear Properties of $[10_6]$ AS4/3501-6 Graphite/Epoxy at High Strain Rates , 22°C (72°F) and 0% Moisture.

Initial Properties

Specimen Number	Strain Rate $(\dot{\gamma}_{12})$, s^{-1}	Modulus (G_{12}) GPa (Msi)
10/0L1	2.60	8.3(1.20)
10/0L2	2.75	8.5(1.23)
10/0L3	3.02	8.9(1.29)
10/0L5	3.58	9.1(1.32)
10/0L6	3.04	9.4(1.37)
10/0L7	3.15	9.1(1.32)
10/0L8	1.10	9.4(1.36)

Ultimate Properties

Specimen Number	Time to Failure (t_f) ,ms	Strength (F_{12}) MPa (Ksi)	Strain (γ_{12}) , %
10/OL1	5.3	71(10.34)	0.96
10/0L2	5.8	76(11.08)	1.03
10/0L3	5.8	78(11.36)	1.13
10/0L5	6.7	90(13.14)	1.30
10/0L6	6.4	90(13.14)	1.12
10/0L7	6.4	91(13.28)	1.25
10/OL8	2.2	77(11.28)	1.02

Table A-22. Shear Properties of [10_6] AS4/3501-6 Graphite/Epoxy at Low Strain Rates , 22°C (72°F) and 1% Moisture.

Initial Properties

Specimen Number	Strain Rate ($\dot{\gamma}_{12}$) , ms^{-1}	Modulus (G_{12}) GPa (Msi)
X3	4.0	8.6 (1.25)
X4	5.7	8.6 (1.25)
X6	4.5	9.5 (1.38)

Ultimate Properties

Specimen Number	Time to Failure (t_f) , ms	Strength (F_{12}) MPa (Ksi)	Strain (γ_{12}) , %
X3	2.2	74.3 (10.77)	1.10
X4	2.2	77.7 (11.27)	1.17
X6	2.2	75.8 (11.00)	—

Table A-23. Shear Properties of $[10_6]$ AS4/3501-6 Graphite/Epoxy at Intermediate Strain Rates , 22°C (72°F) and 1% Moisture.

Initial Properties

Specimen Number	Strain Rate $(\dot{\gamma}_{12})$, s^{-1}	Modulus (G_{12}) GPa (Msi)
F1	0.61	6.3 (0.91)
X1	0.47	8.9 (1.29)
X2	0.58	7.8 (1.13)

Ultimate Properties

Specimen Number	Time to Failure (t_f) , ms	Strength (F_{12}) MPa (Ksi)	Strain (γ_{12}) , %
F1	24.8	75.3 (10.92)	1.48
X1	25.5	79.8 (11.58)	1.17
X2	27.6	92.2 (13.37)	1.61

Table A-24. Shear Properties of $[10_6]$ AS4/3501-6 Graphite/Epoxy at High Strain Rates , 22°C (72°F) and 1% Moisture.

Initial Properties

Specimen Number	Strain Rate $(\dot{\gamma}_{12})$, s^{-1}	Modulus (G_{12}) GPa (Msi)
F2	1.7	8.3 (1.20)
F3	2.0	9.2 (1.33)
F9	1.2	9.4 (1.37)

Ultimate Properties

Specimen Number	Time to Failure (t_f) , ms	Strength (F_{12}) MPa (Ksi)	Strain (γ_{12}) , %
F2	7.9	78.7 (11.42)	1.25
F3	7.8	81.7 (11.83)	1.10
F9	9.3	81.8 (11.90)	1.11

Table A-25. Shear Properties of $[10_6]$ AS4/3501-6 Graphite/Epoxy at Low Strain Rates , 60°C (140°F) and 0% Moisture.

Initial Properties

Specimen Number	Strain Rate $(\dot{\gamma}_{12})$, ms^{-1}	Modulus (G_{12}) GPa (Msi)
S5	3.7	— —
S6	4.0	— —
S7	4.0	— —
Y1	7.8	6.6 (0.96)
Y2	7.2	6.2 (0.90)
Y10	9.5	6.1 (0.89)

Ultimate Properties

Specimen Number	Time to Failure (t_f) , s	Strength (F_{12}) MPa (Ksi)	Strain (γ_{12}) , %
S5	3.6	77.0 (11.17)	1.35
S6	2.7	72.3 (10.48)	1.10
S7	3.7	75.8 (11.00)	1.50
Y1	2.2	72.6 (10.53)	1.59
Y2	2.3	67.1 (9.74)	1.43
Y10	2.2	75.8 (11.00)	1.80

Table A-26. Shear Properties of [10_6] AS4/3501-6 Graphite/Epoxy at Intermediate Strain Rates , 60°C (140°F) and 0% Moisture.

Initial Properties

Specimen Number	Strain Rate ($\dot{\gamma}_{12}$) , s^{-1}	Modulus (G_{12}) GPa (Msi)
S8	—	— —
S9	—	— —
S10	—	— —
Y6	0.44	6.4 (0.93)
ZZ2	0.61	9.4 (1.36)
X9	0.65	9.1 (1.30)

Ultimate Properties

Specimen Number	Time to Failure (t_f) ,m s	Strength (F_{12}) MPa (Ksi)	Strain (γ_{12}) , %
S8	40.5	88.9 (12.90)	—
S9	30.0	63.8 (9.25)	0.96
S10	30.5	87.3 (12.66)	1.60
Y6	26.0	65.4 (9.48)	1.20
ZZ2	26.5	102.7 (14.91)	1.82
X9	26.0	87.3 (12.66)	1.41

Table A-27. Shear Properties of $[10_6]$ AS4/3501-6 Graphite/Epoxy at High Strain Rates , 60°C (140°F) and 0% Moisture.

Initial Properties

Specimen Number	Strain Rate $(\dot{\gamma}_{12})$, s^{-1}	Modulus (G_{12}) GPa (Msi)
S12	1.6	6.9 (1.00)
S13	2.3	7.6 (1.10)
X8	2.0	6.9 (1.00)
Y8	1.6	6.9 (1.00)
Y9	1.8	6.6 (0.96)

Ultimate Properties

Specimen Number	Time to Failure (t_f) ,m s	Strength (F_{12}) MPa (Ksi)	Strain (γ_{12}) , %
S12	8.3	94.5 (13.70)	1.59
S13	8.6	93.8 (13.60)	1.53
X8	7.7	92.4 (13.40)	1.28
Y8	7.4	73.8 (10.70)	1.18
Y9	7.0	75.8 (11.00)	1.30

Table A-28. Shear Properties of $[10_6]$ AS4/3501-6 Graphite/Epoxy at Low Strain Rates , 91°C (196°F) and 0% Moisture.

Initial Properties

Specimen Number	Strain Rate ($\dot{\gamma}_{12}$) , $m\,s^{-1}$	Modulus (G_{12}) GPa (Msi)
ZZ15	5.4	6.9 (1.00)
ZZ13	5.7	8.5 (1.23)
Y5	6.4	5.9 (0.85)
Y3	4.9	6.9 (1.01)

Ultimate Properties

Specimen Number	Time to Failure (t_f) , s	Strength (F_{12}) MPa (Ksi)	Strain (γ_{12}) , %
ZZ15	2.7	79.9 (11.60)	1.60
ZZ13	2.2	81.8 (11.86)	1.46
Y5	2.6	65.2 (9.46)	1.59
Y3	2.6	64.1 (9.30)	1.35

Table A-29. Shear Properties of $[10_6]$ AS4/3501-6 Graphite/Epoxy at Intermediate Strain Rates , 91°C (196°F) and 0% Moisture.

Initial Properties

Specimen Number	Strain Rate ($\dot{\gamma}_{12}$) , s^{-1}	Modulus (G_{12}) GPa (Msi)
ZZ14	0.66	7.2 (1.04)
ZZ11	0.86	6.9 (1.00)
ZZ6	0.80	7.6 (1.10)

Ultimate Properties

Specimen Number	Time to Failure (t_f) , ms	Strength (F_{12}) MPa (Ksi)	Strain (γ_{12}) , %
ZZ14	21.5	75.8 (11.00)	1.41
ZZ11	16.0	76.5 (11.10)	1.35
ZZ6	19.5	84.1 (12.20)	1.52

Table A-30. Shear Properties of $[10_6]$ AS4/3501-6 Graphite/Epoxy at High Strain Rates , 91°C (196°F) and 0% Moisture.

Initial Properties

Specimen Number	Strain Rate ($\dot{\gamma}_{12}$) , s^{-1}	Modulus (G_{12}) GPa (Msi)
F6	1.9	8.9 (1.30)
F10	1.6	1.4 (1.08)
X5	2.1	8.5 (1.23)
ZZ18	2.5	7.6 (1.10)
Y7	2.8	6.9 (1.00)
ZZ12	2.9	7.6 (1.10)
ZZ1	1.1	6.8 (0.98)
ZZ5	2.3	6.9 (1.00)
ZZ7	—	— —
ZZ8	2.1	8.3 (1.20)
ZZ9	1.0	6.6 (0.96)

Ultimate Properties

Specimen Number	Time to Failure (t_f) , ms	Strength (F_{12}) MPa (Ksi)	Strain (γ_{12}) , %
F6	7.2	85.5 (12.40)	1.41
F10	9.0	97.9 (14.20)	1.20
X5	7.7	83.4 (12.10)	1.51
ZZ18	6.7	82.7 (12.00)	1.43
Y7	7.5	87.6 (12.70)	1.69
ZZ12	7.4	97.9 (14.20)	1.77
ZZ1	11.8	68.9 (10.00)	1.20
ZZ5	5.5	70.3 (10.20)	1.30
ZZ7	6.6	79.9 (11.60)	—
ZZ8	7.0	95.8 (13.90)	1.53
ZZ9	8.4	85.5 (12.40)	1.82

Table A-31. Shear Properties of $[10_6]$ AS4/3501-6 Graphite/Epoxy at Low Strain Rates , 91°C (196°F) and 1% Moisture.

Initial Properties

Specimen Number	Strain Rate ($\dot{\gamma}_{12}$) , ms^{-1}	Modulus (G_{12}) GPa (Msi)
KK1	3.4	7.6 (1.10)
KK4	4.0	5.6 (0.82)
X7	8.0	6.3 (0.92)
F8	8.8	7.2 (1.04)

Ultimate Properties

Specimen Number	Time to Failure (t_f) , s	Strength (F_{12}) MPa (Ksi)	Strain (γ_{12}) , %
KK1	3.2	50.5 (7.33)	1.50
KK4	2.5	45.2 (6.60)	0.94
X7	1.9	61.2 (8.90)	1.48
F8	1.8	60.4 (8.80)	—

Table A-32. Shear Properties of [10_6] AS4/3501-6 Graphite/Epoxy at Intermediate Strain Rates , 91°C (196°F) and 1% Moisture.

Initial Properties

Specimen Number	Strain Rate ($\dot{\gamma}_{12}$) , s^{-1}	Modulus (G_{12}) GPa (Msi)
MM4	0.72	8.8 (1.28)
F4	0.02	6.7 (0.98)
X10	0.01	7.0 (1.02)

Ultimate Properties

Specimen Number	Time to Failure (t_f) , s	Strength (F_{12}) MPa (Ksi)	Strain (γ_{12}) , %
MM4	24.0	75.8 (11.00)	1.59
F4	1.7	56.3 (8.17)	1.82
X10	1.6	54.8 (7.95)	1.77

Table A-33. Shear Properties of $[10_6]$ AS4/3501-6 Graphite/Epoxy at High Strain Rates , 91°C (196°F) and 1% Moisture.

Initial Properties

Specimen Number	Strain Rate $(\dot{\gamma}_{12})$, s^{-1}	Modulus (G_{12}) GPa (Msi)
LL9	1.4	6.5 (0.94)
MM1	4.1	6.3 (0.92)
MM5	–	– –
OO1	1.5	5.6 (0.82)
Y4	3.1	5.9 (0.85)

Ultimate Properties

Specimen Number	Time to Failure (t_f) , ms	Strength (F_{12}) MPa (Ksi)	Strain (γ_{12}) , %
LL9	16.8	66.9 (2.70)	2.23
MM1	7.1	70.9 (10.30)	2.25
MM5	8.5	75.8 (11.00)	–
OO1	19.0	60.7 (8.80)	2.23
Y4	7.4	61.4 (8.90)	1.95

Table A-34. Shear Properties of $[10_6]$ AS4/3501-6 Graphite/Epoxy at Low Strain Rates, 128°C (263°F) and 0% Moisture.

Initial Properties

Specimen Number	Strain Rate ($\dot{\gamma}_{12}$), ms^{-1}	Modulus (G_{12}) GPa (Msi)
10/-2H1	66	7.2(1.05)
10/-2H2	77	8.4(1.22)
10/-2H3	70	9.5(1.38)
10/-2H4	79	7.6(1.11)
10/-2H5	88	8.3(1.21)
10/-2H6	10	7.2(1.05)
10/-2H7	32	7.5(1.09)
10/-2H8	40	6.9(1.00)

Ultimate Properties

Specimen Number	Time to Failure (t_f), s	Strength (F_{12}) MPa (Ksi)	Strain (γ_{12}), %
10/-2H1	0.232	64(9.40)	1.74
10/-2H2	0.174	68(9.87)	1.72
10/-2H3	0.158	56(8.15)	1.01
10/-2H4	0.164	59(8.68)	1.54
10/-2H5	0.168	66(9.58)	1.67
10/-2H6	0.131	61(8.95)	1.38
10/-2H7	0.510	67(9.80)	1.45
10/-2H8	0.370	69(10.10)	1.65

Table A-35. Shear Properties of $[10_6]$ AS4/3501-6 Graphite/Epoxy at Intermediate Strain Rates , 128°C (263°F) and 0% Moisture.

Initial Properties

Specimen Number	Strain Rate $(\dot{\gamma}_{12})$, s^{-1}	Modulus (G_{12}) GPa (Msi)
10/-1H1	0.43	8.7(1.27)
10/-1H2	0.34	9.3(1.35)
10/-1H3	0.10	9.1(1.34)
10/-1H4	0.16	9.5(1.38)

Ultimate Properties

Specimen Number	Time to Failure (t_f) ,ms	Strength (F_{12}) MPa (Ksi)	Strain (γ_{12}) , %
10/-1H1	40	67(9.77)	1.51
10/-1H2	36	67(9.76)	1.30
10/-1H3	22	65(9.45)	1.30
10/-1H4	32	61(8.97)	1.44

Table A-36. Shear Properties of [10_6] AS4/3501-6 Graphite/Epoxy at High Strain Rates, 128°C (263°F) and 0% Moisture.

Initial Properties

Specimen Number	Strain Rate ($\dot{\gamma}_{12}$), s^{-1}	Modulus (G_{12}) GPa (Msi)
10/0H1	5.0	10.6(1.54)
10/0H2	5.0	10.9(1.58)
10/0H3	2.2	11.6(1.68)
10/0H4	2.0	10.6(1.54)
10/0H5	2.4	10.1(1.47)
10.0H6	2.2	9.8(1.42)

Ultimate Properties

Specimen Number	Time to Failure (t_f), ms	Strength (F_{12}) MPa (Ksi)	Strain (γ_{12}), %
10/OH1	4	84(12.2)	1.87
10/OH2	3	70(10.3)	1.22
10/0H3	4	86(12.6)	1.87
10/OH4	9	86(12.5)	1.95
10/0H5	8	82(12.0)	1.88
10/0H6	8	88(12.9)	1.98

Table A-37. Tensile Properties of $[0_6]$ AS4/3501-6 Graphite/Epoxy at Low Strain Rates, 22°C (72°F) and 0% Moisture.

Initial Properties

Specimen Number	Strain Rate ($\dot{\varepsilon}_{11}$), ms^{-1}	Modulus (E_{11}) GPa (Msi)	Poisson's Ratio ν_{12}
0/-4L2	0.31	143(20.8)	0.26
0/-4L3	0.37	142(20.6)	0.27
0/-413	0.35	143(20.8)	0.27
0/-415	0.37	144(21.0)	0.27

Ultimate Properties

Specimen Number	Time to Failure (t_f), s	Strength (F_{1T}) MPa (Ksi)	Strain (ε_{1T}), %
0/-412	44	2404(349)	1.55
0/-413	49	2356(342)	1.54
0/-414	56	2452(356)	1.58
0/-415	55	2404(349)	1.55

Table A-38. Tensile Properties of $[0_6]$ AS4/3501-6 Graphite/Epoxy at High Strain Rates, 22°C (72°F) and 0% Moisture.

Initial Properties

Specimen Number	Strain Rate ($\dot{\varepsilon}_{11}$), s^{-1}	Modulus (E_{11}) GPa (Msi)	Poisson's Ratio ν_{12}
0/0L1	1.00	145(21.1)	0.27
0/0L2	1.02	145(21.1)	0.26
0/0L3	1.01	148(21.5)	0.27
0/0L3.1	1.03	150(21.9)	0.26
0/0L4	1.08	148(21.5)	0.25

Ultimate Properties

Specimen Number	Time to Failure (t_f), ms	Strength (F_{1T}) MPa (Ksi)	Strain (ε_{1T}), %
0/0L1	18	2349(341)	1.42
0/0L2	18	2308(335)	1.46
0/0L3	18	2335(339)	1.42
0/0L3.1	19	2335(339)	1.42
0/0L4	16	2273(330)	1.39
0.0L5	14	2377(345)	1.41

Table A-39. Tensile Properties Of $[0_6]$ AS4/3501-6 Graphite/Epoxy at Low Strain Rates , 22°C (72°F) and 1% Moisture.

Initial Properties

Specimen Number	Strain Rate ($\dot{\varepsilon}_{11}$) , ms^{-1}	Modulus (E_{11}) GPa (Msi)	Poisson's Ratio ν_{12}
HH8	5.0	144.8 (21.0)	—
Z4	3.2	143.7 (20.8)	0.28
		144.8 (21.0) x	
Z5	3.3	142.0 (20.6)	—
Z10	3.2	144.1 (20.9)	0.22
		147.1 (21.2) x	
Z12	3.2	145.9 (21.2)	0.27
HH9	4.6	151.7 (22.0)	0.25
HH11	3.9	144.8 (21.0)	0.31

Ultimate Properties

Specimen Number	Time to Failure (t_f) , s	Strength (F_{1T}) MPa (Ksi)	Strain (ε_{1T}) , %
HH8	3.10	2413 (350)	1.58
Z4	—	2082 (302)	1.35
			1.50 x
Z5	4.45	1944 (282)	1.42
Z10	4.50	1985 (288)	1.30
			1.31 x
Z12	4.90	2206 (320)	1.56
			1.45 x
HH9	3.00	2178 (316)	1.43
HH11	2.80	2102 (305)	1.28

Table A-40. Tensile Properties of $[0_6]$ AS4/3501-6 Graphite/Epoxy at Intermediate Strain Rates , 22°C (72°F) and 1% Moisture.

Initial Properties

Specimen Number	Strain Rate ($\dot{\varepsilon}_{11}$) , s^{-1}	Modulus (E_{11}) GPa (Msi)	Poisson's Ratio ν_{12}
Z6	0.37	147.0 (21.3)	0.43
		142.6 (20.6) x	
Z8	0.69	142.7 (20.7)	0.31
		143.1 (20.8)	
Z11	0.24	147.0 (21.3)	0.27
HH10	0.51	144.9 (21.0)	0.29
		144.9 (21.0) x	

Ultimate Properties

Specimen Number	Time to Failure (t_f) , ms	Strength (F_{1T}) MPa (Ksi)	Strain (ε_{1T}) , %
Z6	40.0	2020 (293)	1.40
Z8	21.4	2068 (300)	1.38
Z11	6.3	2234 (324)	1.38
			1.42 x
HH10	32.0	2213 (321)	1.51
			1.54 x

Table A-41. Tensile Properties of $[0_6]$ AS4/3501-6 Graphite/Epoxy at High Strain Rates , 22°C (72°F) and 1% Moisture.

Initial Properties

Specimen Number	Strain Rate $(\dot{\varepsilon}_{11})$, s^{-1}	Modulus (E_{11}) GPa (Msi)	Poisson's Ratio ν_{12}
Z7	0.81	15.5 (21.1)	—
Z9	0.79	147.1 (21.2)	0.27
		149.4 (21.7) x	
HH2	0.97	158.6 (23.0)	0.28
HH3	0.93	230.4 (24.0)	0.48

Ultimate Properties

Specimen Number	Time to Failure (t_f) , ms	Strength (F_{1T}) MPa (Ksi)	Strain (ε_{1T}) , %
Z7	20.0	2213 (321)	1.46
Z9	19.2	2199 (319)	1.46
HH2	16.2	2344 (340)	1.55
HH3	19.6	2380 (345)	1.51

Table A-42 Tensile Properties of $[0_6]$ AS4/3501-6 Graphite/Epoxy at Low Strain Rates , 60°C (140°F) and 0% Moisture.

Initial Properties

Specimen Number	Strain Rate ($\dot{\varepsilon}_{11}$) , ms^{-1}	Modulus (E_{11}) GPa (Msi)	Poisson's Ratio ν_{12}
BB14	—	— —	—
N2	3.3	131.0 (19.0)	—
N12	3.5	— —	—
N15	3.3	— —	—
EE2	3.6	144.8 (21.0)	0.32
EE3	3.6	151.7 (22.0)	0.32
EE6	3.5	144.8 (21.0)	0.33
BB6	4.0	144.8 (21.0)	—
BB10	3.5	151.7 (22.0)	—

Ultimate Properties

Specimen Number	Time to Failure (t_f) , s	Strength (F_{1T}) MPa (Ksi)	Strain (ε_{1T}) , %
BB14	3.6	2309 (335)	—
N2	4.2	2206 (320)	1.40
N12	4.3	2144 (311)	1.51
N15	4.7	2530 (367)	1.56
EE2	4.1	2240 (325)	1.46
EE3	4.1	2240 (325)	1.45
EE6	3.9	2109 (306)	1.36
BB6	3.6	2082 (302)	1.41
BB10	3.9	2364 (343)	1.49

Table A-43. Tensile Properties of $[0_6]$ AS4/3501-6 Graphite/Epoxy at Intermediate Strain Rates , 60°C (140°F) and 0% Moisture.

Initial Properties

Specimen Number	Strain Rate ($\dot{\varepsilon}_{11}$) , s^{-1}	Modulus (E_{11}) GPa (Msi)	Poisson's Ratio ν_{12}
N3	0.48	146.2 (21.2)	0.24
N7	0.47	160.6 (23.3)	0.28
BB4	0.12	147.6 (21.3)	—
BB12	0.45	170.4 (24.7)	0.25
EE12	0.35	160.8 (23.3)	0.34
EE11	0.40	149.6 (21.2)	0.27

Ultimate Properties

Specimen Number	Time to Failure (t_f) , ms	Strength (F_{1T}) MPa (Ksi)	Strain (ε_{1T}) , %
N3	35.0	2427 (352)	1.49
N7	35.0	2330 (338)	1.44
BB4	29.0	— —	—
BB12	35.0	2123 (308)	0.96
EE12	45.0	2254 (327)	1.38
EE11	45.0	2192 (318)	1.45

Table A-44. Tensile Properties Of $[0_6]$ AS4/3501-6 Graphite/Epoxy at High Strain Rates , 60°C (140°F) and 0% Moisture.

Initial Properties

Specimen Number	Strain Rate ($\dot{\varepsilon}_{11}$) , s^{-1}	Modulus (E_{11}) GPa (Msi)	Poisson's Ratio ν_{12}
N9	1.1	157.2 (22.8)	0.24
N14	1.0	181.3 (26.3)	0.26
BB11	1.0	148.9 (21.6)	0.26
BB7	1.1	151.0 (21.9)	—

Ultimate Properties

Specimen Number	Time to Failure (t_f) , ms	Strength (F_{1T}) MPa (Ksi)	Strain (ε_{1T}) , %
N9	18.2	2351 (341)	1.51
N14	16.0	2454 (356)	1.47
BB11	14.6	2206 (320)	1.46
BB7	16.0	2206 (320)	1.48

Table A-45. Tensile Properties of $[0_6]$ AS4/3501-6 Graphite/Epoxy at Low Strain Rates , 91°C (196°F) and 0% Moisture.

Initial Properties

Specimen Number	Strain Rate ($\dot{\varepsilon}_{11}$) , ms^{-1}	Modulus (E_{11}) GPa (Msi)	Poisson's Ratio ν_{12}
EE9	3.83	– –	0.35
BB2	3.61	144.8 (21.0)	–
BB8	3.50	144.8 (21.0)	–
BB16	3.33	151.7 (22.0)	–

Ultimate Properties

Specimen Number	Time to Failure (t_f) , s	Strength (F_{1T}) MPa (Ksi)	Strain (ε_{1T}) , %
EE9	3.90	2164 (314)	1.45
BB2	3.90	2302 (334)	1.47
BB8	4.15	2468 (358)	1.54
BB16	4.20	2364 (343)	1.55

Table A-46. Tensile Properties of $[0_6]$ AS4/3501-6 Graphite/Epoxy at Intermediate Strain Rates , 91°C (196°F) and 0% Moisture.

Initial Properties

Specimen Number	Strain Rate $(\dot{\varepsilon}_{11})$, ms^{-1}	Modulus (E_{11}) GPa (Msi)	Poisson's Ratio ν_{12}
T7	0.42	158.0 (22.9)	0.27
EE7	0.30	158.7 (23.0)	0.28
EE8	0.28	158.7 (23.0)	0.32

Ultimate Properties

Specimen Number	Time to Failure (t_f) ,m s	Strength (F_{1T}) MPa (Ksi)	Strain (ε_{1T}) , %
T7	39.0	2371 (344)	1.51
EE7	55.0	2482 (360)	1.52
EE8	49.5	2227 (323)	1.39

Table A-47. Tensile Properties of $[0_6]$ AS4/3501-6 Graphite/Epoxy at High Strain Rates , 91°C (196°F) and 0% Moisture.

Initial Properties

Specimen Number	Strain Rate $(\dot{\varepsilon}_{11})$, s^{-1}	Modulus (E_{11}) GPa (Msi)	Poisson's Ratio ν_{12}
BB15	1.2	156.5 (22.7)	0.27
BB3	1.3	155.8 (22.6)	0.30
BB1	1.1	157.2 (22.8)	0.30
BB5	1.1	152.4 (22.1)	0.29

Ultimate Properties

Specimen Number	Time to Failure (t_f) ,m s	Strength (F_{1T}) MPa (Ksi)	Strain (ε_{1T}) , %
BB15	16.8	2454 (356)	1.67
BB3	15.6	2289 (332)	1.43
BB1	14.2	2089 (303)	1.33
BB5	16.6	2475 (359)	1.69

Table A-48. Tensile Properties of $[0_6]$ AS4/3501-6 Graphite/Epoxy at Low Strain Rates , 91°C (196°F) and 1% Moisture.

Initial Properties

Specimen Number	Strain Rate ($\dot{\varepsilon}_{11}$) , ms^{-1}	Modulus (E_{11}) GPa (Msi)	Poisson's Ratio ν_{12}
T11	4.04	144.8 (21.0)	0.32
O8	4.30	176.5 (25.6)	0.33
013	—	— —	—
014	—	161.3 (23.4)	—
T9	3.62	— —	—

Ultimate Properties

Specimen Number	Time to Failure (t_f) , s	Strength (F_{1T}) MPa (Ksi)	Strain (ε_{1T}) , %
T11	3.60	2399 (348)	1.52
O8	4.25	2330 (338)	1.51
O13	4.30	2206 (320)	—
O14	—	— —	—
T9	4.00	2275 (330)	1.45

Table A-49. Tensile Properties of $[0_6]$ AS4/3501-6 Graphite/Epoxy at Intermediate Strain Rates , 91°C (196°F) and 1% Moisture.

Initial Properties

Specimen Number	Strain Rate ($\dot{\varepsilon}_{11}$) , s^{-1}	Modulus (E_{11}) GPa (Msi)	Poisson's Ratio ν_{12}
O9	–	– –	–
O10	0.41	158.6 (23.0)	0.36
O11	0.40	155.8 (22.6)	0.27
T2	0.41	151.7 (22.0)	0.36

Ultimate Properties

Specimen Number	Time to Failure (t_f) , ms	Strength (F_{1T}) MPa (Ksi)	Strain (ε_{1T}) , %
O9	50.0	2344 (340)	–
O10	39.0	2123 (308)	1.42
O11	45.5	2420 (351)	1.55
T2	37.0	2275 (330)	1.47

Table A-50. Tensile Properties of $[0_6]$ AS4/3501-6 Graphite/Epoxy at High Strain Rates , 91°C (196°F) and 1% Moisture.

Initial Properties

Specimen Number	Strain Rate ($\dot{\varepsilon}_{11}$) , s^{-1}	Modulus (E_{11}) GPa (Msi)	Poisson's Ratio ν_{12}
HH5	0.80	184 (26.6)	0.33
HH4	1.25	148 (21.6)	0.27
T12	0.90	147 (21.3)	0.27

Ultimate Properties

Specimen Number	Time to Failure (t_f) , ms	Strength (F_{1T}) MPa (Ksi)	Strain (ε_{1T}) , %
HH5	17.8	1999 (290)	1.07
HH4	19.6	2248 (326)	1.51
T12	17.6	2158 (313)	1.51

Table A-51. Tensile Properties of $[0_6]$ AS4/3501-6 Graphite/Epoxy at Low Strain Rates, 128°C (263°F) and 0% Moisture.

Initial Properties

Specimen Number	Strain Rate ($\dot{\varepsilon}_{11}$), ms^{-1}	Modulus (E_{11}) GPa (Msi)	Poisson's Ratio ν_{12}
0/-4H1	0.295	148(21.6)	0.28
0/-4H2	0.324	144(20.9)	0.27
0/-4H3	0.316	150(21.8)	0.30
0/-4H4	0.332	147(21.4)	0.28

Ultimate Properties

Specimen Number	Time to Failure (t_f), s	Strength (F_{1T}) MPa (Ksi)	Strain (ε_{1T}), %
0/-4H1	50	2397(348)	1.46
0/-4H2	51	2328(338)	1.48
0/-4H3	48	2246(326)	1.38
0/-4H4	52	2405(349)	1.44

Table A-52. Tensile Properties of $[0_6]$ AS4/3501-6 Graphite/Epoxy at High Strain Rates, 128°C (263°F) and 0% Moisture.

Initial Properties

Specimen Number	Strain Rate $(\dot{\varepsilon}_{11})$, s^{-1}	Modulus (E_{11}) GPa (Msi)	Poisson's Ratio ν_{12}
0/0H1	0.96	160(23.3)	0.30
0/0H3	0.95	158(23.0)	0.30
0/0H3	1.05	161(23.5)	0.29
0/0H4	1.04	157(22.8)	0.27
0/0H5	0.90	157(22.8)	0.30
0/0H6	0.94	159(23.1)	0.29

Ultimate Properties

Specimen Number	Time to Failure (t_f), m s	Strength (F_{1T}) MPa (Ksi)	Strain (ε_{1T}), %
0/0H1	21	2439(354)	1.37
0/0H2	21	2445(355)	1.40
0/0H3	14	2321(337)	1.33
0/0H4	15	2425(352)	1.43
0/0H5	13	2204(320)	1.11
0/0H6	13	2135(310)	1.23

BIBLIOGRAPHY

1 Daniel, I. M., Hamilton, W. G., and LaBedz, R., "Strain Rate Characterization for Unidirectional Graphite/Epoxy Composite", Composite Materials Testing and Design (Sixth Conference), ASTM STP 787, ed. by I. M. , Daniel, American Society for Testing and Materials, 1892, pp. 394-413.

2 Daniel, I. M., "High Strain Rate Properties of Unidirectional Composites", NASA CR-167969, 1982.

3 Shen, C. H. and Springer, G. S., Journal of Composite Materials, Vol. 10, Jan 1976, pp. 2-20.

4 McKague, E. L., Jr., Reynolds, J. D., and Halkias, J. E., ASME, Journal of Engineering Materials and Technology, Jan. 1976, pp. 92-95.

5 Weitsman, Y., Journal of Composite Materials, Vol. 10, July 1976, pp.193-204.

6 Springer, G. S., Journal of Composite Materials, Vol. 11, Jan. 1977, pp.107-122.

7 Miller, A. K., and Adams, D. F., "Micromechanical Aspects of the Environmental Behavior of Composite Materials", Report UWME-DR-70-11111, Department of Mechanical Engineering, University of Wyoming, Laramie, Jan. 1978.

8 Shen, C. H. and Springer, G. S., Journal of Composite Materials, Vol. 11, Jan.1977, pp. 2-16.

9 Hertz, J., "Investigation inti the High-Temperature Strength Degredation of Fiber-Reinforced Resin Composite During Ambient Aging", Report GDCA-DBG73-005, Contract NAS8-27435, General Dynamics/Convair Aerospace Division, June 1973.

10 Lifshzitz, J. M., and Gilat, A., Experimental Mechanics, Vol. 19, No 12, Dec 1979, pp. 444-449.

11 Lifshzitz, J. M. "Strain Rate, Temperature and Humidity Influences on Strength and Moduli of a Graphite/Epoxy Composite", Composite Technology Review, Spring 1982.

12 Van Amerongen, G. T., Rubber Chemistry Technology, Vol. 37, 1964, pp. 1065-1152.

13 Browning, C. E., Husman, G. E., and Whitney J. M., "Moisture Effects on Epoxy Matrix Composites", ASTM STP 617, American Society for Testing and Materials, 1977, pp. 481-496.

14 Bueche, F., and Kelley, F. N., Journal of Polymer Science, Vol. 45, 1960, pp. 267-273.

15 Tsai, W. S., Hahn H. Thomas, "Introduction to Composite Materials", Technomic 1980.

16 Staverman, A. J. and Schwarzl, F., "Linear Deformation Behavior of High Polymers", Chapter I in Die Physik der Hochpolymeren, Vol. IV, edited by Stuart, H. A., Springer-Verlag, Berlin 1956.

17 Williams, M. L., Landel, R. F., Ferry, J. D., "Temperature Dependence of Relaxation Mechanisms in Amorphous Polymers and Other Glass-Forming Liquids", Journal, A. M. Chemical Soc., Vol. 77, pp. 3701, 1955.

18 Muki, R., and Sternberg, E., "On Transient Thermal Stresses in Viscoelastic Materials With Temperature-Dependent Properties", Journal of Applied Mechanics, pp. 193-207, June 1961.

19 Lohr, J. J., Trans. Soc. Rheol., 9:1 pp. 65, 1965.

20 Chamis, C. C., Lark, R. F., and Sinclair, J. H., "Integrated Theory for Predicting the Hygrothermomechanical Response of Advanced Composite Structural Components", ASTM STP 658, American Society for Testing and Materials.

21 Chamis, C. C. In Composite Materials: Testing and Design, ASTM STP 460, American Society for Testing and Materials, 1970, pp. 336-351.

22 Chamis, C. C. and Sinclair, J. H. "10-Deg Off-Axis Test for Shear Properties in Fiber Composites", Experimental Mechanics, Sept. 1977, pp. 339-346.

23 Dally, D. J., Riley, F. W., "Experimental Stress Analysis", Second Edition, Mc Graw Hill, 1987.

24 Yaniv, G., Peimanidis, G. and Daniel, I. M., "Method for Hygromechanical Characterization of Graphite/Epoxy Composite", Journal of Composites Technology and Research, Spring 1987, pp. 21-25.

25 Fowler, C. C., "Bonding of Elevated Temperature Strain Gages to Humid Aged Graphite Tensile Specimens Through the Use of Anaerobic Adhesives", Air Force Technical Report AFML-TR-75-204, Air Force Materials Lab, Dec. 1975.

26 Crank, J. Transactions at the Faraday Society, Vol. 51, 1955

27 Ferry, J. D. and Stratton, R. A., "The Free Volume Interpretation of The Dependence Of Viscosities and Viscoelastic Relaxation Times on Concentration, Pressure and Tensile Strain", Kolloid-Zeitchrift, Vol 171, pp. 107, 1960.

28 Daniel, I. M., Liber, T., and LaBedz, R., "New Method for Testing Composites at Very High Strain Rates", Experimental Mechanics, Vol. 21, No. 2. Feb. 1981, pp. 71-77.

29 Ishai, O, Gali, S., and Yaniv, G., "Durability of Adhesively Bonded Systems", CR-DAJA37-80-C0303, U.S. Army European Office, June 1981.

30 Kibler, K. G., "Time-Dependent Environmental Behavior of Graphite/Epoxy Composites", Air Force Wright Aeronautical Laboratories, AMWAL-TR-80-4052, May 1980.

31 Kobayashi, T., "Dynamic Crack Propagation Studies in Polymers", Ph.D Thesis, Illinois Institute of Technology, Chicago Il, 1972.

32 Yaniv, G. and Daniel, I. M., "Height-Tapered Double Cantilever Beam Specimen for Study of Rate Effects on Fracture Toughness of Composites", presented at Eight ASTM Symposium on composite Materials: Testing and Design, April 28-30, 1986, Charleston, SC.

33 Yaniv, G., Peimanidis, G., Daniel, I. M., "Envoronmental Effects on High Strain Rate Properties of Graphite/Epoxy Composites", CR-NAG-3-423, NASA, Lewis Research Center, Dec. 1986.

34 Sendeckyj, G. P., Richardson, M. D., and Pappas, J. E., "In Composite Reliability", STP 580, American Society For Testing and Materials, Philadelphia, 1975, pp. 528-548.

35 Whitney, M. J., Daniel, I. M., Pipes, R. B., "Experimental Mechanics of Fiber Reinforced Composite Materials, Society for Experimental Stress Analysis", Monograph No. 4 (SESA), First Edition, 1982.

36 Jones, M. R., "Mechanics of Composite Materials", McGraw-Hill, 1975.

37 Aklonis, J. J., McKnight, J. W., Shen, M., "Introduction to Polymer Viscoelasticity", Whiley-Interscience, 1972.

38 Smith, L. T., "Stress-Strain-Time-Temperature Relationships for Polymers", ASTM Special Technical Publication #325, Symposium on Stress-Strain-Time-Temperature Relationships in Materials, American Society for Testing and Materials, N.Y., 1962.

39 Moehlenpah, A. E., Ishai, O., and DiBeneddetto, A. T., "The Effects of Time and Temperature on the Mechanical Behavior of a Plasticized Epoxy Resin Under Different Loading Modes", Journal of Applied Polymer Science, Vol. 13, 1969, pp. 1231-1245.

40 Minoru Miwa [et al], "Temperature Dependence of the Tensile Strength of Glass-Fiber-Epoxy and Glass Fiber-Unsaturated Polyester Composites", Journal of Applied Polymer Science, Vol. 23, 1979, pp. 2957-2966.

41 Koltunov, M. A., and Troyanovski, I. E., "The Conditions for the Existance of a Temperature-Time Analogy", Polymer Mechanics 6, 2, Jan. 1973, pp.196-200.

42 Williams, J. G., "Fracture Mechanics of Polymers", Ellis Horwood Series in Engineering Science.

43 Hirai, T., and Kline, D. E., "Dynamic Mechanical Properties of Graphite/Epoxy and Carbon/Epoxy Composites", Journal of Composite Materials, April 1973.

44 Gibson, F. R., "Dynamic Mechanical Behavior of Fiber-Reinforsed Composites: Measurement and Analysis", Journal of Composite Materials, Vol. 10, Oct. 1976, pp. 325.

45 Crossman, F. W., Mauri, R. E., and Warren W. J., "Moisture-Altered Viscoelastic Responce of Graphite/Epoxy Composites", Advanced Composite Materials, Environmental Effets, J. R. Vinson, editor, STP 658, American Society for Testing and Materials.

46 Moehlenpah, A. E., Ishai, O., DiBenedetto, A. T., "The Effect of Time and Temperature an the Mechanical Behavior of Epoxy Composites", Polymer Engineering and Science, Vol. 11, No. 2, March 1971, pp. 129-138.

47 Jurf, A. R., Vinson, R. J., "Effect of Moisture on the Static and Viscoelastic Shear Properties of Epoxy Adhesives", Journal of Material Science 20, 1985, pp. 2979-2989.

48 Shirell, C. D., and Halpin, J., "Moisture Absorption and Desorption in Epoxy Composite Laminates", Composite Materials: Testing and Design (Fourth Conference), ASTM STP 617, American Society for Testing and Materials, 1977, pp. 514-528.

49 Delasi, R., and Whiteside, J. B., "Effect of Moisture on Epoxy Resins and Composite Materials-Environmental Effects", ASTM STP 658, J. R. Vinson, editor, American Society for Testing and Materials, 1978, pp. 2-20.

50 Hahn, H. T., "Residual Stresses in Polymer Matrix Composite Laminates", Journal of Composite Materials, Vol. 10, Oct. 1976, pp. 266-278.

51 Shirell, C. D., "Diffusion of Water Vapor in Graphite/Epoxy Composites", Advanced Composite Materials-Environmental Effects, ASTM STP 658, J. R. Vinson, editor, American Society for Testing and Materials, 1978, pp. 21-42.

52 Kowalski, I. M., "Characterizing the Tensile Stress-Strain Nonlinearity of Pan-Based Carbon Fibers", Presented at ASTM 8'th Symposium, Composite Materials Testing and Design, April 29-May 1, 1986, Charleston, SC.

53 Ruland, W., "The Relationship Between Preffered Orientation and Young's Modulus of Carbon Fibers", Applied Polymer Symposia, No. 9, 1969, pp. 293-301.

REPORT DOCUMENTATION PAGE

Form Approved
OMB No. 0704-0188

1. AGENCY USE ONLY (*Leave blank*)	2. REPORT DATE	3. REPORT TYPE AND DATES COVERED
	October 1991	Final Contractor Report

4. TITLE AND SUBTITLE

Environmental and Strain Rate Effects on Graphite/Epoxy Composites

5. FUNDING NUMBERS

WU-505-63-5B
G-NAG3-423

6. AUTHOR(S)

Konstantinos Peimandis

7. PERFORMING ORGANIZATION NAME(S) AND ADDRESS(ES)

Northwestern University
School of Engineering and Applied Science
Evanston, Illinois 60201

8. PERFORMING ORGANIZATION REPORT NUMBER

None

9. SPONSORING/MONITORING AGENCY NAMES(S) AND ADDRESS(ES)

National Aeronautics and Space Administration
Lewis Research Center
Cleveland, Ohio 44135-3191

10. SPONSORING/MONITORING AGENCY REPORT NUMBER

NASA CR-187229

11. SUPPLEMENTARY NOTES

Project Manager, C.C. Chamis, Structures Division, NASA Lewis Research Center, (216) 433-3252. Report was submitted as a thesis in partial fulfillment of the requirements for the degree Master of Science in Theoretical and Applied Mechanics to Northwestern University, Evanston, Illinois in May 1987.

12a. DISTRIBUTION/AVAILABILITY STATEMENT

Unclassified - Unlimited
Subject Category 24

12b. DISTRIBUTION CODE

13. ABSTRACT (*Maximum 200 words*)

An experimental investigation is described which deals with the hygrothermal characterization of unidirectional graphite/epoxy composites over a ranges of strain rates. Special techniques developed for such hygrothermal characterization are also described. The mechanical properties of the composite material were obtained and analyzed by means of a time-temperature-moisture superposition principle. The results show that: (1) the embedded gage technique was thoroughly examined and found to be appropriate for both hygrothermal expansion and mechanical strain measurements, (2) all transverse properties were found to decrease with increasing temperature and moisture content, and (3) ultimate transverse properties were found to increase with strain rate at low temperatures but follow an opposite trend at high temperatures compared to dry specimens.

14. SUBJECT TERMS

Graphite fiber; Composite; Environmental effects; High-strain rate; Embedded gages; Properties; Time-temperature; Superposition; Theory; Figures; Tables

15. NUMBER OF PAGES
292

16. PRICE CODE
A13

17. SECURITY CLASSIFICATION OF REPORT	18. SECURITY CLASSIFICATION OF THIS PAGE	19. SECURITY CLASSIFICATION OF ABSTRACT	20. LIMITATION OF ABSTRACT
Unclassified	Unclassified	Unclassified	

End of Document